

**DEVELOPMENT OF REMOTE SENSING METHODS FOR MEASUREMENT
OF LARGE, GRAVEL-BED, BRAIDED RIVERS**

**A dissertation submitted in fulfilment of the requirements for the
degree of Doctor of Philosophy**

by

Richard M. Westaway
Fitzwilliam College, University of Cambridge
September 2001

DECLARATION

I hereby declare that this dissertation entitled "*Development of remote sensing methods for measurement of large, gravel-bed, braided rivers*" is entirely my own work, and that I have acknowledged all sources of information and collaboration.

I further state that this dissertation is not substantially the same as any other work that has been, or is currently being, submitted for a degree, diploma or other qualification at this or any other University.

I also declare that the length of this dissertation does not exceed 80000 words, as specified by the Degree Committee for the Faculty of Earth Sciences and Geography.

A handwritten signature in black ink that reads "R. M. Westaway". The "R." is capitalized and followed by a period, "M." is capitalized and followed by a space, and "Westaway" is written in a cursive script.

Richard Westaway

THESIS SUMMARY

Riverbed topography is traditionally measured using repeated terrestrial survey of monumented cross-sections. The need for fully three-dimensional morphological information, coupled to limits on the density, spatial extent and frequency of re-survey using terrestrial methods, has led many river scientists to seek new approaches. Remote sensing has provided high-resolution high-quality digital elevation models (DEMs) in a variety of geomorphological settings. However, large gravel riverbeds represent an extreme case, with low relative relief, large spatial extent, presence of water and vegetation, and high spectral contrast between wet and dry areas. Thus, this research aims to assess the ability of two remote sensing techniques, digital photogrammetry and airborne laser scanning (ALS), to measure the topography of large, braided, gravel riverbeds, with sufficient quality to allow changes in bed form through both space and time to be detected. The field-sites selected for this work are two gravel-bed braided rivers of the Canterbury Plains, New Zealand: the North Ashburton and the Waimakariri. To achieve this aim, a number of objectives were addressed.

First, given the extreme nature of the application, project design required particular attention, including consideration of sensor height and photogrammetric block triangulation. Sensor height is important because of the inverse relationship between height (and hence financial cost) and surveyed point density (and hence quality of surface representation). In this research, data were collected photogrammetrically with different flying heights. This suggested that optimum flying height was linked to retention of sufficient image texture, and not simply the effects of image scale upon the precision of derived elevations. Photogrammetric block triangulation was also found to exert an important influence over the quality of DEMs produced, and major improvements resulted from addition of a network of tie-points to help constrain the bundle adjustment.

Second, methodologies were required for dealing with surface water, an issue particular to riverbed topography. Acquisition of remotely-sensed data during low flows minimises this issue, which is traditionally addressed by resorting to terrestrial survey techniques in wetted channels. Recent research has shown the potential for using remote sensing methods to estimate water depth and submerged topography, both for clear water (using through-water digital photogrammetry) and more-turbid water (using image analysis techniques). However, both methods have yet to be used for wider topographic survey of riverbed topography. One reason for this is the difficulty in modelling water surface elevation, which is required if estimated water depths are to be translated into z-elevation values. Thus, water surface elevation was mapped using interpolating water edge elevations derived using digital photogrammetry and ALS across wetted channels. Reach-scale DEMs were then produced by combining digital photogrammetry or ALS in exposed areas with refraction-corrected through-water digital photogrammetry for the clear water North Ashburton and water depth determined empirically from water colour for the more turbid Waimakariri.

Third, the adoption of automated topographic data collection methods mean that it is no longer feasible to identify errors manually. Consequently, automated methods of error detection are urgently required. This research developed two automated post-processing routines. The first, for the North Ashburton River, was used to identify wetted points where the water surface, rather than the submerged bed, had been detected. These points were removed from the surface, and a new elevation was calculated based on the elevation of surrounding, correctly-positioned, points. The second, for the Waimakariri River, was developed to identify and remove discrete zones of error. This was based upon a filtering method, involving comparison with a coarser-resolution DEM. Points that exceeded a maximum tolerated elevation difference were removed, and the correct elevation derived from interpolation of surrounding points.

All three of these developments were assessed in terms of the quality of the surfaces acquired. This was achieved through independently-acquired ground survey points, measured using a combination of Total Station and real-time kinematic GPS. Using this information, systematic, random and gross errors were identified in the DEMs, which helped guide development of post-processing routines. This suggested that application of automated post-processing procedures, both in terms of estimation of submerged topography and identification and removal of errors, permit reductions in DEM surface error. The subsequent improvement in overall surface quality is particularly important in terms of geomorphologically-significant parameters (e.g. water depth distribution, mean bed level).

Finally, the acquired data were used to assess the feasibility of using remote-sensing methods to increase the spatial and temporal resolution of surveyed data for estimating process rates from measured morphological change. In river environments, this has led to attempts to estimate bed load transport rates from a time-series of DEMs. However, it is important to consider whether real morphological changes (which are likely to be small in large gravel-bed river environments relative to spatial extent) can be distinguished from noise, given the errors associated with individual DEM surfaces. In this research, several methods were used to try to assess the feasibility of estimating volume changes and inferring bed load transport rates. These suggested that random errors in individual DEM surfaces impose a minimum level of detection of morphological change in DEMs of difference. However, it was found that given adequate photogrammetric or ALS project design, this threshold level is so small as to represent only a relatively insignificant (10-20%) information loss in terms of the total morphological change information obtained.

ACKNOWLEDGEMENTS

"The following summer there was a party that went down the [Colorado] river consisting of five of us, mapping the additional dam sites. I went along with a phototheodolite loaned to me by the U.S. Geological Survey to make topographical maps of these dam sites by this wonderful phototheodolite process... As we went upstream in very shallow water, trying to line our boats up, they overturned... At that moment, however, I was not so much concerned about the alidade as I was about my phototheodolite, which was bobbing down the stream from wave to wave... One of the boys jumped in a canoe that we had there and dashed downstream and picked the phototheodolite off a sand bar about a mile or so below...that survey was not a very successful one!"

Leon T. Eliel (p.17, 1947) in *Photogrammetric Engineering*.

Although the technology may have changed since Leon Eliel's account of an early photogrammetric survey of the Colorado river, remote measurement of large riverbeds remains a difficult task, and one which often relies on the co-operation between many people and organisations. I would, therefore, like to extend my thanks to those who have made this research possible: the Natural Environment Research Council (studentship GT04/98/54/FS) and the New Zealand Foundation for Research, Science and Technology (contract CO1818) for financial support; Air Logistics (NZ) Ltd, New Zealand and Aerial Precision Surveys, New Zealand for aerial photography; Infoterra Ltd (formerly the National Remote Sensing Centre) and the Zentrum für Datenverarbeitung (Centre for Data Processing), Universität Mainz, Germany (and Norman Kerle) for scanning; AAM Geodan, Australia for the airborne laser scanning survey, and David Turton for subsequent email correspondence; and the National Institute of Water and Atmospheric Research (NIWA) Ltd and Environment Canterbury (EC) for providing field teams and surveying equipment.

On a more personal level, I would also like to thank my supervisors, Stuart Lane and Murray Hicks, for their help, support and enthusiasm over the past three years. I am particularly grateful for their first meeting, at the 4th Gravel-Bed Rivers Workshop in Goldbar, Washington, in 1995. This initiated the collaboration between the University of Cambridge (and later the University of Leeds) and NIWA, and which allowed one very fortunate Ph.D. student the chance to spend 7 months in New Zealand.

In the UK, first in Cambridge and later in Leeds, Stuart provided a near continuous flux of ideas, many of which have found their way into this thesis in one form or another. He also possessed a seemingly boundless supply of energy and enthusiasm, which almost certainly rubbed off on me too. I am also indebted to all those who provided ideas and

help in both Cambridge and Leeds, including Keith, James, Gabriel, Patrice, Steve, Chris, Anthony, Justin, Sam, Rachel, Doug, Katarina, Norman, Elaine, Tim and anyone else I've forgotten. Special thanks must go to Cathryn for providing some sanity amidst all the madness.

In New Zealand, thanks to Murray for successfully managing to juggle his heavy workload in order to find time for me and my work, particularly during my time at NIWA. He also, along with Sandra, Katie and Charlotte (and, of course, Luna), took me under their wing while I was in Christchurch, and laid on some memorable moments. Attempting (badly) to ski, wading round Lake Taupo and the Stewart Island expedition spring immediately to mind! I would also like to thank all the staff at NIWA Christchurch for welcoming and accommodating me, and introducing me to Fotsal, Touch and the Corporate Challenge. In particular, thanks must go to John Fenwick, Graeme Davenport and the Christchurch field team, with whom I shared office space for 6 months, and Maurice Duncan, Jeremy Walsh, Graeme Smart and Ian Hawes for their input into my work.

Finally, a big thank you to my family and friends for their support, encouragement and interest over the last three years. It is, and was, very much appreciated.

TABLE OF CONTENTS

Title page	i
Declaration	ii
Thesis summary	iii
Acknowledgements	v
Table of contents.....	vii
List of figures	xiii
List of tables	xxiii
Chapter 1 . Introduction.....	1
1.1 Research aims and objectives.....	1
1.2 Research context.....	1
1.2.1 Overview	1
1.2.2 <i>Importance of form in contemporary fluvial geomorphology</i>	3
1.2.3 <i>Conventional survey of river environments</i>	7
1.2.4 <i>Remote sensing survey of river environments</i>	12
1.2.5 <i>Summary of research context</i>	14
1.3 Detailed research objectives	14
1.3.1 <i>Objective (i): to establish the project design necessary to yield topographic information from large, gravel riverbeds with a quality that allows channel morphology and morphological change to be determined and measured.</i>	14
1.3.2 <i>Objective (ii): to develop and to apply procedures for dealing with the presence of water on the riverbed.....</i>	16
1.3.3 <i>Objective (iii): to evaluate the quality of surface representation of digital terrain models of braided, gravel riverbeds produced using digital photogrammetry and airborne laser scanning</i>	17
1.3.4 <i>Objective (iv): to develop and to apply automated post-processing procedures to identify and eliminate errors from topographic surfaces obtained using remote sensing methods, and to assess their effectiveness at improving final DEM quality.....</i>	18
1.3.5 <i>Objective (v): to evaluate the reliability of estimates of volumes of erosion and deposition inferred from remotely-sensed digital elevation models of large, gravel-bed rivers, and hence to assess the feasibility of using morphological methods to estimate sediment transport rate</i>	19
1.4 Thesis structure	20

Chapter 2 . Acquisition and quality of remotely-sensed data in river environments	23
2.1 Data acquisition	23
2.1.1 <i>Aerial imagery</i>	23
2.1.2 <i>Photogrammetry</i>	26
2.1.3 <i>Airborne laser scanning</i>	30
2.2 Submerged topography	30
2.2.1 <i>Image analysis</i>	32
2.2.2 <i>Through-water photogrammetry</i>	35
2.3 Data quality.....	36
2.3.1 <i>Types of error</i>	38
2.3.2 <i>Sources of error</i>	39
2.3.3 <i>Error and data acquisition method</i>	39
2.3.4 <i>Error and data distribution and density</i>	42
2.3.5 <i>Error and interpolation method</i>	42
2.3.6 <i>Error and terrain characteristics</i>	43
2.3.7 <i>Assessment of error</i>	44
2.3.8 <i>Assessment of static-DEM error</i>	44
2.3.9 <i>Assessment of dynamic-DEM error</i>	49
2.4 Chapter summary	51
Chapter 3 . Project design and methodology	53
3.1 Introduction.....	53
3.2 Study sites	53
3.2.1 <i>The North Ashburton River</i>	54
3.2.2 <i>The Waimakariri River</i>	55
3.3 Digital photogrammetry	58
3.3.1 <i>Principles</i>	58
3.3.2 <i>Image acquisition</i>	61
3.3.3 <i>Digital image creation</i>	67
3.3.4 <i>Photogrammetric control</i>	69
3.3.5 <i>Block triangulation</i>	72
3.3.6 <i>DEM and ortho-image generation</i>	77
3.4 Airborne laser scanning.....	79
3.4.1 <i>Principles</i>	79
3.4.2 <i>Project design</i>	81
3.4.3 <i>Data acquisition</i>	83

3.4.4 <i>Data post-processing</i>	85
3.5 Independent check data	86
3.6 Chapter summary	89
Chapter 4 . The clear water case: through-water digital photogrammetry	91
4.1 Introduction	91
4.2 The geometry of through-water photogrammetry	92
4.3 Methodology	94
4.3.1 <i>Correction for refraction</i>	94
4.3.2 <i>Post-processing</i>	96
4.3.3 <i>DEM collection parameter values</i>	98
4.4 Application to North Ashburton River: Sub-areas	100
4.4.1 <i>Uncorrected DEM surfaces</i>	100
4.4.2 <i>Depth correction for refraction</i>	103
4.4.3 <i>Automated post-processing</i>	105
4.4.4 <i>DEM quality assessment</i>	106
4.5 Variation of DEM collection parameters	111
4.6 Application to North Ashburton River: Whole study reach	116
4.6.1 <i>Stereo-matching performance</i>	117
4.6.2 <i>Quality assessment</i>	121
4.7 DEM quality assessment using derived parameters	126
4.7.1 <i>Mean bed level</i>	128
4.7.2 <i>Water depth distribution</i>	130
4.8 A simplified refraction-correction method	132
4.9 Chapter summary	134
Chapter 5 . The turbid water case: estimating water depth from water colour ...	136
5.1 Introduction	136
5.2 Theoretical background	137
5.3 Acquisition and preparation of imagery	138
5.4 Development of an empirical relationship between pixel colour and water depth	141
5.5 Quality assessment of depth estimates	145
5.6 Chapter summary	149
Chapter 6 . The turbid water case: dry-bed survey using remote sensing methods	151
6.1 Introduction	151

6.2 Dry-bed survey using digital photogrammetry	152
6.2.1 <i>DEM collection strategy</i>	152
6.2.2 <i>DEM collection</i>	156
6.2.3 <i>Stereo-matching performance</i>	156
6.2.4 <i>Raw DEM quality assessment</i>	161
6.2.5 <i>Post-processing</i>	164
6.2.6 <i>Basic post-processing</i>	165
6.2.7 <i>Individual DEM post-processing: Use of local standard deviation</i>	167
6.2.8 <i>Individual DEM post-processing: Use of coarse resolution DEM</i>	169
6.2.9 <i>Individual DEM post-processing: Comparison of methods</i>	172
6.2.10 <i>Joining of individual DEMs</i>	173
6.2.11 <i>Integration of post-processed dry-bed DEM with water depth estimates</i>	178
6.2.12 <i>Reach-scale post-processing: Systematic error removal</i>	183
6.3 Dry-bed survey using airborne laser scanning	186
6.3.1 <i>DEM generation</i>	186
6.3.2 <i>Integration of dry-bed DEM with water depth estimates</i>	187
6.4 Final DEM quality assessment	187
6.4.1 <i>Qualitative DEM assessment</i>	188
6.4.2 <i>Comparison with independent check data</i>	188
6.4.3 <i>Overlap analysis</i>	194
6.5 Chapter summary	199
Chapter 7 . The feasibility of using the morphological method to infer bedload transport rates in large, braided, gravel-bed rivers.....	201
7.1 Introduction	201
7.1.1 <i>Rationale</i>	202
7.1.2 <i>Theoretical basis</i>	202
7.1.3 <i>DEMs of difference</i>	203
7.1.4 <i>Boundary conditions and sediment routing</i>	203
7.1.5 <i>Limitations of the morphological method</i>	204
7.2 DEMs of difference	206
7.3 Quality assessment of DEMs of difference from post-processed DEMs	207
7.3.1 <i>Reach-averaged elevation change statistics</i>	208
7.3.2 <i>Reach-averaged volume change statistics</i>	211
7.3.3 <i>Error detection</i>	213
7.3.4 <i>Gross error</i>	213

7.3.5 <i>Systematic error</i>	216
7.3.6 <i>Random error: Theory</i>	224
7.3.7 <i>Random error: Deterministic approach</i>	228
7.3.8 <i>Random error: Probabilistic approach</i>	230
7.3.9 <i>Random error: Comparison and discussion</i>	230
7.3.10 <i>Conclusions</i>	238
7.4 Effect of post-processing on DEM of difference quality.....	239
7.4.1 <i>Reach-averaged elevation change statistics</i>	239
7.4.2 <i>Gross error</i>	244
7.4.3 <i>Systematic error</i>	248
7.4.4 <i>Random error</i>	254
7.4.5 <i>Conclusions</i>	255
7.5 Comparison with conventional survey methods	257
7.5.1 <i>Rationale</i>	257
7.5.2 <i>Method</i>	258
7.5.3 <i>Effect of cross-section spacing</i>	260
7.5.4 <i>Effect of post-processing</i>	263
7.6 Chapter summary	263
Chapter 8 . Conclusions	266
8.1 Introduction.....	266
8.2 Research objectives re-visited.....	267
8.2.1 <i>Objective (i): to establish the research design necessary to yield topographic information from large, gravel riverbeds with a quality that allow channel morphology and morphological change to be determined</i>	267
8.2.2 <i>Objective (ii): to develop and to apply procedures for dealing with the presence of water on the riverbed</i>	271
8.2.3 <i>Objective (iii): to evaluate the quality of surface representation of digital terrain models of braided, gravel riverbeds produced using digital photogrammetry and airborne laser scanning</i>	273
8.2.4 <i>Objective (iv): to develop and to apply automated post-processing procedures to identify and eliminate errors from topographic surfaces obtained using remote sensing methods, and to assess their effectiveness at improving final DEM quality</i>	274
8.2.5 <i>Objective (v): to evaluate the reliability of estimates of volumes of erosion and deposition inferred from remotely-sensed digital</i>	

<i>elevation models of large, gravel-bed rivers, and hence to assess the feasibility of using morphological methods to estimate sediment transport rate</i>	275
8.3 Research aim revisited	277
8.4 Wider implications	278
8.5 Critical review and future research	280
Appendix A. OrthoMAX DEM collection parameters.....	283
References	286

LIST OF FIGURES

Chapter 3. Project design and methodology

Figure 3.1 The North Ashburton and Waimakariri Rivers, South Island, New Zealand (Copyright © Microsoft Encarta Virtual Globe 1998). The approximate locations of the study sites are circled in red.....	54
Figure 3.2 The North Branch of the Ashburton River. Flow is towards the camera	55
Figure 3.3 The North Ashburton study reach, looking upstream from Thompson's Track bridge.....	55
Figure 3.4 The Waimakariri River confined at the Lower Gorge. Flow is towards the camera (copyright © Peter Morath/Hedgehog House Press).....	57
Figure 3.5 The Waimakariri study reach from the air, looking downstream. The location of Crossbank is marked (photograph courtesy of Andrew Westaway, December 1999).....	57
Figure 3.6 The Waimakariri field site as seen from the ground. The disparity between spatial extent and vertical relief is clearly demonstrated	58
Figure 3.7 The perspective projection: the assumed relationship between object-space, image-space and camera lens (from Lane <i>et al.</i> , 1993)	59
Figure 3.8 The mean daily discharge record for the North Ashburton River for the period between the May 1995 and February 1999 photogrammetric surveys. (Flow data provided by NIWA and Environment Canterbury)	63
Figure 3.9 The mean daily discharge record for the Waimakariri River for the period between the February 1999 and March 1999 photogrammetric surveys (Flow data provided by NIWA and Environment Canterbury)	65
Figure 3.10 The mean daily discharge record for the Waimakariri River for the period between the February 1999 and February 2000 photogrammetric surveys (Flow data provided by NIWA and Environment Canterbury)	65
Figure 3.11 The relationship between theoretical precision, photograph scale and scanning resolution	66

Figure 3.12 Extracts from the digital images of the North Ashburton and Waimakariri riverbeds	69
Figure 3.13 The marker boards constructed for use as PCP targets (from Hicks <i>et al.</i> , 1999b)	70
Figure 3.14 The three components of the airborne laser scanning (ALS) system (from Fraser <i>et al.</i> , 1999)	81
Figure 3.15 The survey geometry of the Optech 1020 airborne laser scanner (from Fraser <i>et al.</i> , 1999)	83
Figure 3.16 The mean daily discharge record for the Waimakariri River for the period between the February 2000 photogrammetric and May 2000 ALS surveys. (Flow data provided by NIWA and Environment Canterbury)	83
Chapter 4. The clear water case: through-water digital photogrammetry	
Figure 4.1 Geometry of two-media photogrammetry (from Fryer and Kneist, 1985)	93
Figure 4.2 The three-dimensional geometry associated with an analytical solution for through-water photogrammetry (from Butler <i>et al.</i> , 2001b)	94
Figure 4.3 The automated refraction-correction procedure	99
Figure 4.4 The three sub-areas used for development and testing of the refraction-correction procedure: (a) shows the raw images of the three sub-areas; (b) shows the raster images of the raw photogrammetrically-acquired DEMs, scaled from black (lowest elevations) to white (highest elevations); and (c) shows the stereo-matching statistics files that are produced during DEM collection, which give the spatial distribution of matching performance. White points show good matches, with light and dark grey representing fair and poor matches respectively. Black points indicate an unsuccessful match and subsequent interpolation. Each tile is 30 m x 30 m in size and flow is from top to bottom	101
Figure 4.5 Spatial pattern of discrepancies between DEM and surveyed elevation for wet-bed points in the three sub-area DEMs. Circle diameter reflects magnitude of elevation error, following scaling to remove the effect of water depth	103

Figure 4.6	Modelling the water surface elevation: (a) shows the non-directional edge detection image; (b) shows the water edge elevation map; and (c) shows the final estimated water surface.....	104
Figure 4.7	The spatial pattern of corrected water depths (left) and depth corrections made to calculate them (right).....	105
Figure 4.8	The spatial distribution of points eliminated by the automated post-processing routine (left) and elevation changes introduced to the refraction-corrected DEM following re-interpolation (right) for each sub-area. Values of d of 0.00 and 0.06 m were used	107
Figure 4.9	The sub-area DEM surfaces: (a) following application of the refraction-correction; (b) post-processed with $d = 0.00$ m; and (c) post-processed with $d = 0.06$ m	108
Figure 4.10	The relationship between DEM and surveyed wet-bed point elevations for the three sub-areas for uncorrected and refraction-corrected DEMs	110
Figure 4.11	The relationship between apparent and measured water depth. The dashed line ($h:h_a$) shows where apparent depths should approximately plot.....	110
Figure 4.12	The effect of DEM collection parameter perturbation on stereo-matching matching precision and DEM quality for submerged points in each sub-area	112
Figure 4.13	The spatial pattern of elevation changes in the uncorrected sub-area DEMs produced by increasing the maximum parallax parameter to 9 pixels.....	114
Figure 4.14	Digital images used to create photogrammetric DEMs for the North Ashburton River. The spatial resolution of the images has been increased for display	117
Figure 4.15	Uncorrected DEMs of the North Ashburton study reach. The images are scaled from white (high elevations; 53.5 m.a.s.l.) to black (low elevations; 49 m.a.s.l.)	118
Figure 4.16	The spatial pattern of stereo-matching performance for the North Ashburton DEMs. Dark green points are ‘good’ matches, light green points are ‘fair’ matches and yellow points are ‘poor’ matches. Interpolated (non-matched) points are shown in red.....	119

Figure 4.17 The final North Ashburton DEMs. The DEMs are generated using default parameter uncorrected DEMs (dry-bed areas) and increased maximum parallax corrected DEMs (wet-bed areas), and have been detrended and trimmed.....	122
Figure 4.18 The relationship between surveyed water depth and errors from the corrected (maximum parallax = 9; $d = 0.06\text{m}$) May 1995 whole reach DEM	126
Figure 4.19 Error in mean bed level estimates for a range of cross-section spacings for the initial, final and surveyed North Ashburton DEMs. Error is defined with respect to the full resolution ($1\text{ m} \times 1\text{ m}$) DEM derived from survey measurements.....	129
Figure 4.20 Water depth distributions derived from the May 1995 North Ashburton DEM at various stages of correction, and from independent survey measurements	131
Figure 4.21 The differences in refraction-corrected water depth calculated using methods A and B of estimating refractive displacement through water	133
Chapter 5. The turbid water case: estimating water depth from water colour	
Figure 5.1 Rectified and mosaicked aerial imagery of the study reach from each photographic survey	140
Figure 5.2 Results of maximum likelihood, manually-edited classification of mosaicked imagery (Figure 5.1) of the study reach	142
Figure 5.3 The relationship between measured depth and RGB digital numbers (dN) for each survey.....	145
Figure 5.4 Estimated water depth maps for the study reach shown in Figure 5.1 : (a) February 1999; (b) March 1999; (c) February 2000; and (d) May 2000	146
Figure 5.5 The relationship between measured and predicted depth for each survey.....	148
Figure 5.6 Cumulative frequency distributions of surveyed (grey) and estimated (black) water depths	149

Chapter 6. The turbid water case: dry-bed survey using remote sensing methods		
Figure 6.1	The effect of DEM collection parameter perturbation on stereo-matching matching precision and DEM quality for dry-bed points	153
Figure 6.2	The effect of point spacing on DEM visual appearance, the number of stereo-matching points and DEM quality for both test areas	154
Figure 6.3	The approximate areas covered by photographs acquired during each survey. The study reach limits are outlined in blue	157
Figure 6.4	Example of a raw individual DEM (a) before and (d) after trimming based on an area of interest (c) derived manually using the raw DEM and ortho-image (b). The dashed lines in (c) represent neighbouring areas of interest.....	158
Figure 6.5	The (a) classified ortho-image and (b) spatial distribution of dry-bed stereo-matching performance for the individual DEM shown in Figure 6.4 . Dark green points are ‘good’ matches, light green points are ‘fair’ matches and yellow points are ‘poor’ matches. Interpolated (non-matched) points are shown in red.....	159
Figure 6.6	The matching performance for individual Waimakariri riverbed DEM	160
Figure 6.7	Raw DEMs of the whole study reach. For each survey, the top image shows the detrended DEM surface, and the lower image shows the same DEM but with wet-bed areas masked out	162
Figure 6.8	An illustration of the removal of unmatched, wet and vegetated points from the Waimakariri DEM surfaces. The raw DEM has several regions with gross errors present (a), which are near wetted channels, but not eliminated when wet-bed and vegetated areas are masked out (b). The use of the DEM stereo-matching statistics file (c) allows creation of a sparse DEM, comprised of only matched, dry-bed points (d). However, following re-interpolation gross errors remain (e), which are propagated into a modelled water surface elevation (f)	166

Figure 6.9 Maps of local standard deviation used to identify gross errors in the Waimakariri test areas DEM. Standard deviation is scaled from 0 (white) to 3 and above (black). Visual comparison with Figure 6.8a shows a good level of correspondence between standard deviation and error.....	168
Figure 6.10 Effect of different standard deviation radius and tolerance level combinations on DEM quality using automated post-processing method 1	169
Figure 6.11 Identification of gross errors using coarser-resolution DEMs: (a) shows the three spatial resolutions tested; (b) shows the differences in elevation at dry-bed matched points relative to the test areas 1 m DEM surface	171
Figure 6.12 Effect of different DEM resolution and tolerance level combinations on DEM quality using automated post-processing method 2.....	172
Figure 6.13 The best case test area DEMs produced using both post-processing methods: (a) the dry-bed using method 1; (b) the dry-bed using method 2; (c) the modelled water surface from the method 1 dry-bed; and (d) the modelled water surface from the method 2 dry-bed. All DEM surfaces are scaled from 38.5 m (black) to 42.5 m (white)	173
Figure 6.14 Mosaicked post-processed sparse DEMs for each photogrammetric survey.....	175
Figure 6.15 Re-interpolated whole-reach sparse DEM for March 1999. The DEM has been detrended, from -1.5 m (black) to +1.5 m (white), and wet-bed and vegetated points are masked out. The banding effect caused by systematic differences between individual DEMs is visible	176
Figure 6.16 Spatial pattern of individual DEM overlap differences for each photogrammetric survey.....	177

Figure 6.17 Schematic representation of the two contrasting mosaicking strategies used for joining individual overlapping DEMs (a) . Mosaicking of sparse DEMs tends to reinforce elevation discrepancies (b) , while distance-weighted averaging of continuous surfaces minimises elevation discontinuities (c) . The green line shows the final, mosaicked, DEM surface. Vertical scale has been exaggerated	178
Figure 6.18 The re-interpolated whole reach post-processed DEM surfaces. Wet-bed and vegetated areas have been masked out, and the DEM surfaces have been detrended to be scaled from –1.5 m (black) to +1.5 m (white). There is little visual evidence of the banding effect that previously affected the whole reach DEMs (Figure 6.15).....	179
Figure 6.19 Water surface elevation maps for each whole reach DEM, modelled from the post-processed dry-bed DEMs (Figure 6.18). Each is detrended and scaled from –1.5 m (black) to +1.5 m (white). Dry-bed and vegetated areas have been masked out.....	181
Figure 6.20 Final whole reach DEMs for the Waimakariri study reach, following post-processing, mosaicking and incorporation of estimated water depth maps. Each DEM has been detrended relative to the same linear trend surface	182
Figure 6.21 Maps of height discrepancies between the post-processed DEM surfaces and PCP elevations. Areas shaded red indicate that the final DEM surface is too low. Areas in green represent areas where final DEM elevations are too high. Zones of no shading are within ±2.5 cm of surveyed PCP position. The location of individual PCPs is marked.....	184
Figure 6.22 The post-processing stages used to create reach-scale photogrammetric DEMs of the Waimakariri study-reach.....	185
Figure 6.23 Water surface elevation map for the May 2000 ALS DEM. It has been detrended and is scaled from –1.5 m (black) to +1.5 m (white). Dry-bed and vegetated areas have been masked out	187
Figure 6.24 Final whole reach DEM for the Waimakariri study reach calculated using ALS. Elevations have been detrended with the same linear trend surface used in Figure 6.20	188

Figure 6.25 The effect of the post-processing procedure on dry-bed and wet-bed DEM quality for the whole reach DEMs of the Waimakariri River. The bars represent ME (DEM accuracy) with the vertical error bars indicating \pm SDE (DEM precision). Approximately two-thirds of errors fall within the bounds of each error bar.....	190
Figure 6.26 The spatial distribution of dry-bed (red) and wet-bed (blue) independent check point measurements. They have been superimposed on the classified images of the riverbed shown in Figure 5.2	193
Figure 6.27 The relationship between upstream and downstream elevations for individual DEM overlaps shown in Figure 6.16 . The mean elevations in the overlap area are shown, with error bars representing the standard deviation of individual DEM elevations. The overlaps are colour-coded to reflect the DEM outlines in Figure 6.3	196
Figure 6.28 Overlap analysis for the three flight passes used in the ALS survey	198
Chapter 7. The feasibility of using the morphological method to infer bedload transport rates in large, braided, gravel-bed rivers	
Figure 7.1 Post-processed DEMs of difference for the North Ashburton and Waimakariri study reaches.....	209
Figure 7.2 Distribution of elevation differences that comprise the post-processed DEMs of difference	211
Figure 7.3 Classified maps of the assumed wet-dry history of riverbed pixels, created by comparing binary classified images of wet-bed and dry-bed areas from the start and end of each epoch spanned by the post-processed DEMs of difference	218
Figure 7.4 Comparison of cut (red) and fill (green) volumes for the whole study reaches, with respect to the three geomorphological assumptions. NA is North Ashburton May 95 – Feb 99; W1 is Waimakariri Feb 99 – Mar 99; W2 is Waimakariri Feb 99 – Feb 00; and W3 is Waimakariri Feb 00 – May 00	220
Figure 7.5 The positions of the four sub-areas in bar-top (BT) and braid-belt (BB) locations.....	221

Figure 7.6	Comparison of cut (red) and fill (green) volumes for the Waimakariri sub-areas, with respect to the three geomorphological assumptions. W1 is Waimakariri Feb 99 – Mar 99; W2 is Waimakariri Feb 99 – Feb 00; and W3 is Waimakariri Feb 00 – May 00	223
Figure 7.7	Distributions of morphological change in terms of cut (red) and fill (green) volumes for the post-processed DEMs of difference (Figure 7.1).....	225
Figure 7.8	Mean estimated information loss in terms of cut (red) and fill (green) volumes due to random error for each predicted LOD _{min} value using both deterministic (D) and probabilistic (P) approaches	232
Figure 7.9	Recalculation of the W2 (Waimakariri; Feb 99 – Feb 00) post-processed DEM of difference (Figure 7.1c) to illustrate the effect of random error elimination using both deterministic and probabilistic methods. Two levels of detection are illustrated both each approach ...	234
Figure 7.10	Cumulative information loss totals (relative to total volumes of cut and fill) derived from the post-processed DEMs of difference. NA is North Ashburton May 95 – Feb 99; W1 is Waimakariri Feb 99 – Mar 99; W2 is Waimakariri Feb 99 – Feb 00; and W3 is Waimakariri Feb 00 – May 00	236
Figure 7.11	The North Ashburton (May 95 – Feb 99) DEMs of difference produced from DEMs at various stages of post-processing.....	241
Figure 7.12	The W1 (Feb 99 – Mar 99) DEMs of difference produced from DEMs at various stages of post-processing.....	242
Figure 7.13	The W2 (Feb 99 – Feb 00) DEMs of difference produced from DEMs at various stages of post-processing	243
Figure 7.14	The W3-1 (Feb 00 – May 00) DEM of difference produced from unprocessed DEMs.....	244
Figure 7.15	The effect of post-processing on the resultant DEMs of difference. Cut volumes are in red and fill volumes in green. Both are reach-averaged	247

Figure 7.16 The volume of change associated with statistically-identified gross errors in the DEMs of difference at various stages of post-processing. Values are expressed relative to the total volumes of cut, fill and net change calculated from the corresponding DEM of difference surfaces (Table 7.21). Cut volumes are in red and fill volumes in green.....	251
Figure 7.17 Comparison of cut (red) and fill (green) volumes for the reach-scale DEMs of difference at various stages of post-processing with respect to the three geomorphological assumptions.....	253
Figure 7.18 Loss of cut (red) and fill (green) volumes for DEMs of difference at various stages of post-processing for different LOD _{min} values	257
Figure 7.19 The results of mean bed level change analysis using various cross-sections spacings for each post-processed DEM of difference. Mean bed level change is plotted in black. The standard deviation of mean bed level change calculations for a given cross-section spacing are plotted in grey. Both are relative to the value calculated using the minimum (1 m) cross-section spacing	261
Figure 7.20 The results of mean bed level change analysis using various cross-sections spacings for each unprocessed (black) and post-processed (red) DEM of difference. Mean bed level change is plotted in solid lines. The standard deviation of mean bed level change calculations for a given cross-section spacing are plotted in dashed lines.....	264

LIST OF TABLES

Chapter 1. Introduction

Table 1.1	A summary of gravel-bed river monitoring programmes undertaken using terrestrial survey techniques (modified from Lane, 1998)	9
------------------	---	---

Chapter 2. Acquisition and quality of remotely-sensed data in river environments

Table 2.1	Examples of studies that have used aerial imagery to study river environments.....	24
------------------	--	----

Table 2.2	A summary of studies that have used photogrammetry to study river environments.....	28
------------------	---	----

Table 2.3	A summary of studies that have used airborne laser study to study river environments.....	31
------------------	---	----

Table 2.4	A summary of studies that have used image analysis techniques to determine water depth from remotely-sensed water colour	34
------------------	--	----

Table 2.5	Types and sources of error in conventional, terrestrial survey, digital photogrammetry and airborne laser scanning (Cooper and Cross, 1988; Butler <i>et al.</i> , 1998; Huisng and Gomes Pereira, 1998; Baltsavias, 1999a; Favey <i>et al.</i> , 1999; Lane <i>et al.</i> , 2000)	40
------------------	--	----

Table 2.6	Examples of internal methods of error assessment used to assess the quality of terrain surfaces	48
------------------	---	----

Table 2.7	Propagation of error in simple functions (modified from Squires, 1968).....	51
------------------	---	----

Chapter 3. Project design and methodology

Table 3.1	Details of the aerial photography of the North Ashburton River	63
------------------	--	----

Table 3.2	Details of the aerial photography of the Waimakariri River	64
------------------	--	----

Table 3.3	Specifications relating to the creation of digital images	68
------------------	---	----

Table 3.4	Calculation of the theoretical vertical photogrammetric precision permitted by the digital imagery used in this study	68
------------------	---	----

Table 3.5	Estimation of image texture from the standard deviation of dNs.....	70
------------------	---	----

Table 3.6	Summary of the lens distortion parameters and fiducial data required by the OrthoMAX block tool, and the corresponding values for the cameras and lens used in this study	73
------------------	---	----

Table 3.7	Fiducial RMSE calculated by the OrthoMAX block tool	74
Table 3.8	Initial results from block triangulation for both study reaches using only PCP information	76
Table 3.9	Results from block triangulation for both study reaches using both PCP and tie-point information. Change from previous blocks (calculated using only PCPs) given in brackets	78
Table 3.10	Comparison of features of digital photogrammetry and airborne laser scanning (Baltsavias, 1999a; Hansen and Jonas, 2000)	82
Table 3.11	Independent check data collected for the two study reaches	87
Chapter 4. The clear water case: through-water digital photogrammetry		
Table 4.1	The matching precision of the initial sub-area DEMs for dry-bed and wet-bed points.....	101
Table 4.2	Quality assessment of the three raw sub-area DEMs for wet-bed and dry-bed DEM points	102
Table 4.3	Number of points removed by the automated post-processing routine for both threshold levels tested	106
Table 4.4	The effect of applying the refraction-correction and post-processing procedures on the quality of wet-bed points in the sub-area DEMs. Underlined values are significantly improved at the 95% confidence level.....	109
Table 4.5	The collection parameters considered and parameter values used.....	111
Table 4.6	The effect of correction parameter variation on the quality of uncorrected wet-bed points in the sub-area DEMs. Underlined values are significantly improved at the 95% confidence level	113
Table 4.7	The effect of increasing the maximum parallax collection parameter on dry-bed point DEM stereo-matching precision and quality.....	115
Table 4.8	The effect of applying the refraction-correction and post-processing procedure on the quality of wet-bed points in the sub-area DEM generated using the increased maximum parallax collection parameter set. The values are underlined if errors are significantly reduced from previous stage of processing at the 95% confidence level.....	115

Table 4.9	Comparison of wet-point quality, at different stages of correction, between DEM generated using default and increased maximum parallax collection parameter sets. The values are underlined if reductions in error are significant at the 95% confidence level	116
Table 4.10	Stereo-matching performance for whole reach DEMs of the North Ashburton study reach	120
Table 4.11	The effect of the refraction-correction and post-processing procedure on default and optimised parameter whole reach DEMs of the North Ashburton River. Underlined values represent significant decreases in error from the previous stage of correction at the 95% confidence level	123
Table 4.12	The change in DEM quality using an increased maximum parallax parameter, as compared with the default value, for the whole reach DEMs of the North Ashburton River. Underlined values represent significant improvements in DEM quality at the 95% confidence level.....	124
Table 4.13	A comparison of sediment storage volumes obtained from uncorrected and corrected photogrammetry, and from evenly-spaced cross-sections, as with a conventional monitoring programme. Error in volume is unsigned and determined with respect to the storage volume calculated from the entire ground survey data-set.....	130
Table 4.14	DEM quality assessment of corrected DEMs using both refraction-correction methods.....	134
Chapter 5.	The turbid water case: estimating water depth from water colour	
Table 5.1	Details of the aerial photographs used in this study.....	138
Table 5.2	Classification accuracy statistics for each of the photographic surveys. Kappa statistics that are underlined are significant at the 95% confidence level	141
Table 5.3	Details of river conditions and depth measurements at the time of photography	143

Table 5.4	Results of the multivariate analyses between pixel colour and measured water depth for each epoch. Underlined values of R^2 are statistically significant ($p < 0.05$)	144
Table 5.5	Quality assessment of the water depth estimates.....	147
Table 5.6	Depth prediction quality and maximum predicted depth (MPD) reported in similar studies	147
Chapter 6. The turbid water case: dry-bed survey using remote sensing methods		
Table 6.1	Summary of DEM point spacings and collection details	153
Table 6.2	Summary of stereo-matching performance for each photographic survey.....	159
Table 6.3	Quantitative DEM quality assessment of the raw reach-scale DEMs	161
Table 6.4	Summary of best case DEM quality obtained using both post-processing methods	169
Table 6.5	The effect of the post-processing procedure on dry-bed and wet-bed DEM quality for the whole reach photogrammetric DEMs of the Waimakariri River. Underlined values represent significant decreases in error from the previous stage of correction at 95% confidence level	189
Table 6.6	Final DEM quality for all four reach-scale DEM surfaces of the Waimakariri River.....	191
Table 6.7	Estimation of reach-averaged DEM quality based on the relative proportion of dry-bed and wet-bed area.....	192
Table 6.8	Comparison between number of DEM points in dry- and wet-bed areas and the number of surveyed check points used to assess DEM quality.....	194
Table 6.9	Aggregated overlap analysis statistics for the photogrammetrically-derived DEMs.....	195
Table 6.10	Overlap analysis statistics for the ALS-derived DEM	197
Chapter 7. The feasibility of using the morphological method to infer bedload transport rates in large, braided, gravel-bed rivers		

Table 7.1	Details of the four epochs for which DEMs of difference were calculated for the North Ashburton and Waimakariri study reaches	208
Table 7.2	Reach-averaged elevation change statistics derived from the post-processed DEMs of difference	210
Table 7.3	Reach-averaged volume change statistics derived from the post-processed DEMs of difference	212
Table 7.4	Detection of gross errors in the post-processed DEMs of difference based on maximum expected local elevation difference.....	214
Table 7.5	Revised reach-averaged volume change statistics derived from the post-processed DEMs of difference with gross errors removed. The figures in brackets represent the change from the raw reach-averaged volume changes (Table 7.3)	215
Table 7.6	Volume change statistics derived from the post-processed DEMs of difference divided by wet-dry history zone. Data have been coloured-coded to reflect the geomorphological assumption (identified above) to which they most closely relate: assumption 1 in blue; assumption 2 in red; and assumption 3 in green.....	219
Table 7.7	Volume change statistics for the four sub-areas divided by wet-dry history zone. Data have been coloured-coded to reflect the geomorphological assumption (identified above) to which they most closely relate: assumption 1 in blue; assumption 2 in red; and assumption 3 in green. W1 is Waimakariri Feb 99 – Mar 99; W2 is Waimakariri Feb 99 – Feb 00; and W3 is Waimakariri Feb 00 – May 00	222
Table 7.8	Parameterisation of the precision associated with the post-processed DEMs	226
Table 7.9	Parameterisation of the precision estimated for the post-processed DEMs of difference (from Equation 2.12).....	227
Table 7.10	Examples of <i>t</i> values, probabilities and weights calculated from given elevation changes and LOD _{min} values	228
Table 7.11	Estimated LODmin for the four types of morphological change defined in Figure 7.3	229

Table 7.12	Calculation of morphological change less than LOD _{min} for each type of morphological change and summation of total information loss for the entire study reaches. NA is North Ashburton May 95 – Feb 99; W1 is Waimakariri Feb 99 – Mar 99; W2 is Waimakariri Feb 99 – Feb 00; and W3 is Waimakariri Feb 00 – May 00	229
Table 7.13	Calculation of information loss relative to total cut and fill volumes (Table 7.3) for each predicted LOD _{min} value using a deterministic approach	231
Table 7.14	Calculation of morphological information loss due to probability-weighting for each type of morphological change and summation of total information loss for the entire study reaches. NA is North Ashburton May 95 – Feb 99; W1 is Waimakariri Feb 99 – Mar 99; W2 is Waimakariri Feb 99 – Feb 00; and W3 is Waimakariri Feb 00 – May 00	232
Table 7.15	Calculation of information loss relative to total cut and fill volumes (Table 7.3) for each predicted LOD _{min} value using a probabilistic approach	233
Table 7.16	Estimated DEM of difference precision and DEM precision required to fulfil given information loss tolerances	236
Table 7.17	Summary of all of the DEMs of difference assessed for errors. Those in bold are the final, post-processed DEMs that were analysed in Section 7.3	240
Table 7.18	Reach-averaged elevation change statistics for the post-processed DEMs of difference. Post-processed DEMs of difference are displayed in bold	245
Table 7.19	Reach-averaged volume change statistics derived from the DEMs of difference calculated from DEMs at various levels of post-processing (Table 7.17). Post-processed DEMs of difference are displayed in bold	246
Table 7.20	Detection of gross errors in the DEMs of difference based on maximum expected local elevation difference	249
Table 7.21	Decrease in volumes of cut and fill following the removal of gross error and the effect on net volume change for DEMs of difference at various stages of post-processing (Table 7.17)	250

Table 7.22	Volume change statistics derived from the DEMs of difference at various stages of post-processing divided by wet-dry history zone Data have been colour-coded to reflect the geomorphological assumption to which they most closely relate	252
Table 7.23	Values of LOD _{min} used to examine information loss due to random error in the DEMs of difference at various stages of post-processing....	255
Table 7.24	Calculation of information loss relative to total cut and fill volumes for the corresponding DEM of difference (Table 7.17) for each predicted LOD _{min} value, using a probabilistic approach	256
Table 7.25	A comparison of sediment storage volumes obtained from uncorrected and corrected photogrammetry, and from evenly-spaced cross-sections, as with a conventional monitoring programme. Error in volume is unsigned and determined with respect to the storage volume calculated from the entire ground survey data-set.....	262

CHAPTER 1. INTRODUCTION

1.1 Research aims and objectives

The overall aim of this research is:

to assess the ability of remote sensing, based upon digital photogrammetry and airborne laser scanning, to measure the morphology of large, braided, gravel-bed rivers with sufficient quality to allow changes in bed morphology in space and time to be detected.

To achieve this aim, five research objectives have been identified:

- (i) to establish the project design necessary to yield topographic information from large, gravel riverbeds with a quality that allows channel morphology and morphological change to be determined;
- (ii) to develop and to apply procedures for dealing with the presence of water on the riverbed;
- (iii) to evaluate the quality of surface representation of digital elevation models of braided, gravel riverbeds produced using digital photogrammetry and airborne laser scanning;
- (iv) to develop and to apply automated post-processing procedures to identify and eliminate errors from topographic surfaces obtained using remote sensing methods, and to assess their effectiveness at improving final DEM quality;
- (v) to evaluate the reliability of estimates of volumes of erosion and deposition inferred from remotely-sensed digital elevation models of large, gravel-bed rivers, and hence to assess the feasibility of using morphological methods to estimate sediment transport rate.

1.2 Research context

1.2.1 Overview

In large, braided rivers, the continual and mutual interrelationship between river channel processes and river channel form (Ashworth and Ferguson, 1986) is most visually manifest in the physical morphology of the riverbed. This makes observation, measurement and representation of riverbed morphology and morphological change an essential component of fluvial geomorphology. In recent years, there has been a rapid growth in the use of digital elevation models (DEMs) within geomorphology (Pike, 2000). DEMs are regularly-spaced gridded arrays of point elevations that represent

ground surface form. They were established as a tool for landform representation in the 1960s (e.g. Miller and Laflamme, 1958). However, it is only with rapid development of automated survey techniques, the increasing use of Geographic Information Systems (GIS) and the ongoing revolution in computing power that the full potential of DEMs is being realised in geomorphology.

Terrestrial survey techniques may be unable to provide morphological information at sufficient spatial density for reliable DEM derivation, especially at larger spatial scales of investigation, and alternative survey tools are increasingly sought. Remote survey methods are now at a stage of development where techniques such as high density global positioning system (GPS) survey, digital photogrammetry (from both airborne and satellite platforms), airborne laser scanning (ALS) and synthetic aperture radar (SAR) interferometry increasingly represent cost effective ways of surveying large landforms with a precision that permits comparatively small changes in morphology to be detected. This means that traditional benefits associated with aerial photography, including the large, synoptic, areal coverage, apply without the constraint of only being able to resolve morphological change in two dimensions. Accordingly, DEMs have been used in geomorphic applications as diverse as watershed run-off modelling (e.g. Quinn *et al.*, 1991; Montgomery *et al.*, 1998), floodplain inundation modelling (e.g. Bates *et al.*, 1998); slope stability analyses (e.g. Brunsden and Chandler, 1996), glacial mass balance studies and ablation modelling (e.g. Willis *et al.*, 1998; Turpin *et al.*, 1998) and coastal and estuarine management (e.g. Pethick, 1998; Hardisty *et al.*, 1998).

However, fluvial geomorphologists have arguably been relatively slow to adopt a DEM-based research strategy. As a result, measurement and numerical representation of riverbed topography frequently remains relatively basic (Pike, 1995), often centred around monumented channel cross-sections (Lane, 1998). However, many river scientists see the development and application of remote survey techniques in fluvial environments as an important step towards observation and understanding of river channel form and change (Ashmore and Church, 1998; Lane, 1998; Paola, 2001).

Braided, gravel-bed rivers are an important landform on which to test and develop these remote sensing methods for two reasons. First, it is at the spatial scale of large, gravel riverbeds that the inadequacies of conventional, terrestrial survey techniques are most keenly felt, and where developments using remote sensing methods may be most beneficial. Furthermore, the dynamism of braided rivers means that rapid or even instantaneous measurement is critical if information on riverbed morphology is to be obtained and used to create meaningful DEMs. Second, a relatively small proportion of

riverbed area is submerged at mean flows and, where inundation is present, water depths are generally small. Thus, taking the riverbed as a whole, the contribution of topographic errors associated with remote sensing survey of inundated areas (where data quality is likely to be decreased) is relatively small. If remote sensing methods are abandoned altogether in inundated regions, the ground survey needed to recover gaps in the DEM surface is relatively modest. The ability to survey such rivers during low flow conditions (which, because of the skewed nature of most flow duration curves toward low flows, occur most frequently) is important as it permits measurement of the morphological effect of large, less frequent, flood events.

In addition, large, gravel riverbeds also represent a significant test for the emerging remote survey methods themselves (Lane, 2000). First, the vertical relief of large, gravel riverbeds is typically small (less than 2 m) relative to the spatial extent (greater than 100 m). This makes the quality of survey measurements critical, as they must be sufficiently precise to detect morphological change. Areal coverage of remote sensing methods is usually inversely related to point density and hence surface quality (Lane, 2000), and is ideally maximised to reduce cost and data volume. Thus, a balance must be achieved such that spatial coverage is maximised for a given level of survey precision. Second, correct DEM representation of riverbed topography necessarily requires consideration of both exposed and submerged areas, and the presence of shallow water introduces additional procedures that must be developed and adopted in addition to the remote sensing of dry areas of riverbed.

1.2.2 Importance of form in contemporary fluvial geomorphology

Geomorphologists have always placed great importance in the role of observation (Rhoads and Thorne, 1996). Given that form is commonly easier to observe than process, this frequently means that morphology and morphological change assume key importance in geomorphological studies. Several emerging research themes in contemporary fluvial geomorphological research have ensured that river channel form remains an important consideration today (Lane, 2000).

First, there has been increased interest in the morphology of riverbeds as a basis for understanding the spatial organisation and possible scale dependency of river networks, and notably their degree of self-similarity as expressed by fractal measures (Pike, 2000). To date, studies of the fractal structure of river channels have been made for both individual river channels (e.g. Nikora, 1991; Sapozhnikov and Foufoula-Georgiou, 1996; Nykanen *et al.*, 1998; Hicks *et al.*, 1999a) and for drainage networks as a whole (e.g. Tarboton *et al.*, 1988; La Barbera and Rosso, 1989; Peckham, 1995;

Rinaldo *et al.*, 1998). The frequently observed spatial orderliness of river systems has been suggested by some researchers to indicate self-organised criticality, a dynamic state related to principles of energy dissipation (Phillips, 1995) and which has been observed in many disciplines of physical and earth sciences (Bak, 1997). It is typically characterised by fractal (power-law) scaling in space and time of relevant (in this case, channel forming) processes, and has been demonstrated statistically for both meandering (e.g. Stølum, 1996) and braided (e.g. Sapozhnikov and Foufoula-Georgiou, 1997; Sapozhnikov and Foufoula-Georgiou, 1999) river systems. The concept of self-organised criticality in river settings is important given the links that have been demonstrated between the fractal geometry of river systems and other hydrological characteristics (Pike, 2000), such as the distributions of discharge and energy dissipation (Rogriguez-Iturbe *et al.*, 1992), and the clear management implications these links provide. However, it is becoming clear that current understanding of the spatial organisation of river systems is lacking in two important areas. First, all work to date has studied only the two-dimensional spatial organisation of rivers, with the geometric properties of river planform typically determined from aerial photographs or satellite imagery. Apart from the well-rehearsed problems associated with the water level dependence of aerial imagery interpretation (e.g. Ferguson and Ashworth, 1992; Lawler, 1993), it is unlikely that the scaling properties of a three-dimensional system will be adequately derived from two-dimensional measurements. This is particularly important given the disparity between the length scales typically associated with the two-dimensions previously studied (i.e. cross-stream and downstream directions) and the length scale typically associated with vertical relief of a gravel-bed river. Second, despite the links established between the scaling of river form and river processes (e.g. Rogriguez-Iturbe *et al.*, 1992), relatively few studies have explicitly examined the geometric properties of river processes, and in particular the scale dependence of morphological change. So, whilst interest in river system scaling has heightened interest in riverbed form, it has also demonstrated that advances in both areas will only be made once three-dimensional information of river channel form (and hence river channel change) is available.

Second, there is growing recognition of the role of form as a control over flow processes. It is now widely accepted that a mutual interrelationship exists between distributed river channel morphology and river channel processes, at least in conceptual terms (Ashworth and Ferguson, 1986; Richards, 1988). Field and flume measurements appear to support this theory, in terms of both the effects of morphology on flow processes (e.g. Ashworth and Ferguson, 1986; Dietrich and Whiting, 1989;

Ashmore *et al.*, 1992) and on sediment entrainment and transport (e.g. Hassan and Reid, 1990; Clifford *et al.*, 1992; Ferguson *et al.*, 1992). Changes in river channel form caused by these processes will reflect both the magnitude-frequency regime and the sensitivity to change of the environment in question (Lane, 1998). In particularly dynamic fluvial environments, these changes may be almost continual, and will exhibit a spatially distributed character: spatially-distributed differences in bed elevation cause spatial variations in process and hence spatially variable changes in form. Mass continuity means that morphological changes at one location necessarily influence morphological changes at other spatially- and temporally-distant locations, and through changes in form, river channel processes. This demands greater consideration of both the spatial contingency of local boundary conditions (Lane and Richards, 1997) and of the importance of historical evolutionary trajectories (Lane *et al.*, 1996), whereby existing morphology exerts a conditioning influence upon future patterns of river channel change. Ultimately, these findings require much greater emphasis being placed on the role of topography in channel- and reach-scale process studies (Lane *et al.*, 1994).

Third, and given the link that has been established between flow processes and channel morphology, some researchers have suggested the use of morphological information as a means of understanding river channel processes (e.g. Ashmore and Church, 1998; Lane, 1998). Qualitative observations of river channel morphology and its change through time have been used for some time to classify styles of channel change, both in flume and field environments (e.g. Rundle, 1985; Ashmore, 1991; Ferguson, 1993). The use of regularly-spaced DEMs makes such observations easier and numerically rigorous (e.g. Lane *et al.*, 1996; Heritage *et al.*, 1998). Furthermore, the recognised failure of some process-based studies to determine and to predict river form reliably has led to calls for a reversal of the traditional methodology used to estimate sediment transport rates. Instead, average transport rates are inferred from measured changes in river channel morphology (e.g. Carson and Griffiths, 1989; Ferguson and Ashworth, 1992; Goff and Ashmore, 1994; Martin and Church, 1995; Lane *et al.*, 1995a; Ashmore and Church, 1998; Nicholas and Sambrook-Smith, 1998; McLean and Church, 1999; Ham and Church, 2000; Smith *et al.*, 2000). It follows that distributed information on river channel form is central to the adoption of such a morphological method in fluvial geomorphology (Lane, 1998), and accurate representation of three-dimensional topography has therefore become an important research goal.

Fourth, detailed channel morphology is required for numerical simulation of the interaction between river channel form and process, both to provide initial boundary conditions and for the purpose of validating model predictions. Numerical simulations of river channel environments have been developed at a range of scales. At the grain scale, specification of surface topography is essential for river channel hydraulic studies, and grain size characteristics have been central to estimation of flow and sediment transport (e.g. Parker *et al.*, 1982; Andrews, 1983). Due to the difficulties of obtaining accurate representation of gravel surfaces, numerical simulation of grain scale processes has typically been carried out using generic representations of riverbed morphology with uniform grain size (e.g. Wallbridge *et al.*, 1999; Jia *et al.*, 2001; McEwan *et al.*, 2001) which potentially limits its applicability in a field setting.

At the channel scale, rapid advances in our understanding of flow processes have been made in recent years through numerical modelling, with increases in computer power permitting increasingly complex two- and three-dimensional simulations of flow and transport processes using computational fluid dynamics (CFD) models (e.g. Lane and Richards, 1998; Nicholas and Sambrook-Smith, 1999; Bradbrook *et al.*, 2000). Given the continued expansion of computer resources and model sophistication, it is likely that channel topographic representation will become the major obstacle facing researchers in coming years. This is an issue of particular importance given the obvious and inevitable link between initial boundary conditions (in the form of topographic data) and model results (e.g. Carter and Shankar, 1997; Nicholas, 2001).

At the reach scale, river channels are increasingly being regarded as complex, multi-scale systems, within which the dynamic behaviour at any given level in the hierarchy of scales may be dominated by only a few crucial aspects of the dynamics at the next level below (Werner, 1999). Consequently, despite the potential ability of CFD to handle simulations of channel processes over larger spatial scales, it is increasingly argued that it is not worth modelling all of the lower level dynamics if only a relatively small proportion of these processes actually contribute to dynamics at the higher (and by implication larger) levels of interest (e.g. Paola, 2001). Instead, those few key aspects of lower level behaviour that are thought to matter should be focused upon and modelled. As a result, reach scale simulations of flow dynamics have become dominated by cellular models of braided channels (e.g. Murray and Paola, 1994, 1997; Webb, 1995), grounded upon relatively simple water routing and sediment flux relations. To date, such models have been tested largely using randomly-generated bed topographies (e.g. Murray and Paola, 1994). However, the potential of such a

modelling strategy to reliably simulate braided channels can perhaps only be tested by using actual reach-scale riverbed DEMs.

Finally, there is now an increased appreciation of the importance of environmental and ecological considerations in river management. River channel morphology is a fundamental control over the availability and nature of river channel habitats, and consideration of habitat distribution and change now forms a significant aspect of any river management strategy (e.g. Klingeman, 1998). This involves consideration of riverbed morphology at a range of spatial scales, such as the distribution of morphological units at the reach scale (e.g. Glova *et al.*, 1998) and importance of pebble clusters and void space at the grain scale (Carboneau *et al.*, in press).

A feature common to all of these issues is that riverbed morphology is of great significance. Consequently, any method that can increase the ease and speed with which morphological information can be obtained will be of real importance (Butler *et al.*, 2001a),

1.2.3 Conventional survey of river environments

Despite the importance of channel topography and the desire of many geomorphologists to adopt a DEM-based approach to fluvial studies, river channel form often remains poorly measured and described. Lane (1998) suggests that this is perhaps one of the legacies of the large-scale adoption of engineering principles across geomorphology in the mid twentieth century, and their influence in much research carried out since. Given this historical legacy, coupled with practical difficulties associated with collecting, collating and storing topographic data using conventional survey methods (Brasington *et al.*, 2000), monumented channel cross-sections remain prevalent in contemporary fluvial geomorphological research. For example, river monitoring research programmes frequently remain based on repeat survey of established cross-sections (e.g. Ferguson and Ashworth, 1992; Goff and Ashmore, 1994; Nicholas and Sambrook-Smith, 1998; McLean and Church, 1999), as does much river management, for example, the rivers of Canterbury, New Zealand (e.g. Blakely and Mosley, 1987; Connell, 2001).

This study focuses on the North Ashburton and the Waimakariri Rivers. These are two of the several large, braided, gravel-bed rivers that flow across the Canterbury Plains, South Island, New Zealand. These rivers are up to 200 km in length and may have active riverbeds of up to 1.5 km wide. The regional council, Environment Canterbury (EC), has the responsibility to manage and hence monitor these rivers. A cross-section approach is used, with the position of measured points determined using either

conventional levelling or with a Total Station and data logger. For example, on the Waimakariri River, successive profiles are typically positioned at least two active riverbed widths apart, with complete survey of all the cross-sections (which determines the minimum re-survey frequency) taking up to five years (Blakely and Mosley, 1987). In the Waimakariri study reach considered in this study, the EC cross-sections are spaced 800 m apart (Hicks *et al.*, 1999b). Similar survey specifications are used on many rivers of the Canterbury Plains, and repeat survey of cross-sections provides all the necessary morphological information upon which significant management decisions are made. These include selection of stopbank height based on at-a-section bed level (Williman and Lowe, 1988), evaluation of the effects of channel confinement (Connell, 2001) and estimation of appropriate gravel extraction volumes based on bed level change between surveys (Griffiths, 1991). However, it is not clear whether this monitoring strategy can effectively and reliably represent riverbed morphology and morphological change. Yet, with finite time and resources available, there is no feasible way of increasing either the temporal or the spatial density of measurements with conventional surveying methods.

The spatial-temporal resolution of measurements in any topographic survey involves a trade-off between: (i) the spatial extent of the field area, (ii) the spatial density of information required, and (iii) the frequency with which re-survey is undertaken through time. Given finite time and resources, improvement in any one of these factors requires a trade-off with one or both of the others. For instance, in order to increase the frequency of surveys, either the spatial density of sampled points or the area under consideration must be reduced. The effects of this trade-off are most apparent at larger spatial scales, such as those associated with the braided, gravel-bed rivers of the Canterbury Plains. **Table 1.1** provides a summary of recent attempts to monitor river channel topography in dynamic gravel-bed using terrestrial survey methods with reference to these three factors.

The use of such a survey strategy to monitor large, gravel-bed rivers has a number of potential weaknesses. First, topographic survey in river environments has been typically dominated by repeat levelling (Lane, 1998). Levelling generally requires manual logging in the field, which decreases the rate at which topographic information can be obtained. Furthermore, cross-sections must be levelled one at a time, requiring the instrument to be set up as many times as necessary (Bannister *et al.*, 1998). Since the 1980s, the development and adoption of electromagnetic distance measurement systems and Total Station theodolites have afforded terrestrial surveys a greater degree of automation and flexibility (Bannister *et al.*, 1998; Keim *et al.*, 1999). Data is

logged electronically, making the method faster than other terrestrial survey techniques and meaning that the topographic data can be transferred directly into a computer for subsequent and immediate analysis. Researchers who have conducted Total Station surveys have reported data collection speed of 240 points per hour (e.g. Lane *et al.*, 1994; Keim *et al.*, 1999), which may be increased further by using a device which automatically tracks the prism (Hicks *et al.*, 1999b; Chandler and Ashmore, 2001).

Researcher(s)	River	Method (survey used)	Reach length (m)	Downstream survey spacing ^a (m)	Frequency of re-survey (days)
Cheetham (1979)	Spjelffjelldal, Norway	X-S (L)	150	40	15
Fenn and Gurnell (1987)	Tsidjiore Nuove and Bas Arolla, Switzerland	X-S (L)	200	50	8 ^b
Ashworth and Ferguson (1986)	Lyngsdalsevia, Norway	X-S (L)	50	5	1
Lane (1990)	Haut Arolla, Switzerland	X-S (L)	50	5	2
Ferguson <i>et al.</i> (1992)	Sunwapta, Canada	X-S (L)	35	5	3
Ferguson and Ashworth (1992)	White, USA	X-S (L)	25	5	3
Goff and Ashmore (1994)	Sunwapta, Canada	X-S (L)	60	10	1
Lane <i>et al.</i> (1994)	Haut Arolla, Switzerland	P (TS) ^c	50	0.5	<1
Nicholas and Sambrook-Smith (1998)	Virkisa, Iceland	X-S (L)	250	10	3

X-S – Cross-sections; P – Planimetric; L – Levelling; TS – Total Station

^a Downstream spacing refers to cross-section interval for cross-section based surveys and average downstream point spacing for planimetric surveys.

^b One cross-section on Tsidjiore Nuove was also re-surveyed daily for 50 days and hourly for 3 days.

^c Submerged bed only (exposed areas surveyed using analytical photogrammetry)

Table 1.1 A summary of gravel-bed river monitoring programmes undertaken using terrestrial survey techniques (modified from Lane, 1998).

A feature common to most terrestrial survey methods is that they are best suited to relatively small spatial study areas. However, at spatial scales such as those

associated with large, gravel-bed rivers, their reliability is reduced. In the case of levelling, positioning of heights has traditionally been made with stadia tacheometry (Lane, 1998). However, the quality of height determination using this method is based on the distance to the elevation being sighted. Given a typical relation of $100\Delta x$, where x is the difference between the upper and lower stadia hairs, this means a quality of elevation determination of ± 0.01 m could produce a distance estimate as poor as ± 1 m (Lane, 1998). Planimetric errors such as these will be particularly significant in the presence of sudden breaks of slope, such as channel banks on gravel riverbeds. Total Station theodolites are recommended for surveys where 95% of measurements are under 500 m (Bannister *et al.*, 1998). Over greater distances, errors may result from both frequency drift and atmospheric refraction. Discrepancies can lead to heighting errors of up to 0.50 m over a horizontal distance of 1.5 km, even though the final measurement will be displayed and recorded in millimetre resolution (Cooper, 1998). The widely used Geodimeter 400 series of Total Station has a quoted precision of ± 0.005 m + 5 ppm (Barker *et al.*, 1998).

More recently, high density global positioning system (GPS) surveys have been utilised in river environments (e.g. Brasington *et al.*, 2000). This is a satellite-based positioning technique that provides three-dimensional position with suitable ground receiving equipment (Van Sickle, 1996). In particular, the development of real-time kinematic (RTK) positioning, whereby instantaneous coordinate and elevation fixes are possible through the use of a radio link between a moving receiver and stationary base station (Cooper, 1998), offers great potential. Unlike previous terrestrial techniques, the quality of topographic data obtained is independent of the area under study. However, the use of GPS survey introduces new uncertainties. These include systematic error associated with autocorrelation of GPS measurements (e.g. Satalich and Ricketson, 1998; Brasington *et al.*, 2000), related to atmospheric effects on the GPS signal (Cooper, 1998; Brasington *et al.*, 2000).

Second, there is a wider philosophical issue associated with the use of terrestrial survey techniques to measure gravel riverbeds. The spatial distribution of points is critical to the quality of representation of any terrain surface. Given sufficient density of points, the bias associated with individual point measurements due to surface roughness could, theoretically, be eliminated, as every point on the surface would be surveyed. Physical constraints (both time and the dimensions of the survey pole) mean this can never be the case and uncertainty is introduced, resulting from sampling being carried out at a lower spatial frequency than is contained in the true surface (Lane, 1998). The issue of correct terrain representation becomes even more critical when

terrain surfaces are compared to estimate morphological development, as errors in the terrain surfaces used will propagate into artefacts in volumetric calculations of change.

During terrestrial riverbed surveys, the choice of position of measured points, although informed by the nature of the topography and the location of breaks of slope, is essentially subjective. Often a hierarchical approach will be adopted, whereby given limited time to complete the survey, the largest morphological features will be measured preferentially, with smaller features represented depending on the time available. For small study areas, levelling or Total Station theodolite can successfully be used to represent all morphological features at scales greater than the grain-scale. However, if the area of interest is increased, then a form of aliasing will inevitably occur, as representation of smaller morphological units is sacrificed in favour of larger topographic features, in order to complete the survey in the allocated time. For example, in small (less than 100 m) study reaches, successive cross-sections are typically spaced every 5-10 m (**Table 1.1**). In longer reaches, cross-sections are surveyed at wider downstream intervals (e.g. Cheetham, 1979; Ferguson and Werry, 1983; Fenn and Gurnell, 1987; Martin and Church, 1995; McLean and Church, 1999).

Third, geomorphologically-significant morphological changes in riverbed form will only be detected if the temporal frequency of re-survey is commensurate with the rate of morphological change. This is governed by the time-scale at which the channel forming processes operate (Lane, 1998). Of the three terrestrial survey variables discussed above, the appropriate frequency of re-survey is most strongly fixed, as it is dictated by the rate of change of the landform in question (Lawler, 1993). In rapidly changing environments, this may render conventional survey techniques inadequate, and the more rapidly a landform is changing, the more serious this problem becomes. In the case of small-scale proglacial, braided rivers, it has been common to use a frequency of re-survey of 24 hours or greater (**Table 1.1**). However, while such time-scales will yield information about the net effect of a diurnal discharge fluctuation, topographic changes occurring within the diurnal cycle will go undetected. Furthermore, these time-integrated measures of morphological change are often incorrectly linked with instantaneous measures of process, such as within-channel flow and sediment transport processes (e.g. Ferguson and Ashworth, 1992; Goff and Ashmore, 1994). It is only possible to make such links when the process measurements are at an equivalent time-scale to the morphological changes with which they are associated, and not the morphological changes defined by the sampling strategy (Lane, 1998). Even within-diurnal surveys frequencies may be inadequate in certain environments. For example, Lane (1990) reported that a survey of six cross-sections of a proglacial braided stream

took around four hours. In the same study reach, planform channel bar growth was observed at 0.5 m per hour.

Finally, an emphasis on repeat surveying implies a commitment to return to the same cross-sections (Lane *et al.*, 1993). Research design is therefore constrained by initial evaluation of the field site, rather than evolving as understanding of the landform grows. This issue is particularly relevant in dynamic river environments, where wetted channel migration or avulsion may leave river channel cross-sections no longer orthogonal to the direction of flow (e.g. Coldwell, 1957; Lewin, 1990) or even dry during later surveys. Conversely, selected cross-sections may show little change during the period of study, despite the potential for large changes to occur due to flood flows or channel switching (e.g. Nicholas and Sambrook-Smith, 1998). Planimetric survey of an entire active riverbed reduces the chance of either scenario occurring, but requires either longer in the field to complete one survey or a lower spatial density of surveyed points.

1.2.4 *Remote sensing survey of river environments*

Progress in the issues outlined above might come from the incorporation of remote sensing methods in fluvial geomorphology. “Remote sensing” is used here to refer to any non-contact method used to determine landform surface properties.

Remote sensing techniques have the potential for widespread application to the study of fluvial systems, both as a means of detecting and mapping change and as a means of measuring some of the physical variables cause those changes (Milton *et al.*, 1995). The use of remote sensing techniques breaks down the trinity of factors that conventionally determine the spatio-temporal sampling frequency of measurements. First, the spatial extent of area over which data is collected becomes limited only by the spatial coverage of remotely sensed data. Remote sensing offers the potential of observing river systems at the reach scale or larger and within their geomorphological setting. Given the spatial links between flow, sediment transport and channel morphology (Lane and Richards, 1997), understanding of the wider geomorphic setting of single river reaches may be necessary for correct interpretation of local observations. Second, the sampling density of points obtained using remote sensing methods is limited, at least in theory, only by the spatial resolution with which data is obtained. This can vary from grain-scale detail in airborne aerial photographs to a sampling interval of metres or more with commonly used satellite-based sensors. Even at the coarsest end of the scale, this may still represent a large increase on what it is possible to collect with terrestrial, manual methods. Furthermore, because remote

sensing data is usually handled digitally, the additional time and cost necessary to interrogate high spatial resolution data is only marginally greater than that required to examine the same data at lower resolutions. Third, the temporal sampling frequency is potentially much greater than with terrestrial methods. By offering a synoptic view of river environments, repeat measurements are possible whenever and wherever the sensor makes a subsequent pass across the area of interest. However, if commercial sensors are used, there may be relatively little control over when this happens. In addition, remote sensing allows the use of archival imagery to reconstruct longer-term river channel change. One of the main problems in geomorphology has been the observation and estimation of process rates that are characteristically slow (Thornes and Brunsden, 1977). If sufficient historical imagery is available to form a time-based sequence, then the nature, distribution and effects of these processes can be accurately assessed and quantified (Chandler and Cooper, 1988), over a period far greater than the average duration of research funding.

The physical basis of using remote sensing in fluvial environments is grounded in three basic assumptions (Milton *et al.*, 1995). First, it is assumed that the spatio-temporal changes of interest in river channel produce observable and measurable changes in the spatial-temporal pattern of electromagnetic radiation detected at the sensor. Second, it is assumed that remote sensing systems have a known level of data quality, even if that quality cannot be determined absolutely. For riverbed changes to be deemed significant they must exceed the uncertainty associated with the measurements derived from the sensor used to observe them. Third, it is assumed that geometric distortions introduced by the sensor's properties and position/orientation can be modelled such that displacements of observed image features are known to be real. The second and third assumptions are particularly important with non-imaging sensors, such as ALS, where there is no recognisable photo-like image produced.

The pace with which remote sensing technologies are being developed and adopted by geomorphologists has led to suggestions that issues of data quality are being neglected due to the sheer volume of data available and the rush to produce results (Cooper, 1998). Consequently, assessment of data error and the effects of error on derived parameters has become a much needed area of research. Despite considerable progress in this area (e.g. Torlegård *et al.*, 1986; Li, 1988, 1994; Butler *et al.*, 1998; Huisings and Gomes Pereira, 1998; Baltsavias, 1999a; Gooch *et al.*, 1999; Brasington *et al.*, 2000; Lane *et al.*, 2000; Hofton *et al.*, 2000; Wise, 2000), there is still much to learn regarding the overall feasibility of using remote sensing methods in many geomorphological settings.

1.2.5 Summary of research context

Current fluvial geomorphological research places great emphasis on the importance and role of river channel form, and creates a substantive need for high-quality morphological information. Traditionally, riverbed morphology has been measured using cross-sections measured using terrestrial survey techniques. However, problems associated with the inevitable trade-off between spatial extent, spatial resolution, and temporal frequency of re-survey, has placed doubts over the reliability of topographic information obtained in this way, particularly for large study reaches such as those considered in this research. The development of remote sensing methods has provided a possible alternative method of obtaining topographic data, although the quality of information derived remains poorly quantified. With this research context in mind, the five research objectives outlined in **Section 1.1** are now explained in more detail.

1.3 Detailed research objectives

1.3.1 *Objective (i): to establish the project design necessary to yield topographic information from large, gravel riverbeds with a quality that allows channel morphology and morphological change to be determined and measured.*

The potential challenge offered to remote survey technologies by large, gravel-bed rivers means that consideration of project design is essential if high quality topographic data are to be obtained. Large, gravel riverbeds have a number of features that need to be considered when planning topographic survey using remote sensing.

First, there is a large disparity between the scales of vertical relief and spatial extent (Lane, 2000). In large, braided, gravel-bed rivers, the riverbed width is often three or four orders of magnitude greater than average channel depth. When viewed from above, the riverbed can appear almost totally lacking in relief. In many ways, the braiding process itself depends on this disparity. Small differences in vertical relief across the riverbed permit the active channels to migrate and avulse relatively easily. The wide lateral expanse of gravel allows these processes to act in an unconstrained manner, which is often seen as an important condition for braiding (e.g. Murray and Paola, 1994). Riverbeds where there is greater vertical relief or a confined riverbed may deviate from a classic braided channel pattern (e.g. Werry and Ferguson, 1980; Carson and Griffiths, 1987). However, the relative lack of vertical relief associated with large, gravel riverbeds also makes them difficult to survey. The riverbed consists of both large areas of low relief and local areas of sudden relief change, such as at active or abandoned channels with steep gravel banks. Any survey method which is to

represent braided riverbed morphology correctly must be capable of deriving elevations for large, and often featureless, areas of low relief, but with a sufficiently high spatial resolution in areas where there are sudden breaks in slope associated with channel banks.

The use of remote sensing in gravel-bed river environments reduces the spatial coverage problem, but in so doing introduces a number of other issues. In particular, a key feature of using remote sensing to derive morphological information is the trade-off that must occur between precision and spatial coverage. Precision can be improved by lowering the flying height used to collect the raw imagery (increasing the image scale). However, this means that the area covered by each image will be reduced, requiring more ground control points, more DEMs and a larger volume of data. These result in increased time for, and cost of, data generation. A critical aspect of this trade off, with respect to braided riverbeds, is the number of flying lines needed to cover the entire riverbed width.

A second issue specific to photogrammetric survey of gravel riverbeds is photograph contrast. With both analogue and digital photogrammetry, it is important to obtain well exposed images with the object of interest represented by a wide range of radiance values (Chandler *et al.*, 2001). With low camera-to-object distances, gravel surfaces have the potential to provide an abundance of texture in resulting imagery (e.g. Pyle *et al.*, 1997; Butler *et al.*, 1998; Carboneau *et al.*, in press). However, the need to maximise flying height with respect to the required precision in large, gravel-bed river settings, in order to increase spatial coverage on each image, means that this texture might be reduced or even lost. Consequently, aerial photography of gravel riverbeds will often contain two distinct spectral signals, the light areas (low digital numbers, DNs) associated with exposed gravel and dark areas (high DNs) constituting the wetted channels. The difference between these two spectral signals, combined with the lack of a spectral signal from intermediate DNs, can cause exposure problems at the time of photography, leading to imagery with inadequate contrast. This is a particular problem given the reduced texture associated with photographing exposed gravel areas from high flying heights, where contrast determines grain-scale recognition on the imagery and hence the success of automated stereo-matching. It remains unknown whether aerial photography of gravel riverbeds, taken at a scale at least in part determined by spatial coverage considerations, can be of sufficient quality to allow adequate stereo-matching for digital terrain generation.

With these issues in mind, this study will examine the project design necessary for acquisition of topographic information from large, gravel riverbeds using digital photogrammetry and ALS.

1.3.2 *Objective (ii): to develop and to apply procedures for dealing with the presence of water on the riverbed.*

Rivers, by definition, convey water. Thus, an important requirement of topographic survey of active riverbeds is the ability to measure submerged morphology. Conventional, terrestrial, survey techniques have typically required a surveyor to wade into active channels to permit a survey measurement to be made (e.g. Ferguson and Ashworth, 1992; Lane *et al.*, 1994). Where the water becomes too deep, a survey staff may be lowered into the channel from a boat (e.g. Davoren and Mosley, 1986). In addition, echo-sounding or sonar techniques, common hydrographic mapping techniques for topographic measurement of shallow coastal waters (Morang *et al.*, 1997), have been successfully adopted to determine river depth (e.g. Neill, 1969; Dinehart, 1992; McLean and Church, 1999). In previous applications of remote sensing of river environments, terrestrial survey measurements have been retained in the wetted channels (e.g. Lane *et al.*, 1994). Thus, the benefits associated with remote measurement of exposed riverbed areas are reduced. However, the development of a digital photogrammetric refraction correction for shallow clear water (Butler *et al.*, 2001b) and image analysis techniques for estimating water depth based on water colour (Lyzenga, 1981; Winterbottom and Gilvear, 1997) leave open the possibility of ‘total’ remote survey of braided river channels.

Wetted channels in braided gravel-bed river systems are typically shallow (less than 2 m), meaning that the submerged bed is visible in most areas of the riverbed if turbidity is sufficiently low. Thus, remote sensing techniques here have the potential to provide water depth or bed elevation measurements, although different procedures are required based on the extent to which the water is clear.

Where water is sufficiently clear (transparent) to allow the bed texture to be clearly visible on the imagery used, two media photogrammetry, incorporating a correction for refraction at an air-water interface, can be used directly to survey submerged topography. Through-water photogrammetry was originally proposed in the 1960s for use with coastal bathymetry measurements (e.g. Tewinkel, 1963), and recent research has applied and tested the two-media correction procedure developed for use with analytical photogrammetry (e.g. Rinner, 1969) to correct the elevation of submerged points survey with digital photogrammetry in a gravel-bed river setting (Butler *et al.*,

2001b). However, this work concentrated on large-scale imagery of gravel surfaces in a flume bed. Digital photogrammetry has rarely been applied to river environments in a reach-scale field setting. In clear water, ALS has the potential to measure submerged topography (e.g. Hickman and Hogg, 1969; Lyzenga, 1985; Harris *et al.*, 1987; Penny *et al.*, 1989; Irish and Lilycrop, 1999; Guenther *et al.*, 2000), and hydrographic surveys in water depths of up to 70 m have been reported (Wehr and Lohr, 1999). However, for this to be achieved, dual or multiple frequency systems are required, incorporating a longer wavelength laser that can penetrate the water column (Wehr and Lohr, 1999). Single frequency systems will tend to have a shorter wavelength that is normally absorbed at the water surface (Huisings and Gomes Pereira, 1998).

If water is slightly-turbid (translucent) then submerged topography is still likely to be seen on the source imagery, although the bed texture will be less distinct. As digital photogrammetry relies on image texture in order to identify conjugate points on overlapping images, a digital photogrammetric approach cannot necessarily be used in these areas. An alternative approach uses image analysis to derive an empirical relationship between water depth and water colour. The ability to derive water depth estimates from water colour has long been recognised (e.g. Grange Moore, 1946). However, it is only with the development of multi-spectral sensors and digital image processing that the method has been more widely adopted (e.g. Lyzenga, 1981; Cracknell *et al.*, 1987; Lyon *et al.*, 1992; Kumar *et al.*, 1997; Winterbottom and Gilvear, 1997; Gilvear *et al.*, 1998). To date, this approach has only been used to estimate water depth. The water depth maps produced have not been re-incorporated within a fully three-dimensional survey framework, meaning that whilst its potential has been demonstrated, it may have yet to be fully realised.

Thus, this research seeks to develop, to test and to automate approaches to derive submerged topography for both clear and slightly-turbid water, and to integrate them into fully three-dimensional digital photogrammetric and ALS surveys of large, gravel-bed braided rivers.

1.3.3 *Objective (iii): to evaluate the quality of surface representation of digital terrain models of braided, gravel riverbeds produced using digital photogrammetry and airborne laser scanning.*

Surface quality is conventionally measured in terms of accuracy, precision and reliability as compared to independent elevation measurements (Cooper and Cross, 1988). However, Wise (2000) suggests that because these measures are based on a relatively small number of points (i.e. those points for which an equivalent

independently-acquired check elevation value is available) it may be that surface quality is better estimated with reference to derived parameters, which are more sensitive to errors in the digital terrain surface (Ley, 1986; Wise, 1998). For braided, gravel-bed rivers, there are a number of derived parameters which are likely to be used by river scientists and river managers, including water depth, mean bed level (MBL), sediment storage volumes, local slope and aspect, and morphological scaling properties. DEMs of difference also represent derived data, and are perhaps one of the most useful data quality assessment methods for DEMs of dynamic riverbeds.

In this context, this research will investigate several different methods of error assessment, including conventional empirical measures, parameters derived from single DEMs, and parameters derived from DEM of difference surfaces obtained from sequential DEMs .

1.3.4 Objective (iv): to develop and to apply automated post-processing procedures to identify and eliminate errors from topographic surfaces obtained using remote sensing methods, and to assess their effectiveness at improving final DEM quality.

A crucial but often neglected element of digital elevation modelling is the post-processing necessary to identify and to remove errors from the final topographic surface. The automation of topographic data acquisition has two main consequences with respect to data quality. First, it becomes easy to believe that the raw digital terrain output is free of errors (Cooper, 1998). However, this is rarely the case, and consequently these errors may be propagated into parameters derived from the terrain surface (Wise, 2000). Second, the volume of data generated using automated methods makes actual error assessment more difficult.

Traditionally, errors in terrain surfaces have been identified by a human operator using a rendered or three-dimensional visualisation of the calculated elevation surface (Carrara *et al.*, 1997). However, this does not guarantee that all errors are removed. For example, human visualisation artefacts have been noted such as the “firth effect” (Hunter and Goodchild, 1997). Automation of terrain modelling methods has taken away the fundamental role of the photogrammetrist in setting a stereomark over a point of interest (Lane, 2000), such that point mismatching can occur undetected. In any case, the associated dramatic increase in the number of points that can be surveyed makes manual checking of each point increasingly unfeasible. Consequently, automated post-processing techniques are recognised as being urgently required (e.g. Lane, 2000; Wise, 2000).

A particular source of error in remote sensing survey methods is the presence of vegetation. Remote sensing methods are line-of-sight technologies, in that measurements are only possible for those features visible on the raw imagery. The imagery used is typically acquired aerially and near-vertical, meaning that the top of the vegetative canopy, rather than the true ground surface, will be detected in vegetated areas. Consequently, photogrammetric and ALS surveys will always tend to contain a systematic bias associated with vegetation height (e.g. Lane *et al.*, 2000). If individual trees and bushes exist, then ‘spikes’ may be present in the surveyed data (e.g. Ritchie *et al.*, 1994; Charlton *et al.*, 2001). The dynamic nature of braided rivers causes individual channels to migrate across the riverbed and this, coupled with frequent (intra-annual) bankfull floods, means that vegetation often has little time to establish in these environments. This is particularly true for gravel-bed channels, which are frequently devoid of any significant vegetation cover. Nevertheless, isolated trees and bushes may persist, and more stable areas of the riverbed may develop which allow more extensive grass and shrub coverage. Furthermore, the errors introduced by the remote survey of a treetop (rather than riverbed surface) would potentially be significant given the low local vertical relief. Hence, despite the relative lack of vegetation cover expected on braided riverbeds as a whole, it is critically important to deal with the presence of riverbed vegetation.

An important requirement of any automated post-processing procedure is that it effectively removes errors in a digital terrain surface without compromising the quality of correctly represented points. This effectiveness can be judged with respect to surface quality *per se*, or with respect to parameters that are derived from the surface. As it has been suggested that such parameters should be used to determine the quality of digital terrain surfaces (Wise, 2000; Lane, 2000), it follows that derived measures are also perhaps more useful for assessing the success of automated post-processing.

This research will aim to develop automated post-processing methods for riverbed DEMs to identify and eliminate errors from the raw DEM surfaces, to include consideration of errors caused by the presence of both surface water and vegetation. The design and success of the post-processing procedures developed will be informed by their effect upon DEM quality.

1.3.5 Objective (v): to evaluate the reliability of estimates of volumes of erosion and deposition inferred from remotely-sensed digital elevation models of large, gravel-bed rivers, and hence to assess the feasibility of using morphological methods to estimate sediment transport rate.

One goal of employing remote sensing to monitor landforms is to utilise the subsequent increase in the volume of topographic information obtained to infer process rates from morphological change. Whether this is possible for large, gravel-bed rivers remains largely untested and unknown, particularly in a field setting, although two groups of potential problems have been identified (Lindsay *et al.*, *in review*): (i) those inherent with morphological-based calculations of sediment transport; and (ii) those linked to the quality of topographic data available. Given that there is little vertical relief in braided riverbeds (Lane, 2000), it follows that the vertical magnitude of change is also likely to be small. Thus, it is important to consider whether remote sensing technologies can be used to acquire digital terrain surfaces with sufficient quality to allow significant morphological change to be detected in these environments. If the DEM surfaces themselves are of insufficient quality, such that real morphological change cannot be distinguished from background errors, then invalid conclusions could be made about the physical processes that the data are intended to help understand (Fryer *et al.*, 1994). A linked question that must also be addressed is whether a minimum surface quality can be determined, with respect to the correct calculation of volumes of erosion and deposition. Such a figure would provide an important baseline surface quality necessary for effective deployment of remote sensing to monitor gravel-bed rivers.

This study will seek to assess the feasibility of applying the morphological method to riverbed DEMs of difference derived from topographic information measured using digital photogrammetry and ALS. The quality of morphological change estimates will be investigated in terms of the ability to separate real morphological changes from artefacts created by the presence of errors.

1.4 Thesis structure

Chapter 2 presents a review of monitoring and modelling of riverbed environments using remote sensing techniques in terms of data acquisition methods and data quality. First, the use of aerial imagery is examined and potential weaknesses considered. Then, the two remote survey technologies used in this research, digital photogrammetry and ALS, are introduced and previous applications of both technologies in fluvial geomorphology analysed. The determination of water depth and submerged topography using remote sensing methods is also reviewed. Next, errors and error detection in digital terrain representation are considered in the context of the

digital elevation model. Error detection is discussed in terms of errors associated with both static (or single) and dynamic (or difference) DEM surfaces. This section will also highlight the range of terminology used in the literature to describe types and statistical measurements of error in terrain surfaces, and in so doing establish the nomenclature to be used in this research.

Chapter 3 outlines the common methodology used in this research to obtain digital terrain surfaces of two large, gravel riverbeds using both digital photogrammetry and ALS. First, the basic principles of each technique is explained. Next, issues regarding project design and data acquisition methods are discussed, and the specific design and methods used in this research explained and justified. Common to both technologies is the trade off between spatial coverage and surface representation. This issue was particularly important given the disparity between spatial extent and vertical relief in large, gravel-bed rivers. Consequently, this aspect of project design is given particular consideration. Finally, the concurrent collection of independent check data is detailed.

Chapter 4 presents the application of digital photogrammetry to the clear-water North Ashburton River. This involves the development of an automated two-media geometric correction for refraction at the air-water interface, and the subsequent development of an automated post-processing routine to deal with mismatching of underwater points. The dry- and wet-bed quality of the resultant DEMs is judged with respect to independent check data and by using the derived parameters of water depth and mean bed level. Quality assessment also provides an indication of the need for and success of the refraction-correction process.

Chapters 5 and 6 apply digital photogrammetry and ALS to the much larger and more turbid-water Waimakariri River. **Chapter 5** explains the method for estimating water depth, based on an empirical relation developed between water colour and measured water depth. The quality of water depth estimates is assessed by comparison with additional independent water depth measurements. **Chapter 6** describes the remote survey of dry-bed areas using digital photogrammetry and airborne laser scanning (ALS). For digital photogrammetry, this comprises DEM generation, automated post-processing routines developed to identify and remove errors and integration of water depth information to estimate the submerged topography. For ALS, this includes DEM generation and integration of water depth information to estimate the submerged topography. For DEMs generated using both methods, the quality of riverbed representation and the success of post-processing methods is examined using both independent check data and overlap analysis.

Chapter 7 examines the estimates of volumes of erosion and deposition that can be obtained from between-survey difference DEMs, in order to evaluate the potential utility of using remotely-sensed digital terrain surfaces as input for morphological methods of inferring process rates in braided, gravel-bed rivers. The quality of post-processed DEMs of difference is assessed with respect to three types of error (gross, systematic and random), each of which has a particular effect on DEM of difference quality. This approach is also used to assess the effect of the post-processing procedures developed for the riverbed DEM surfaces on resultant DEMs of difference. Finally, the effect of cross-section spacing on the morphological change information recovered is examined. This is important because both rivers studied in this research are monitored using widely-spaced cross-sectional surveys. However, the reliability of calculated changes in sediment storage made based on such information is not known.

Chapter 8 closes the thesis by re-visiting the overall research aim and specific research objectives, and by proposing some wider implications of this work. Potential directions for future research are also suggested.

CHAPTER 2. ACQUISITION AND QUALITY OF REMOTELY-SENSED DATA IN RIVER ENVIRONMENTS

In this chapter, issues surrounding the use of remotely-sensed data in river environments are examined. First, data acquisition is addressed (2.1), and past and present uses of remote sensing in fluvial geomorphology are reviewed, including aerial imagery (2.1.1), photogrammetry (2.1.2) and airborne laser scanning (2.1.3). The acquisition of data from inundated areas of riverbed is also discussed (2.2), and the two methods commonly used to infer water depth and submerged topography are examined: depth determination based on remotely-sensed water colour (2.2.1); and through-water photogrammetry (2.2.2). Next, data quality is considered, with respect to digital representation of surface terrain (2.3). First, the different types of error that may occur (2.3.1) are identified. Then, their sources are discussed (2.3.2), including data acquisition method (2.3.3), point density and distribution (2.3.4), interpolation method (2.3.5) and terrain characteristics (2.3.6). Finally, methods of error identification and surface quality assessment are examined (2.3.7), based on whether the DEMs involved are ‘static’ (representing morphology) (2.3.8) or dynamic (representing morphological change) (2.3.9).

2.1 Data acquisition

Although river scientists have traditionally relied upon field-based investigations to obtain data on channel and floodplain behaviour (Milton *et al.*, 1995), remote sensing has been used in a variety of ways to inform fluvial geomorphological studies. Aerial photographs have been used to supplement field investigations of river channels and floodplains since the 1920s (Putnam, 1947), multi-spectral sensors have been available since the 1960s (Milton *et al.*, 1995) and data from satellite platforms have been accessible since the 1970s (Muller *et al.*, 1993). The historical and contemporary use of three types of remote sensing in fluvial geomorphology will be considered here: aerial imagery; photogrammetry; and airborne laser scanning (ALS).

2.1.1 Aerial imagery

Aerial imagery, consisting of any spatially-distributed optical data obtained from airborne and satellite platforms, has commonly been used in geomorphology to provide both qualitative and quantitative information on landform features. Examples of fluvial geomorphic studies incorporating aerial imagery are given in **Table 2.1**.

PLATFORM AND SENSOR USED			
Purpose of research	Air photos	Multi-spectral imagery (airborne)	Satellite imagery
Bank erosion	Painter <i>et al.</i> (1974); Miles (1976)		
Channel change	Smith (1941); Whitehouse (1944); Sundborg (1956); Crickmay (1960); Schumm and Lichy (1963); Pels (1964); Speight (1965a,b); Fernando (1966); Wolman, 1967; Fahnestock and Bradley (1973); Hitchcock (1977); Werritty and Ferguson (1980); Leeks <i>et al.</i> (1988); Gilvear and Winterbottom (1992); Kondolf and Swanson (1993); Warburton <i>et al.</i> (1993); Gurnell <i>et al.</i> (1994); Winterbottom (2000)	Bryant and Gilvear (1999)	Salo <i>et al.</i> (1986); Philip <i>et al.</i> (1993)
Channel width	Beschta (1983); Reinfelds (1997)		
Drainage network	Shaw (1953); Howe, (1960); Sternberg (1961)		Rinaldo <i>et al.</i> (1988); Costa-Cabral and Burges (1997)
Flood inundation mapping	Parker <i>et al.</i> (1970); Gilvear <i>et al.</i> (1994); Reinfelds (1995)		Green <i>et al.</i> (1983); Blasco <i>et al.</i> (1992); Nagarajan <i>et al.</i> (1993); Bates <i>et al.</i> (1997); Townsend and Walsh (1998); Horritt and Bates (2001)
Floodplain geomorphology	Lueder (1959); Kelly and McGuire (1955); Price (1965); Rundle (1985); Carson (1986); Schumann (1989); Sapozhnikov and Foufoula-Georgiou (1996)	Wright <i>et al.</i> (2000)	Hamilton and Lewis (1990); Muller (1992); Thorne <i>et al.</i> (1993); Sapozhnikov and Foufoula-Georgiou (1996); Nykanen <i>et al.</i> (1998)
Flow velocity	Linton (1952); Oros (1952)		
Grain delineation	Iriondo (1972); Adams (1979); Church (2001)		
Paleo-channel mapping	Smith (1941)		Jacobberger (1988); Ramasamy <i>et al.</i> (1991)
Suspended sediment			Mertes <i>et al.</i> (1993); Nellis <i>et al.</i> (1998)
Water temperature		Torgersen <i>et al.</i> (2001)	

Table 2.1 Examples of studies that have used aerial imagery to study river environments.

Although experiments taking pictures from kites and balloons date back to the 19th century (Reeves, 1927), it was not until the first World War (with the accelerated need to evaluate territory from afar) that the value of using aircraft-mounted cameras to study terrain was realised (Smith, 1941; Putnam, 1947). The ability to identify and to map surface topography, particularly using stereoscopic methods, was quickly recognised. Drainage features and river channels, in particular, were found to be suited to mapping from aerial photographs (Shaw, 1953), with “the relative height and symmetry of the banks, the breadth and openness of the stream bed, the presence of islands, rocks, sand bars, and shoals, and the occurrence of bare sand, vegetation and channel scars above water level” all able to be determined (Smith, p.125, 1943).

By the 1960s, aerial photography was a commonly-used qualitative tool in fluvial geomorphology (e.g. Sundborg, 1956; Crickmay, 1960; Schumm and Lichy, 1963; Peels, 1964; Fernando, 1966; Wolman, 1967). The extraction of quantitative information from aerial photographs was more infrequent, though early examples include derivation of Manning’s n roughness coefficient using terrestrial stereoscopic imagery by the United States Geological Survey (reported in Lohman and Robinove, 1964) and power spectrum analysis of river meanders (Speight, 1965a). By this time, the ability to infer channel processes directly from aerial photographs had also been recognised. This included using aerial photography to estimate wave conditions (e.g. Putnam, 1947) and analysis of sequential photographs to calculate river surface flow velocities (e.g. Linton, 1952; Oros, 1952).

Contemporary fluvial geomorphological research still relies heavily upon aerial photographs at a range of scales, for instance to delineate individual pebble clasts and clusters (e.g. Church, 2001), to help understand channel-scale flow processes (e.g. Rundle, 1985), to observe and classify reach-scale geomorphology (e.g. Schumann, 1989) and to explore scaling properties associated with large, braided rivers (e.g. Sapozhnikov and Foufoula-Georgiou, 1996). Over the last twenty years, multi-spectral sensors and satellite platforms have complemented traditional air photographs, allowing study of larger river systems (Milton *et al.*, 1995) such as the Amazon (Salo *et al.*, 1986), the Ganges (Philip *et al.*, 1993) and the Brahmaputra (Thorne *et al.*, 1993). However, the development of airborne multi-spectral scanners and thematic mappers in the last few years promises a re-emergence of interest in reach scale issues (e.g. Lyon *et al.*, 1992; Hardy *et al.*, 1994; Winterbottom and Gilvear, 1997; Wright *et al.*, 2000).

In fluvial geomorphology, aerial images are perhaps at their most valuable when channel change is considered, and the ability to use aerial photographs in this context has long been recognised (Lohman and Robinove, 1964; Fezer, 1971). A knowledge of

channel planform and changes in its position through time is critical to many geomorphological and river management issues (Milton *et al.*, 1995). Using time-series of aerial imagery, positional change of river channels can easily be identified qualitatively (e.g. Whitehouse, 1944; Sundborg, 1957; Pels, 1964; Fernando, 1964; Fahnstock and Bradley, 1973; Werrity and Ferguson, 1980; Kondolf and Swanson, 1993; Warburton *et al.*, 1993). The recent development of commercial geographical information systems (GIS) software, which readily allows photographs taken at different dates and scales to be georeferenced to a common spatial framework and compared, has permitted more quantitative description of river channel change (e.g. Gurnell *et al.*, 1994; Bryant and Gilvear, 1999; Winterbottom, 2000). This is an important step towards estimation of volumetric change from patterns of channel change (e.g. Carson and Griffiths, 1989; Ham and Church, 2000).

Despite this progress, two basic limitations exist which constrain the exclusive use of aerial images in river environments. First, channel planform identified in an unconfined river is generally stage dependent. This means that mapping channel boundaries at different dates from aerial photographs or satellite imagery is not necessarily a reliable guide to channel change (Lawler, 1993), because stage effects may be confused with actual channel changes (Ferguson and Ashworth, 1992). Second, aerial images are two-dimensional. Consequently, planform variation has dominated studies of channel change, meaning that river environments frequently remain categorised and described by planform appearance alone (e.g. Sapozhnikov and Foufoula-Georgiou, 1996; Nykanen *et al.*, 1998; Winterbottom, 2000), despite the three-dimensional nature of river channel processes and morphology.

2.1.2 Photogrammetry

Both of these limitations are addressed by taking image interpretation one stage further and extracting quantitative, three-dimensional information about the landform under investigation using photogrammetry. Photogrammetry is a mature discipline, with its potential applicability to topographic survey first recognised and developed in the late nineteenth century (e.g. Deville, 1893). There are several natural benefits of photogrammetric survey that are particularly advantageous in geomorphological studies of landform change (Lane *et al.*, 1993). Photogrammetry extracts fully-distributed three-dimensional morphological information using a method that can be retrospective and that is non-invasive. The photograph records all points within the area covered at a resolution that is in theory only limited by the resolution of the film used. The method also records a significant amount of extra, explanatory information, and can be repeated at a time-scale appropriate to the rate of landform change, provided there is reasonable control over the position of an appropriate platform.

Archive photographs, providing there is sufficient overlap and photo control points can also be used (e.g. Chandler and Cooper, 1988; Chandler and Cooper, 1989; Chandler and Clark, 1992; Brunsden and Chandler, 1996).

Table 2.2 provides a summary of studies to date that have incorporated photogrammetry in fluvial environments. In general, photogrammetric techniques have been applied to rivers in two main ways: to measure bank erosion; and to monitor channel change. Photogrammetric determination of channel bank erosion rate appears to offer great potential (Lawler, 1993), not least because of the non-contact nature of photogrammetry and the potential fragility of stream-banks (Collins and Moon, 1979). Terrestrial cameras are set up along a baseline, usually established approximately opposite and parallel to the bank under investigation. Artificial targets are constructed at the bank and these points are then surveyed from fixed control stations away from zones of possible erosion, allowing photogrammetric reconstruction of the three-dimensional morphology of the bank.

Painter *et al.* (1974) made the first reported terrestrial photogrammetric measurements of stream-bank erosion as part of a wider study of the effect of afforestation on erosion processes at Plynlimon, Wales. Collins and Moon (1979) and Dickinson and Scott (1979) conducted photogrammetric studies concentrating solely on bank erosion, examining the sediment yield from the stream-banks of several southern Ontario streams. Williams *et al.* (1979) used stereoscopic viewing of aerial photograph pairs to study riverbank erosion and recession of the Ottawa River over a 50-year period. More recently, Barker *et al.* (1997) and Dixon *et al.* (1998) have used analytical photogrammetry in an attempt to identify the relative importance of bank erosion in supplying sediment yield to the River Yarty, Devon. The whole bank face was measured using a regularly-spaced grid, with extra points measured in areas of most rapid change in relief. Pyle *et al.* (1997) employed digital photogrammetry to study a section of bank of the proglacial stream at the Haut Glacier d'Arolla, Switzerland, using the OrthoMAX module of ERDAS Imagine to create regularly-spaced DEMs.

The second group of studies uses photogrammetric techniques to examine morphology and morphological changes in river environments as a whole. Such studies use either aerial or terrestrial photography, depending on the size of the field site and on the availability of suitable vantage points. In this context, photogrammetry has been employed in fluvial geomorphological studies at a range of spatial and temporal scales.

Researcher(s)	River	Purpose of research	Photograph type (and platform)	Photogrammetric method
Eliel (1947)	Colorado, USA	Dam site mapping	Oblique (vantage points)	Manual
Forrester (1960)	Rideau, Canada	Water current velocity	Vertical (airborne)	Manual
Lo and Wong (1973)	Ephemeral gully, Hong Kong	Channel change (3D)	Vertical (camera tripod)	Manual
Painter <i>et al.</i> (1974)	Cyff, Wales	Bank erosion	Oblique (opposite bank)	Manual
Collins and Moon (1979); Dickinson and Scott (1979)	Various, Ontario, Canada	Bank erosion	Oblique (opposite bank)	Manual
Williams <i>et al.</i> (1979)	Ottawa, Canada	Bank erosion	Vertical (airborne)	Manual
Lewin and Manton (1975); Lewin and Hughes (1976)	Various, Wales	Channel change (2D)	Vertical (airborne)	Manual
Lewin and Weir (1977)	Lower Spey, Scotland	Channel change (2D)	Vertical (airborne)	Manual
Sherstone (1983)	Muskwa, Canada	Channel change (3D)	Vertical (airborne)	Manual
Welch and Jordan (1983)	Lampkin Branch, USA	Channel change (3D)	Vertical (gantry)	Manual
Lane <i>et al.</i> (1994)	Haut Arolla, Switzerland	Channel change (3D)	Oblique (vantage points)	Manual
Carter and Shankar (1997)	North Ashburton, New Zealand	Gridding method comparison	Vertical (airborne)	Automated
Barker <i>et al.</i> (1997); Dixon <i>et al.</i> (1998)	Yarty, Devon	Bank erosion	Oblique (opposite bank)	Manual
Pyle <i>et al.</i> (1997)	Haut Arolla, Switzerland	Bank erosion	Oblique (opposite bank)	Automated
Butler <i>et al.</i> (1998); Butler <i>et al.</i> (2001a)	Affric, Scotland	Grain size information	Vertical (gantry)	Automated
Dixon <i>et al.</i> (1998)	Upper Severn, Wales	Channel change (2D)	Vertical (airborne)	Manual
Heritage <i>et al.</i> (1998)	Various, Northumberland	Low relief mapping	Oblique (vantage points)	Automated
Lane (1998)	Haut Arolla, Switzerland	Channel change (3D)	Oblique (vantage points)	Automated
Lapointe <i>et al.</i> (1998)	Ha! Ha!, Canada	Channel change (3D)	Vertical (airborne)	Automated
Stojic <i>et al.</i> (1998)	Hydraulic model	Channel change (3D)	Vertical (gantry)	Automated
Chandler <i>et al.</i> (2001)	Hydraulic model	Channel change (3D)	Vertical (gantry)	Automated
Chandler and Ashmore (2001); Stojic (2001)	Sunwapta, Canada	Channel change (3D)	Oblique (vantage points)	Automated
Smart and Brasington (2001)	Hydraulic model	Drainage network evolution	Vertical (gantry)	Automated
Connell (2001)	North Ashburton, New Zealand	Topography for numerical modelling	Vertical (airborne)	Automated
Smart <i>et al.</i> (2001)	Waimakariri, New Zealand	Grain size information	Vertical (gantry)	Automated

Table 2.2 A summary of studies that have used photogrammetry to study river environments.

At the micro-scale, Butler *et al.* (1998) used close-range digital photogrammetry to study rough river gravel surfaces. Images were obtained from a reach of the clear-water gravel-bedded River Affric, Scotland, using a calibrated camera mounted on a gantry. The resulting DEMs allowed the development of a watershed segmentation method to allow the identification of individual grains and characterisation of surface roughness (Butler *et al.*, 2001a). A similar methodology has been employed by Smart *et al.* (2001) in order to describe surface roughness for a small section of exposed gravel on the Waimakariri riverbed, New Zealand. Close-range digital photogrammetry has also been employed by Stojic *et al.* (1998), to produce DEMs of a 1:20 hydraulic model of a braided, gravel-bed stream in order to study sediment transport rates. Further successful application of close-range digital photogrammetry in a laboratory setting has been reported by Chandler *et al.* (2001), for gravel- and sand-bedded flume studies, and by Smart and Brasington (2001), for an actively-eroding basin under simulated rainfall, both using an uncalibrated digital camera.

At the channel-scale, Lane *et al.* (1994) and Lane (1998) describe how analytical and subsequently digital photogrammetry have been used to monitor and model river topography for a 50 m length of actively braiding proglacial stream at Haut Glacier d'Arolla, Switzerland. Photogrammetric survey was combined with rapid tacheometric survey of sub-aqueous zones in order to monitor the interrelated effect on channel morphological change of both discharge and sediment supply variations (Lane *et al.*, 1996). The DEMs and DEMs of difference obtained were subsequently used to visualise channel changes and describe within reach spatial patterns of process and channel adjustment (Lane *et al.*, 1995b, 1996), to make morphological estimations of time-integrated bed load transport rate (Lane *et al.*, 1995a), and as the topographic boundary conditions for process-based flow modelling (Lane and Richards, 1998; Bradbrook *et al.*, 2000). At a similar scale, Heritage *et al.* (1998) used a Close-Range Digital Workstation (CDW) to apply terrestrial photogrammetry on a variety of low relief fluvial geomorphic features (lateral, point and mid-channel bars) ranging from 10 to 100 m² for two gravel-bed rivers in Northumberland, UK. Terrestrial digital photogrammetry has also been utilised by Chandler and Ashmore (2001) and Stojic (2001) to model river channel changes for the Sunwapta River, Canada, using an uncalibrated digital camera and three camera stations around 125 m above and overlooking the study area.

At the reach-scale, initial uses of photogrammetry tended to concentrate on planform channel position and floodplain geometry. For example, Lewin and Manton (1975), Lewin and Hughes (1976) and Lewin and Weir (1977) used analogue photogrammetry to create detailed contour plots for various river floodplains of Wales and Scotland.

More recently, Dixon *et al.* (1998) used analytical photogrammetry with 1:5000 colour vertical air photographs taken in 1984 and 1992 to produce bank lines for a section of the Upper River Severn, Wales. Few published examples exist in which the full three-dimensional potential of photogrammetry has been harnessed at the reach scale. An early application is reported by Sherstone (1983), in which the volume of a newly-created 600 m long channel on the Muskwa River, Canada was estimated. However, the use of manual photogrammetric methods restricted data collection to ten equally-spaced channel cross-sections. More recently, automated photogrammetric methods have allowed a rapid increase in the density of data collection. For example, Carter and Shankar (1997) described the collection of a 1.6 m spaced DEM of a 500 m x 150 m reach of the North Ashburton River, New Zealand, using digital photogrammetry. Similarly, Lapointe *et al.* (1998) used “computer-assisted” photogrammetry to examine the response of a 34km reach of the Ha! Ha! River, Quebec, to a large flood event. In the study, pre-flood and post-flood DEMs were constructed from 30000 and 40000 data points, respectively.

2.1.3 Airborne laser scanning

Airborne laser scanning (ALS) is a much newer technology than photogrammetry and, as a consequence, it has been used on fewer occasions in fluvial geomorphology.

Table 2.3 provides a summary of studies that have applied ALS in river environments.

In contrast to photogrammetric studies of river environments, the most significant motivation behind ALS surveys of riverbeds has been the determination of topographic boundary conditions for numerical flow simulation. In particular, ALS data have been used as the input for two-dimensional modelling of floodplain flow to predict peak discharges and inundation extents for standard flood events (e.g. Gomes Pereira and Wicherson, 1999; Marks and Bates, 2000; Evans *et al.*, 2001; Thompson and Maune, 2001). Airborne laser scanning has also been employed in studies of channel change, and used to estimate post-flood volumes of erosion and deposition in both Iceland (Finnegan *et al.*, 2001) and Missouri, USA (Kesarwani *et al.*, 2001).

2.2 Submerged topography

An important issue that must be addressed when using any remote sensing technique to study river environments is how to deal with submerged areas of riverbed. Frequently, because the effects of surface water are perceived as uncertain, data collection is restricted to exposed areas of riverbed. This strategy has been implemented in several different ways. In studies investigating channel pattern or floodplain geometry alone, it is the position or boundaries of wetted channels that are of greatest interest. In this case, the nature of the water or submerged bed is of little

consequence, and the riverbed can be treated as a binary (i.e. dry and wet) feature, allowing channel planform geometry to be mapped (e.g. Shaw, 1953; Speight, 1965a,b; Sapozhnikov and Foufoula-Georgiou, 1996; Reinfelds, 1997; Nuykanen *et al.*, 1998; Lane, 2001) and riverbed changes identified (e.g. Werrity and Ferguson, 1980; Salo *et al.*, 1986; Thorne *et al.*, 1993; Warburton *et al.*, 1993; Gurnell *et al.*, 1994; Winterbottom, 2000; Winterbottom and Gilvear, 2000).

Researcher(s)	River	Purpose of research
Ritchie <i>et al.</i> (1994)	Goodwin Creek and Little Washita watershed, USA	Channel cross-sections
Bollweg (1999)	Rhine, Germany	Water level
Gomes Pereira and Wicherson (1999)	Ijssel, Netherlands	Topography for numerical modelling
Marks and Bates (2000)	Stour, Devon	Topography for numerical modelling
Evans <i>et al.</i> (2001)	Eamont, Cumbria	Topography for numerical modelling
French (2001)	Orwell, Essex	Topography for numerical modelling
Charlton <i>et al.</i> (2001)	Coquet, Northumberland	Mapping of channel topography
Finnegan <i>et al.</i> (2001)	Skeiðarársandur, Iceland	Channel change (3D)
Kesarwani <i>et al.</i> (2001)	Missouri, USA	Channel change (3D)
Schmidt <i>et al.</i> (2001); Thompson and Maune (2001)	Various, North Carolina, USA	Topography for numerical modelling

Table 2.3 A summary of studies that have used airborne laser scanning (ALS) to study river environments.

Elsewhere, it may be that exposed features are the focus of interest, meaning that wetted areas and the effect of surface water need not be considered. Examples include characterisation of grain-scale roughness (e.g. Church, 2001; Butler *et al.*, 2001a), evidence of erosional scars (e.g. Kelly and McGuire, 1955), mechanisms of bank failure (e.g. Gilvear *et al.*, 1994) and identification of maximum flood inundation (e.g. Parker *et al.*, 1970; Reinfelds, 1995; Bates *et al.*, 1997).

Even when three-dimensional channel changes are being studied, data collection may still be restricted to exposed areas of the riverbed. Acquiring imagery at low flow reduces this problem to a certain extent but, assuming the channel does not dry up altogether, some parts of the riverbed will always be excluded from measurement. For instance, investigations of bank erosion have focussed exclusively on those parts of the bank that are above the water surface (e.g. Painter *et al.*, 1974; Collins and Moon,

1979; Dickinson and Scott, 1979; Williams *et al.*, 1979; Barker *et al.*, 1997; Pyle *et al.*, 1997; Dixon *et al.*, 1998) even though the focus of erosion will often be below the water surface. A similar approach has been used in studies of riverbed morphology and morphological change, with only exposed areas being measured (e.g. Lewin and Manton, 1975; Lewin and Hughes, 1976; Lewin and Weir, 1977; Ritchie *et al.*, 1994; Dixon *et al.*, 1998; Heritage *et al.*, 1998; Chandler and Ashmore, 2001; Charlton *et al.*, 2001; Finnegan *et al.*, 2001; Kesarwani *et al.*, 2001). Likewise, collection of topographic boundary conditions for numerical flow simulation is frequently restricted to exposed floodplain areas, which only permits routing of flood flows (e.g. Gomes Pereira and Wicherson, 1999; Marks and Bates, 2000; Connell, 2001; Thompson, 2001). Commonly, data from the submerged areas are collected using additional, terrestrial, survey methods. For example, the submerged bed may be estimated using a measure of average upstream channel depth (e.g. Sherstone, 1983) or measured with rapid tacheometric survey (e.g. Lane *et al.*, 1994; Carter and Shankar, 1997; Lapointe *et al.*, 1998), and then integrated with remotely sensed topographic data from surrounding exposed areas of riverbed. Occasionally, remote sensing methods can be applied directly to the complete riverbed, including wetted channels. For example, some multiple return airborne laser scanning systems do allow the beds of shallow water bodies to be mapped (Wehr and Lohr, 1999), with the first (quickest) laser return describing the water surface and a second (slower) return describing the submerged bed (Charlton *et al.*, 2001). Another approach, although one typically only possible in laboratory experiments involving hydraulic models, is to drain the river channel prior to taking photographs (e.g. Stojic *et al.*, 1998; Chandler *et al.*, 2001). Although this allows the entire flume-bed to be photographed, the morphological consequences of repeated draining and inundation are uncertain.

Assuming that a multiple frequency airborne laser scanning system is not available, and that real river channels cannot be drained, the presence of surface water presents an important issue that must be addressed if remote sensing technologies are to be used to measure riverbed morphology. Remote sensing methods have been used in two main ways to address this problem: (i) image analysis to relate water colour to water depth (**Section 2.2.1**); and (ii) two-media photogrammetry to correct photogrammetric measurements of submerged points for the effects of refraction at an air-water interface (**Section 2.2.2**).

2.2.1 *Image analysis*

It has long been recognised that, when viewed from above, changes in water colour reflect changes in water depth (e.g. Smith, 1943; Dietz, 1947; Putnam, 1947). The first standard method for quantitative estimation of water depth based on water colour was

proposed by Grange Moore (1947) using the “transparency method” of depth determination. It was found that when a sandy beach was photographed vertically from the air through a colour filter, the brightness varied in a simple way with depth and the clarity of water over it. If the clarity (or extinction coefficient) of the water was known, then the water depth could be determined by measuring brightness at different points on a single air photograph. If an absolute value of the extinction coefficient was not known, comparison of brightness profiles prepared from photographs taken simultaneously using two contrasting lens filters allowed estimation of water depth. It was concluded that, in average coastal waters, depths of 6 m or more could be measured to a precision of $\pm 10\%$ (Grange Moore, 1947). Ensuing research relating water colour to water depth was dominated by shallow coastal environments (e.g. Duntley, 1963; Geary, 1968; Schneider, 1968; Lankes, 1970; Specht *et al.*, 1973), despite recognition of the potential for submerged riverine features to be mapped in the same way (e.g. Lohman and Robinove, 1964; Fezer, 1971).

Renewed interest in remotely-sensed water depth techniques and bathymetric mapping has generally occurred coincident with the development of new sensors and platforms, but has again generally remained restricted to coastal environments. Airborne multi-spectral scanners were used in a number of studies of shallow coastal waters (e.g. Yost and Wenderoth, 1968; Helgeson, 1970; Lyzenga, 1978; Lyzenga, 1981; Lyzenga, 1985; Cracknell *et al.*, 1987), allowing application of surface reflection corrections and radiometric techniques not readily possible with conventional aerial photography (Lyzenga, 1978). The development of satellite platforms has also been significant, with photography (e.g. Lepley, 1968) and multi-spectral data (e.g. Lyzenga, 1981; Cracknell *et al.*, 1982; Spitzer and Dirks, 1987; Cracknell *et al.*, 1987; Ibrahim and Cracknell, 1990; Sabins, 1997) from spaceborne sensors increasingly used in studies of shallow water bathymetry. In general, two approaches to recovering shallow coastal water depth information from aerial imagery have been developed. One approach, in line with early studies, empirically relates observed water colour to observed water depth (e.g. Grange Moore, 1947; Lyzenga, 1978; Lyzenga, 1981; Cracknell *et al.*, 1982; Lyzenga, 1985; Cracknell *et al.*, 1987; Ibrahim and Cracknell, 1990). The second approach reflects a more physically-based approach to depth determination, and attempts to model water depth from general laws governing the behaviour of electromagnetic radiation through a water body (e.g. Paredes and Spero, 1983; Spitzer and Dirks, 1987; Philpot, 1989; Lee *et al.*, 1999).

Determination of water depth using aerial imagery has only relatively recently been applied to fluvial environments (Milton *et al.*, 1995). **Table 2.4** provides a summary of published attempts at bathymetric mapping from remotely-sensed data.

Researcher(s)	River	Purpose of research	Imagery type (and platform)	Method used
Lyon <i>et al.</i> (1992)	St. Mary's, USA	Bathymetric mapping	Multi-spectral (airborne)	Physically-based
Hardy <i>et al.</i> (1994)	Green, USA	Habitat mapping	Multi-spectral videography (airborne)	Empirical
Acornley <i>et al.</i> (1995)	Test, Hampshire	Habitat mapping	Multi-spectral (airborne)	Empirical
Kumar <i>et al.</i> (1997)	Rupnarayan-Hooghly, India	Bathymetric mapping	Single-band (satellite)	Empirical
Winterbottom and Gilvear (1997)	Tummel, Scotland	Bathymetric mapping	Multi-spectral / Black & white (airborne)	Empirical
Gilvear <i>et al.</i> (1998)	Faith Creek, USA	Channel change	Black & white / Colour (airborne)	Empirical
Bryant and Gilvear (1999)	Tay, Scotland	Channel change	Multi-spectral (airborne)	Empirical
Marcus <i>et al.</i> (2001)	Lamar, USA	Habitat mapping	Multi-spectral (airborne)	Empirical

Table 2.4 A summary of studies that have used image analysis techniques to determine water depth from remotely-sensed water colour.

The first identified study is that of Lyon *et al.* (1992) who used an airborne multi-spectral scanner to evaluate bottom sediment types and water depths for a reach of the St. Mary's River, Michigan, USA. A broadly physically-based approach was used, based on estimating extinction from Secchi disk depths for several different bottom types. In several other attempts to estimate river water depth from remote sensed data, it has been the identification and classification of fish habitats that has been the driving force. Hardy *et al.* (1994) showed that high resolution multi-spectral video imagery could be used to successfully map river depth and mesoscale hydraulic features for the Green River, Utah, USA. Acornley *et al.* (1995) report on the use of an airborne multi-spectral scanner to map salmonid spawning habitat in a 1 km reach of the River Test, Hampshire. More recently, Marcus *et al.* (2001) demonstrated the use of a high spatial resolution multi-spectral scanner to map water depth for the Lamar River, Wyoming, USA. Other studies have attempted to quantify bathymetric change, for example, due to a large flood event (Bryant and Gilvear, 1999) or produced by gold placer mining (e.g. Gilvear *et al.*, 1998). Although the majority of river-based studies have used multi-spectral imagery, under certain conditions colour or even black and white photographs may be used to derive quantitative estimates of water depth (Milton *et al.*, 1995). For example, Winterbottom and Gilvear (1997) produced a water depth map of a 500 m section of the River Tummel, Scotland, from black and white imagery and Gilvear *et al.*

(1998) generated a water depth map for a 2 km reach of Faith Creek, Alaska, USA, from a combination of colour and black and white imagery.

All of the above studies are restricted to determination of water depth rather than absolute elevation of the submerged bed. Consequently, the output is in the form of two-dimensional water depth maps, rather than maps of submerged topography. For these to be obtained, the water depth estimates must be transformed to bed elevation values (Lane, 2000), and incorporated within a wider riverbed survey of exposed areas. Progress can be made by linking two-dimensional image analysis with three-dimensional measurement of channel morphology and morphological change (Lane, 2001), in which channel edge elevations are used to estimate water surface elevations, from which water depths can be subtracted and bed elevation values calculated. As far as is known, this has yet to be achieved for river environments.

2.2.2 *Through-water photogrammetry*

If water clarity and depth permit, sub-aqueous features may be identified on vertical aerial images of water bodies. This was recognised in early applications of photogrammetry to shallow coastal and river environments (e.g. Lee, 1922; Dietz, 1947), although suitable water conditions for the use of analogue stereoscopic methods were often difficult to obtain (Grange Moore, 1947). It was not until the 1960s, with the development and adoption of more rigorous analytical photogrammetric methods, that the two-media problem presented by subaqueous topography was addressed numerically. Empirical testing of the error caused by application of photogrammetry through water, to measure submerged points on the bed, found that measured depths were consistently too small (and hence bed elevation consistently too high) by a factor of 1.3 to 1.5 (Tewinkel, 1963). Subsequent theoretical treatment of the two-media situation incorporated Snell's Law to model the refraction of light at the air-water interface. This demonstrated that the systematic bias was determined by the refractive index of water (1.340 for ocean water, 1.333 for distilled water), but varied based on several factors including camera separation distance, radial distance from the perspective centre and water surface conditions (e.g. Tewinkel, 1963; Meijer, 1964; Shmutter and Bonfiglioli, 1967; Rinner, 1969). Early applications of through-water photogrammetry were generally confined to shallow ocean water, using simultaneous photography with infra-red film to model water surface elevation (as water molecules absorb radiation in this region of the electromagnetic spectrum; Reilly, 1965). Studies were mainly based around mapping of shallow ocean-floor topography (e.g. Reilly, 1965; Harris and Umbach, 1972; Rosenhschein *et al.*, 1977; MacPhee *et al.*, 1981), although applications as diverse as shipwreck mapping (Höhle, 1971) and

determination of fish size (Harvey and Shortis, 1996; Shortis and Harvey, 1998) have been reported.

Few of these studies report rigorous testing of data quality obtained using through-water photogrammetric methods. Harris and Umbach (1972) used withheld control points to calculate a root mean square error of 0.55 m and a maximum error of 1.4 m in water up to 12 m in depth. Elsewhere, results have been reported for depths up to 30 m, given favourable lighting and sea surface conditions (e.g. Tewinkel, 1963; Höhle, 1971), although much lower maximum depths have also been encountered (e.g. Rosenshein *et al.*, 1977; MacPhee *et al.*, 1981).

A different spatial scale of study has been used by Fryer and co-workers to derive three-dimensional coordinates of small areas of sea bottom features and coral reefs (e.g. Holmes, 1982; Fryer, 1983; Tan, 1983; Yong, 1984; Fryer and Kniest, 1985; Fryer, 1987). This work was conducted using a camera mounted on a floating gantry, with a Perspex-covered 6 m x 4 m base area providing a flat water surface of known relative elevation. Using this device and an uncalibrated camera, underwater points up to 3 m below the surface were measured with a standard error in the z-direction of ± 0.014 m (Fryer, 1983). At a similar spatial scale, Butler *et al.* (2001b) examined the roughness of natural gravel beds using a through-water correction for digital photogrammetry. Small areas of gravel riverbed were photographed in both a flume and field environment. In both cases, a Perspex 'lid' was used to flatten the water surface at the time of exposure. The quality of through-water DEMs was assessed using independent check points. Errors in the corrected DEMs were not significantly different from the equivalent one-media DEM (0.000 ± 0.0015 m) for a water depth of 0.12 m (-0.0035 ± 0.0018 m), but degraded for a water depth of 0.25 m (-0.0726 ± 0.0013 m).

2.3 Data quality

Remote sensing methods now permit collection of a wide range of environmental information. In the context of three-dimensional morphological information, Cooper (1998) asserts that the ease with which digital terrain surfaces can now be produced has tended to divert attention away from the quality of the data and towards methods and procedures for manipulating and analysing them. This issue is reinforced by the problem of acquiring sufficient independent check data to reliably assess the quality of data collected by remote sensing methods, due to the increase in data volume permitted by automation of collection and processing procedures.

In many earth and environmental science applications, digital terrain representations serve as inputs for detailed spatial analyses. In hydrology and geomorphology, DEMs

are increasingly being employed as boundary conditions for numerical models of surface water processes and pathways at scales ranging from river catchments to individual channel confluences (e.g. Moore *et al.*, 1991; Romanowicz *et al.*, 1993; Lane and Richards, 1998; Bradbrook *et al.*, 2000). For such applications, appreciation of global and spatially distributed DEM quality can be critical: small variations in surface elevation could dramatically impact modelled surface run-off routes (e.g. Burrough and McDonnell, 1998). Thus, undetected errors can lead to invalid conclusions about the physical processes that the data are intended to help understand (Fryer *et al.*, 1994). The importance of assessing data quality becomes even more critical if two or more surfaces are to be compared to evaluate morphological change (e.g. Lane *et al.*, 1994; Brunsden and Chandler, 1996; Deroose *et al.*, 1998; Willis *et al.*, 1998; Brown and Arbogast, 1999). It is essential to ensure that the coordinate datums are identical and a careful assessment of the magnitudes of errors in the datasets is required before any conclusions can be made about changes in actual terrain (Cooper, 1998).

In this thesis, the term “uncertainty” is used to refer to a lack of knowledge of a true value. This can be thought of as the value that would be obtained if an error-free observation were made using a perfect instrument (Hunter and Goodchild, 1997). Used in this way, it includes uncertainties associated with both the remote sensing methods and data handling procedures used and with any independent measurements used to determine data quality. “Error” is used to denote explicit differences between data obtained from a DEM surface and some true or expected value for that data, although (from the above definition) this value will itself contain uncertainties.

In this research, topographic data was manipulated and presented in the form of regularly-gridded digital elevation models (DEMs) which consisted arrays of elevation measurements (Z-coordinates) ordered by planimetric (X, Y) position. Given that errors occur in three dimensions (X, Y and Z), the correct specification of any point error is the three-dimensional vector difference (\equiv) between the true and measured X, Y, Z position of a corresponding point. However, raster DEMs are based on fixed X, Y arrays meaning that the scope for determining \equiv is reduced. Thus, the smallest planimetric error that can be determined is equivalent to the DEM point spacing in the X and Y directions. In practice this is usually ignored, and it is assumed that a shift in X, Y datums will cause a detectable systematic error in Z-coordinates. Hence, in regularly-gridded DEMs, errors are usually conceptualised as an incorrect assignment of elevation value (E_Z) in just one direction (Z). In reality, the value of E_Z for any given DEM point comprises of systematic error due to datum shifts in the X , Y and/or Z directions and a random distribution of errors values around E_Z (based on the precision

of the method used to collect data). This assumption is also made for information derived from a DEM surface.

2.3.1 Types of error

When any physical quantity is measured, the value obtained is unlikely to be exactly equal to the true value, and uncertainties will always be present. Correspondingly, and irrespective of how they are derived, all DEM surfaces will contain error. Surveyors, and more recently photogrammetrists, have divided errors associated with a measured terrain surface into three groups: random; systematic; and gross (Cooper and Cross, 1988; Cooper, 1998; Butler *et al.*, 1998). Hence, to describe fully the quality of surveyed measurements, it is necessary to consider errors from each category (Cooper and Cross, 1988).

Random error is inherent in any set of measurements, and in the absence of systematic error, causes successive readings to be distributed about the true value of a quantity (Squires, 1968). These inconsistencies cannot be removed by refining the data collection process or by applying corrections. Although the exact effect of random error on a DEM surface and derived parameters is difficult to determine, they can often be assessed and quantified using statistical methods based on a Gaussian distribution. Statistical tests of hypotheses (e.g. Koch, 1987) enable a decision, at a given confidence level, of whether the quality of the measurements is satisfactory. The term “precision” is commonly used in relation to random error (Squires, 1968; Cooper and Cross, 1988; Wise, 2000), and a measurement is said to be precise if the spread of random error is small. Random error may also be quantified experimentally by taking repeat measurements to produce a mean value which approaches more and more closely the true value being measured (Squires, 1968).

A systematic error is one that involves regular or repeated error throughout a set of measurements (Squire, 1968). Unlike random error, they are avoidable in theory and occur through the use of inexact functional models and improperly calibrated equipment (Cooper, 1998). Repeated measurements with the same equipment or functional model neither reveal nor reduce a systematic error, and instead produce a spread of measurements about some displaced value. Consequently, systematic error is potentially more important than random error in a dataset. However, it is often assumed to be negligible and, by implication, unimportant. For instance, the substitution of root mean square error for standard deviation of error in DEM quality assessment (e.g. Torlegård *et al.*, 1986; Monckton, 1996) presupposes an absence of systematic error (Li, 1988). This is discussed further in **Section 2.3.8**. The term

“accuracy” is conventionally used to describe the magnitude of systematic error (Squires, 1968; Cooper and Cross, 1988).

Gross errors, also called blunders, arise through incorrect procedures or intermittent failings in the functional model used. They are inevitable in any set of measurements but can be minimised through incorporation of redundant (duplicate) data. Gross error is often assumed to arise through human mistakes (e.g. Cooper, 1998), but the arrival of automated survey techniques has demonstrated that it can equally arise when measurement is automated (e.g. Nagao *et al.*, 1988; Chandler, 1999). The term “reliability” is used in the context of gross error. Internal reliability relates to the ease with which individual blunders that arise during the survey process can be identified (Cooper and Cross, 1988), with the internal reliability of a DEM used to refer to the size of the marginally detectable gross error. The smaller this value is (such that only gross errors and not true topographic variation is detected), the higher the internal reliability. External reliability relates to the effect of an undetected blunder on information computed from a measurement (Cooper and Cross, 1988), and so on parameters derived from a DEM surface. It has been demonstrated that a high internal reliability necessarily results in a high external reliability (e.g. Pelzer, 1979). However, independent, quantitative measures of both are recommended (Cooper and Cross, 1988).

2.3.2 Sources of error

Error in DEMs is dependent on a number of factors: (i) the way in which data are acquired; (ii) the density and distribution of elevation points measured; (iii) the interpolation method used to transform discrete elevations into a continuous or quasi-continuous surface; and (iv) the characteristics of the terrain being modelled (Desmet, 1997). In reality, these factors are closely interrelated. For example, interpolation quality is closely linked to the spacing of points and the characteristics of the surface, as well as the interpolation method itself (Kubik and Botman, 1976).

2.3.3 Error and data acquisition method

First, the method used to collect data is of fundamental importance. It determines the baseline quality of any measurements, as all information derived is necessarily of equal or lesser quality than the original data. All survey methods will contain random, systematic and gross error, so it is helpful to separate the causes and effects of each before their importance can be properly assessed. **Table 2.5** presents some of the sources of error associated with terrestrial survey, digital photogrammetric and ALS data.

Type of error	Source/cause of error
Random error (precision)	(i) Terrestrial survey – Variation in repeat measurements. (ii) Digital photogrammetry – Low signal-to-noise ratio in source imagery; errors in photo-control point measurement and positioning; terrain type (iii) Airborne laser scanning – Low signal-to-noise ratio of received signal; width of laser beam; timing accuracy of the electronics; laser beam divergence; laser wavelength variations; positional uncertainty of GPS and inertial reference system (IRS); atmospheric transmission properties; terrain type.
Systematic error (accuracy)	(i) Terrestrial survey – Incorrect instrument calibration; atmospheric and geoid effects; instrument errors and incorrect pointing. (ii) Digital photogrammetry – Insufficiently convergent imagery; incorrect camera calibration; incorrect bundle adjustment; non-optimal DEM collection parameters. (iii) Airborne laser scanning – Laser detector bias and gain; laser pulse delay; positional bias of GPS and IRS; use of non-intelligent filtering methods; grain noise.
Gross error (internal reliability, IR, and external reliability, ER)	(i) Terrestrial survey – Incorrect measuring/recording procedures (IR); effect of blunders on derived data (ER). (ii) Digital photogrammetry – Data input errors (IR); mismatches during stereo-matching process (IR); poor block triangulation (IR); effects of viewing geometry and shadow (IR); edge effects (IR); effect of mismatches on derived data (ER). (iii) Airborne laser scanning – Data input errors (IR); multiple signal returns (IR); near-nadir elevation artefacts (IR); loss of phase lock (IR); effect of blunders on derived data (ER).

Table 2.5 Types and sources of error in conventional, terrestrial survey, digital photogrammetry and airborne laser scanning (Cooper and Cross, 1988; Butler et al., 1998; Huisings and Gomes Pereira, 1998; Baltsavias, 1999a; Favey et al., 1999; Lane et al., 2000).

The use of digital photogrammetry to acquire topographic information requires careful consideration of conventional controls upon photogrammetric quality (e.g. Shearer, 1990), as well as recognition of the additional controls introduced by digitisation and automation (Lane et al., 2000). The precision of topographic measurements made using digital photogrammetric methods (p_T) has a one-to-one correspondence with the pixel dimensions of the imagery used, δX (Lane, 2001). Both are related to the flying height (which determines image scale) and the scanning resolution used to convert hard-copy photographs to digital images. For digital cameras this is translated as the flying height and size of pixel array used, but because digital cameras were not used in

this study, they are not considered further. This means that it is possible to predict the maximum precision with which elevation measurements can be made (Shearer, 1990) before the photogrammetric analysis has taken place. The pixel dimensions (in metres), and thus the theoretical vertical precision of photogrammetric measurements (in meters), are given by:

$$\delta X = s \times (\delta x / 1000000) = p_T \quad (2.1)$$

where the photograph scale is 1:s and δx is the scanning resolution used (in microns). The vertical precision, refers to the standard deviation of error (SDE) associated with distribution of photogrammetric measurements, such that a stated precision, $\pm p_T$, is equivalent to one standard deviation. This means that approximately 68% of measurements would be within $\pm p$ of the true value, and around 95% of measurements would be within $\pm 2p$ of the true value.

Digital photogrammetry automates the final stages of the photogrammetric process. In so doing it presents several new uncertainties that have yet to be adequately quantified. Lane *et al.* (2000) identify two particular generic issues. First, digital image creation, usually by scanning hard-copy photographs, can introduce error into the photogrammetric process. Scanning should minimise image distortion and not introduce any systematic errors into derived elevation data. This suggests that high spatial-resolution photogrammetric scanners are required (Smith *et al.*, 1997), and that photographic diapositives should be used (Chandler, 1999) to avoid the possibility of negative-to-print distortions. Second, automation of the stereo-matching process uses numerical algorithms, rather than a human operator, to match corresponding points on the stereo-images. Consequently, the nature of the algorithm and the DEM collection parameters chosen are likely to exert an influence upon final data quality (e.g. Smith *et al.*, 1997; Butler *et al.*, 1998; Gooch *et al.*, 1999).

Airborne laser scanning includes many more variables and unknowns than photogrammetric survey (e.g. Baltsavias, 1999b) making analytical derivation of theoretical error models, assessment of data quality and error propagation analyses more complicated (Baltsavias, 1999a). Nonetheless, several authors have attempted to ascribe an inherent vertical measurement precision to ALS systems, usually around $\pm 0.10\text{-}0.15$ m (e.g. Jonas and Byrne, 1999; Fowler, 2000; Hansen and Jonas, 2000). Airborne laser scanning may also contain systematic error, due mainly to GPS positional inaccuracies in the order of 0.05-0.20 m plus 0.005-0.020 m per 100 m of flying height (Baltsavias, 1999a; Turton and Jonas, 1999). Using ALS, sensor positioning error leads to a rapid heighting quality decrease with scan angle, especially for high flying heights (Baltsavias, 1999a). Data quality with photogrammetric survey

tends to be more homogeneous within the image format used. Furthermore, laser surveys are often flown without accompanying aerial photographs of the area surveyed, making subsequent post-processing and filtering particularly difficult (e.g. Charlton *et al.*, 2001) as there is no simple visual check on surface quality. Ackermann (1999) termed airborne laser scanning a “blind” system because particular objects or features are not optically-distinguished.

2.3.4 Error and data distribution and density

A second control over surface quality is the density and distribution of surveyed points. A terrain surface is a continuous phenomena, so unless every surface point is measured (such that the point spacing in the X and Y direction, δX and δY , tend to zero) there will be error due to spatial sampling. Traditional manual data collection methods (including terrestrial survey and analytical photogrammetry) employ a vector-based sampling strategy, due to limits on δX and δY caused by the trade-off between the spatial extent of study area, spatial density of measured points and the temporal frequency of re-survey. This means that a human operator has control over the distribution of collected points. Such control has been found to be critical, for example, the importance of including features such as breaklines in landform surfaces (e.g. Li, 1992, 1994; Lane *et al.*, 1994; Gong *et al.*, 2000). The movement towards automated DEM collection, produced either using high spatial resolution automated stereomatching (as in digital photogrammetry) or by high spatial resolution randomly sampled points (as in ALS), means that δX and δY relate to pixel size. Because the spatial density of points is only barely related to its cost (Huang, 2000), remote sensing techniques permit a vastly increased spatial resolution of measurements, and values of δX and δY typically much less than those associated with manual methods. Although neither method uses the surface characteristics to explicitly inform collection strategy (Baltsavias, 1999a; Lane *et al.*, 2000), specific feature representation is theoretically less important as relatively small morphological features (in relation to survey area extent) are able to be detected. The main costs are increased file size and increased data generation and processing time (Smith *et al.*, 1997).

2.3.5 Error and interpolation method

A third source of error is the interpolation method used to create a continuous surface from point elevation data measurements. The method chosen will determine the quality of the overall surface as errors in source data will be propagated through the modelling surface to the resulting DEM (Li, 1993b; Wise, 1998). However, and in contrast to the first two factors, relatively little work has been done in this area. As a result, much less is known about error arising during interpolation (Desmet, 1997). Yet, in both digital

photogrammetric and ALS surveys, the method of interpolation used is potentially critical. For ALS, in which a randomly-distributed point elevation dataset, the importance of interpolation algorithm is clear. For digital photogrammetry, because of the raster DEM output ultimately produced, the importance of interpolation may be overlooked. However, assuming that the stereo-matching success rate is less than 100% (in which case a true raster DEM is produced), the initial output from the automated stereo-matching process will also be a randomly-distributed point elevation dataset. Interpolation is subsequently performed, as part of the automated process, to convert this vector coverage into a raster gridded DEM. Thus, the importance of interpolation increases as stereo-matching performance deteriorates. For the purpose of gridding high-resolution datasets, the interpolation scheme should be able to handle large quantities of data and should, as far as possible, honour the sampled data points (Carter and Shankar, 1997). Commonly, bilinear interpolation (e.g. Delaunay triangulation) or kriging are used to grid surface data. However, Desmet (1997) found that for regularly-spaced data, kriging produced topographic artefacts which negatively affected the quality of the DEM surface. It is likely that optimum interpolation type is terrain and data-distribution specific, with computational time and resources an important additional consideration.

2.3.6 Error and terrain characteristics

Finally, the characteristics of the terrain surface itself will control the ability of remotely sensed topographic measurements and the resulting modelled surface to represent it correctly. It is well established that terrain roughness exerts a strong control over the quality of DEM surface (e.g. Li, 1993a,b; Huisng and Gomes Pereira, 1999; Huang, 2000). This has been demonstrated experimentally on several occasions for a variety of scales and terrain types, using both digital photogrammetry and ALS (e.g. Torlegård *et al.*, 1986; Smith *et al.*, 1997; Butler *et al.*, 1998; Kraus and Pfeiffer, 1998; Gomes Pereira and Wicherson, 1999; Petzold *et al.*, 1999; Gong *et al.*, 2000; Lane *et al.*, 2000).

There are a number of explanations for this. First, complex relief can lead to small lateral displacements in X,Y position being translated as significant errors in Z elevation (Huisng and Gomes Pereira, 1998; Baltsavias, 1999a). If a surface is relatively flat, errors in X and Y will be less significant, but planimetric errors will become increasingly significant on sloped or complex terrain (Baltsavias, 1999a). Second, the presence of vegetation or surface water will introduce errors into remote measurements of ground surface elevation. Where vegetation occurs, the vegetative top will be detected by both digital photogrammetry (e.g. Deroose *et al.*, 1998; Brown and Arbogast, 1999; Lane *et al.*, 2000) and ALS (e.g. Ritchie *et al.*, 1994; Ritchie 1996; Hofton *et al.*, 2000). For

inundated areas, digital photogrammetry will either see a distorted inundated bed due to the effects of refraction (e.g. Butler *et al.*, 2001b) or will fail to identify successfully any corresponding points from the raw imagery (e.g. Brown and Arbogast, 1999). Single-frequency ALS systems will generally represent water bodies as planar surfaces (e.g. Ritchie *et al.*, 1994), although Huisings and Gomes Pereira (1998) report that waves in shallow coastal water reflected the laser beam differentially.

There are also sensor specific issues that should be considered. Digital photogrammetry, like any passive optical sensor, will be affected by shadow and apparent relief displacement effects, which are likely to exert indirect influence over measurement quality through mismatching (e.g. Deroose *et al.*, 1998; Lane *et al.*, 2000; Carbonneau *et al.*, in press). These factors are most important when relief is great relative to camera height, or when sun angle is low relative to relief. Airborne laser scanning can produce large errors or failed measurements in areas of rough terrain. A laser scanner typically operates with a phase measurement technique requiring an initial vertical accuracy of about 75 m. If local relief exceeds this value, the phase lock may be lost and measurements will not be made (Favey *et al.*, 1999).

2.3.7 Assessment of error

The importance of error in determining the utility of a DEM makes correct designation of error magnitude in DEM surfaces an important topic. However, there appears to be no single method of parameterising DEM quality that has universal support. Instead, a number of alternative methods exist. Furthermore, the terms employed to examine types of error and error detection techniques are often incorrectly defined and used.

In the context of the aims of this research, methods of error assessment will be divided into two broad categories: (a) those associated with single DEM surfaces, here called static measures of error; and (b) those associated with DEMs of difference, here referred to as dynamic measures of error.

2.3.8 Assessment of static-DEM error

There are four types of methods that may be applied to single DEM surfaces in order to detect error: (i) visual assessment; (ii) external assessment; (iii) internal assessment; and (iv) assessment of derived parameters.

First, qualitative assessment of DEM surfaces using visualisation techniques such as raster images, shaded relief maps, ortho-rectified imagery and, more recently, three dimensional viewsheds and photo-realistic views, allow rapid qualitative assessment of how closely a DEM surface resembles the known terrain (e.g. Carrara *et al.*, 1997; Pyle *et al.*, 1997; Huisings and Gomes Pereira, 1998; Brown and Arbogast, 1999; Walker and

Wilgoose, 1999; Lane *et al.*, 2000; Chandler *et al.*, 2001). Gross error can be easily identified as ‘spikes’ or ‘pits’ in the DEM surface (e.g. Ritchie *et al.*, 1994; Brunsden and Chandler, 1998; Butler *et al.*, 1998; Huisng and Gomes Pereira, 1998). In many cases visual assessment should form an important first step in determining the nature of DEM error, helping to inform subsequent quantitative error assessment methods.

Second, external or “empirical” (Li, 1992) methods are those which quantitatively compare a DEM surface to independent check measurements made to a known higher order of quality (Shearer, 1990; Wise, 2000). Conventionally, the degree of correspondence between DEM heights and true heights is reported as the root mean square error (RMSE), given by:

$$\text{RMSE} = \pm \sqrt{\frac{\sum_{i=1}^n d_i^2}{n}} \quad (2.2)$$

where d is height difference between the DEM and check point, and n is the number of check points. Traditionally, error in topographic measurements and DEMs has been reported in terms of RMSE (e.g. Harris and Umbach, 1972; Ackermann, 1978; Torlegård *et al.*, 1986; Huisng and Gomes Pereira, 1998; Satalich and Ricketson, 1998; Brown and Arbogast, 1999; Gomes Pereira and Wicherson, 1999; Gong *et al.*, 2000; Wise, 2000; Chandler *et al.*, 2001), and error specifications from commercial bodies are also frequently in terms of RMSE (e.g. USGS, 1987; OS, 1992; FEMA, 2000). The term “standard error” is also sometimes employed to describe the same measure of error (Shearer, 1990; e.g. Lo and Wong, 1973; Fryer, 1983; Bolstad and Stowe, 1994). Li (1988) has advocated reporting the standard deviation of error (SDE) in place of the RMSE, given by:

$$\text{SDE} = \pm \sqrt{\frac{\sum_{i=1}^n (d_i - ME)^2}{n}} \quad (2.3)$$

with

$$ME = \sum_{i=1}^n \frac{d_i}{n} \quad (2.4)$$

and where the mean error, ME, is necessarily reported too (Monckton, 1996). The only difference between **Equations 2.2** and **2.3** is the inclusion of ME in the expression for SDE, reinforcing the assumption made when RMSE is calculated that there is no mean error, meaning no systematic bias, in the DEM surface (Li, 1988). This assumption is frequently ignored in practice, with RMSE calculated and stated even when a systematic bias has been shown to exist (e.g. Bolstad and Stowe, 1994; Huisng and

Gomes Pereira, 1998; Satalich and Ricketson, 1998; Gomes Pereira and Wicherson, 1999). Hence, RMSE is both presumptive of negligible systematic bias (Li, 1988) and conflates systematic and random error (Wise, 2000) which are correctly considered independent of each other. The coupled use of ME and SDE is gradually being adopted (e.g. Li, 1992; Monckton, 1996; Desmet, 1997; Butler *et al.*, 1998; Lane *et al.*, 2000), with ME a measure of systematic error (and DEM accuracy) and SDE an indicator of random error (and DEM precision).

Gross error in DEM surfaces are assessed empirically with reference to extreme errors. The values of extreme errors are given by d_{min} and d_{max} , which represent the largest negative and positive elevation deviations between DEM and check point elevations (e.g. Li, 1988, 1992; Desmet, 1997; Heritage *et al.*, 1998). However, in the context of assessing DEM internal reliability and identifying gross errors in a DEM surface, this measure is not particularly useful as it will, by definition, include all gross error values. Instead, a measure of maximum error expected based on an assumed Gaussian distribution is sometimes proposed (e.g. Torlegård *et al.*, 1986; Shearer, 1990) whereby maximum expected error (MEE) is ± 3 SDE. Given that 99.73 % of deviations are expected to fall between -3 SDE and $+3$ SDE of the mean (ME), this measure excludes the extreme 0.27 % of deviations (or the maximum and minimum 0.135 % of deviations, respectively) which can be assumed to be blunders.

An inherent feature of empirical measures of DEM quality is that a form of space-time substitution is assumed. Point error is most correctly determined by repeat measurement at the same point, which allow a distribution of errors to be obtained and ME and SDE calculated (e.g. Squires, 1968; Taylor, 1997). However, the equivalent measures of error associated with a DEM surface are determined by making one set of simultaneous measurements at several points in space. In so doing, the resulting distribution of errors combines errors related to measurement technique itself with uncertainties associated with the spatial sampling used to obtain the independent check points.

Other criticisms have also been levelled at empirical measures of error. These are often centred around the fact that they are invariably based on a very small sample of check points (typically less than 5% of all DEM points; e.g. Butler *et al.*, 1998; Huisings and Gomes Pereira, 1998; Lane *et al.*, 2000). Thus, they are unlikely to be representative of the DEM surface as a whole (Wise, 2000). Furthermore, these measures are “global” (Hannah, 1981) and aggregated across the entire DEM surface, so they tell us little about local variations in error (although, apart from obtaining a

sufficient density of check points, there is nothing to prevent measures such as ME and SDE being calculated on a more local basis).

The third type of static DEM error assessment methods are internal measures, which refer to any error assessment method which uses only information held within the DEM surface. These are particularly appropriate when no or little independent check data are available. Such methods are often based on traditional geostatistical techniques, formerly used to estimate unknown values but now employed to assess surface uncertainty (Atkinson, 1999). Generally, they are based on comparison of pixel values with neighbouring pixels, leading to identification of the spatial structure of error present in a DEM surface. These descriptors of error have been variously termed “theoretical models” (Li, 1993; Monckton, 1996) and “simulation methods” (Liu and Jezek, 1999), and are often considered more “local” (Hannah, 1981; Polidori *et al.*, 1991) than the measures of ME, SDE and RMSE.

A summary of internal methods used to assess the quality of DEM surfaces is given in **Table 2.6**. Of these, a particularly elegant method is proposed by Felicísmo (1994), employing the elevation difference between each DEM pixel and the elevation of the same point as interpolated from neighbouring pixels. This allows production of a distribution of elevation differences, which if assumed to be Gaussian in shape, allows statistical tests to be performed to determine whether each individual deviation value belongs to the population of deviations (Felicísmo, 1994). Disadvantages of such techniques include: (i) that many are based on mathematical models of terrain which are unlikely to apply in the real world (Monckton, 1996); (ii) that they may require tedious and computationally-demanding mathematical procedures (Florinsky, 1998); and (iii) that they do not represent a reliable estimate of DEM quality (Li, 1994). In addition, they are inevitably suited to smooth terrain (Wise, 2000), as sudden breaks of slope will generally be identified as in error (e.g. Hannah, 1981).

An alternative strategy for internal assessment of DEM errors is to perform overlap analysis, also called “crossover analysis” (Hofton *et al.*, 2000). This entails using any areas of data overlap to calculate elevation deviations, and then treating the distribution of deviations in the same way as when independent check data is available (i.e. calculation of ME, SDE, RMSE, MEE, etc.). Despite reporting of this method for both digital photogrammetry (e.g. Pyle *et al.*, 1997; Stojic *et al.*, 1998; Huang, 2000) and ALS (e.g. Fraser *et al.*, 1999; Hofton *et al.*, 2000), it does not appear to have been widely adopted. However, it is potentially a very attractive method of assessing DEM quality in the absence of independent check data.

Internal method of error assessment	Examples
Point elevation comparison with immediate neighbours	Hannah (1981); Nagao <i>et al.</i> (1988); Felicísmo (1994)
Elevation histograms	Carrara <i>et al.</i> (1997)
Autocorrelation and semi-variogram construction	Kubik and Botman (1976); Frederiksen <i>et al.</i> (1986); Polidori <i>et al.</i> (1991); Brown and Bara (1994); Liu and Jezek (1999); Lane (2000)
Autocorrelated random fields	Ehschlaeger <i>et al.</i> (1997); Hunter and Goodchild (1997)
Principle component analysis	Lopez (1997)
Fourier analysis	Makarović (1972; 1974); Frederiksen (1981); Liu and Jezek (1999)
Spectral analysis	Tempfli (1980)
Monte Carlo simulation	Openshaw <i>et al.</i> (1991); Lee <i>et al.</i> , (1992); Davis and Keller (1997)
Stochastic conditional simulation	Kyriakidis <i>et al.</i> (1999)

Table 2.6 Examples of internal methods of error assessment used to assess the quality of terrain surfaces.

The final type of static DEM error assessment method uses derived parameters. An important general limitation of all static DEM error assessment methods considered up to now is that they consider only point elevation values, in which relatively small errors could lead to larger errors in parameters derived from the DEM surface such as slope and aspect (Wise, 1998). Hence, one of the most potentially fruitful approaches to error assessment, yet one which is not particularly widely developed nor adopted (Lane, 2000), involves assessment of derived parameters or external reliability. Rather than focusing on elevation values, it considers some intended purpose of a DEM, and will likely be more sensitive to errors and artefacts (Ley, 1986). Work in this field has centred on empirical approaches (Wise, 2000), including visual assessment of plots of derivative values (e.g. Wood and Fisher, 1993; Lane *et al.*, 2000) and comparison of derived values with independently-measured data (e.g. Bolstad and Stowe, 1994; Giles and Franklin, 1996). Such work is a step towards approaches in which the quality of a DEM surface is judged in terms of the quality of output produced from it, for example, variations in predictions of floodplain extent (Lee *et al.*, 1992), predictions of soil erosion (Desmet, 1997) and derivation of drainage networks (Wise, 2000).

A key point to emerge from analyses of this type is that the assessment of DEM quality should be carried out in the context of the purpose of the DEM. Inaccurate points in a DEM surface are not necessarily a serious problem if those inaccuracies have minimal effect upon the derived parameters that are of interest (Lane, 2001) and, therefore, DEM quality is sufficient for the particular task (Wise, 2000).

2.3.9 Assessment of dynamic-DEM error

In the context of assessing the feasibility of using the morphological method to estimate sediment transport rates, we need to be confident that changes observed and quantified in the DEMs of difference represent 'real' morphological change, as opposed from those produced by errors in each surface. Elevation change at each pixel (Δh) is given by:

$$\Delta h = m_b - m_a \quad (2.5)$$

where m is the measured elevation of a corresponding point in successive DEM surfaces, a and b . Since each measured point elevation will consist of the true elevation value and an error, elevation change is more correctly given by

$$\Delta h = (h_b \pm e_b) - (h_a \pm e_a) \quad (2.6)$$

where h is the true elevation and e is the associated error of a corresponding point in successive DEM surfaces. In the absence of knowledge about the precision of each point (i.e. e in **Equation 2.6**), a global measure of precision is used, conventionally RMSE (**Equation 2.2**) or, more correctly, SDE (**Equation 2.3**). This expression forms the basis for all DEM of difference calculations.

The magnitude of Δh will be affected by systematic, random and gross error in the DEM surfaces used. Systematic error will tend to introduce bias into the value of Δh , which translate into apparent yet erroneous elevation increases or decreases in the DEM of difference. Visual or statistical assessment of a DEM of difference will not necessarily highlight systematic bias, unless there is prior knowledge of the maximum elevation change that occurred or of zones of no change (which in principle allows systematic error to be detected and the DEM of difference 'calibrated' to reduce it to a negligible level). Gross error will appear as erroneous elevation change, often in the form of one or a few grouped pixels showing erroneously large elevation change. It is typically relatively easy to identify and eliminate using visual or numerical methods.

The effect of random error in a DEM of difference is to introduce uncertainty about the minimum elevation change that can be distinguished from background noise. When calculating a DEM of difference, since both surfaces used will contain random error, it becomes necessary to define the minimum level of detection (Brasington *et al.*, 2000) that it is possible to achieve. In the absence of systematic error, analytical error propagation theory can be used to predict the total uncertainty associated with random errors in a mathematical function (e.g. Squires, 1968; Taylor, 1997; Burrough and McDonnell, 1998).

To estimate the maximum random error associated with differencing of DEMs, the precision associated with DEMs h_a and h_b are assumed to be $\pm p_a$ and $\pm p_b$, where p_a and p_b are a function of the spread of the error distribution (i.e. RMSE or SDE; Taylor, 1997). Hence, the maximum probable random error, e_{max} , associated with the function $\Delta h = h_b - h_a$ is given by:

$$e_{max} = \pm(p_a + p_b) \quad (2.7)$$

However, this expression will invariably overestimate average uncertainty due to random error (Taylor, 1997), because for the actual value of e to equal its highest or lowest extreme, both h_a and h_b would have to be overestimated or underestimated by their full amounts, $\pm p_a$ and $\pm p_b$. If h_a and h_b are independent of each other and the uncertainties are random, there is a relatively small probability that this will happen. For example, if p_a and p_b represent SDE and are from a normally distributed population, the probability that both h_a and h_b are underestimated by their full amounts is only around 2% ($15.7\% \times 15.7\%$). Given that there is an equally low probability that both h_a and h_b are overestimated to their full amounts, it is far more likely that the true uncertainty will fall somewhere in between the two extreme positions.

Consequently, a more realistic measure of final uncertainty due to random errors is given when the precision (or SDE) values themselves are added in quadrature (i.e. the root of the sum of squares). Following the proof of Squires (1968), and again considering the case of $\Delta h = h_b - h_a$, where $\pm p_a$ and $\pm p_b$ are the associated precision (SDE), then the error associated in Δh ($e_{\Delta h}$) is:

$$e_{\Delta h} = c_a p_a + c_b p_b \quad (2.8)$$

where the coefficients c_a and c_b are given by:

$$c_a = \frac{\delta \Delta h}{\delta h_a} \quad \text{and} \quad c_b = \frac{\delta \Delta h}{\delta h_b} \quad (2.9)$$

The partial derivatives are evaluated at $a = a_0$, $b = b_0$, so from **Equation 2.8**:

$$e_{\Delta h}^2 = c_a^2 p_a^2 + c_b^2 p_b^2 + 2c_a c_b p_a p_b \quad (2.10)$$

Taking the average for pairs of values of h_a and h_b , and assuming h_a and h_b to be independent, the average value of $p_a p_b$ is zero. Therefore:

$$e_{\Delta h}^2 = c_a^2 p_a^2 + c_b^2 p_b^2 \quad (2.11)$$

From **Equation 2.9**, $c = 1$ for a linear function (Squires, 1968). Therefore, the global precision, $e_{\Delta h}$, predicted due to random error in a DEM of difference ($\Delta h = h_b - h_a$) is given by:

$$e_{\Delta h} = \sqrt{p_a^2 + p_b^2} \quad (2.12)$$

This will always produce a final uncertainty less than that predicted by **Equation 2.7** (Taylor, 1997).

This discussion also highlights the potential utility of using DEMs of difference as a method of assessing DEM quality. By subtracting one surface from another, the relative uncertainty associated with the final surface is the largest that can be obtained with any simple arithmetic function (**Table 2.7**), and consequently, subtraction of surfaces is often advised against (e.g. Burrough and McDonnell, 1998). However, if considered spatially, the high relative errors obtained tend to highlight areas where errors are likely to be present in the DEMs used in the differencing procedure. Therefore, DEMs of difference are potentially a very powerful DEM quality assessment tool.

Relation between u and a,b	Analytical propagation of random error	$a \pm d_a$	$b \pm d_b$	Final value, u	Final error, d_u	Relative error (%)
$u = a + b$	$(d_u)^2 = (d_a)^2 + (d_b)^2$	12±2	8±1	20	±2.24	±11.2
$u = a - b$		12±2	8±1	4	±2.24	±56.0
$u = ab$	$(d_u/u)^2 = (d_a/a)^2 + (d_b/b)^2$	12±2	8±1	96	±19.7	±20.8
$u = a/b$		12±2	8±1	1.25	±0.260	±20.8
$u = a^2$	$(d_u/u)^2 = 2(d_a/a)$	12±2	n/a	144	±48.0	±33.3
$u = a^3$	$(d_u/u)^2 = 3(d_a/a)$	12±2	n/a	1728	±862.5	±50.0
$u = \log_e a$	$d_u = d_a/a$	12±2	n/a	2.48	±0.167	±6.7
$u = e^a$	$d_u/u = d_a$	12±2	n/a	162755	±3255	±2.0

Table 2.7 Propagation of error in simple functions (modified from Squires, 1968).

2.4 Chapter summary

The problems identified in **Chapter 1** with using conventional, terrestrial survey techniques to obtain morphological information from river environments, particularly if the spatial area is large, has led many researchers to seek alternative methods. One possibility is the use of remote sensing.

This chapter has presented a review of applications of remote sensing techniques, focussing in particular on the use of aerial imagery, photogrammetry and ALS. Special consideration was given to acquiring topographic data from submerged areas of the riverbed. For this purpose, image analysis techniques and through-water photogrammetry have both been successfully used. Previous work that has been

carried out in this area represents the context for this research, and informs the project design required for the implementation of digital photogrammetric and ALS surveys of large, gravel-bed rivers (**Chapter 3**).

Given the increasing automation of remote sensing-based data collection methods and the increased data volume which often results, the quality of information acquired is an important consideration. Recognition of three distinct types of surface error (systematic, random and gross) helped allow their respective sources to be identified. It also assisted in the identification of different error assessment methods, and consideration was given to how different methods could be used to quantify different types of error. Analytical error propagation, to estimate the random error associated with DEMs of difference, was also undertaken. This interpretation of types of error, sources of error and error assessment methods will be used to inform decisions about the quality of DEMs (**Chapters 4 and 6**) and DEMs of difference (**Chapter 7**) generated for large, gravel riverbeds later in this study.

CHAPTER 3. PROJECT DESIGN AND METHODOLOGY

From the discussion of the problems associated with conventional, terrestrial methods of obtaining topographic data from river environments (Chapter 1), and given the ability of remote sensing techniques to address these issues (Chapter 2), digital photogrammetry and airborne laser scanning represent two potentially attractive methods of surveying gravel riverbeds. However, large, gravel riverbeds represent an extreme case, meaning that project design becomes critical (3.1). In this chapter, the Canterbury Plains are introduced (3.2), and the Waimakariri (3.2.1) and North Ashburton (3.2.2) study reaches are described. Next, the theoretical and practical aspects of acquiring DEMs of large, gravel riverbeds using digital photogrammetry (3.3) and airborne laser scanning (3.4) are detailed, including discussion of the specific project design used in this research. For digital photogrammetry, this comprises basic principles (3.3.1), image acquisition (3.3.2), digital image creation (3.3.3), photogrammetric control (3.3.4), block triangulation (3.3.5) and DEM and ortho-image creation (3.3.6). For airborne laser scanning, this comprises basic principles (3.4.1), project design (3.4.2), data acquisition (3.4.3) and data post-processing (3.4.4). Finally, the independent check measurements made to help with quality assessment of the remote surveys are described (3.5).

3.1 Introduction

Project design is a critical aspect of any topographic survey. This is particularly true when data is to be obtained using remote sensing techniques, given the trade-off between the extent of image coverage and surface representation (Lane, 2000). Large, braided, gravel riverbeds represent an extreme case due to their large spatial extent (typically $10^2\text{--}10^3$ m width) relative to small vertical relief (typically less than 2 m). In order to use remote sensing methods to survey this topography successfully, as well as to detect the breaks of slope that may be necessary for good surface representation (Li, 1992; Lane *et al.*, 1994), lower flying heights and larger scale imagery are desirable. However, for reasons of financial cost, processing time and data management, it is preferable to use a larger flying height and smaller scale imagery. Thus, any remote sensing project must be designed so as to give sufficient data density and precision with as wide a spatial coverage as is possible (Lane, 2000). Two aspects of project design are considered here: selection of study sites; and acquisition and processing of remote-sensed data.

3.2 Study sites

For this research, two study sites were selected: the North Ashburton River and the Waimakariri River. Both are large, braided rivers that flow eastwards across the

Canterbury Plains, South Island, New Zealand (**Figure 3.1**). The Canterbury Plains extend for about 180 km along the eastern coast of South Island, and are divided into sections by a sequence of large, braided rivers that drain the Southern Alps.

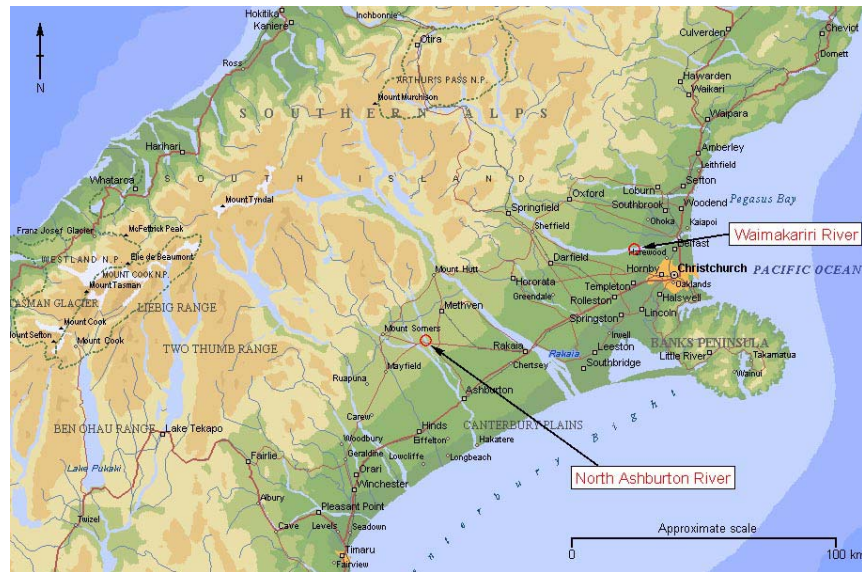


Figure 3.1 The North Ashburton and Waimakariri Rivers, South Island, New Zealand (Copyright © Microsoft Encarta Virtual Globe 1998). The approximate locations of the study sites are circled in red.

3.2.1 The North Ashburton River

The North Branch of the Ashburton River (**Figure 3.2**) drains around 300 km² of steep greywacke terrain in the Southern Alps and has been described in detail by Laronne and Duncan (1992). The lower catchment, across the inland Canterbury Plains from the alpine foothills to the confluence with the South Branch, comprises of around 80 km² of Pleistocene gravels and sands. The study reach (**Figure 3.3**) is around 400 m in length, and is located immediately upstream of Thompson's Track bridge. Here, the riverbed is around 100 m wide, although it has been substantially narrowed from an earlier width of about 500 m by the planting of willow-trees. Aggradation has been measured in the reach since 1937, with a wedge of bed material accumulating at an average rate of 0.058 m per year. The braidplain surface is characterised by a mixture of medium to coarse gravels and sand, with d_{50} reported as 25.8 mm by Laronne and Duncan (1992). At normal-low flows (20 m³/s), the North Ashburton is a shallow river with clear water (very low turbidity), meaning that in most areas the bed can be clearly seen on vertical aerial photographs. The entire riverbed is submerged at flows of around 100 m³/s (Duncan, pers. comm.).



Figure 3.2 The North Branch of the Ashburton River. Flow is towards the camera.



Figure 3.3 The North Ashburton study reach, looking upstream from Thompson's Track bridge.

The study site was chosen due to prior availability of stereo photographs and an extensive independent ground survey dataset, measured using Total Station (Willsman, 1995), and available for use as check data. Good road access and comparative lack of vegetation were also important considerations for subsequent surveys.

3.2.2 The Waimakariri River

The Waimakariri is one of the largest rivers of the Canterbury Plains, and has been described previously by Griffiths (1979b). The headwaters of the river occupy relatively

confined bedrock channels. After emerging from the high mountains, the river develops a large, braided form, interrupted only by three narrow gorges (**Figure 3.4**). Downstream of the Lower Gorge, the river flows in a progressively shallowing trench across the Canterbury Plains. The river reaches Plains level around 18 km from the river mouth. Downstream of this, the degree of braiding decreases until about 10 km from the mouth, where the river becomes essentially single-thread (Carson and Griffiths, 1989). The riverbed remains gravel-bedded until around 2.5 km from the mouth, at which point it becomes a sand bed river.

The field site chosen for this research was a 3.3 km long reach of the lower Waimakariri River (**Figure 3.5**), approximately centred on Crossbank. Crossbank is a major transverse stopbank, part of a large network of groynes and stopbanks that have dramatically narrowed the active riverbed in the last 70 years to protect the city of Christchurch. It is located a few kilometres to the south and built partly on former Waimakariri floodplain. The width of the active bed has been reduced from around 4 km to around 1 km at the study reach. Consequently, the entire bed becomes inundated in flood flows greater than about 800-1000 m³/s (Hicks *et al.*, 2001), which typically happen several times each year. The mean flow is approximately 120 m³/s, so that under normal flow conditions much of the active riverbed is exposed (**Figure 3.6**). The vertical relief in the study reach is small, generally less than 2 m, with a mixed gravel bed with a d₅₀ of around 28 mm (Carson and Griffiths, 1989). Average channel depth during low flows is typically less than 1.3 m (Hicks *et al.*, 1999b), but the higher water turbidity of the Waimakariri compared to the Ashburton means that although the bed is visible the bed texture is not distinct on vertical colour aerial photographs.

Following reconnaissance of several potential sites on the lower Waimakariri, the study reach was chosen for a number of reasons (Hicks *et al.*, 1999b), including proximity to the NIWA office in Christchurch, comparatively pronounced vertical relief, relatively shallow and distributed flow, a lack of vegetative cover and the history of previous work, most notably by Griffiths (1979b) and Carson and Griffiths (1989). The study reach occupies a significant position in the Waimakariri long profile, centred on Crossbank, which is believed to be the current location of the river's hinge point (Griffiths, 1979b). Upstream of this point the Waimakariri has historically degraded, while downstream it has aggraded (Hicks *et al.*, 1999b). The choice of study reach length was based on the step length (900 m) and meander wavelength (1400 m) proposed by Carson and Griffiths (1979). The 3.3 km reach used in this study exceeds three step lengths and two meanders, and includes five of the approximately 800 m-spaced cross-sections used by the local regional council, Environment Canterbury (EC), for long term monitoring of bed level changes (Hicks *et al.*, 1999b).



Figure 3.4 The Waimakariri River confined at the Lower Gorge. Flow is towards the camera (copyright © Peter Morath/Hedgehog House Press).



Figure 3.5 The Waimakariri study reach from the air, looking downstream. The location of Crossbank is marked (photograph courtesy of Andrew Westaway, December 1999).



Figure 3.6 The Waimakariri field site as seen from the ground. The disparity between spatial extent and vertical relief is clearly demonstrated.

Topographic data was acquired from both reaches using two remote sensing methods, digital photogrammetry and airborne laser scanning (ALS). The latter was only used for the Waimakariri.

3.3 Digital photogrammetry

3.3.1 Principles

The majority of remote sensing surveys carried out for this research were performed using digital photogrammetry. The photogrammetric method is explained at length elsewhere (e.g. Slama, 1980; Ghosh, 1988; Lane *et al.*, 1993; Wolf and Dewitt, 2000). It is based upon the geometric relationship between a three-dimensional object, a two-dimensional image of the object, and the camera lens. To illustrate this, we can assume a perspective projection (Slama, 1980), whereby a straight line passes through a point in the object space (*A*), the perspective centre of the camera lens (*O*) and the image of that point in the image space (*a*) (**Figure 3.7**).

Under this condition, the relationship between the two-dimension coordinates of any image point and its corresponding three-dimensional object-space position can be described as (Ghosh, 1988):

$$\begin{bmatrix} x \\ y \\ -c \end{bmatrix} = kM \begin{bmatrix} X - X_0 \\ Y - Y_0 \\ Z - Z_0 \end{bmatrix} \quad (3.1)$$

where (x,y) are the co-ordinates of point *a* in the image space, (X,Y,Z) are the co-ordinates of point *A* in the object space, c is the focal length of the camera, (X_0,Y_0,Z_0)

are the co-ordinates of the perspective centre of the camera lens in the object space, k is a scale factor, and M is the rotation matrix:

$$\begin{matrix} m_{11} & m_{12} & m_{13} \\ m_{21} & m_{22} & m_{23} \\ m_{31} & m_{32} & m_{33} \end{matrix} \quad (3.2)$$

where $m_{11}\dots m_{33}$ are functions of camera orientation, ω , ϕ , and κ (**Figure 3.7**).

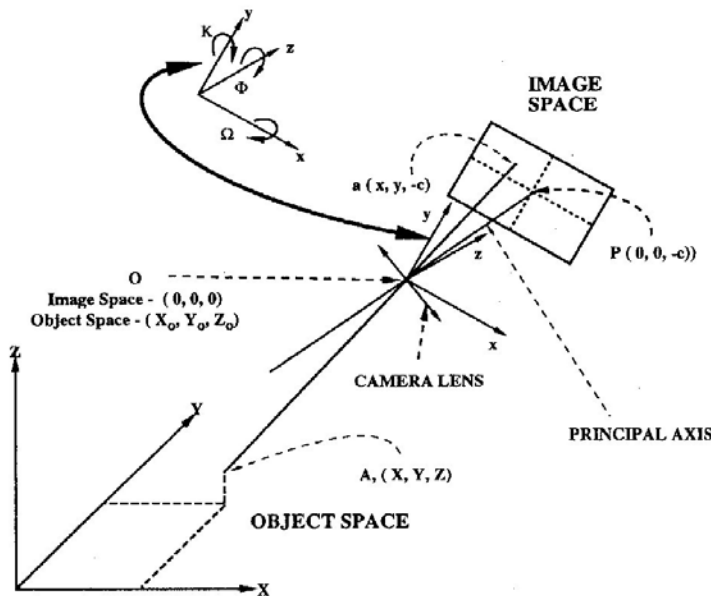


Figure 3.7 The perspective projection: the assumed relationship between object-space, image-space and camera lens (from Lane et al., 1993).

The elements of matrix M , scale factor k and (X_0, Y_0, Z_0) may be considered collectively as the external orientation parameters of the camera (Ghosh, 1988). **Equation 3.1** can be expanded into the collinearity equations, such that the location of every point in the image is described by two equations:

$$x = \frac{-c[m_{11}(X - X_0) + m_{12}(Y - Y_0) + m_{13}(Z - Z_0)]}{[m_{31}(X - X_0) + m_{32}(Y - Y_0) + m_{33}(Z - Z_0)]} \quad (3.3)$$

$$y = \frac{-c[m_{21}(X - X_0) + m_{22}(Y - Y_0) + m_{23}(Z - Z_0)]}{[m_{31}(X - X_0) + m_{32}(Y - Y_0) + m_{33}(Z - Z_0)]} \quad (3.4)$$

Using **Equations 3.3** and **3.4**, the image-space coordinates of the same point measured on two overlapping images is sufficient to calculate the unique (X, Y, Z) position of the corresponding point in the object space, assuming the camera external orientation parameters are first known. These are commonly determined by back-calculation using photograph control points (PCPs), which are natural or artificial

features that can be identified on the imagery (Chandler and Moore, 1989) and for which three-dimensional coordinates are known (Lane *et al.*, 1993). This can be done using a number of mathematical solutions, the most powerful of which is the bundle adjustment (Granshaw, 1980). This solves the collinearity equations using a simultaneous least squares solution. A minimum of three co-ordinated PCPs are necessary, but more points are frequently used (usually at least five) to introduce redundancy into the least squares calculation, in order to increase the precision of parameter estimates (Chandler and Moore, 1989).

In practice, the special case of a perspective projection rarely occurs due to disturbances such as lens distortion and atmospheric refraction (Lane *et al.*, 1993). Atmospheric effects are usually assumed to be negligible for the range of flying heights commonly used in photogrammetric surveys. Lens distortion can be modelled by testing the camera lens under laboratory conditions in order to calculate several well-established lens distortion parameters. Once satisfactory camera parameters are obtained, the collinearity equations can be extended to model these effects (Chandler and Moore, 1989).

The final photogrammetric task is to calculate the three-dimensional coordinates of points in the object-space by identifying corresponding image points on overlapping photographs. Conventionally, this final task was performed manually, with point collection rate and point quality defined by the collection technique selected and skill of the operator. For example, Lane (1994) was able to collect 200 points per hour on average using an Intergraph analytical plotter (Lane *et al.*, 1994). However, digital photogrammetry represents a new phase of photogrammetry (Saleh, 1996) in which the computer becomes the host environment, creating the possibility for new and extended operational concepts and, in particular, process automation (Ackermann, 1996).

Chandler (1999) identified three advantages associated with digital photogrammetry compared with other survey techniques and traditional photogrammetric methods. First, and most importantly, the technique allows the production of high spatial-resolution DEMs using fully automated stereo-matching and image-processing algorithms. This automation allows regularly-spaced raster DEMs of quantifiable precision to be derived at rates exceeding 100 times those provided by earlier manual photogrammetric methods (e.g. Lane, 1994), and exceeding 1,000 times those provided by conventional ground survey methods (e.g. Ferguson and Ashworth, 1986). Second, software packages that carry out the photogrammetric processing are now available commercially, such as ERDAS Imagine OrthoMAX, PCI/EASI-PACE, R-WEL/Desktop Mapping System and VirtuoZo (Chandler, 1999). This software has been developed for

a wide market, including non-photogrammetrists, and so the technique has been opened to a far greater range of users (Chandler and Padfield, 1996). Third, because such software runs on relatively cheap and readily available UNIX and NT workstations, it is now unnecessary to invest in specialised and expensive photogrammetric hardware.

Digital photogrammetric processing involves several stages: image acquisition; creation of digital images; photogrammetric control; block triangulation; and DEM and ortho-image generation.

3.3.2 *Image acquisition*

Photogrammetric survey relies on the acquisition of suitable stereo-imagery. Overlapping images may be obtained terrestrially (e.g. Lo and Wong, 1973; Lane *et al.*, 1994; Pyle *et al.*, 1997; Chandler and Ashmore, 2001), from an airborne platform (e.g. Salgueiro, 1965; Brunsden and Chandler, 1996; Derose *et al.*, 1998; Brown and Arbogast, 1999; Lane *et al.*, 2000) or from a satellite platform (e.g. Gugan and Dowman, 1988; Bolstad and Stowe, 1994; Giles and Franklin, 1996). The decision on the method of image acquisition rests on both theoretical and practical considerations.

The theoretical basis of photogrammetric design can be used to determine the design required to obtain a required vertical precision. It is well established that the vertical precision of photogrammetric measurements is directly related to the image pixel dimensions in the object-space (Lane, 2001). This means the theoretical precision can be estimated using **Equation 2.1**. The best possible spatial resolution is about five times the object-space pixel dimensions (Lane *et al.*, 2000). Thus, for a given application of photogrammetry, a desired spatial resolution and/or level of precision can be established by altering either image scale (therefore, flying height) or scanning resolution accordingly. Scanning resolution is often constrained by the physical limits imposed by the scanner and consideration of digital file size. Digital file size will increase by four as scanning resolution is doubled, which means that scanned image files often become very large. For example, a standard format aerial photograph scanned at 15 microns will produce a digital file of over 200 Mb in size. Consequently, flying height is more usually altered in order to provide the desired photogrammetric spatial resolution and precision. In principle, this means that low flying heights are preferable, since the density and precision of photogrammatically-measured points will be maximised. However, the disadvantage of reducing flying height is that the spatial coverage per image is reduced, which means that multiple flying lines, increased data volume, and increased processing time will be required. Consequently, it is desirable to maximise flying height for a given level of photogrammetric precision.

The main practical consideration is the availability of suitable sensor platforms. For terrestrial photogrammetry, this requires vantage points overlooking the study site, with a recommended minimum angle of incidence of 30° (e.g. Chandler and Ashmore, 2001). In the case of gravel-bed rivers, this has previously been achieved by establishing exposure stations on areas of high relief immediately adjacent to the area of interest (e.g. Lane *et al.*, 1994; Stojic, 2000; Chandler and Ashmore; 2001). For airborne and satellite-mounted sensors, the main practical consideration is the temporal control available. This is maximised if specially-commissioned aerial photography is used, but else is limited to when aerial photographs are available, or by the frequency of satellite passes. Temporal control of imagery can also be reduced by poor visibility or cloud cover.

For the study reaches selected for this research, terrestrial photography was neither feasible due to the relative lack of relief in the surrounding areas nor appropriate given the width of the gravel riverbeds measured. For example, to obtain an angle of incidence of 30° to the Waimakariri channel centre, a bank-mounted camera would have had to be positioned at a height of over 400 m. Satellite-mounted sensors, despite recent increases in the spatial density of points such as the 1 m panchromatic scans available from IKONOS and OrbView (Jensen, 1996; Lane, 2001), are still unable to match airborne photography in terms of spatial resolution. Given the relationship between object-space pixel dimensions, photogrammetric planimetric point spacing and photogrammetric vertical precision explained above, 1 m pixels (the smallest currently available from commercial satellites) would represent a minimum point spacing of 5 m and a theoretical vertical precision of ±1 m. At this spatial resolution, many smaller riverbed features (e.g. channel banks and smaller channels) would not be well represented, and the vertical precision would not be acceptable relative to the typical riverbed relief (less than 2 m) (Lane, 2001). Furthermore, specially-commissioned aerial photographs were available for this research which offered far greater temporal control with respect to capturing the riverbeds at low flows between flood events.

For the purpose of this research, an aircraft-mounted camera was used to obtain purpose-flown near-vertical colour aerial photographs of each study reach. Flights were scheduled for days when discharge was low, such that a large proportion of the riverbed was not inundated, and when there were clear or lightly overcast skies (Hicks *et al.*, 1999b). All photography was carried out between 11:00 and 15:00, during the summer months, to ensure that the sun was high in the sky and to minimise shadows and water surface glare.

For the North Ashburton River, two sets of aerial photographs were obtained (**Table 3.1**). Both flights were operated by Air Logistics (NZ) Ltd (formerly Aerial Surveys Ltd), using a Zeiss LMK15 metric camera with a 266636B lens and no filter. Camera lens distortion parameters, fiducial mark positions and the focal length were provided in a camera calibration certificate. The May 1995 photographs were flown as part of a previous, unconnected, project which aimed to use digital photogrammetry to produce a detailed topographic map of the Thompson's Track reach for use with the 2DE braided river model (Willsman, 1995; Carter and Shankur, 1997). For this work, a photographic scale of 1:3000 was selected and a flight-line selected which was orthogonal to direction of flow, meaning the entire study reach was covered in one photograph overlap. The same photograph survey specifications were used on 16th February 1999, during a period of even lower river flow. The mean daily discharge record between May 1995 and February 1999 (**Figure 3.8**) shows the occurrence of several floods, perhaps five of which would likely have produced peak flows greater than 100 m³/s, causing complete riverbed inundation.

Date	Photograph scale	Number of flying lines required to span riverbed	Number of photos required to give total coverage	Mean daily discharge (m ³ /s)
19/05/1995	1:3000	1	2	7.3
16/02/1999	1:3000	1	2	2.8

Table 3.1 Details of the aerial photography of the North Ashburton River.

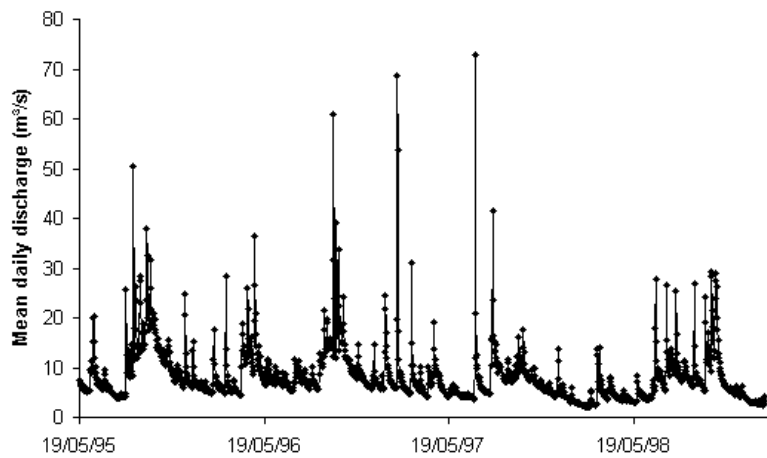


Figure 3.8 The mean daily discharge record for the North Ashburton River for the period between the May 1995 and February 1999 photogrammetric surveys. (Flow data provided by NIWA and Environment Canterbury).

For the Waimakariri River, the choice of scale of photography was critical due to the trade-off between spatial extent and surface representation. In total, three sets of photographs were obtained (**Table 3.2**). For the February and March 1999 photographs, a Zeiss LMK15 metric camera was used with a 266636B lens and no filter. For the February 2000 photographs, a Wild RC8 camera was used, with a UAg #470 lens and a Wild AV 2.2x Ni3763 filter. For both cameras, lens distortion parameters, fiducial mark positions and focal lengths were obtained from camera calibration certificates. All three flights were operated by Air Logistics, and in each case the direction of flight was parallel to the direction of flow.

Date	Photograph scale	Number of flying lines required to span riverbed	Number of photos required to give total coverage	Instantaneous discharge (m ³ /s)
16/02/1999	1:5000	2	16	27.0
19/03/1999	1:5000	2	18	56.0
23/02/2000	1:4000	2	22	64.8

Table 3.2 Details of the aerial photography of the Waimakariri River.

The choice of survey dates was related to the temporal scales of interest. The first survey (16th February 1999) was chosen to coincide with a particularly low discharge in order to maximise the exposed area that could be measured photogrammetrically. On 28th February 1999, a flood event occurred (**Figure 3.9**), with a peak flow of 780 m³/s, which inundated most of the riverbed (Hicks *et al.*, 1999b). The decision was made to conduct another survey immediately after this event once discharge had returned to normal low-flow conditions, and a second set of photographs were flown on 19th March 1999. This gave pre-flood and post-flood surveys, which was hoped would give an idea of the morphological change caused by a single flood event. The third set of photographs were obtained during low flow conditions on 23rd February 2000, to give an indication of the nature and magnitude of annual change. The mean daily discharge record for February 1999 to February 2000 (**Figure 3.10**) shows several flood events, of which up to eight contained peak flows greater than 800 m³/s and inundated the majority of the riverbed.

For both study reaches, selection of photograph scale was determined in the first instance by the level of photogrammetric precision required. The theoretical precision of a photogrammetric survey places a basic limit on the quality of DEMs derived (Lane *et al.*, 2000). Next, photograph scale was maximised such that the required theoretical precision was obtained. Commonly, **Equation 2.1** is used to estimate this limit as there is a one-to-one relationship between object space pixel dimensions and vertical precision of a photogrammetric survey (Lane, 2001). Given the low vertical relief in the

study reaches relative to the spatial extent, the theoretical precision needed to be high. This was particularly important since one potential use of the riverbed DEMs was to calculate morphological change. Based on the propagation of random error in a DEM of difference (**Equation 2.12**), in order to be confident of detecting elevation changes as small as ± 0.10 m, a DEM precision of ± 0.07 m is required. Within the constraints of scanning resolution available, this necessitated a relatively large image scale and low flying height (**Figure 3.11**).

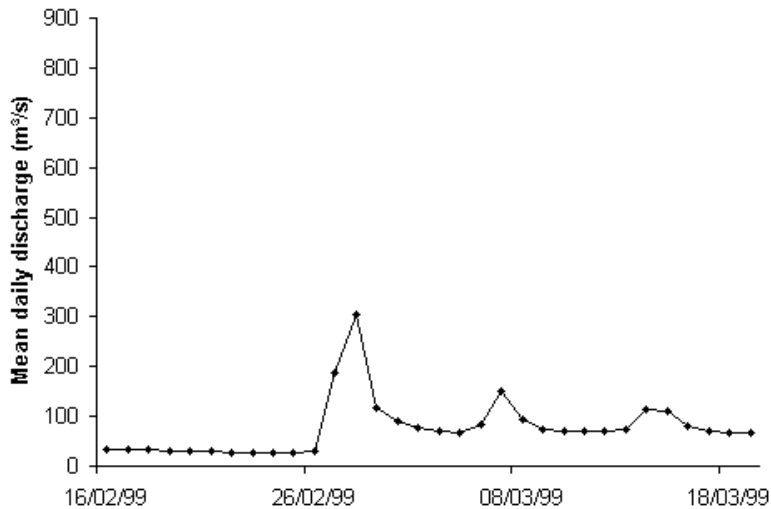


Figure 3.9 The mean daily discharge record for the Waimakariri River for the period between the February 1999 and March 1999 photogrammetric surveys (Flow data provided by NIWA and Environment Canterbury).

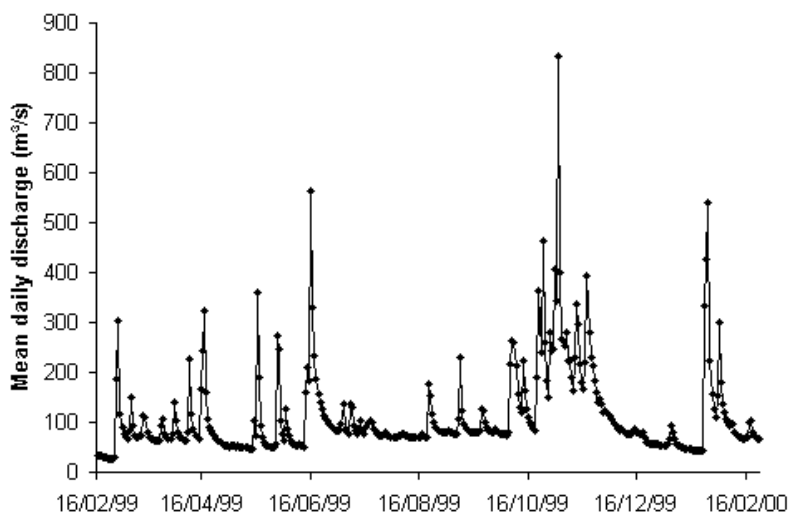


Figure 3.10 The mean daily discharge record for the Waimakariri River for the period between the February 1999 and February 2000 photogrammetric surveys (Flow data provided by NIWA and Environment Canterbury).

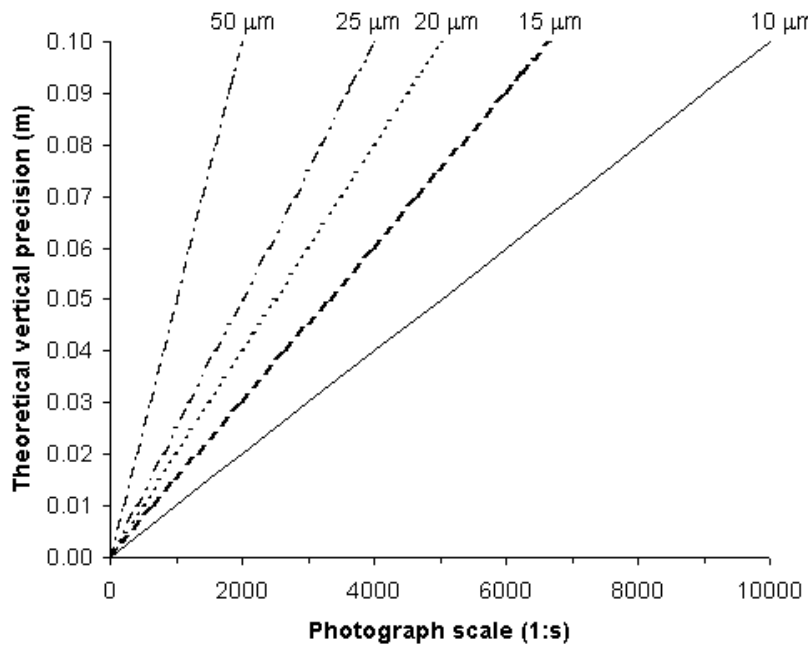


Figure 3.11 The relationship between theoretical precision, photograph scale and scanning resolution.

A disadvantage of increasing image scale is that the area of coverage of each image is reduced, requiring a greater number of images to cover a given area. For the standard aerial photograph format size (0.235 m), a photograph scale of 1:3000 gives single image coverage of 705 m x 705 m, and overlap area of 420 m x 705 m (assuming the conventional 60% overlap is achieved). Assuming a scanning resolution of 15 microns, from **Equation 2.1**, this gives a theoretical vertical precision of ± 0.045 m. For the North Ashburton, 1:3000 photography was appropriate, as it allowed the 400 m x 100 m study reach to be covered in one pair of overlapping photographs with greater than the desired precision.

For the Waimakariri, the situation was more complicated. In order to obtain a theoretical precision of around ± 0.07 m, and given the desire to restrict scanning resolution to around 15 microns due to the size of digital file produced, a photograph scale of 1:5000 was considered preferable. This gave an acceptable theoretical photogrammetric precision of ± 0.07 m if scanned at 15 microns (**Figure 3.11**). For standard aerial photographs, 1:5000 imagery gives a spatial coverage per image of 1175 m x 1175 m and an estimated overlap area of 705 m x 1175 m (downstream x cross-stream). Thus, because riverbed width in the study reach varies from around 800 to 1200 m, the decision to use 1:5000 scale imagery meant that two flying lines were

needed to span the entire active riverbed. This doubled the number of images needed to cover the complete reach, and also increased the computational time and resources required during photogrammetric analysis. However, had a single flying line been used, image scale would have been confined to a practical minimum of 1:8000 and, from **Equation 2.1**, theoretical photogrammetric precision would decrease to around ± 0.12 m for a scanning resolution of 15 microns.

Due to a lack of riverbed texture recorded in the 1:5000 scale photographs obtained in February 1999 and March 1999 (discussed in **Section 3.3.3**), the photograph scale was increased to 1:4000 for the February 2000 survey. This gives single image coverage of 940 m x 940 m and an estimated overlap area of 560 m x 940 m (downstream x cross-stream). To prevent having to increase the number of flight lines further, this required considerable skill on behalf of the aircraft pilot to position the plane correctly such that the whole study reach was recorded on overlapping photographs without leaving any gaps in the coverage. Despite this, a small area of the reach at the extreme upstream end was not covered satisfactorily to allow photogrammetric measurement. However, the increase in photograph scale did permit an increase in the theoretical vertical precision to ± 0.06 m for the same scanning resolution (**Equation 2.1**).

The use of three different photograph scales (1:3000, 1:4000 and 1:5000) also allowed assessment of the effect of photograph scale on automated stereo-matching performance and on final DEM quality.

3.3.3 Digital image creation

In order to perform automated photogrammetry, softcopy or digital images are required. These can be acquired directly through use of a digital camera (e.g. Chandler and Ashmore, 2001; Chandler *et al.*, 2001; Stojic, 2001), although large format digital cameras remain expensive. Digital images are more commonly obtained by scanning hardcopy photographic diapositives, negatives or prints (e.g. Brunsden and Chandler, 1996; Pyle *et al.*, 1997; Derose *et al.*, 1998; Butler *et al.*, 1998; Stojic *et al.*, 1998; Lane *et al.*, 2000). Diapositives or negatives should be used as they avoid additional distortions associated with the photographic printing process.

The May 1995 North Ashburton photographs had previously been scanned in-house by Air Logistics (NZ) Ltd, at a resolution of 23 microns. Other sets of photographs were scanned using photogrammetric-standard scanners at the National Remote Sensing Centre, UK, and the Zentrum für Datenverarbeitung (Centre for Data Processing), Universität Mainz, Germany. Photogrammetric-standard scanners are high quality, high spatial resolution scientific flatbed scanners designed specifically for the

photogrammetric community (Smith, 1997). They are typically capable of achieving linear measurement resolutions of 1 to 2 microns, a spatial accuracy of ± 3 to 5 microns RMSE on each axes, and minimum pixel sizes of 8 to 10 microns (Petrie, 1996). These quality requirements are similar to those required for analytical photogrammetric plotters (Petrie, 1996). Images were scanned with a resolution of 14 microns, which was considered to be the smallest possible given the large digital file sizes produced. Information about the scanning specifications is given in **Table 3.3**.

Photograph set	Photo scale	Diapositive format size (m)	Scanning resolution (microns)	Object-space pixel size (m)	Digital file size (Mb)
North Ashburton – May 1995	1:3000	0.235	23.0	0.075	100
North Ashburton – Feb. 1999	1:3000	0.235	14.0	0.042	269
Waimakariri – February 1999	1:5000	0.235	14.0	0.070	269
Waimakariri – March 1999	1:5000	0.235	14.0	0.070	269
Waimakariri – February 2000	1:4000	0.235	14.0	0.056	269

Table 3.3 Specifications relating to the creation of digital images.

From **Equation 2.1**, the theoretical vertical precision of photogrammetric measurements can be calculated. These are presented for each of the photograph sets collected for the North Ashburton and Waimakariri Rivers in **Table 3.4**. On each occasion, the theoretical precision was close to the desired maximum value of ± 0.07 m.

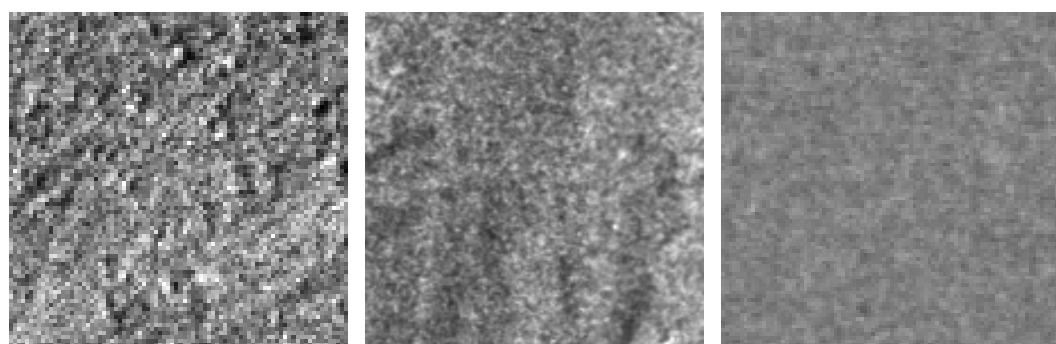
Photograph set	Best theoretical precision (m) (from Equation 2.1)
North Ashburton – May 1995	± 0.075
North Ashburton – February 1999	± 0.042
Waimakariri – February 1999	± 0.070
Waimakariri – March 1999	± 0.070
Waimakariri – February 2000	± 0.056

Table 3.4 Calculation of the theoretical vertical photogrammetric precision permitted by the digital imagery used in this study.

The digital output was in the form of 256 grey-scale tagged image format (TIF) files, supplied on CD-ROM. Examples of the quality of image output are given in **Figure 3.12**. Each image shows an area of approximately 6 m x 6 m of exposed gravel bed. It is clear that the different combinations of image scale and scanning resolution influence the digital image texture. A quantitative estimate of image texture is given by the standard deviation of pixel digital numbers (dNs) within these image extracts. The dNs range from 0 (black) to 255 (white) in 256 grey-scale images (**Table 3.5**). These

indicate that image scale is strongly related to image texture. The influence of scanning resolution seems less important: the image texture was highest in the May 1999 North Ashburton image which was scanned at almost twice the resolution of any other image. Given that the automated stereo-matching algorithm is based on brightness differences on corresponding images (**Section 3.3.6**), the effect of image texture on stereo-matching performance and final photogrammetric DEM quality is potentially important. This will be examined for the North Ashburton River in **Chapter 4** and the Waimakariri River in **Chapter 6**.

(a) North Ashburton – 05/95 (b) North Ashburton – 02/99 (c) Waimakariri – 02/99



(d) Waimakariri – 03/99 (e) Waimakariri – 02/00

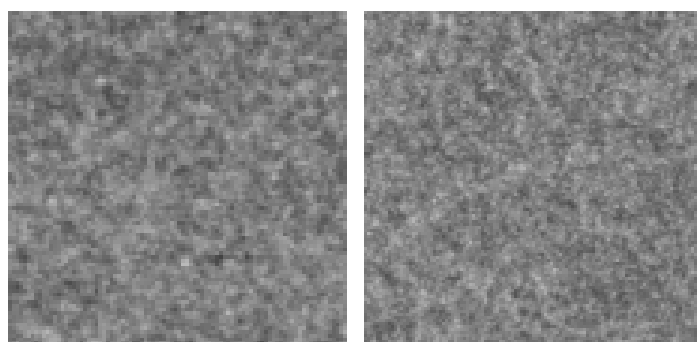


Figure 3.12 Extracts from the digital images of the North Ashburton and Waimakariri riverbeds.

3.3.4 Photogrammetric control

Before image acquisition, it is necessary to ensure that appropriate photograph control is available (Chandler *et al.*, 2001). Although natural features may be used, artificial targets are preferable for this purpose (Chandler and Moore, 1989), with a minimum of three visible on any one photograph. Further, a three-dimensional object-space coordinate system must be established, and the position of photo-control points (PCPs) must be measured to a fixed datum using terrestrial survey methods such as Total Station or GPS. The quality of the three-dimensional positioning depends on the aim of the study (Dixon *et al.*, 1998), but the quality of photogrammetric measurements is

determined by the quality of photograph control on which it is based (Wolf and Dewitt, 2000), although no better than the limits defined by the object-space pixel dimensions.

Photograph set	Photograph scale	Scanning resolution (microns)	Image texture (standard deviation of dNs)
North Ashburton – May 1995	1:3000	23.0	32.9
North Ashburton – February 1999	1:3000	14.0	14.0
Waimakariri – February 1999	1:5000	14.0	8.4
Waimakariri – March 1999	1:5000	14.0	9.5
Waimakariri – February 2000	1:4000	14.0	12.8

Table 3.5 Estimation of image texture from the standard deviation of dNs.

For this study, PCP markers comprised of a 2 m x 2 m square of dark polythene plastic, a cross formed by two 1.2 m x 0.3 m panels of plywood painted white, and a central target formed by two black and two white triangles (**Figure 3.13**). The survey peg was at the centre of this arrangement. The size of the PCP target was planned with respect to the object-space pixel size (**Table 3.3**). The white plywood cross spanned at least 15 x 15 image pixels, and the central target was at least 4 x 4 image pixels in size.

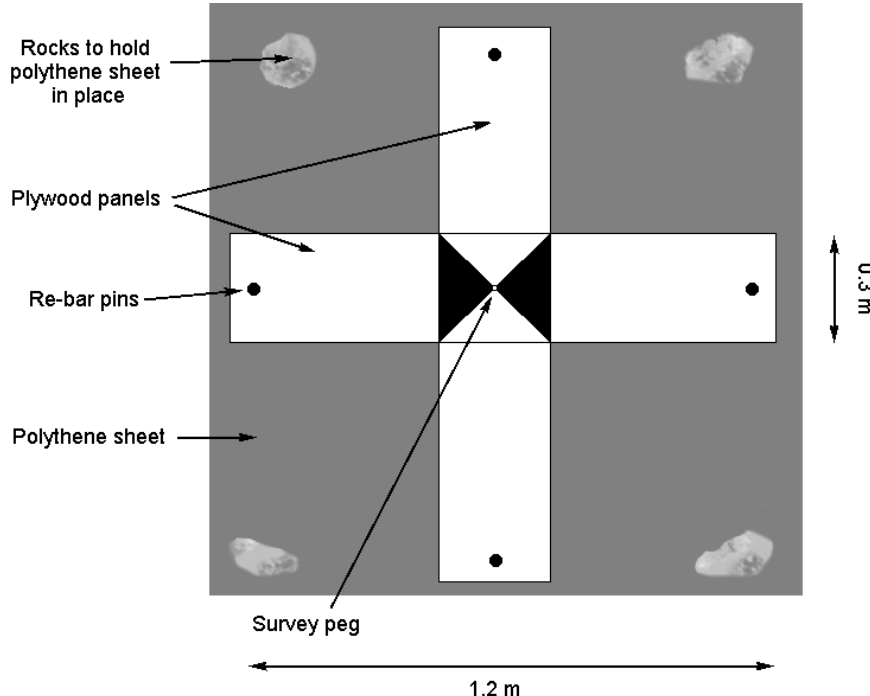


Figure 3.13 The marker boards constructed for use as PCP targets (from Hicks et al., 1999b).

It was decided to aim for inclusion of at least six PCPs per photograph overlap area. For the North Ashburton, these were laid out prior to photography, and spread out on the exposed riverbed across the complete extent of the study reach (Willsman, 1995). Two parallel lines of three PCPs were established, and labelled according to line (right or left bank), and downstream position (north, centre or south). In May 1995, a three-dimensional coordinate system was established using an arbitrary datum, established from a fixed benchmark located on Thompson's Track bridge. The position of the PCPs was measured using Total Station, and so a precision in the order ± 0.005 m is assumed (Barker *et al.*, 1998). In February 1999, the same datum was used, and the photo control points were re-established as close as possible to their original positions (Willsman, 1999). Again, Total Station was used to survey PCP position.

For the Waimakariri, due to the large number of photographs and much larger study area, positioning the PCPs to achieve six per overlap became far more critical. Prior to the February and March 1999 surveys, 45 PCPs were set out over the study reach (Hicks *et al.*, 1999b). This involved nine cross-stream lines of markers, spaced 400 m apart, and labelled A-I, going upstream. The five PCPs in each line (labelled 1-5 from the true left bank) were stratified across the riverbed so that the central three appeared in photographs from both flight lines. The positioning of PCPs was planned from a 1:10000 scale colour photograph-mosaic of the study reach (provided by Peter Ball of SkyCam). When laminated, this also served as a map to locate the PCPs in the field (Hicks *et al.*, 1999b).

For the February 2000 survey, the image scale was increased (to 1:4000) which increased the number of photograph overlaps on the riverbed in the downstream direction. Consequently, the number of PCPs was increased to 55, with two additional cross-stream lines (J and K). The system of positioning and labelling of PCPs was unchanged. In the field, prior to all three photographic surveys, the PCP markers were laid out by two to three NIWA field teams during one day and surveyed by EC surveyors in two days, using a Trimble real-time kinematic GPS (Hicks *et al.*, 1999b). The three-dimensional co-ordinate system was established within the WGS84 global reference datum, and adjusted to the local Mount Pleasant coordinate system. The positioning of PCPs using GPS is expected to give three-dimensional co-ordinates to within a few centimetres of true position, with a slightly lower precision expected in the vertical (Z) plane (Barker *et al.*, 1998; Satalich and Ricketson, 1998; Brasington *et al.*, 2000).

3.3.5 *Block triangulation*

The purpose of block triangulation is to recover the precise three-dimensional position and orientation of the camera at the time of exposure of each photograph. This is achieved by determining camera location through measurement of the two-dimensional image-space coordinates of PCPs of known three-dimensional position in the object-space. Deviations from the special case of a perspective projection, fiducial marks and the focal lengths were determined from the camera calibration certificates.

Various commercial software packages are available to perform automated photogrammetry (Chandler, 1999), but the ERDAS Imagine OrthoMAX package is popular in the UK academic community because of its low cost when purchased through the CHEST (Combined Higher Education Software Team) licensing arrangement (Chandler *et al.*, 2001). The 8.3 version of this software was available at the University of Cambridge, installed on several UNIX machines including both Sun and Silicon Graphics workstations. It has previously been successfully used in a variety of projects (e.g. Pyle *et al.*, 1997; Butler *et al.*, 1998; Lane, 1998; Lane *et al.*, 2000; Chandler *et al.*, 2001).

The stages of digital photogrammetric block triangulation mirror those associated with conventional photogrammetry, but use digital images rather than photographic prints (Lane *et al.*, 2000). These consist of two phases: interior orientation; and exterior orientation. In the ERDAS Imagine OrthoMAX environment, both phases are carried out within the 'Block Tool' module.

The interior orientation phase may be defined as the restoration of the interior geometry of the camera at the time of exposure (Dixon *et al.*, 1998). Initially, this requires specification of camera lens distortion parameters, the photograph fiducial system, the number of images used and the surveyed object-space position of PCPs. Then, the interior geometry of the camera is established, using position of the fiducial marks on the photographs to mathematically tie the digital imagery pixel coordinates to the fiducial system of the original photographs (Smith, 1997).

For this study, five photogrammetric blocks were established, one for each photographic survey (i.e. two for the North Ashburton and three for the Waimakariri). Despite the considerable differences in study reach size, and hence number of photographs required, the same procedure was used for each block. Over the course of the five photographic surveys, two large-format metric cameras were used, and full camera calibration details supplied for each. This provided values for all of the lens distortion parameters and fiducial positions initially required by OrthoMAX (**Table 3.6**). Next, the digital images were imported and added to their respective block, and each

image was automatically assigned a sequential reference number (ERDAS, 1995). Information about the three-dimensional coordinated position of PCPs was supplied by the NIWA and EC field teams in X,Y,Z format in ASCII files, which were imported directly into OrthoMAX.

Lens distortion parameters and fiducial positions (microns)	Zeiss LMK15 (266626B)	Wild RCS (Uag #470)
Focal length	152213	151548
Principle point of autocollimation, (x_0, y_0)	(-10.0, +10.0)	(0.0, -50.0)
Radial distortion parameter, k_0	+1.134e ⁻⁰⁴	-2.283e ⁻⁰⁴
Radial distortion parameter, k_1	-1.018e ⁻¹⁴	+4.455e ⁻¹⁴
Radial distortion parameter, k_2	+7.428e ⁻²⁶	-1.765e ⁻²⁴
Fiducial position e, (x, y)	(0.00, -155590)	(0.00, -149910)
Fiducial position f, (x, y)	(-155570, 0.00)	(-149900, 0.00)
Fiducial position g, (x, y)	(0.00, +155540)	(0.00, +149910)
Fiducial position h, (x, y)	(+155590, 0.00)	(+149910, 0.00)

Table 3.6 Summary of the lens distortion parameters and fiducial data required by the OrthoMAX block tool, and the corresponding values for the cameras and lens used in this study.

The interior orientation of the images used was determined by on-screen positioning of fiducial marks for each image, aided by an image magnification facility and an option which, after the pixel coordinates of two fiducial marks have been measured, estimates the remaining fiducial positions. This estimate was only used as the starting point for manual re-measurement of these fiducial positions. Once all fiducial marks have been located, the RMSE of the measurements is calculated in both pixels (image space) and microns (film space) (ERDAS, 1995). Given correct positioning of the fiducial marks, this error estimate refers to image distortions that create discrepancies between theoretical and actual fiducial pixel coordinates. These are known to occur in aerial photography, usually as a result of poor performance of the vacuum system used to hold the film flat in the image plane (Fryer *et al.*, 1994).

In this study, the positioning of four fiducial marks on each image gave the RMSE values shown in **Table 3.7**. A considerable range of results was obtained, generally higher than the RMSE values of 3.4 microns and 4.1 microns obtained by Lane *et al.* (2001) for 1:3000 imagery scanned at 25 microns and comparable with those obtained with analytical methods using hardcopy imagery (*cf.* Welch and Jordan, 1983; Lane, 1994). Nonetheless, all results compare favourably with the average 15 μm image measurement precision assigned to manual photogrammetric measurement (Baltsavias, 1999a). The higher RMSE values associated with the North Ashburton

May 1995 imagery may reflect the higher scanning resolution used (23 microns as compared with 14 microns for all other imagery), as this will degrade the quality of fiducial mark representation on the images (Smith, 1997), making them harder to position correctly on-screen.

Photogrammetric block	Fiducial RMSE for individual images (microns)	Mean fiducial RMSE (microns)
North Ashburton – May 1995	12.8; 13.7	13.3
North Ashburton – Feb 1999	12.4; 12.6	12.5
Waimakariri – Feb 1999	1.5; 3.0; 4.2; 5.6; 5.7; 6.1; 6.1; 6.3; 6.5; 7.5; 7.5; 8.6; 8.8; 8.9; 12.1; 12.4	6.9
Waimakariri – March 1999	3.4; 4.4; 5.5; 5.9; 6.8; 6.9; 7.1; 7.4; 8.0; 8.1; 8.1; 9.0; 9.3; 10.5; 10.9; 14.7; 15.8; 17.7	8.9
Waimakariri – Feb 2000	0.0; 0.3; 0.9; 0.9; 1.1; 1.4; 1.4; 1.5; 1.8; 2.0; 2.0; 2.0; 2.2; 2.2; 2.3; 2.3; 2.5; 2.7; 2.8; 3.3; 6.2	1.9

Table 3.7 Fiducial RMSE calculated by the OrthoMAX block tool.

The second phase of block creation is the establishment of the exterior (or absolute) orientation of the photogrammetric block. This phase is carried out to rotate and translate the photogrammetric block to the desired scale and orientation relative to the horizontal datum defined by the PCPs (Dixon *et al.*, 1998). This requires the image-space position of PCPs to be identified and recorded for overlapping images. Finally, automated block triangulation is performed, involving a simultaneous least-squares bundle adjustment to solve the unknown camera parameters (position and orientation) through space resection from the measured PCPs (Smith, 1997).

In OrthoMAX, the external orientation phase begins with the location and measurement of the image-space pixel coordinates of visible PCPs. This is performed using the ‘Ground Point Measurement’ tool, which allows on-screen viewing of up to three images simultaneously. An image magnification facility and ‘auto-place’ functionality assist the human operator. Auto-placing helps to automate the measurement of corresponding PCPs appearing on multiple images (Chandler *et al.*, 2001), using the normalised cross-correlation coefficient to locate optimum conjugate point matches (ERDAS, 1995). Next, is the block triangulation calculation itself. This is performed automatically by OrthoMAX using an iterative least squares bundle adjustment. The number of iterations (0-20) and a convergence value are defined by the user (ERDAS, 1995). The convergence value is used to determine when the iterative process is complete, by defining the maximum spatial adjustment to ground points that will initiate another iteration.

The success of the bundle adjustment solution is assessed by a number of internally-generated statistics. Three of these statistics were considered in this research. First, the standard deviation of unit weight, which measures the conformance of the bundle adjustment to estimated parameters and specified parameter precision (ERDAS, 1995), and is often considered to represent an indication of the overall quality of the least squares solution. The value should be around 1.0, and always between 0.5 and 2.0 (ERDAS, 1995). The second and third important statistics are the standard deviations of the residuals associated with the exposure station (i.e. camera lens) and with the PCP positions. These represent deviations from the best fit of the collinearity equations (**Equations 3.3 and 3.4**) to all PCP ground coordinates, image measurements and camera lens parameters (ERDAS, 1995). Small standard deviations, with respect to the object-space pixel size and expected precision of surveyed PCP positions, suggest that the real life object-to-image geometry closely approaches the theoretical condition of collinearity. This means that bundle adjustment has been able to triangulate the block successfully. In terms of these measures, and based at this stage on solely on the coordinated PCP targets, the initial results from the blocks triangulated for this research were generally encouraging (**Table 3.8**): the standard deviations of unit weight were within the acceptable bounds (0.5-2.0), mean exposure station residual standard deviation values were generally less than ± 0.010 m and mean PCP residual standard deviation values were generally less than ± 0.005 m. There were two main exceptions. First, the standard deviation of unit weight for the February 1999 North Ashburton and Waimakariri blocks appeared to be too low (suggesting the bundle adjustment solution is under-constrained; ERDAS, 1995). Second, the mean exposure station and PCP residual standard deviations for the May 1995 North Ashburton block appeared exceptionally high, with the exposure station in the X direction particularly anomalous.

In an attempt to improve these statistics, tie-points were added to the block. Tie-points are additional PCPs with poorly known or completely unknown horizontal and vertical coordinates (ERDAS, 1995), which help to constrain by least-squares calculation by adding further redundancy into the solution. In this instance, riverbed points that could be visually identified on-screen on both overlapping images were used as tie points (e.g. Stojic *et al.*, 1998; Chandler *et al.*, 2001).

Photogrammetric block	Standard deviation of unit weight	MEAN EXPOSURE STATION RESIDUAL STANDARD DEVIATION (m)			MEAN PCP RESIDUAL STANDARD DEVIATION (m)		
		X	Y	Z	X	Y	Z
North Ashburton – May 1995	1.28	1.257	0.526	0.399	0.079	0.092	0.115
North Ashburton – Feb 1999	0.41	0.260	0.120	0.093	0.024	0.027	0.032
Waimakariri – Feb 1999	0.55	0.088	0.084	0.061	0.025	0.023	0.034
Waimakariri – March 1999	0.98	0.097	0.102	0.081	0.041	0.037	0.052
Waimakariri – Feb 2000	0.89	0.110	0.119	0.052	0.032	0.032	0.050

Table 3.8 Initial results from block triangulation for both study reaches using only PCP information.

This was performed in a systematic manner, by adding additional rows of tie-points between existing rows of PCPs until little further change was observed in the bundle adjustment solution. The auto-place feature was again found to be helpful. Finally, the blocks were re-triangulated as before, and the bundle adjustment solution statistics obtained are shown in **Table 3.9**. Inclusion of tie-points had two main effects. First, those standard deviation values that were especially high are reduced to more acceptable values. Second, the three Waimakariri blocks are much more consistent in terms of all measures of block quality, suggesting that the bundle solutions used are relatively robust. For these reasons, it was decided to use these blocks for subsequent DEM and ortho-photo generation.

3.3.6 DEM and ortho-image generation

Once appropriate bundle adjustment solutions had been obtained, DEMs and ortho-images were generated using the ‘DEM Tool’ and ‘Ortho Tool’ processes of the OrthoMAX module.

Automated DEM extraction is achieved by the Vision Algorithm, which relies on variations in contrast and brightness in two overlapping images. The system uses an area-based correlator to identify corresponding points on each image, and employs a hierarchical approach, in which correlations are performed at increasingly higher resolutions by generating a range of reduced resolution dataset (RRDS) files from the source imagery. The hierarchical approach both compensates for large changes in DEM elevation and constrains matching at the next resolution, such that false fixes between largely disparate points is prevented (ERDAS, 1995). At a given resolution and for a given point, local models of terrain produced at coarser resolutions are used to ortho-rectify patches at evenly-spaced elevations above and below the predicted elevation (ERDAS, 1995). At each elevation, patches are matched to determine levels of correlation until a successful match is made (Lane *et al.*, 2000). Prior to DEM generation using OrthoMAX, the user is able to adjust 12 DEM collection parameters which guide the operation of the Vision algorithm. These parameters are listed and explained in **Appendix 1**. Improvements in matching precision and overall surface quality have been reported by varying relevant collection parameters prior to DEM collection (e.g. Pyle *et al.*, 1997; Smith *et al.*, 1997; Gooch *et al.*, 1999; Butler *et al.*, 1998; Lane *et al.*, 2000), so correct specification is important.

Photogrammetric block	Tie-points added	Standard deviation of unit weight	MEAN EXPOSURE STATION RESIDUAL STANDARD DEVIATION (m)			MEAN PCP RESIDUAL STANDARD DEVIATION (m)		
			X	Y	Z	X	Y	Z
North Ashburton – May 1995	11	0.88 (-0.400)	0.515 (-0.742)	0.191 (-0.335)	0.215 (-0.184)	0.054 (-0.025)	0.062 (-0.030)	0.070 (-0.045)
North Ashburton – Feb 1999	7	0.42 (+0.010)	0.179 (-0.081)	0.066 (-0.054)	0.083 (-0.010)	0.025 (+0.001)	0.027 (0.000)	0.031 (-0.001)
Waimakariri – Feb 1999	94	1.04 (+0.490)	0.082 (-0.006)	0.088 (0.004)	0.061 (0.000)	0.038 (+0.013)	0.038 (+0.015)	0.052 (0.018)
Waimakariri – March 1999	113	1.13 (+0.150)	0.071 (-0.026)	0.076 (-0.026)	0.059 (-0.022)	0.040 (-0.001)	0.039 (+0.002)	0.051 (-0.001)
Waimakariri – Feb 2000	88	0.94 (+0.050)	0.080 (-0.030)	0.091 (-0.028)	0.045 (-0.007)	0.031 (-0.001)	0.031 (-0.001)	0.049 (-0.001)

Table 3.9 Results from block triangulation for both study reaches using both PCP and tie-point information. Change from previous blocks (calculated using only PCPs) given in brackets.

There are two further decisions which must be made by the operator prior to DEM generation in OrthoMAX: (i) the source image must be selected; and (ii) the DEM point spacing must be chosen. Based on the precision of the bundle adjustment solution, the minimum DEM grid spacing is approximately five times greater than the object-space pixel size (and hence the theoretical photogrammetric precision) (Lane *et al.*, 2000).

After each DEM is created, OrthoMAX generates a summary of the results for each RRDS level of processing. Emphasis is usually placed on the finest resolution RRDS as these relate to the final level of DEM processing (Gooch *et al.*, 1999). They give a first indication of the quality of the derived DEM surface, and have frequently been used for DEM quality assessment in previous applications of OrthoMAX to geomorphological projects (e.g. Pyle *et al.* 1997; Butler *et al.*, 1998; Stojic *et al.*, 1998; Lane *et al.*, 2000). A statistics file is also produced which indicates the spatial distribution of matching success, in terms of the strength of correlation between corresponding image points. Four classes of points are identified by OrthoMAX: ‘good’; ‘fair’; ‘poor’; and ‘interpolated’ (or not matched). The DEM collection results for the DEMs generated in this study will be discussed in **Chapter 4** for the North Ashburton River and **Chapter 6** for the Waimakariri River.

Once DEMs have been created, OrthoMAX allows production of two digital orthorectified images (ortho-images) for each DEM (one from each overlapping source image used to generate the DEM). Softcopy ortho-rectification involves the re-sampling of raw imagery to remove the distorting effects of sensor geometry and terrain variation. The OrthoMAX Ortho Tool uses rational functions to compute image pixel coordinates associated with a given X,Y position and Z elevation interpolated from a DEM, using a patch-based method to accelerate processing time (ERDAS, 1995). Bilinear re-sampling is used to preserve the geometric and radiometric fidelity of the ortho-rectified imagery. Ortho-images may be used for qualitative DEM quality assessment (e.g. Pyle *et al.*, 1997), for quantitative detection of DEM errors through stereo-matching of two ortho-images (e.g. Lane, 2000) and for integration of two-dimensional image analysis techniques with three-dimensional DEM surfaces (e.g. Butler *et al.*, 2001a). In this study, an ortho-image was produced for each DEM generated and these are discussed further in **Chapters 4** (North Ashburton) and **6** (Waimakariri).

3.4 Airborne laser scanning

3.4.1 Principles

Airborne laser scanning (ALS) is an aircraft-mounted laser system that is used to acquire X,Y,Z coordinates of terrain and terrain features. The principle of the method

and hardware used have been given various other titles including airborne laser altimetry (ALA; Favey *et al.*, 1999; Hofton *et al.*, 2000), light detection and ranging (LiDAR; FEMA, 2000; Charlton *et al.*, 2001), laser detection and ranging (LADAR; Wehr and Lohr, 1999) and airborne laser terrain mapper (ALTM; Hansen and Jonas, 2000). The distance between the sensor and the ground is determined by precise measurement of the return time of pulses of laser light. If the exact three-dimensional position of the sensor and the angle of the laser beam can be recovered, a dense network of three-dimensional ground coordinates can be calculated. A primitive version of ALS was first tested in the 1960s, but it was not until the 1970s and 1980s that the first experimental systems were developed and attached to light aircraft (Ackermann, 1999; Wehr and Lohr, 1999). By the early 1990s, the integration of real-time kinematic GPS positioning and the adoption of two-dimensional scanners over one-dimensional profilers heralded the widespread adoption of ALS by the surveying community (Wehr and Lohr, 1999).

There are three fundamental components of any ALS system (Hansen and Jonas, 2000; **Figure 3.14**). First, the aircraft's position must be determined, commonly using real time kinematic GPS, at around one second epochs. Second, the aircraft's orientation and attitude must be continually monitored. This is achieved approximately 50 times each second, using a sensitive, onboard, Inertial Reference System (IRS). Third, a high accuracy laser range-finder device scans beneath the aircraft to produce a wide swathe over which the distance from the aircraft to the ground is precisely measured for every laser pulse. There are typically 5000 to 25000 laser pulses emitted and received each second. Standard ALS systems measure the timing of single wavelength laser pulses, usually configured to record either the initial ("first return") or final ("last return") reflection received (Huising and Gomes Pereira, 1998; Jonas and Byrne, 1999). More sophisticated models can record multiple returns (Baltsavias, 1999a), or utilise two or more laser frequencies (Irish and Lilycrop, 1999), allowing determination of vegetation height and water depth (e.g. Ritchie, 1996, Wehr and Lohr, 1999). Post-processing software subsequently combines the scanner's position, attitude and laser transit times to derive X,Y,Z coordinate positions. As they are determined using GPS, the raw elevations acquired are initially computed as WGS84 ellipsoid heights. These should be converted to orthometric heights based on the local geoid-spheroid separation distance (Fraser *et al.*, 1999).

Airborne laser scanning is frequently compared to digital photogrammetry in terms of the respective methods' ability to provide three-dimensional topographic data. **Table 3.10** provides a summary of the main similarities and differences between the two systems in terms of project design.

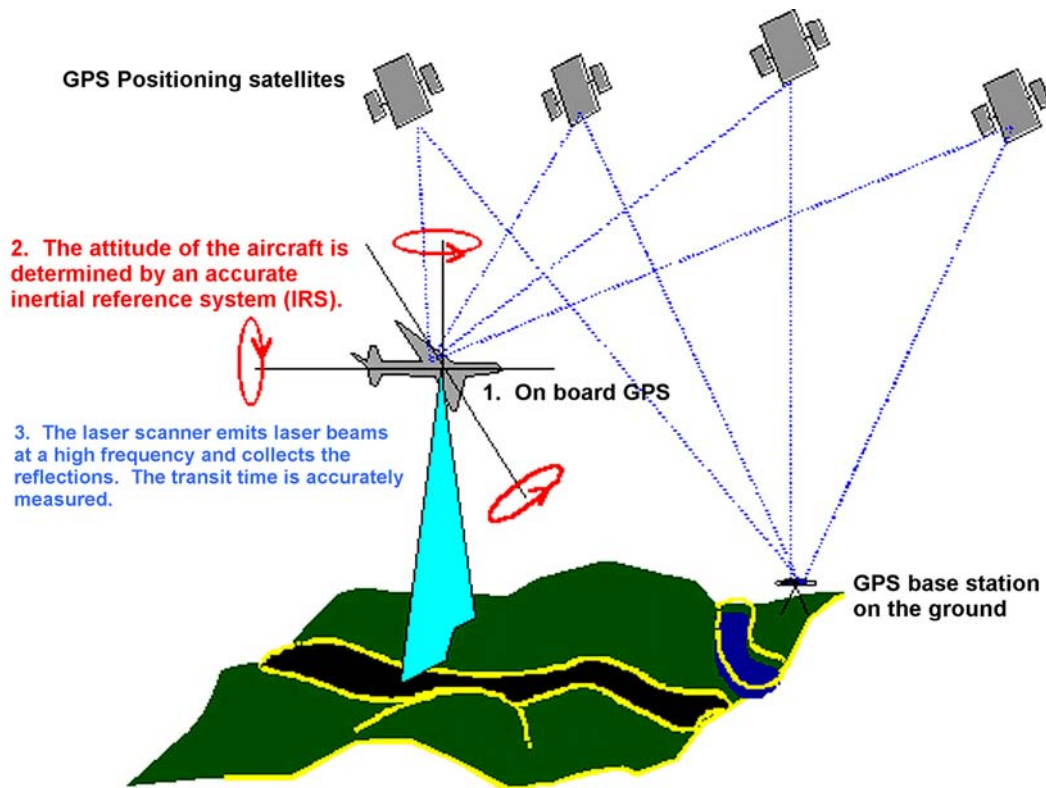


Figure 3.14 The three components of the airborne laser scanning (ALS) system (from Fraser et al., 1999)

3.4.2 Project design

For this research, an ALS survey of the Waimakariri River study reach was conducted by AAM Geodan, a joint venture between Dutch company Geodan Geodesie B.V. and AAM Surveys Ltd of Queensland, Australia. Geodan Geodesie has developed laser scanning since 1993 (Fraser et al., 1999), and has close links with TopScan GmbH, the German company which developed much of the software and algorithms used to post-process ALS data (Jonas and Byrne, 1999). Since 1998, AAM Geodan have employed ALS technology for a range of different applications and environments (e.g. Fraser et al., 1999; Jonas and Byrne, 1999; Turton, 1999; Hansen and Jonas, 2000; Witte et al., 2000; Jonas, 2001a; Jonas, 2001b), although gravel-bed river environments had not previously been surveyed.

The equipment used by AAM Geodan for the Waimakariri survey consisted of an Optech 1020 ALS scanner mounted in an Aerocommander 680 survey aircraft (Fraser et al., 1999). The Optech 1020 permits data to be acquired at 5000 points per second over a swathe width of up to 700 m from a maximum flying height of 1000 m. The scanner uses a single-frequency (1.04 micron) wavelength laser which can be configured to record either first or last return. At the normal operating altitude, the

emitted laser beam is approximately 0.30 m in diameter when it reaches the ground surface and is directed in a swathe across the ground by a rotating mirror (Turton and Jonas, 1999). The forward motion of the aircraft causes this to be translated as a zig-zag track on the ground (**Figure 3.15**).

Consideration	Digital photogrammetry	Airborne laser scanning
Vertical precision	<ul style="list-style-type: none"> Depends on image scale and resolution 	<ul style="list-style-type: none"> Estimated at $\pm 0.10\text{--}15$ m, but depends on system used
Ground resolution	<ul style="list-style-type: none"> defined by project requirements trade-off between DEM point spacing and processing time 	<ul style="list-style-type: none"> typical point spacing of 3 m multiple sensor passes may be used to increase point density
Ground support	<ul style="list-style-type: none"> photo control required independent ground points provide check data 	<ul style="list-style-type: none"> base station within 50 km required independent ground points provide check data
Flight planning	<ul style="list-style-type: none"> relatively wide area covered per image at given flying height (75° effective field-of-view) 60% overlap required between images 	<ul style="list-style-type: none"> relatively narrow swathe width at given flying height (20–40° scan angle) requires careful route planning to avoid missed terrain more flying hours needed to cover same ground area
Flight timing	<ul style="list-style-type: none"> clear skies and daylight required high sun angle (to avoid shadows) 	<ul style="list-style-type: none"> clear skies and daylight not required theoretically possible in any weather conditions, though wind and rain may degrade results visibility of 5–6 GPS satellites required
Processing	<ul style="list-style-type: none"> semi-automated (some human intervention required) some intermediate steps required (digital image creation, bundle adjustment) processing time depends on dataset size and DEM specifications 	<ul style="list-style-type: none"> fully-automated processing time more constant (time-scale of weeks)
Data format	<ul style="list-style-type: none"> grid-based DEM in grey-scale raster format 	<ul style="list-style-type: none"> random spot heights in X,Y,Z coordinates in ascii format
Vegetation penetration	<ul style="list-style-type: none"> visible surface measured (vegetation or topography) 	<ul style="list-style-type: none"> single return system measures visible surface multiple return system can measure true ground surface
Imagery	<ul style="list-style-type: none"> inherent by-product 	<ul style="list-style-type: none"> separate sensor required

Table 3.10 Comparison of features of digital photogrammetry and airborne laser scanning (Baltsavias, 1999a; Hansen and Jonas, 2000).

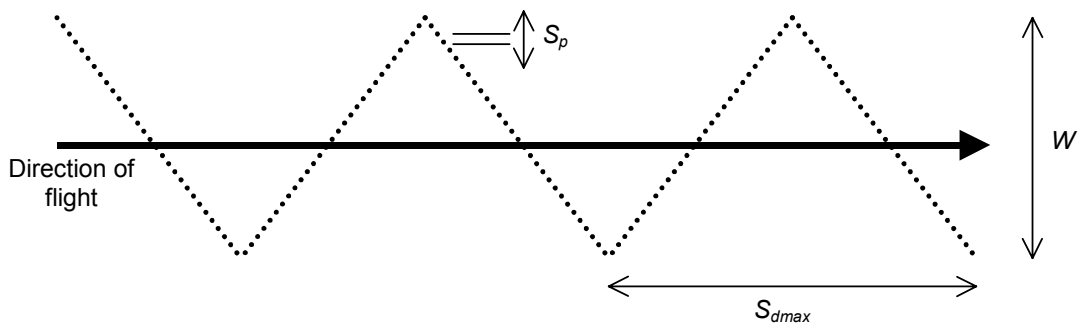


Figure 3.15 The survey geometry of the Optech 1020 airborne laser scanner (from Fraser et al., 1999).

An ALS survey consists of two distinct phases: data acquisition and data post-processing.

3.4.3 Data acquisition

An ALS survey was undertaken of the Waimakariri study reach on 25th May 2000. This fourth riverbed survey was separated from the final digital photogrammetric survey (23rd February 2000) by three months. The intervening flow record is dominated by one large flood event in April, with a smaller flood event that may also have caused riverbed inundation (**Figure 3.16**). Consequently, it was hoped that this would demonstrate the morphological change that occurs during an intermediate time-scale (as compared to the time spanned by the photogrammetric surveys).

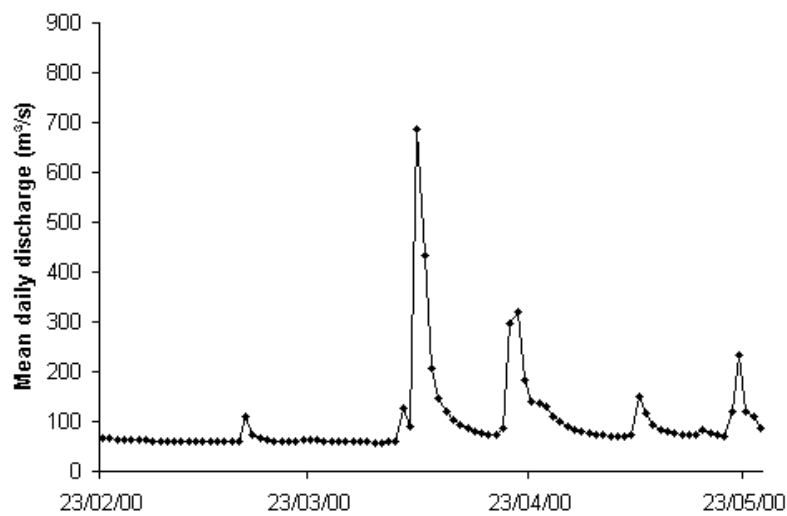


Figure 3.16 The mean daily discharge record for the Waimakariri River for the period between the February 2000 photogrammetric and May 2000 ALS surveys. (Flow data provided by NIWA and Environment Canterbury).

Prior to an ALS survey, careful flight planning is required to determine optimum swathe width and point density for each survey. The system parameters of laser frequency, swathe width, flying height and aircraft velocity can all be adjusted to meet the desired specifications for each project (Turton and Jonas, 1999), within the physical capabilities on the system used. As with photogrammetry, there is a trade-off between flying height (which increases swathe width and decreases flying time and cost) and point density (which improves surface representation). The overall point spacing is a function of the point spacing in both the direction-of-flight (or downstream) and perpendicular (or cross-stream) directions (**Figure 3.15**).

Maximum point spacing in the direction of flight, S_{dmax} , is given by (Baltsavias, 1999)

$$S_{dmax} = \frac{V}{F_s} \quad (3.5)$$

where V is the aircraft velocity (m/s) and F_s is the laser scanner frequency (Hz), the number of scan lines per second (Baltsavias, 1999b). Because of the zig-zag path taken by the laser beam (**Figure 3.15**), average point spacing in the direction of flight (S_d) is approximately half of S_{dmax} (Fraser *et al.*, 1999).

$$S_d = \frac{0.5V}{F_s} \quad (3.6)$$

The point spacing perpendicular to the direction of flight, S_p , is directly related to laser swathe width, W , in metres (Fraser *et al.*, 1999), with

$$S_p = \frac{2WF_s}{F_p} \quad (3.7)$$

where F_p is pulse frequency (Hz), which is how often laser pulses are emitted. Swathe width is calculated by (Fraser *et al.*, 1999)

$$W = 2htan\theta \quad (3.8)$$

where h is flying height (m) and θ is scanner angle in degrees from vertical.

The overall average point spacing can be estimated from the geometric arrangement of surveyed points (**Figure 3.15**). The number of ground points, p , recorded by each diagonal pass of the laser beam across the swathe is given by

$$p = \frac{W}{S_p} \quad (3.9)$$

and the ground area (in m²) that these points cover (a) is

$$a = \frac{S_d W}{2} = S_d W \quad (3.10)$$

From **Equations 3.9** and **3.10**, the average density of points (d , per m^2) may be calculated from

$$d = \frac{W}{S_d S_p W} = \frac{1}{S_d S_p} \quad (3.11)$$

Substituting **Equations 3.6** and **3.7**, this gives an expression for average point density as

$$d = \frac{1}{2WF_s/F_p \times 0.5V/F_s} = \frac{F_p}{VW} \quad (3.12)$$

Hence, average point spacing (S_a) can be estimated from

$$S_a = \sqrt{\frac{VW}{F_p}} \quad (3.13)$$

For the purposes of this study, a minimum point spacing of around 1 m was desired. For this to be achieved, given an aircraft velocity of 70 m/s and a pulse frequency of 5000 Hz (Turton, pers comm.), a swathe width of 70 m would be needed (**Equation 3.13**). Given that the width of the riverbed bed in the study reach is 800-1200 m, this would require up to 17 flying lines to be used. Instead, the survey was limited to three flying lines, each of which had a swathe width of 575 m, requiring a flying height of 800 m. This gave an average horizontal point spacing of 2.8 m, which was reduced to be closer to the target spacing of 1 m by flying the reach three times (AAM Geodan, 2000; Hicks and Jonas, 2000). These survey specifications gave an average downstream spacing of 1.7 m (**Equation 3.6**) and an average cross-stream point spacing of 4.6 m (**Equation 3.7**) for each of the three survey flights.

A GPS base station was operated in Christchurch, about 20 km away from the study reach. The aircraft was also fitted with a large format metric camera, to allow simultaneous acquisition of colour aerial photographs (Hicks and Jonas, 2000).

3.4.4 Data post-processing

An integral part of the ALS solution is the post-processing software. The post-processing performed by AAM Geodan consists of two main phases. First, the topography is reconstituted based on the GPS, IRS and laser beam timing records. This results in a raw dataset of X, Y, Z point coordinates, which is adjusted with respect to the local reference ellipsoid (in this case, the NZGD1949 Mount Pleasant circuit for horizontal and Littleton 1937 for vertical; AAM Geodan, 2000). Second, a

morphological filter is applied to separate the raw ALS points into “ground” and “non-ground” points based on changes in slope for a given terrain type (Fraser *et al.*, 1999). Non-ground points corresponded to areas of surface water and vegetation.

A final dataset of approximately two million X,Y,Z coordinates in space delimited ascii format was supplied on CD-ROM (AAM Geodan, 2000). This comprised of six files, with separate ground and non-ground data for each of the three flights made. In total, 89% of all X,Y,Z coordinates were classified as ground contacts, giving over 1.8 million surface points at an estimated point spacing of 1.6 m (AAM Geodan, 2000). In order to create a DEM of the riverbed surface, the three ground point files were merged, and a surface was generated with bilinear interpolation using the ‘Create Surface’ tool in the Data Preparation module of ERDAS Imagine. The DEM point spacing was set to 1 m, to match the spatial resolution ultimately chosen for the photogrammetric DEMs. The DEM created from the ALS data is considered further in **Chapter 6**.

3.5 Independent check data

The only truly independent means of assessing the quality of DEM surfaces is to compare extracted elevations or derived parameters with independently acquired ground measurements (Torlegård *et al.*, 1986). Although not required for either photogrammetric or ALS processing, this is a crucial aspect of any remotely-sensed topographic survey as it allows an assessment of DEM quality to be obtained (e.g. Butler *et al.*, 1998; Heritage *et al.*, 1998; Fraser *et al.*, 1999; Lane *et al.*, 2000; Chandler *et al.*, 2001). For this research, NIWA and EC field teams provided independent check data for both the North Ashburton and Waimakariri study reaches (**Table 3.11**). The riverbeds were surveyed concurrent with the acquisition of each set of the aerial photographs, meaning that the North Ashburton was surveyed in May 1995 and February 1999, and the Waimakariri was surveyed in February 1999, March 1999 and February 2000. The Waimakariri study reach was also surveyed simultaneously with the ALS survey in May 2000.

The North Ashburton study reach was surveyed using a Total Station and automatic data logger, to the same datum used to survey the PCPs, established from a fixed benchmark on Thompson’s Track bridge. In May 1995, exposed areas over the entire study reach were surveyed with an average spacing of 7 m. In wetted channels, the survey spacing was reduced to 2 m. At each submerged point, water depth was also measured (Willsman, 1995). In February 1999, only the submerged riverbed was surveyed, again using a 2 m survey spacing (Willsman, 1999). No water depths were logged, but water edge locations were labelled to allow depths to be estimated from water level elevations (Willsman, 1999).

Topographic survey	Survey type	Field team	Type of points surveyed	Number of points surveyed	Additional data recorded
North Ashburton – May 1995	Total Station	NIWA	Dry	1890	Grain size ^a
			Wet	1613	Grain size ^a ; water depth
North Ashburton – Feb 1999	Total Station	NIWA	Wet	1127	Point code ^b ; water depth
Waimakariri – Feb 1999	Total Station	EC	Dry	5653	Point code ^b
			Wet	5638	
	RTK GPS	NIWA	Dry	208	
			Wet	9300	Water depth (selected)
	RTK GPS & Echo-sounder	NIWA	Wet	64699	Water depth
Waimakariri – March 1999	Total Station	EC	Dry	831	Point code ^b
			Wet	3415	
Waimakariri – Feb 2000	Total Station	EC	Dry	4056	Point code ^b
			Wet	5757	
	RTK GPS	NIWA	Dry	16	
			Wet	4245	
	RTK GPS & Echo-sounder	NIWA	Wet	76187	Water depth
Waimakariri – May 2000	RTK GPS	NIWA	Dry	707	
			Wet	7653	Water depth

^a Estimated from five size classes

^b Points coded based on four classes (bank top; bank bottom; water edge; water level)

Table 3.11 Independent check data collected for the two study reaches.

The Waimakariri riverbed was surveyed using a combination of Total Station and Trimble RTK GPS survey (Hicks *et al.*, 1999b), to the same datum used to position the PCPs. The spatial extent of the Waimakariri study area is such that survey measurements were concentrated towards the downstream end of the reach. The Total Station was operated by EC, and involved continuous data collection using an automatic data logger and an instrument which automatically tracked the survey prism (Hicks *et al.*, 1999b). Using two operators (one at the instrument and one moving the prism), EC collected approximately 1200 points per day. A common datum was established using fixed EC benchmarks on the channel bank. The GPS survey comprised of two Trimble real-time kinematic (RTK) GPS sets (e.g. Satalich and Ricketson, 1998), each allowing rapid point collection by one person. A base station was established approximately 400 m downstream of Crossbank, which allowed good radio links over the whole study reach (Hicks *et al.*, 1999b). Data collection using RTK

GPS was quicker than Total Station, but was subject to satellite-forced delays. It was estimated that 4-5 days continuous RTK GPS survey by two survey teams would be sufficient to cover all of the wadable wetted channels in the 3.3 km study reach (Hicks *et al.*, 1999b). All Total Station and GPS data were converted to the local Mount Pleasant coordinate system.

For exposed areas of the riverbed, a combination of Total Station and RTK GPS was used to provide a large number of check point elevations. Many of these were coded, based on whether they were at water's edge or water level. Compared to the total number of points surveyed, relatively few were on exposed areas of riverbed, and most of these were located close to wetted channels, in order to assess the quality of representation of channel edge zones. Time constraints meant that dry-bed check points were obtained from a relatively small area of the study reach.

For submerged topography, a much denser network of check points was required, as error assessment was considered more critical in wet-bed zones due to the additional uncertainty introduced into remote sensing survey of these areas. Furthermore, these points were designed to be used as a secondary method of deriving wet-bed topography, albeit at a lower spatial resolution than the dry-bed photogrammetric and ALS surveys, should the remote sensing methods planned not succeed.

In February 1999, the GPS unit was mounted on a quad bike for water depths of up to about 0.6 m, and 'hand-held' for water depths up to 1.0 m. In deeper, navigable channels, a jet boat fitted with GPS and an echo-sounder provided a large number of water depth measurements. However, problems navigating the jet boat in shallow water meant that this approach was abandoned for later wet-bed surveys. Instead, in both the February 2000 and May 2000 check point surveys, water depths were measured by installing a Trimble RTK GPS and echo-sounder in a wooden kayak. This was moved to-and-fro across each wetted channel. In this way, depths were obtained for a far greater proportion of the study reach than had been possible in February 1999.

In March 1999, a different strategy was tested. This involved using a Total Station to measure point elevations for a large number of wetted points, which were then indexed based on whether they were on exposed or submerged gravel, or at the water's edge. Thus, it was possible to derive a data set of estimated water depths based on the elevation of the bed and local water surface.

The check data collected was subsequently used both to assess the quality of remotely-sensed water depths, and to assess the quality of the riverbed DEM surfaces before, during and after post-processing (**Chapters 4, 5 and 6**).

3.6 Chapter summary

Topographic surveys with digital photogrammetry and ALS, as with any survey technique, require careful consideration of project design. This is particularly critical with respect to large, gravel-bed rivers, which represent an extreme case due to the disparity between spatial extent and vertical relief. Survey time and cost is minimised by reducing image scale. Image texture is improved by increasing image scale. In the context of investigating the project design required to obtain topographic information from large, gravel-bed rivers, the two rivers used, the North Ashburton and Waimakariri, have been introduced, and the reasons for the selection of the reaches studied discussed.

Next, the remote sensing technologies of digital photogrammetry and ALS were explained. In each case, this initially consisted of a brief summary of the physical principles upon which the methods are based. From this understanding, a number of phases of data collection and processing were identified, each of which is likely to influence final data quality. Each phase must be considered in the context of the project aims, as many of the parameters involved can be tailored to meet project requirements. In the case of digital photogrammetry, the point spacing and theoretical vertical precision of final DEM surfaces are controlled by the scale of imagery and scanning resolution used. These determine a baseline level of data quality that should be achieved. It was found that addition of tie-points at the block triangulation stage had a positive effect on the quality of the solution to the least-squares bundle adjustment. For ALS, the point spacing can be varied by altering flying height and aircraft speed. It is important to remember, for both digital photogrammetry and ALS, that correct selection of parameters must occur *a priori*, before data acquisition actually occurs. Once surveyed, data density and quality can only be degraded and not increased. In both cases, decisions regarding the number of flying lines required to cover the riverbed were informed by estimation of the quality of surface representation that would result.

Finally, the collection of independent check data was described. The assessment of DEM quality is an important stage of any project that uses remotely-sensed topographic survey, as it is an effective way of quantifying the presence and magnitude of different types of error in the data. Consequently, measurement of riverbed topography using conventional, terrestrial methods formed an important part of project design.

The methods for collecting topographic data described above provide raw datasets. Before the data can be used to answer geomorphological questions, they must be post-processed to deal with the effects of water, vegetation, and other errors, and the

associated improvements in DEM quality must be quantified. Two different methods have been developed to recover submerged topography, based on whether there is clear water or more turbid water. For the clear-water North Ashburton River, through-water photogrammetry was used to recover the topography of submerged zones (**Chapter 4**). For the more turbid Waimakariri River, this involved deriving an empirical relationship between water colour and water depth (**Chapter 5**). In both cases, the measurement of submerged topography was automated and integrated into wider post-processing routines that also attempted to identify and remove vegetation and other errors. The degree of post-processing success will be judged with reference to improvements in both the quality of DEMs *per se* and the quality of parameters derived from them.

CHAPTER 4. THE CLEAR WATER CASE: THROUGH-WATER DIGITAL PHOTOGRAMMETRY

Successful application of remote sensing in river environments requires measurement of both exposed and submerged areas of the riverbed (4.1). In an optimum case, the water is clear and shallow and the bed is visible, allowing through-water photogrammetry to be used to measure submerged topography directly. However, refraction at the air-water interface will systematically bias estimated elevations (4.2). In this chapter, a strategy for dealing with a shallow, clear-water river is developed (4.3), based on the use of a post priori refraction-correction for through-water digital photogrammetry (4.3.1). The presence of water will downgrade image content such that fewer points are successfully stereo-matched and more mismatches occur. Thus, DEM post-processing is required to filter out points where the submerged bed has not been seen (4.3.2). The effect of water on automated stereo-matching performance is also considered in terms of specifying DEM collection parameters (4.3.3). The refraction-correction and post-processing procedure is developed and tested on three small sub-areas of the North Ashburton River (4.4), and subsequently re-applied with an optimised collection parameter set (4.5). Ultimately, corrected DEMs are generated of the whole study reach (4.6). The effectiveness of the correction process is first assessed in terms of DEM quality as compared with independent check data, and then using the derived parameters of mean bed level and water depth distribution (4.7). Finally, a simplified correction algorithm is suggested (4.8).

4.1 Introduction

An obvious and important issue related to using remote sensing methods to study rivers is that most river channels have water in them. If complete morphology and morphological change are to be measured remotely, then treatment of submerged topography is an important consideration. In **Chapter 2**, existing applications of remote sensing in river environments were reviewed. It was shown that, for many existing applications of digital photogrammetry and ALS to riverbeds, this issue was avoided by either not considering inundated areas of the riverbed (e.g. Heritage *et al.*, 1998; Chandler and Ashmore, 2001) or by supplementing remotely sensed data with conventional, terrestrial survey measurements (e.g. Lane *et al.*, 1994). It was also demonstrated that whilst image analysis and through-water photogrammetry offer progress in this area (e.g. Lyzenga, 1981; Hardy *et al.*, 1994; Winterbottom and Gilvear, 1997; Fryer, 1983; Butler *et al.*, 2001b), both have more frequently been applied to shallow coastal environments. In this chapter, the clear-water case is addressed, by applying through-water photogrammetry to the North Ashburton River.

The integration of two-dimensional image analysis methods and three-dimensional DEMs (Lane, 2000) allows submerged elevation data to be produced for the entire riverbed.

4.2 The geometry of through-water photogrammetry

The basis of two-media photogrammetry has been widely addressed (e.g. Tewinkel, 1963; Meijer, 1964; Schmutter and Bonfiglioli, 1967; Rinner, 1969; Höhle, 1971; Harris and Umbach, 1972; Slama, 1980; Shan, 1994). Basic optical principles and empirical results suggest that through-water photogrammetry is theoretically possible. The main issue is that refraction at an air-water interface causes a systematic bias to be introduced to photogrammetrically-measured points. If this is ignored, object-space elevations will be corrupted by a real/apparent depth effect (Butler *et al.*, 2001b).

Specifically, the presence of water results in a departure from the relationship that forms the basis of the collinearity equations (**Equations 3.3 and 3.4**), and which allow the object co-ordinates of a point to be calculated based on the associated image co-ordinates. The geometry of the two-media problem is shown in **Figure 4.1**. Rays of light originating from an underwater point P are refracted at the air-water interface (P_a and P_b) before arriving and being recorded in the image located at exposure stations A and B . If no correction is applied, the two collinear lines $A-P_a$ and $B-P_b$ intersect at point P'' , the (incorrect) apparent depth of underwater point P (Butler *et al.*, 2001b). The exact location of this point will depend on the object-space position and orientation of the two exposure stations. If repeated for many points across a submerged bed, this will produce a surface that lies above (i.e. at a higher elevation than) the real surface.

However, this systematic bias can be modelled. Rays of light passing through the air-water interface are shifted according to the Snel/Descartes law of refraction:

$$\frac{\sin r}{\sin i} = \frac{h}{h_a} = n \quad (4.1)$$

where i is angle of incidence of a ray of light originating from point P below the water surface, r is the angle of the refracted ray above the water surface, h is the actual water depth, h_a is the apparent water depth and n is the refractive index, related to the optical properties of the two media (Fryer and Kniest, 1985). It is known that the refractive index of clear water is relatively constant, varying from 1.340 by less than ± 0.007 for temperatures in the range 0 to 30°C (Jerlov, 1976). Application of **Equation 4.1** to h_a for each underwater point re-validates the assumption of a perspective projection for that point (Fryer and Kniest, 1985).

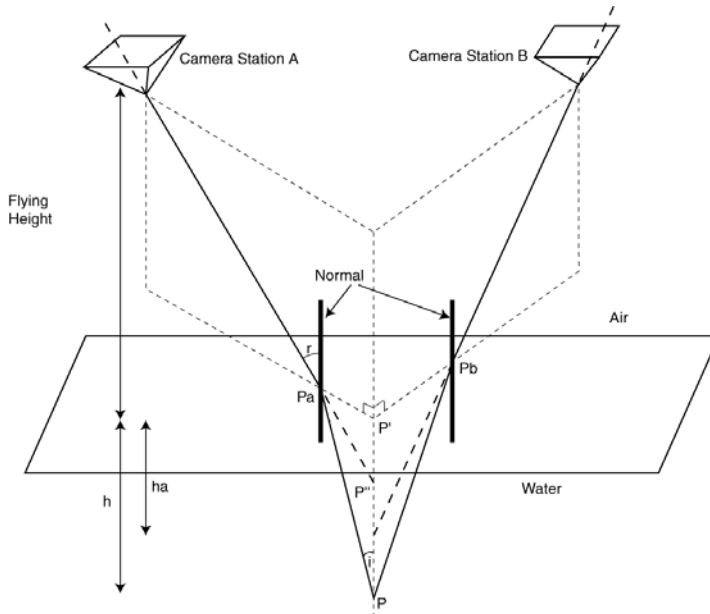


Figure 4.1 Geometry of two-media photogrammetry (from Fryer and Kneist, 1985)

Conventional (analytical) approaches developed to deal with two-media photogrammetric situations have adjusted image coordinates during establishment of the photogrammetric block (e.g. Rinner, 1969, Harris and Umbach, 1972; Newton, 1989; Harvey and Shortis, 1998). This has involved using submerged PCPs to compute radial distortions in the images due to refraction and to allow modification of the bundle of rays to conform to the perspective projection. A disadvantage with this approach, in the context of digital photogrammetry, is that it requires modification of the bundle adjustment solution which is not readily achievable with most commercially available software packages (Butler *et al.*, 2001b).

Once confined to a *post priori* solution, there are two alternative solutions for refraction-correction algorithms (Butler *et al.*, 2001b): adjustment of the object X,Y,Z coordinates for each successfully stereo-matched DEM point; or adjustment of individual vertical Z values to compensate for refraction at each X,Y location. The first option is similar to the analytical two-media solution, except that corrections are made to the object-space coordinates of derived DEMs rather than the image-space coordinates of refracted control points. However, alteration of the planimetric position of DEM points would require re-sampling and re-interpolation to construct and fill the original grid, introducing additional uncertainty into the procedure. Modification of only the Z coordinate automatically retains the grid-based format of the DEM, and is, therefore, preferable.

The Z coordinate adjustment approach was used in research by Butler *et al* (2001b) to develop a refraction-correction algorithm that could be applied *post priori* to a regular grid-based DEM, after the block adjustment phase. The correction procedure was then used to derive DEMs of large-scale gravel surfaces using close-range digital photogrammetry in both laboratory and field settings. This research seeks to build on this work, by developing a similar correction procedure that can be applied to large, gravel-bed rivers at the reach-scale.

4.3 Methodology

4.3.1 Correction for refraction

The refraction model used in this study was derived from the optimum three-dimensional geometry associated with the two-media photogrammetric problem (**Figure 4.2**).

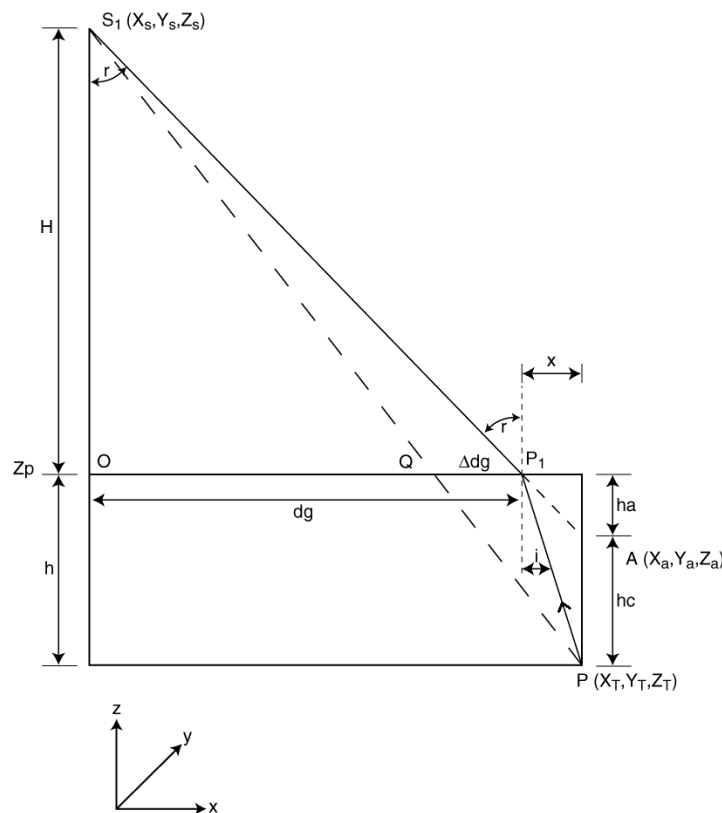


Figure 4.2 The three-dimensional geometry associated with an analytical solution for through-water photogrammetry (from Butler *et al.*, 2001b)

From **Figure 4.2**, the true (h) and apparent (h_a) depth of water can be expressed in terms of the angles of refracted and incident light respectively, with:

$$h = \frac{x}{\tan i} \quad (4.2)$$

and:

$$h_a = \frac{x}{\tan r} \quad (4.3)$$

Hence:

$$h = \frac{h_a \tan r}{\tan i} \quad (4.4)$$

Substituting **Equation 4.1** into **Equation 4.4** gives:

$$h = \frac{h_a \tan r}{\tan \left(\arcsin \left(\frac{\sin r}{n} \right) \right)} \approx \frac{h_a \tan r}{\tan \left(\frac{r}{n} \right)} \quad (4.5)$$

demonstrating that, provided the angle of incidence (i) is known, the true water depth (h) can be calculated from the apparent water depth (h_a).

At present, i is not known, but it can be approximated as follows. First, the straight-line distance (d) from the camera (S_1) to the apparent point (A) is calculated:

$$d = \sqrt{(X_a - X_s)^2 + (Y_a - Y_s)^2 + (Z_a - Z_s)^2} \quad (4.6)$$

where (X_a, Y_a, Z_a) is the position of the apparent point and (X_s, Y_s, Z_s) is the position of the camera lens.

The angle of refraction (r) is formed by the intersect between line $A-S_1$ and S_n , the normal to the horizontal plane (in this case the water surface, Z_p). This normal has a direction cosine of $(0,0,-1)$, and the angle between the two lines ($\cos r$) is given by the product of the two vectors:

$$\cos r = \left(\frac{X_a - X_s}{d} \cdot 0 \right) + \left(\frac{Y_a - Y_s}{d} \cdot 0 \right) + \left(\frac{Z_a - Z_s}{d} \cdot -1 \right) = -\left(\frac{Z_a - Z_s}{d} \right) \quad (4.7)$$

We know that:

$$Z_a = Z_p - h_a \quad (4.8)$$

where Z_p is the elevation of the water surface and h_a is the apparent depth. Substituting this into **Equation 4.7** gives:

$$\cos r = \frac{-(Z_p - Z_s - h_a)}{d} \quad (4.9)$$

Hence:

$$r = \arccos\left(\frac{h_a + Z_s - Z_p}{d}\right) \quad (4.10)$$

Equation 4.10 can then be substituted into **Equation 4.5** to give an expression for true water depth (h):

$$h = \frac{h_a \tan\left(\arccos\left(\frac{h_a + Z_s - Z_p}{d}\right)\right)}{\tan\left(\frac{1}{n} \arccos\left(\frac{h_a + Z_s - Z_p}{d}\right)\right)} \quad (4.11)$$

where all the variables are known or can be estimated: h_a can be calculated as the difference between the apparent elevation and the modelled water surface elevation at a point; Z_s is the elevation of the exposure station calculated during the bundle adjustment; Z_p is the water surface elevation; n is the refractive index; and d can be calculated using **Equation 4.6**, because the three-dimensional co-ordinates of both the camera position (from the bundle adjustment) and the apparent point (from the DEM surface) are known. It is common for this procedure to be carried out for both the overlapping photographs to obtain two values of h for each wet-bed point (Butler, 2001b). The average of both calculations is used to determine the true water depth.

4.3.2 Post-processing

In practice, this optimum situation is complicated by two main factors. First, there is a need to know or to model accurately the position of the water surface (Kniest, 1990). Linked to this is the assumption that the water surface is planar. Second, the magnitude of the required correction depends on the angle of incidence (Fryer and Kniest, 1985), and increases with radial distance from the perspective centre of the camera lens (Tewinkel, 1963; Meijer, 1964). This implies that a spatially-variable correction might be necessary, based on the distance from this point.

In a field setting, three additional issues must be addressed. First, water surface irregularities, such as water surface disturbances, surface waves, quasi-random patches of white water and sunlight glare, may all be important depending on the nature of the river in question. Second, the visibility of the submerged riverbed is likely to be variable both spatially (due to water surface irregularities) and temporally (due to factors including light levels, shadows and river stage). Third, small deviations from the refractive index of water (1.340) might also be expected in river water due to water turbidity. Turbidity might also be spatially variable across the area of interest.

The identification of these factors helped to develop a number of additional research issues. First, it was necessary to establish whether the refraction-correction procedure

for two-media photogrammetry could be used at this scale, and whether it improved representation of submerged topography to a significant extent. This was achieved by assessing the quality of both raw and refraction-corrected DEM surfaces, with reference to both independent check point measurements and derived parameters (water depth distribution and mean bed level). Second, it was important to assess whether lateral distance from the image centre and water turbidity cause significant deviation from the optimum optical geometry shown in **Figure 4.2**. This was assessed by studying the magnitude of the apparent/true water depth effect, and whether it varied spatially across the submerged bed.

A third issue was the modelling of water surface elevation, as this will be critical in subsequent estimations and corrections of water depth. For close-range through-water applications of photogrammetry, Perspex sheets have been used to artificially flatten the water surface and provide control over water surface elevation (e.g. Fryer, 1983; Fryer and Kneist, 1985; Butler *et al.*, 2001b). In this case, such control was neither available nor feasible. Instead, the water surface elevation was modelled by interpolating dry-bed DEM points along the water edges across the wetted channels. This was undertaken by merging the raw DEM with a non-directional edge detection of the original ortho-photo, to produce a map of water edge elevations, which was interpolated to produce a map of estimated water surface elevations. It was found that a smoother water surface was produced when an inexact interpolation algorithm (such as kriging, as in this study, or minimum curvature) was used. Exact interpolators (such as triangulation) were found to produce a faceted and angular water surface. Once the water surface elevation had been estimated, **Equation 4.11** was applied to estimate the refraction-corrected water depth (h) at each wet-bed DEM point. Subsequently, the maps of corrected water depth were converted to maps of corrected submerged bed elevations by subtracting h from Z_w , the elevation of the water surface, at each wet-bed pixel.

Fourth, there was the issue of water surface irregularities. These effects, exaggerated by time lag between exposures, potentially produce brightness differences between corresponding points on overlapping photographs, which may cause the automated stereo-matching algorithm to fail. For close-range through-water photogrammetric work, two cameras can be used, ensuring simultaneous exposure and meaning this problem is minimised (e.g. Fryer, 1983; Fryer and Kneist, 1985; Butler *et al.*, 2001b). However, the use of aerial imagery necessitates a lag between exposures while the aircraft carrying the sensor passes between exposure stations. Differences between image content for identical areas of riverbed were expected to introduce increased levels of both mismatching and interpolation into the photogrammetrically-derived

submerged bed surface. To correct for this, points where it was thought that the photogrammetry had not detected the bed were eliminated. This was based upon the premise that in locations where corrected submerged elevation was within a threshold vertical distance of the estimated water surface elevation, yet was not near the water edge, the photogrammetry was actually detecting the water surface. The areas where points had been eliminated were set to zero and re-interpolated to give the final, corrected submerged bed elevation map. These were merged with the exposed DEM to produce the final, corrected DEM.

In the context of assessing the overall feasibility of using digital photogrammetry in river environments, identification of a threshold water depth, above which the submerged riverbed is no longer visible, was also of interest. This value will define the spatial and temporal limits of where and when through-water photogrammetry can be used to survey inundated riverbeds.

This whole process (**Figure 4.3**) was automated using the Spatial Modeller module of ERDAS Imagine, so that given an input of a raw DEM, a map of estimated water surface elevations, a classified ortho-image (into wet-bed and dry-bed areas) and the (X,Y,Z) position of both exposure stations in the object space, the final corrected DEM was produced without any further user intervention. The estimate of h was made twice (once for each camera location) and averaged for every wet-bed pixel to give a map of corrected water depth for the three sub-areas (Butler *et al.*, 2001b). However, the differences between refraction-corrected water depths (h) estimated from each camera were negligible (the largest being less than 0.001 m), and not statistically significant ($p < 0.05$).

4.3.3 DEM collection parameter values

The theoretical and practical issues identified above are not independent of established controls upon digital photogrammetric performance. Hence, in submerged zones, DEM collection parameter perturbation may also be required. From **Appendix 1**, there are several DEM collection parameters in the OrthoMAX module which may be relevant in the case of through-water photogrammetry. In general, the presence of water downgrades the information content of imagery where the topography is submerged. Parameters used to control stereo-matching performance have previously been shown to improve DEM quality where information content is poor (e.g. Gooch *et al.*, 1999). For example, the minimum threshold and noise threshold parameters can both be reduced in order to increase the number of successfully stereo-matched points.

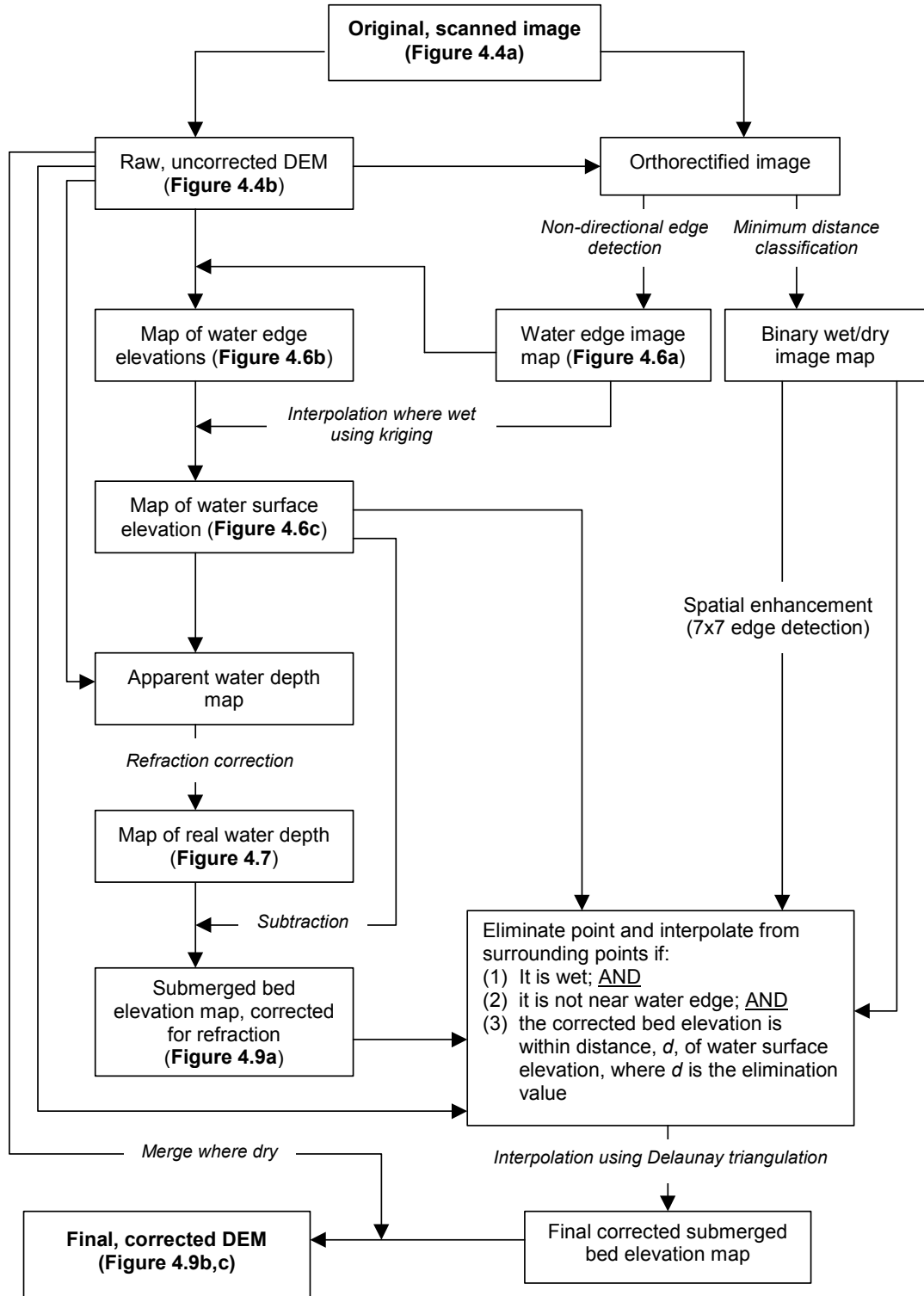


Figure 4.3 The automated refraction-correction procedure

Specifically, the presence of surface water is likely to introduce elevation errors into wet-bed measured points, due to the difficulties associated with the correct vertical positioning of points through water. Refraction causes radial displacement of image coordinates in the image space as compared with a perspective projection. As deeper

water implies greater height differences, larger radial displacements in the x-parallax will occur. Hence, the minimum parallax value must be set higher in order to increase the x,y image-space search distance. Also, the rejection factor may become important, as it can be used to eliminate anomalous high or low points in the dataset, for example, where the water surface was detected rather than the underwater bed. The presence of water may additionally cause the epipolar constraint to operate incorrectly. The epipolar constraint reduces the spatial extent over which the matching algorithm must search, and so increasing the lateral search extent (through increasing the template size) may also help improve submerged point quality.

The importance of these parameters on both the stereo-matching precision and DEM quality was tested using a sensitivity analysis strategy. Each relevant collection parameter was systematically varied, and DEMs recollected for each sub-area. The resulting DEMs were subsequently subjected to the refraction-correction procedure and automated post-processing routine to study how changes in initial DEM quality were propagated through to final the DEMs.

4.4 Application to North Ashburton River: Sub-areas

The refraction-correction procedure was developed and tested using three adjacent 30 m x 30 m sub-areas (**Figure 4.4a**) to reduce processing time during development of the method. The chosen sub-areas contained a large number of ground survey points (388) and exhibited approximately equal areas of submerged and exposed topography. DEMs were generated for each sub-area with a horizontal point spacing of 0.371 m, the smallest point spacing recommended by OrthoMAX. This figure is around five times greater than the object-space pixel size (Lane *et al.*, 2000).

4.4.1 Uncorrected DEM surfaces

The raw DEMs for each of the sub-areas are shown in **Figure 4.4b**. Prior to post-processing or refraction-correction, the position and configuration of the wetted channels is evident. The proportion of matched pixels in dry-bed areas across all three sub-areas (mean of 64%; **Table 4.1**) is lower than reported in previous geomorphological applications of digital photogrammetry (e.g. Butler *et al.*, 1998; Stojic *et al.*, 1998; Lane *et al.*, 2000). This might reflect the scale of photography used, because in areas where the gravel texture of the riverbed becomes indistinct, image texture will be lessened or even lost. This will be especially critical given the low relative relief of the riverbed, as sudden breaks of slope (and the difference in texture and lighting that these produce) will also be absent over large portions of the riverbed.

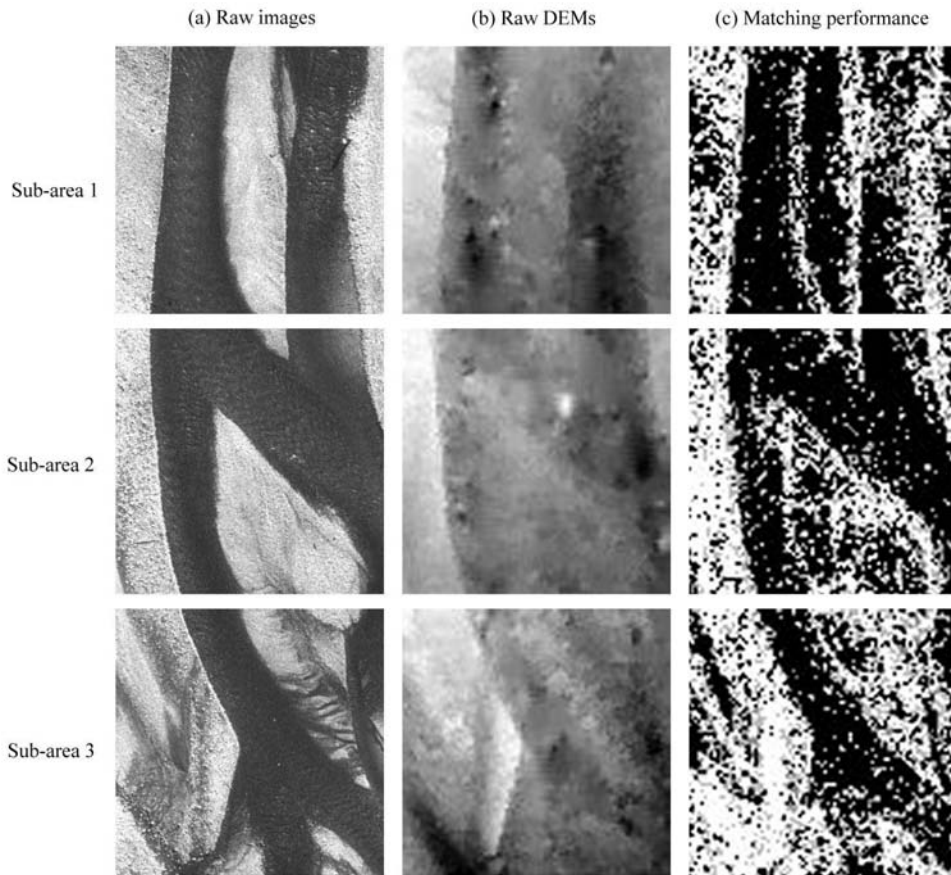


Figure 4.4 The three sub-areas used for development and testing of the refraction-correction procedure: (a) shows the raw images of the three sub-areas; (b) shows the raster images of the raw photogrammetrically-acquired DEMs, scaled from black (lowest elevations) to white (highest elevations); and (c) shows the stereo-matching statistics files that are produced during DEM collection, which give the spatial distribution of matching performance. White points show good matches, with light and dark grey representing fair and poor matches respectively. Black points indicate an unsuccessful match and subsequent interpolation. Each tile is 30 m x 30 m in size and flow is from top to bottom.

Sub-area	STEREO-MATCHED PIXELS IN DRY-BED AREAS (%)				STEREO-MATCHED PIXELS IN WET-BED AREAS (%)			
	Good	Fair	Poor	Total	Good	Fair	Poor	Total
1	28.4	18.2	5.0	51.7	11.4	15.3	5.9	32.6
2	41.6	20.6	3.4	65.5	7.5	11.7	4.3	23.5
3	47.1	23.0	5.6	75.9	24.0	19.4	6.8	50.2

Table 4.1 The matching precision of the initial sub-area DEMs for dry-bed and wet-bed points.

As expected, the proportion of matched pixels is consistently lower for wet-bed points than for dry-bed points (**Table 4.1**). This is assumed to be because the presence of water downgrades image quality and causes the automated stereo-matching algorithm to match fewer points successfully (**Figure 4.4c**). These areas can be identified in the raster images (**Figure 4.4b**) by 'blurring', for example in the centre of the left-hand channel in sub-area 1. There are also some exposed areas that appear to be heavily interpolated, such as the centre of the mid-channel bar in sub-area 1. Nonetheless, the spatial density of matched points is considerably greater than would be obtained using a traditional terrestrial monitoring program. In each sub-area there are approximately 4000 pixels in inundated areas of riverbed: even in the worst case (24%) this gives almost 1000 point elevations in a 30 m x 30 m area.

To obtain an estimate of the quality of the sub-area DEMs, an automated correspondence algorithm was used to associate the location of each DEM point to the location of the nearest survey point, provided it was within a given search radius. A search radius of 0.15 m was used, which guaranteed that the survey point was within the corresponding DEM pixel (0.371 m). This allowed both mean error (ME) and standard deviation (SDE) to be calculated (**Table 4.2**), indicating DEM accuracy and precision, respectively (**Section 2.3.1**). Although the quality of wet-bed points is of most interest here, the procedure was also carried out for dry-bed points, to give an indication of the maximum accuracy and precision that could reasonably be expected in wet-bed areas.

DRY-BED DEM POINTS				WET-BED DEM POINTS		
Sub-area	No. of pixels compared with check points	ME (m)	SDE (m)	No. of pixels compared with check points	ME (m)	SDE (m)
1	34	+0.008	0.084	54	+0.184	0.144
2	23	+0.012	0.074	48	+0.075	0.091
3	18	-0.067	0.098	23	+0.062	0.090

Table 4.2 Quality assessment of the three raw sub-area DEMs for wet-bed and dry-bed DEM points.

The trend suggested by the matching statistics (**Table 4.1**) is also manifest in the quality assessments of the three sub-areas. Mean error associated with dry-bed points is relatively low in all three sub-areas, and the SDE is as good as could be expected given the precision of photo control points used in the block triangulation (**Table 3.9**). In all three sub-areas, the quality of wet-bed points is lower, and a positive systematic error (as would be expected in the presence of water) is evident. On average, the elevation of points on the submerged riverbed in the three sub-areas is around 0.11 m

higher than their surveyed value. There is no clear spatial pattern to the discrepancies between DEM and surveyed elevations for wet-bed points (**Figure 4.5**), suggesting that there is no readily quantifiable spatial pattern of error caused by distance from image perspective centre or water turbidity.

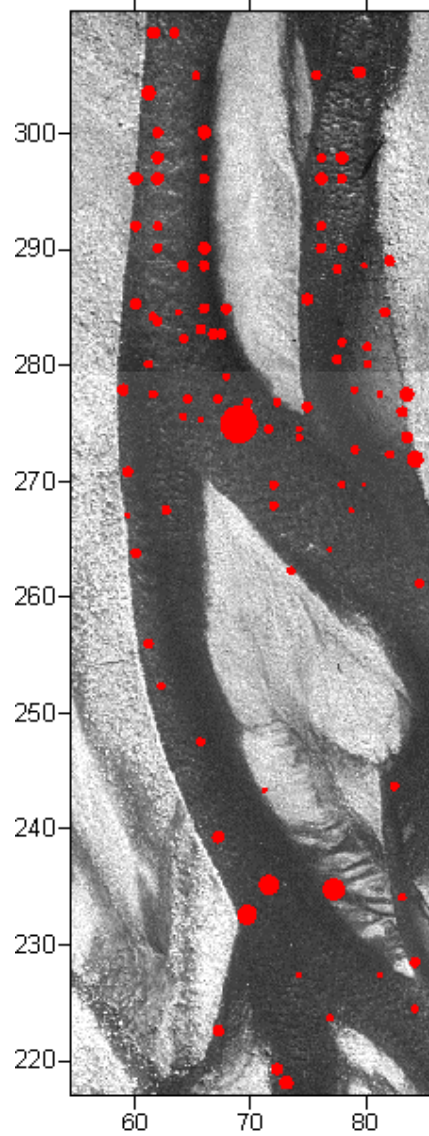


Figure 4.5 Spatial pattern of discrepancies between DEM and surveyed elevation for wet-bed points in the three sub-area DEMs. Circle diameter reflects magnitude of elevation error, following scaling to remove the effect of water depth.

4.4.2 Depth correction for refraction

It is clear from the uncorrected DEMs that the presence of surface water considerably degrades the quality of surface representation. To try to improve the quality of underwater points, the automated refraction-correction procedure (**Figure 4.3**) was applied to the North Ashburton sub-area DEMs. Apart from the raw sub-area DEMs

(Figure 4.4b), the necessary input data consisted of water surface elevation maps, classified ortho-images and the object-space coordinates of each exposure station. The exposure station coordinates were extracted from the bundle adjustment results file. Ortho-images were created for each sub-area using the ‘Ortho Tool’ module of OrthoMAX with the same grid spacing as the DEM surfaces (0.371 m) to ease their integration. Binary wet-dry images were created from the ortho-images using a two-way unsupervised classification. Water surface elevation maps were created using the method described earlier (Section 4.3.2), and are illustrated in Figure 4.6 for sub-area 1. First, a non-directional edge filter was applied to the ortho-images in order to emphasise the boundaries of wetted channels (Figure 4.6a). These were then merged with the raw DEM surfaces to give maps of water edge elevations (Figure 4.6b), and subsequently interpolated across the wetted channels using kriging to produce estimated water surface elevation maps (Figure 4.6c).

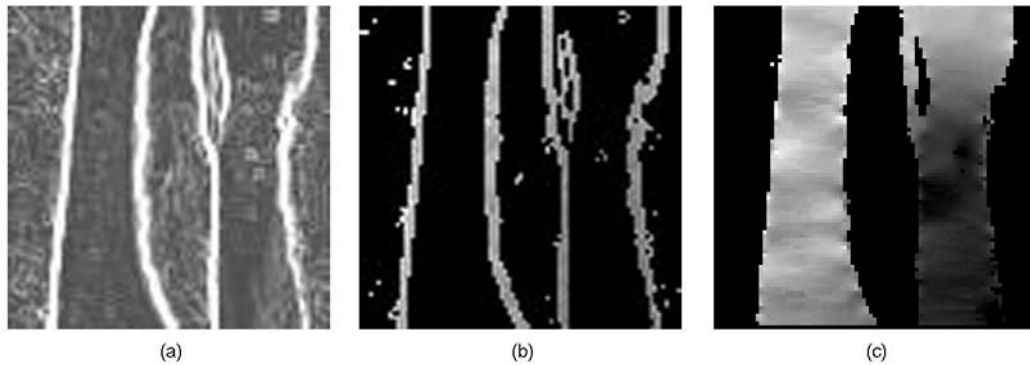


Figure 4.6 Modelling the water surface elevation: (a) shows the non-directional edge detection image; (b) shows the water edge elevation map; and (c) shows the final estimated water surface.

Once all input data had been obtained, Equation 4.11 was used to calculate refraction-corrected water depths (Figure 4.7a) based on apparent depths calculated as the difference between the water surface maps and the raw DEMs. Negative apparent depths were set to zero, and these points (where some point above the water surface had been measured) were later removed during post-processing (Figure 4.3). Figure 4.7 quantifies the vertical depth corrections computed by the refraction-correction model for wet-bed points in each sub-area, which range from approximately 0.01 m to 0.20 m. As expected, the spatial pattern of depth corrections closely resembles that of corrected water depths since the size of depth correction is proportional to apparent depth. The corrected depth values were translated into corrected bed elevation values by subtraction from the modelled water surface elevation.

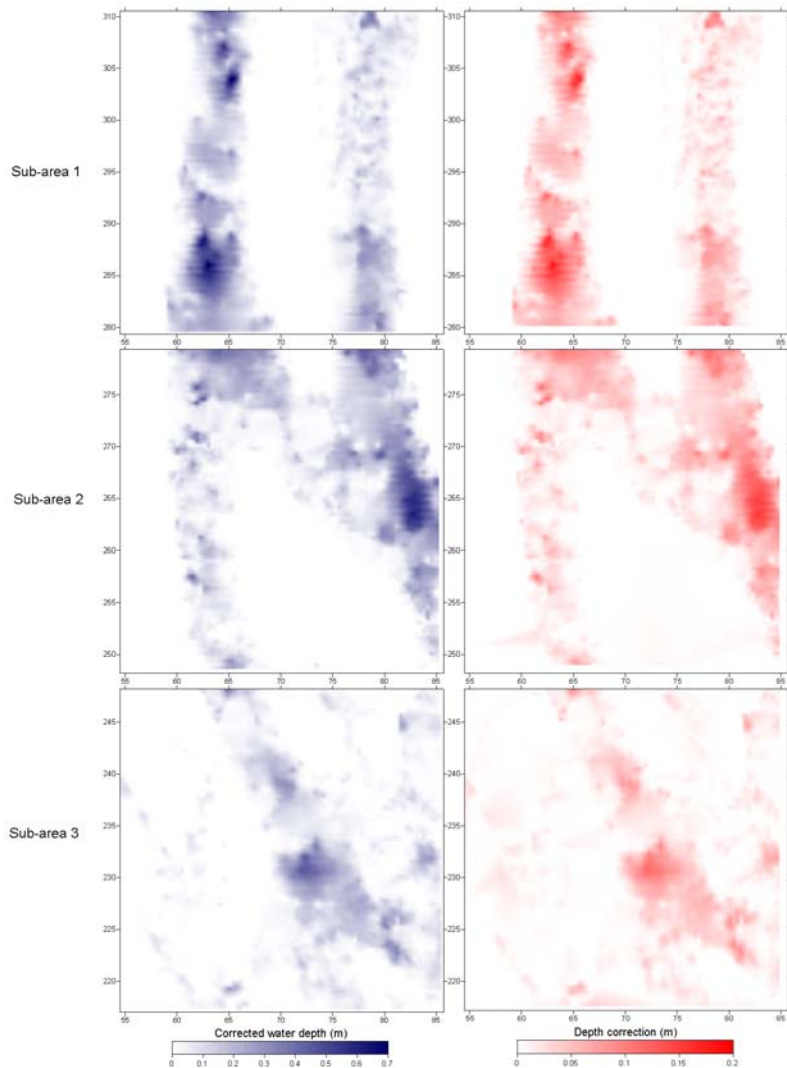


Figure 4.7 The spatial pattern of corrected water depths (left) and depth corrections made to calculate them (right).

4.4.3 Automated post-processing

The final phase of the automated refraction-correction procedure (**Figure 4.3**) was the elimination of points within a threshold distance (d) below the modelled water surface. At these points, it was assumed the submerged bed had not been correctly measured due to point mismatching or detection of the water surface rather than the bed. Following removal of points, the submerged bed was re-interpolated using Delaunay Triangulation. It was recognised that towards the edges of wetted channels, water depths would typically be small and hence points might fall within d of the water surface elevation and yet correctly represent the submerged bed. Consequently, an additional filter was included that meant points that fell within 1 m of the channel edge (as defined by the classified ortho-image) were not considered.

Given the range of measured water depths in the three sub-areas (0.0-0.7 m) and the precision associated with photogrammetrically-derived dry-bed point elevations (mean 0.085 m), corrected DEM surfaces were generated for two values of d : 0.00m and 0.06 m. The points eliminated and the elevation corrections made at these points (from the refraction-corrected bed surface) for both values of d are shown in **Figure 4.8**.

As expected, increasing the d value increases the number of points eliminated from the refraction-corrected DEM surfaces (**Table 4.3**), although relatively few of the points removed produced large (greater than 0.5 m) elevation corrections. However, the range of corrections made was greater than those associated with the refraction-correction itself (**Figure 4.7**). This is not surprising: the refraction-correction merely increased water depths where it was assumed the bed had been seen; the automated post-processing phase attempted to re-impose a wetted channel where it was assumed it had not. Removal of wet-bed points places increased importance upon the interpolation method used to re-establish a continuous bed surface, particularly in areas of shallow beds where a high proportion of points are removed. Re-interpolation of a bed surface from surrounding bed points may result in channel over-deepening in these zones. DEM quality assessment should highlight whether or not this is a particular problem in this case.

Sub-area	$d = 0.00\text{ m}$	$d = 0.06\text{ m}$
1	238	831
2	545	1295
3	425	1140

Table 4.3 Number of points removed by the automated post-processing routine for both threshold levels tested.

4.4.4 DEM quality assessment

The sub-area DEMs, after both the refraction-correction and the automated post-processing stages, are shown in **Figure 4.9**. Visually, it is hard to discern many differences between the raw (**Figure 4.4b**) and the refraction-corrected and post-processed DEM surfaces (**Figure 4.9**).

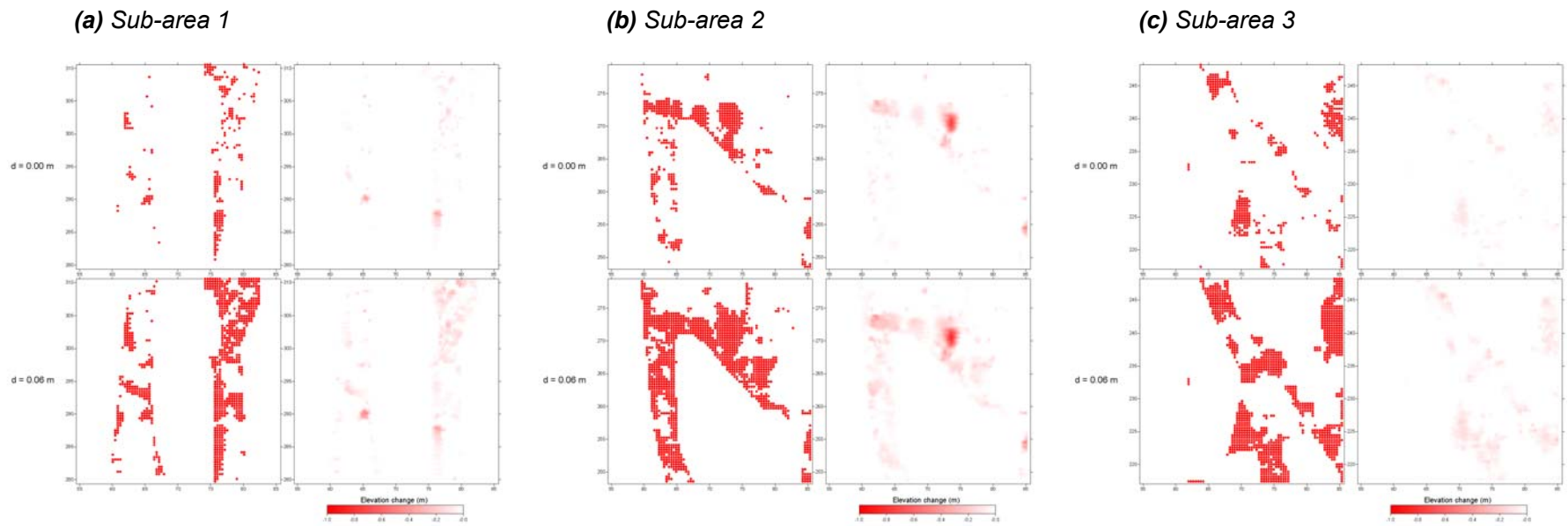


Figure 4.8 The spatial distribution of points eliminated by the automated post-processing routine (left) and elevation changes introduced to the refraction-corrected DEM following re-interpolation (right) for each sub-area. Values of d of 0.00 and 0.06 m were used.

To quantify the effect of the refraction-correction procedure on the wet-bed point quality in the sub-area DEMs, the automated correspondence algorithm was again used to associate DEM points with survey measurements (**Table 4.4**). The reduction in ME suggests that wet-bed point accuracy is improved by the refraction-correction procedure in all three sub-area DEMs, though the improvement in quality is only statistically significant ($\rho < 0.05$) in sub-areas 1 and 2. As expected, the precision (indicated by SDE) remains relatively unchanged as the refraction-correction should not change the spread of errors.

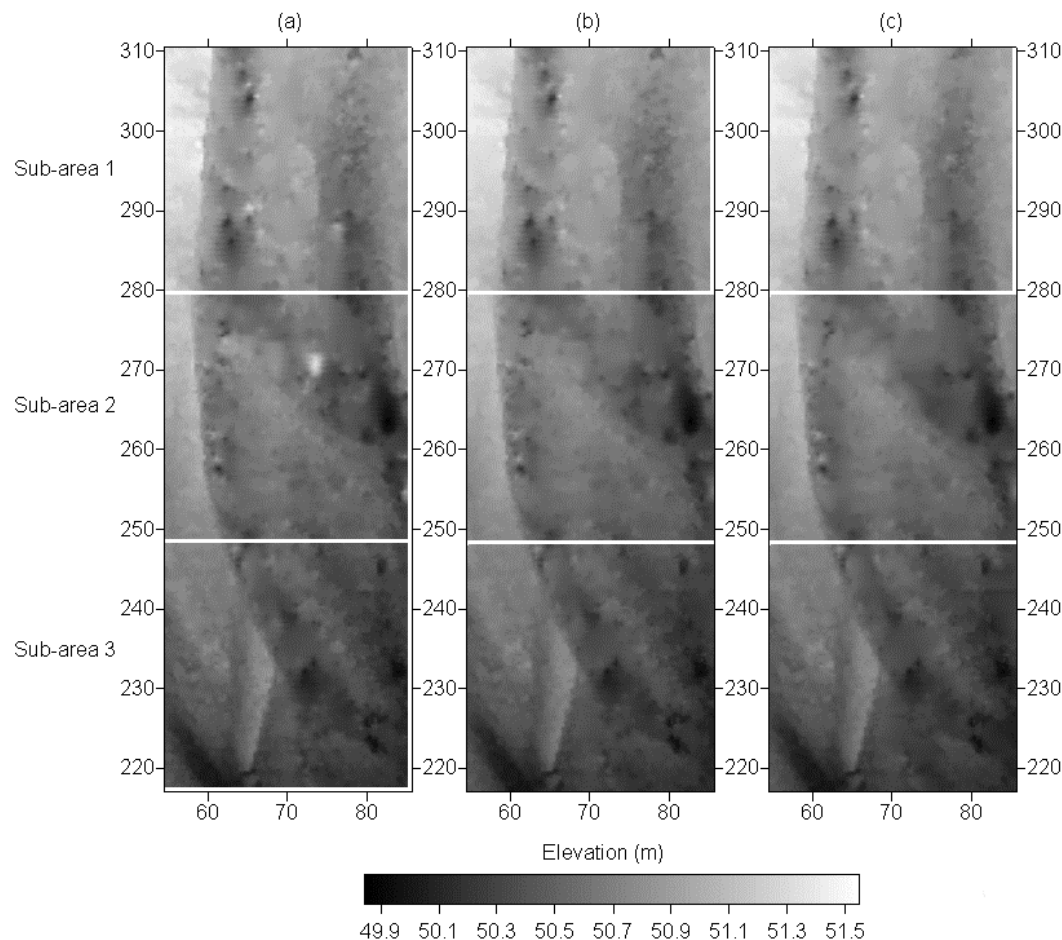


Figure 4.9 The sub-area DEM surfaces: (a) following application of the refraction-correction; (b) post-processed with $d = 0.00\text{ m}$; and (c) post-processed with $d = 0.06\text{ m}$.

The effect of the refraction-correction procedure can be further understood with reference to **Figure 4.10** which shows the relationship between DEM and surveyed elevations for wet-bed points for all three sub-areas. Theoretically, the points should plot near the displayed line of equality. However, refraction produces a systematic error which causes points to plot above this level (i.e. uncorrected DEM elevation $>$ DEM

elevation). The refraction-correction effects a datum shift towards the line of equality (e.g. Butler *et al.*, 2001b) but in this case the shift is not sufficiently large to eliminate all systematic bias.

DEM	SUB-AREA 1		SUB-AREA 2		SUB-AREA 3	
	ME (m)	SDE (m)	ME (m)	SDE (m)	ME (m)	SDE (m)
Raw DEM	+0.184	0.144	+0.075	0.091	+0.062	0.090
Refraction-corrected DEM	<u>+0.160</u>	<u>0.138</u>	<u>+0.048</u>	<u>0.101</u>	+0.055	0.084
Post-processed DEM: $d = 0.00$ m	<u>+0.152</u>	<u>0.138</u>	<u>+0.037</u>	<u>0.099</u>	+0.035	0.079
$d = 0.06$ m	<u>+0.141</u>	<u>0.138</u>	<u>+0.025</u>	<u>0.097</u>	<u>+0.019</u>	<u>0.087</u>

Table 4.4 The effect of applying the refraction-correction and post-processing procedures on the quality of wet-bed points in the sub-area DEMs. Underlined values are significantly improved at the 95% confidence level.

This can be demonstrated by examining the relationship between surveyed and photogrammetrically-derived apparent (i.e. prior to refraction-correction) water depths (**Figure 4.11**). If clear-water refraction was the sole cause of systematic bias, then the surveyed depths would be around 1.3-1.4 times greater than the apparent depths derived from the DEM surfaces. As the plotted points for each sub-area demonstrate, this is not the case, particularly for sub-area 3. Consequently, it cannot be expected that the refraction-correction procedure alone will remove the systematic bias associated with wet-bed point elevations. The systematic error is further reduced, but not removed, by the automated post-processing routine. Following application, ME falls in all three sub-areas, and this further improvement in DEM quality (relative to the refraction-corrected DEMs) is statistically significant ($p < 0.05$) in sub-areas 1 and 2 for the threshold value of 0.06 m.

Another feature of **Figures 4.10** and **4.11** is the high degree of scatter, reflecting the high value of SDE relative to ME (**Table 4.4**). The precision (and hence SDE) of wet-bed DEM points is, in principle, addressed by the automated post-processing procedure, which should remove noise (i.e. water surface detection and mismatches) from the submerged topographic surface. However, the quality assessment statistics show that this has not been the case.

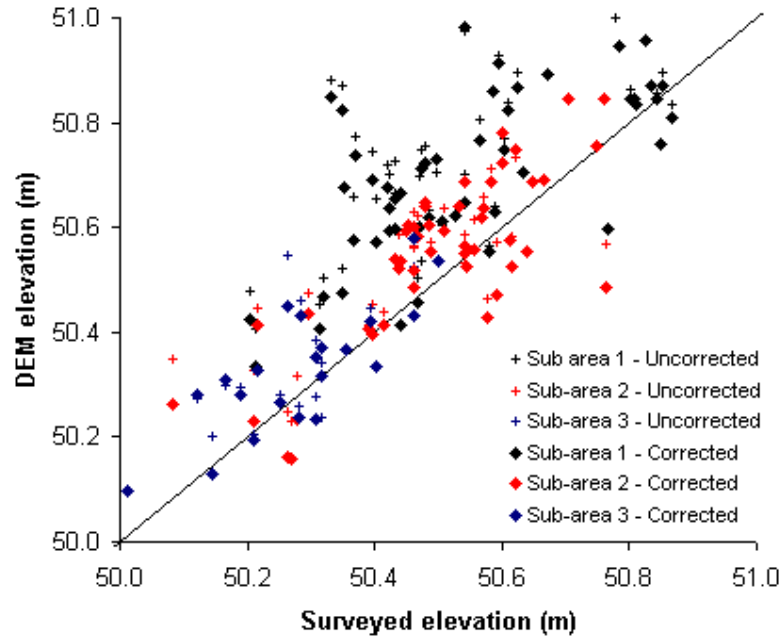


Figure 4.10 The relationship between DEM and surveyed wet-bed point elevations for the three sub-areas for uncorrected and refraction-corrected DEMs.

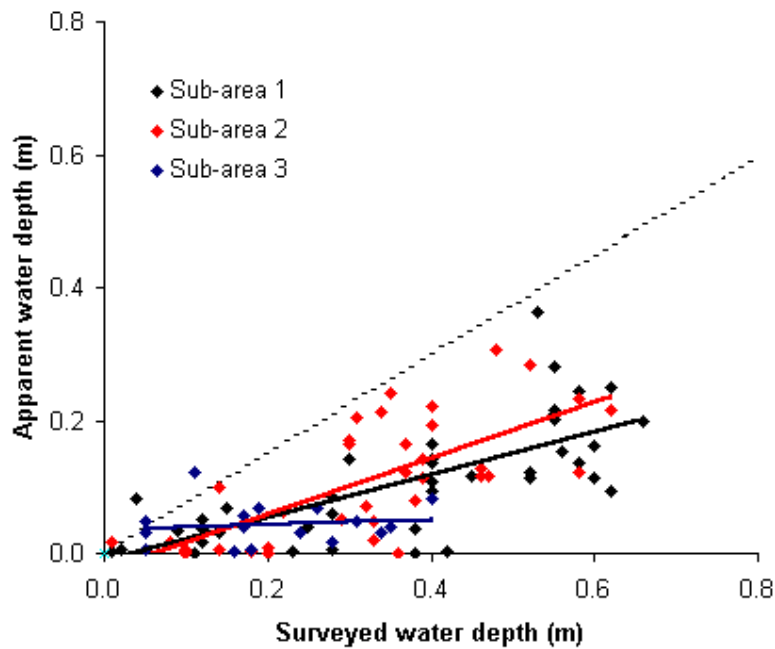


Figure 4.11 The relationship between apparent and measured water depth. The dashed line ($h:h_a$) shows where apparent depths should approximately plot.

4.5 Variation of DEM collection parameters

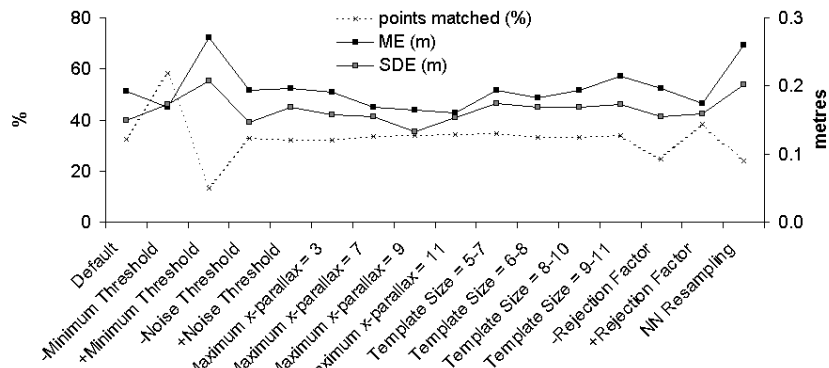
Further improvements in both DEM accuracy and precision might result from modifications to the automated stereo-matching algorithm, through changes made to the user-defined DEM collection parameters (**Appendix 1**). Previous research has found that these can be important controls over quality of derived DEMs (e.g. Pyle *et al.*, 1997; Smith *et al.*, 1997; Gooch *et al.*, 1999; Butler *et al.*, 1998; Lane *et al.*, 2000). The presence of water essentially reduces the texture of the riverbed surface, so those parameters that are known to help deal with poor image quality (ERDAS, 1995; Gooch *et al.*, 1999; Lane *et al.*, 2000), as well as those that have previously been shown helpful in two-media applications of digital photogrammetry (Butler *et al.*, 2001b), were considered particularly relevant (**Table 4.5**). To test the effect of parameter perturbation on stereo-matching performance and DEM quality, raw (uncorrected) DEMs of the three sub-areas were re-collected using a variety of collection parameter sets.

Collection parameter	Default value	Other values tested
Minimum threshold	0.6	0.4; 0.8
Noise threshold	0.4	0.2; 0.6
Maximum parallax	5	3; 7; 9; 11
Template size (min-max)	7-9	5-7; 6-8; 8-10; 9-11
Rejection factor	1.5	1.0; 2.0
Re-sampling	On	Off

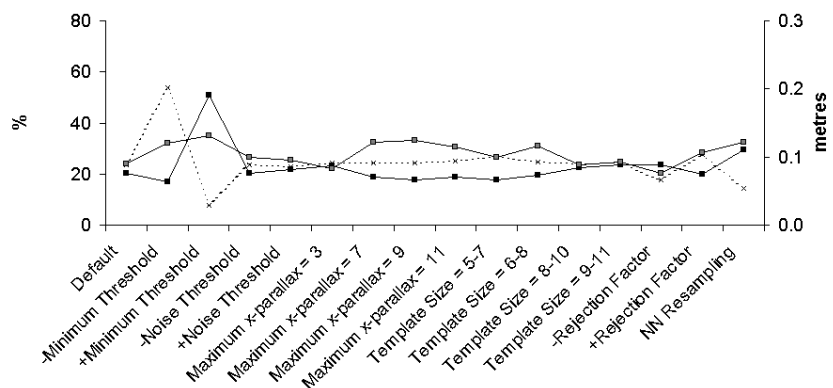
Table 4.5 The collection parameters considered and parameter values used.

The effect of parameter perturbation on the stereo-matching matching performance is shown in **Figure 4.12**. The largest variations in matching success are associated with the minimum threshold and rejection factor parameters. Together, these parameters determine the criteria that must be fulfilled for a point to be accepted as successfully matched. Hence, changes in the proportion of matched points following changes to these parameters do not signify an actual improvement in the precision of the matches, only that greater or fewer points have been approved. This is demonstrated by the lack of correspondence between changes in the proportion of matched points due to these parameter changes and the difference in wet-bed point quality (as indicated by ME and SDE) for the same changes (**Figure 4.12**).

(a) Sub-area 1



(b) Sub-area 2



(c) Sub-area 3

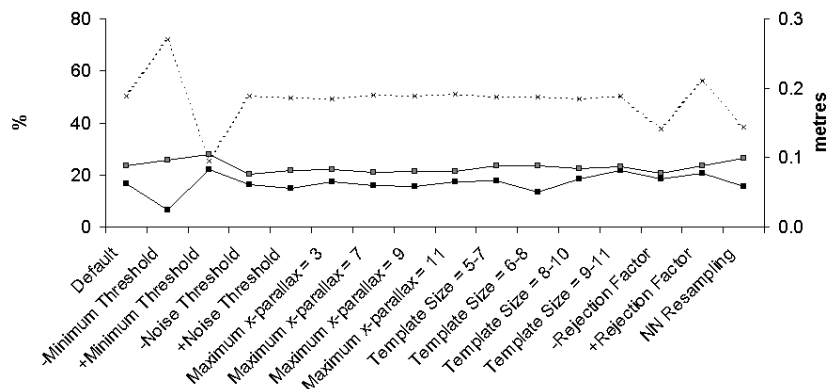


Figure 4.12 The effect of DEM collection parameter perturbation on stereo-matching matching precision and DEM quality for submerged points in each sub-area.

The change in DEM quality in wet-bed zones due to collection parameter perturbation was judged by assessing the wet-bed point quality of each DEM based on the independent check point measurements (**Table 4.6**). It was found that the effects of collection parameter variation were variable both within and between the three sub-areas. No parameter change produced an improvement in both accuracy and precision in all three sub-areas. However, increasing the maximum parallax parameter reduced

ME in all three sub-areas and SDE in sub-areas 1 and 3. The improvement in quality was significant in sub-area 1 ($p < 0.05$), which is known to contain the largest range of water depths. In the context of through-water photogrammetry, the theoretical basis for wet-bed quality improvements due to increasing this parameter has already been established (i.e. it controls the range of elevations considered either side of the expected elevation during stereo-matching; **Appendix 1**) Thus, despite the slight increase in SDE in sub-area 2, it was felt that increasing the maximum parallax parameter to 9 pixels was desirable, given the likely range of water depths at the reach scale.

Collection parameters	SUB-AREA 1		SUB-AREA 2		SUB-AREA 3	
	ME (m)	SDE (m)	ME (m)	SDE (m)	ME (m)	SDE (m)
Default	+0.184	0.144	+0.075	0.091	+0.062	0.090
Minimum threshold = 0.4	+0.168	0.173	+0.064	0.120	+0.024	0.114
Minimum threshold = 0.8	+0.271	0.208	+0.191	0.132	+0.083	0.105
Noise threshold = 0.2	+0.193	0.147	+0.076	0.099	+0.061	0.076
Noise threshold = 0.6	+0.196	0.169	+0.082	0.096	+0.056	0.081
Maximum x-parallax = 3	+0.191	0.158	+0.087	0.083	+0.065	0.083
Maximum x-parallax = 7	<u>+0.168</u>	<u>0.155</u>	+0.070	0.122	+0.060	0.079
Maximum x-parallax = 9	<u>+0.165</u>	<u>0.133</u>	+0.067	0.124	+0.059	0.080
Maximum x-parallax = 11	<u>+0.161</u>	<u>0.154</u>	+0.070	0.115	+0.065	0.080
Template size = 5-7	+0.194	0.174	+0.066	0.099	+0.067	0.088
Template size = 6-8	+0.182	0.168	+0.073	0.116	+0.050	0.088
Template size = 8-10	+0.194	0.168	+0.084	0.088	+0.069	0.084
Template size = 9-11	+0.214	0.173	+0.089	0.092	+0.082	0.087
Rejection factor = 1.0	+0.197	0.155	+0.075	0.096	+0.069	0.078
Rejection factor = 2.0	+0.174	0.159	+0.075	0.106	+0.077	0.088
Re-sampling = Off	+0.260	0.202	+0.110	0.122	+0.059	0.099

Table 4.6 The effect of correction parameter variation on the quality of uncorrected wet-bed points in the sub-area DEMs. Underlined values are significantly improved at the 95% confidence level.

The spatial pattern of elevation changes produced by increasing the maximum parallax parameter in the uncorrected sub-area DEMs is shown in **Figure 4.13**. Changes ranged from approximately -0.9 m to $+0.4$ m, with the largest changes occurring in the wetted channels. The mean elevation change in wetted channels is a lowering of the submerged bed by around 0.005 m, although the spatially-variable nature of change reduces the meaning of an average value. Of greater significance is that the

submerged bed is lowered in the vicinity of those points where the largest positive systematic errors occurred in the uncorrected default parameter DEM (**Figure 4.5**). For dry-bed DEM points, increasing the maximum parallax had negligible effect on DEM quality although slightly more points were successfully stereo-matched (**Table 4.7**).

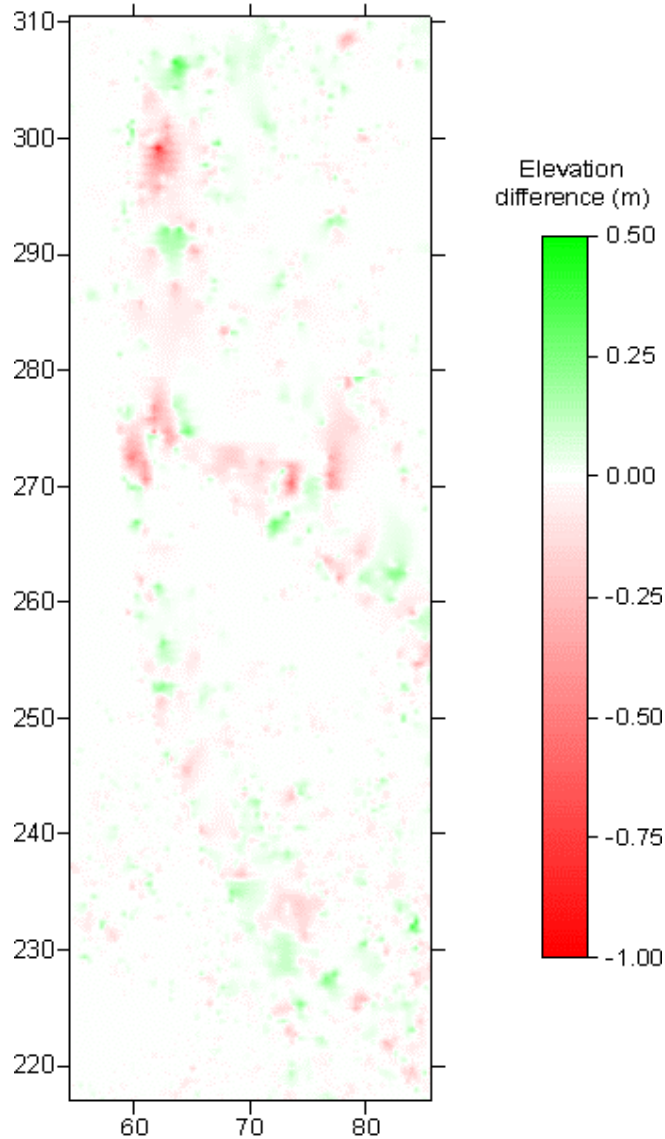


Figure 4.13 The spatial pattern of elevation changes in the uncorrected sub-area DEMs produced by increasing the maximum parallax parameter to 9 pixels.

The final test involved assessing whether the initial improvements in wet-bed point DEM quality obtained due to the increased maximum parallax would propagate through the correction procedure, as compared with the default case. This was achieved by applying the refraction-correction and automated post-processing routines to DEM

generated using an increased maximum parallax parameter of 9 pixels. Analysis of results addressed two main issues: (i) examination of the change in wet-bed point quality due to application of the refraction-correction and post-processing routines (**Table 4.8**); and (ii) examination of the difference between corrected wet-points derived from DEMs generated using the default and increased maximum parallax collection parameter sets (**Table 4.9**).

DEFAULT MAXIMUM PARALLAX PARAMETER (5 PIXELS)				WET-BED POINT OPTIMISED MAXIMUM PARALLAX PARAMETER (9 PIXELS)		
Sub-area	Points matched (%)	ME (m)	SDE (m)	Points matched (%)	ME (m)	SDE (m)
1	51.7	+0.008	0.084	53.2	+0.008	0.087
2	65.5	+0.012	0.074	65.4	+0.012	0.072
3	75.9	-0.067	0.098	76.4	-0.067	0.094

Table 4.7 The effect of increasing the maximum parallax collection parameter on dry-bed point DEM stereo-matching precision and quality.

DEM	SUB-AREA 1		SUB-AREA 2		SUB-AREA 3	
	ME (m)	SDE (m)	ME (m)	SDE (m)	ME (m)	SDE (m)
Raw DEM	+0.159	0.122	+0.074	0.091	+0.061	0.078
Refraction-corrected DEM	<u>+0.123</u>	<u>0.119</u>	<u>+0.034</u>	<u>0.153</u>	<u>+0.053</u>	<u>0.094</u>
Post-processed DEM: $d = 0.00$ m	+0.118	0.116	+0.025	0.140	+0.029	0.090
$d = 0.06$ m	<u>+0.108</u>	<u>0.116</u>	<u>+0.016</u>	<u>0.097</u>	<u>+0.009</u>	<u>0.090</u>

Table 4.8 The effect of applying the refraction-correction and post-processing procedure on the quality of wet-bed points in the sub-area DEM generated using the increased maximum parallax collection parameter set. The values are underlined if errors are significantly reduced from previous stage of processing at the 95% confidence level.

Application of the refraction-correction and post-processing routines, results in a general decrease in both ME and SDE of wet-bed points (**Table 4.8**). Wet-bed point quality ($p < 0.05$) is significantly improved in all three sub-areas with a threshold (d) value of 0.06 m. The resulting SDE is similar that calculated for dry-bed points (**Table 4.2**; mean SDE = 0.09 m), which is the best that can be expected from wet-bed areas. In sub-areas 2 and 3, the ME of wet-bed DEM points is less than 2 cm, but remains considerably higher in sub-area 1.

DEM	SUB-AREA 1		SUB-AREA 2		SUB-AREA 3	
	ΔME (m)	ΔSDE (m)	ΔME (m)	ΔSDE (m)	ΔME (m)	ΔSDE (m)
Raw DEM	-0.025	-0.022	-0.001	+0.000	-0.001	-0.012
Refraction-corrected DEM	-0.037	-0.019	-0.014	+0.052	-0.002	+0.010
Post-processed DEM: $d = 0.00$ m	-0.036	-0.022	-0.012	+0.041	-0.006	+0.011
$d = 0.06$ m	-0.033	-0.022	-0.009	+0.000	-0.010	+0.003

Table 4.9 Comparison of wet-point quality, at different stages of correction, between DEM generated using default and increased maximum parallax collection parameter sets. The values are underlined if reductions in error are significant at the 95% confidence level

Consideration of the changes in wet-bed point quality (**Table 4.9**), as compared with those obtained using the default collection parameter set, shows that improvements in quality in the uncorrected DEM generated with an increased maximum parallax are maintained through the correction process. In terms of ME, the correction process actually appears slightly more effective with the optimised collection parameters, with improvements in all three sub-areas. The effect on wet-bed point precision is more variable, decreasing in sub-areas 2 and 3, which given the increase in accuracy highlights the complex relationship between collection parameter specification and DEM quality. The reduction in error is significant ($p < 0.05$) in sub-areas 1 and 2, both after refraction-correction and following post-processing with a d value of 0.06 m.

4.6 Application to North Ashburton River: Whole study reach

Based upon the apparent success of the refraction-correction and post-processing procedures in increasing wet-bed DEM quality, especially in terms of point accuracy (ME), the process was repeated for the complete study reach. DEMs and ortho-images were generated of the entire study area from the May 1995 and February 2000 aerial photographs (**Figure 4.14**). DEM point spacing was increased to 1 m to reduce data volume. First, DEMs were generated with the default collection parameters (**Appendix 1**). Second, based on experience from the three sub-area DEM, whole reach DEMs were also collected with the maximum parallax collection parameter set to its optimised value of 9 pixels.

The water surface elevation was modelled as before, and the refraction-correction and post-processing procedures (**Figure 4.3**) were applied to the DEMs.

(a) May 1995



(b) February 1999



→ Flow Approximate scale
0 50 100 m

Figure 4.14 Digital images used to create photogrammetric DEMs for the North Ashburton River. The spatial resolution of the images has been increased for display.

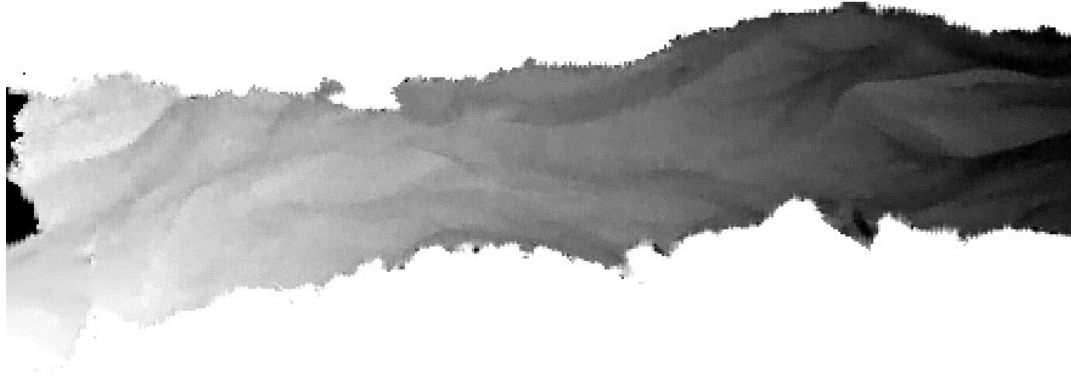
4.6.1 Stereo-matching performance

The raw DEMs of the study reach are shown in **Figure 4.15**. Visually, both DEMs are encouraging, with riverbed features clearly visible, even in the wetted channels, despite the relatively low relief relative to spatial extent. Overhanging bank-edge vegetation (masking the riverbed), particularly in the February 1999 imagery, reduced the useful DEM width by up to 20 m.

(a) May 1995



(b) February 1999

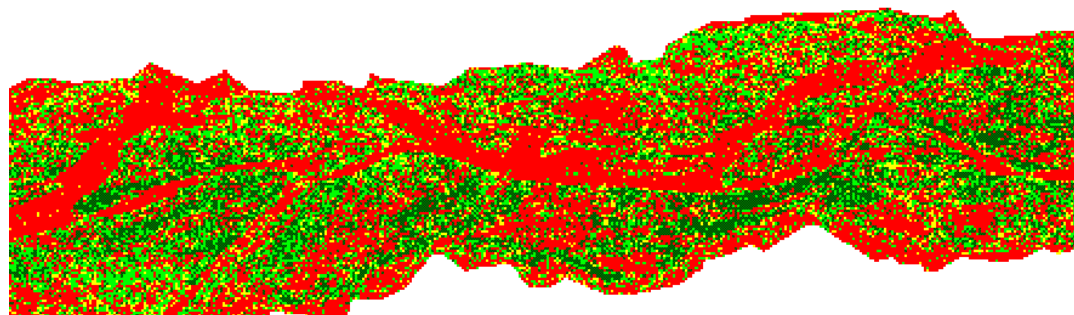


→ Flow Approximate scale
0 50 100 m

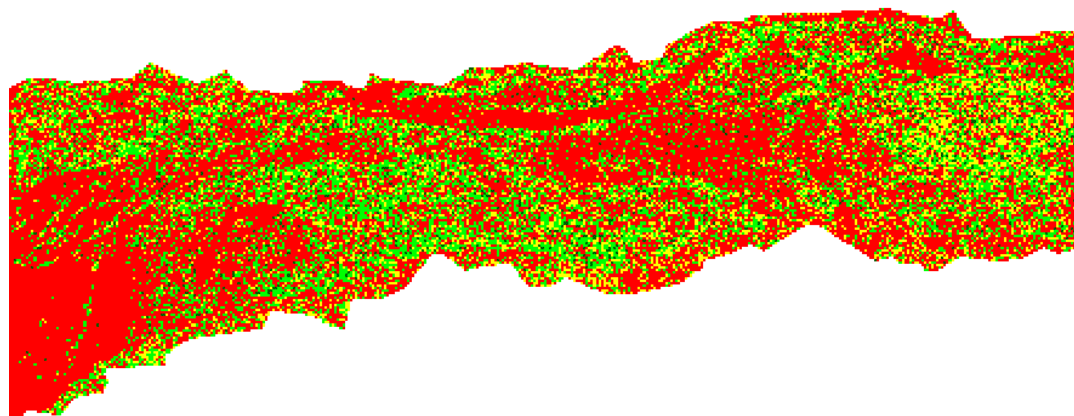
Figure 4.15 Uncorrected DEMs of the North Ashburton study reach. The images are scaled from white (high elevations; 53.5 m.a.s.l.) to black (low elevations; 49 m.a.s.l.).

As observed in the three sub-areas, the number of points matched in exposed gravel areas is considerably higher than in inundated parts of the riverbed (Figure 4.16). In addition, the February 1999 DEM exhibits a region at the extreme upstream end of the reach where stereo-matching has failed, which is translated as a region of extremely low elevations in the DEM surface itself (Figure 4.15b). This was interpreted as an edge effect, as this part of the riverbed was very near the border of both February 1999 digital images. Previous work using ERDAS Imagine OrthoMAX has shown that this can introduce large errors into DEM surfaces (e.g. Butler *et al.*, 1998; Butler *et al.*, 2001b). Edge errors are a common consequence in digital photogrammetry because lens distortion is much more uncertain at the margins of an image, and the magnitude of uncertainty is greater. Thus, there is an increased probability of stereo-matching failure and erroneous elevations.

(a) May 1995



(b) February 1999



→ Flow Approximate scale
0 50 100 m

Figure 4.16 The spatial pattern of stereo-matching performance for the North Ashburton DEMs. Dark green points are ‘good’ matches, light green points are ‘fair’ matches and yellow points are ‘poor’ matches. Interpolated (non-matched) points are shown in red.

The precision of the automated stereo-matching process was assessed using the performance statistics generated during DEM collection (**Table 4.10**). The statistics were sub-divided into dry-bed and wet-bed areas based on a binary (dry-wet) classified image derived from the reach ortho-images. The stereo-matching precision for the May 1995 whole reach DEMs closely resembles the pattern shown by the sub-area DEMs (**Table 4.1**). Using the default collection parameters, just over 50% of all dry-bed points are successfully stereo-matched on the overlapping photographs. In wet-bed areas,

this figure drops to around 40%. Given that the area of study is approximately 40000 m², totals of 22000 (May 1995) and 13000 (February 1999) successfully matched points equate to average point spacings of 1.3 m and 1.8 m, respectively. Both represent a considerable decrease from that commonly feasible using conventional, terrestrial survey methods. When the increased maximum parallax value is used, the number of matched points is slightly increased in both wet-bed and dry-bed areas.

DEM	Total		Good	Fair	Poor	Average point spacing of matched points (m)	
	No. points	(%)	(%)	(%)	(%)		
<i>Default collection parameters</i>							
May 1995	Dry-bed	16898	50.7	19.8	22.1	8.8	1.4
	Wet-bed	5514	39.0	11.2	18.8	9.0	1.6
February 1999	Dry-bed	12243	42.5	3.2	26.0	13.3	1.5
	Wet-bed	1021	34.4	1.2	18.4	14.8	1.7
<i>Optimised collection parameters (maximum parallax = 9 pixels)</i>							
May 1995	Dry-bed	17154	51.5	20.0	22.5	9.0	1.4
	Wet-bed	5683	40.0	11.3	19.7	9.2	1.6
February 1999	Dry-bed	12221	42.5	3.2	26.3	12.9	1.5
	Wet-bed	1141	38.5	1.3	21.0	16.1	1.6

Table 4.10 Stereo-matching performance for whole reach DEMs of the North Ashburton study reach.

For the February 1999 DEM, the number of stereo-matched points using default collection parameters is lower, with around 40% and 35% of points successfully stereo-matched in dry-bed and wet-bed areas, respectively. Very few matches were classed as ‘good’. Increasing the maximum parallax slightly improves matching performance in wet-bed areas, although marginally fewer dry-bed points are successfully stereo-matched. This is perhaps linked to image texture, which was found to be higher for the May 1995 images (**Figure 3.12; Table 3.5**). Furthermore, the contrast (or range of brightness values) in the digital images created from the February 1999 photographs is visibly different to those from May 1995 (**Figure 4.14**). Taken as a whole, the riverbed area of the May 1995 digital image utilises the full range of grey scale tones (black to white, equating to pixel values of 0-255). In the February 1999 image, this range is only 46-255. Consequently, a similar range of riverbed features are represented by fewer grey scale tones, and digital image texture is lessened. In some parts of the riverbed, particularly the upstream part of the reach, the February 1999 digital image saturated at maximum brightness (i.e. white; pixel value of 255). In these areas, grain scale

texture became indistinct or even invisible. The automated stereo-matching algorithm relies heavily upon image texture, explaining why fewer points were successfully matched.

Next, the automated refraction-correction and post-processing routines were applied to the DEMs (**Figure 4.3**). At the reach-scale, riverbed vegetation was also considered because vegetation may introduce systematic error into photogrammetrically-derived DEMs (e.g. Deroose *et al.*, 1998; Lane *et al.*, 2000). At the time of the May 1995 survey, the riverbed was clear from any significant vegetative growth, so vegetation was not considered explicitly. At the time of the February 1999 photogrammetric survey, some scrub-like vegetation was present in the reach. This was identified manually, based on a binary wet-dry maximum likelihood classified image of the reach. Once identified, vegetated points in the DEM surface were eliminated, and their elevation re-interpolated based on surrounding points.

4.6.2 Quality assessment

The final DEM surfaces produced in this way are shown in **Figure 4.17**. The low vertical relief in the study reach means that the downstream trend in mean bed elevation tends to dominate scaling of the whole reach DEMs and obscures bedform-scale features (Sear and Milne, 2000). Consequently, the final DEMs are detrended to emphasise local topographic variation by removing a two-dimensional trend surface. Bed features can be identified as residuals in the resulting surface. The DEMs are also trimmed to eliminate vegetation and (in the case of the February 1999 DEM) to exclude edge effect errors at the upstream end of the reach.

The quality of DEMs was assessed using the automated correspondence algorithm to match DEM points to proximal, independently-surveyed, points. The maximum correspondence distance was set to 0.5 m (half the DEM grid spacing). The DEM quality results were assessed in two ways: (i) to examine the change in quality as a result of applying the correction procedure to DEMs generated using default and increased maximum parallax parameter sets (**Table 4.11**); and (ii) to examine the effect of increasing the maximum parallax parameter at each stage of correction (**Table 4.12**).

Dry-bed point quality was calculated as comparison for the May 1995 DEM, but no independent check measurements were made in dry-bed areas during the February 1999 survey. For the dry-bed areas in the May 1995 DEM, ME is negligible and SDE is low compared to the vertical relief of the reach.

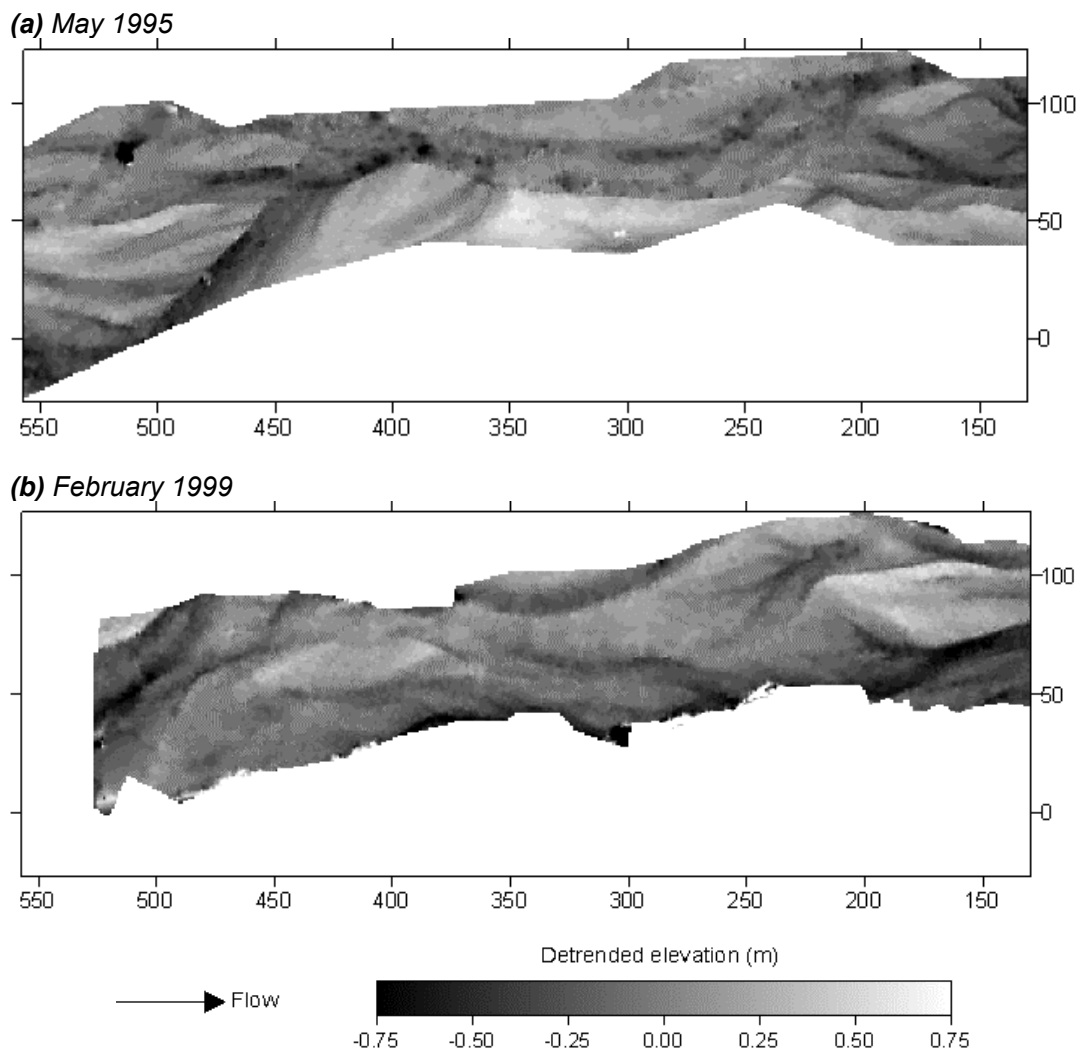


Figure 4.17 The final North Ashburton DEMs. They are generated using default parameter uncorrected DEMs (dry-bed areas) and increased maximum parallax corrected DEMs (wet-bed areas), and have been detrended and trimmed.

Overall, the refraction-correction and post-processing procedure improves wet-bed point quality in the North Ashburton DEMs. For the May 1995 default parameter DEM, the refraction correction procedure proved most effective at improving wet-bed quality, and error was significantly reduced ($\rho < 0.05$). For the February 1999 default parameter DEM, the post-processing to deal with mismatches proved most effective, significantly improving wet-bed DEM quality. The same pattern was repeated when an increased maximum parallax parameter was used, with further, significant ($\rho < 0.05$) improvements resulting in the final, post-processed DEM surfaces. For the February 1999 DEM, this further decrease in wet-bed ME was only achieved at the expense of an increased SDE.

DEM	Points compared	DEFAULT COLLECTION PARAMETERS		MAXIMUM PARALLAX = 9 PIXELS	
		ME (m)	SDE (m)	ME (m)	SDE (m)
May 1995					
Dry-bed	871	-0.021	0.116	-0.026	0.165
Wet-bed					
Raw DEM	717	+0.199	0.233	+0.184	0.242
Refraction-corrected DEM	717	<u>0.173</u>	<u>0.240</u>	<u>+0.145</u>	<u>0.257</u>
Post-processed DEM: $d = 0.00$ m	717	+0.166	0.233	+0.139	0.245
$d = 0.06$ m	717	+0.164	0.232	+0.137	0.244
February 1999					
Dry-bed		<i>No independent check data collected from exposed areas</i>			
Wet-bed					
Raw DEM	231	+0.208	0.182	+0.213	0.250
Refraction-corrected DEM	231	+0.208	0.182	+0.208	0.290
Post-processed DEM: $d = 0.00$ m	231	<u>+0.155</u>	<u>0.149</u>	<u>+0.140</u>	<u>0.223</u>
$d = 0.06$ m	231	<u>+0.149</u>	<u>0.153</u>	<u>+0.128</u>	<u>0.222</u>

Table 4.11 The effect of the refraction-correction and post-processing procedure on default and optimised parameter whole reach DEMs of the North Ashburton River. Underlined values represent significant decreases in error from the previous stage of correction at the 95% confidence level.

These findings are consistent given the image quality and flow conditions associated with each survey. The refraction correction would be expected to make larger positional corrections where the average water depth is deeper (since the vertical displacement introduced by refraction is proportional to water depth). The mean daily discharge at the time of the May 1995 survey was more than double that of February 1999 (**Table 3.1**), implying that wetted channels would have typically been deeper. Furthermore, a higher discharge might have increased the hydraulic efficiency of wetted channels, reducing the proportion of shallow water zones. The automated post-processing routine was designed to remove noise in areas of submerged topography by eliminating points where it was assumed that the bed had not been measured. The presence of fewer ‘good’ stereo-matched points in the February 1999 DEM (**Table 4.10**), despite the lower discharge, may explain the higher SDE of uncorrected wet-bed points (**Table 4.11**). This could be due to the inferior image quality discussed above. It may also be a function of water depth itself, as shallow water is more likely to exhibit surface

disruptions, waves and white water, meaning that there were fewer locations where corresponding underwater points can be identified. As a result, the post-processing procedure proved more effective for the February 1999 DEM, as some of these points are removed.

DEM	ΔME (m)	ΔSDE (m)
May 1995		
Dry-bed	+0.007	+0.049
Wet-bed		
Raw DEM	<u>-0.015</u>	<u>+0.009</u>
Refraction-corrected DEM	<u>-0.028</u>	<u>+0.017</u>
Post-processed DEM: $d = 0.00$ m	<u>-0.027</u>	<u>+0.012</u>
$d = 0.06$ m	<u>-0.027</u>	<u>+0.012</u>
February 1999		
Dry-bed		<i>No data</i>
Wet-bed		
Raw DEM	+0.005	+0.068
Refraction-corrected DEM	+0.000	+0.108
Post-processed DEM: $d = 0.00$ m	<u>-0.015</u>	<u>+0.074</u>
$d = 0.06$ m	<u>-0.021</u>	<u>+0.069</u>

Table 4.12 The change in DEM quality using an increased maximum parallax parameter, as compared with the default value, for the whole reach DEMs of the North Ashburton River. Underlined values represent significant improvements in DEM quality at the 95% confidence level.

Based on experience in the three sub-areas, increasing the maximum parallax parameter improved stereo-matching performance and DEM quality for underwater points. Given that water depths were on average deeper at the time of image acquisition for the May 1995 survey, it is not surprising that larger improvements are made to this DEM surface by increasing this parameter, than to the February 1999 DEM surveyed when water depths were on average less. It is also possible that the different image characteristics, and lower texture in particular, lessen the improvements in stereo-matching performance in inundated areas that arise from changing the maximum parallax.

The highest quality of wet-bed point representation for both May 1995 and February 1999 DEMs is obtained with the increased maximum parallax DEM after refraction-correction and post-processing with $d = 0.06$ m. This suggests that different collection

parameter sets are required for dry-bed and wet-bed areas: in dry-bed areas, the default parameters give better results. This is not surprising since the correct set of image parameters is a function of image content (Gooch *et al.*, 1999). However, OrthoMAX does not allow multiple collection parameter sets to be specified for a single DEM simultaneously. Thus, the final corrected DEMs were produced by creating a DEM using each parameter set, applying the refraction-correction and post-processing procedure (with $d = 0.06$ m), and merging wet-bed and dry-bed areas based on a binary wet-dry image of the riverbed.

The quality associated with DEM points from obtained from exposed riverbed areas (**Table 4.11**) represents the limits of accuracy and precision that it is reasonable to expect from wet-bed areas. Based on this, although wet-bed point quality in terms of ME and SDE is improved by the correction procedure, the presence of water still appears to degrade final DEM quality. Following correction, an average systematic error remains of around 0.15 m for both whole reach DEMs, while SDE is also greater than for dry-bed points. This implies that both that the systematic correction for refraction is insufficient in magnitude and that the presence of water introduces more noise than is removed by post-processing.

As **Figure 4.18a** demonstrates, there remains a strong relationship between surveyed (true) water depth and corrected DEM error for the May 1995 corrected DEM (maximum parallax = 9; $d = 0.06$ m). The correlation coefficient of 0.61 is statistically significant ($p < 0.05$). **Figure 4.18b** shows the relationship between ME and SDE and water depth. Below depths of around 0.20 m, the ME (and accuracy) associated with wet-bed points is little different to that obtained from dry-bed areas (**Table 4.11**), although it increases rapidly with water depth thereafter. Standard deviation of error (and hence corrected DEM precision) does not seem to be as strongly related to water depth. It follows that corrected DEM accuracy will be controlled, at least in part, by water depth. Thus, river stage at the time of image acquisition imposes a key control on that maximum photogrammetric data quality that can be obtained.

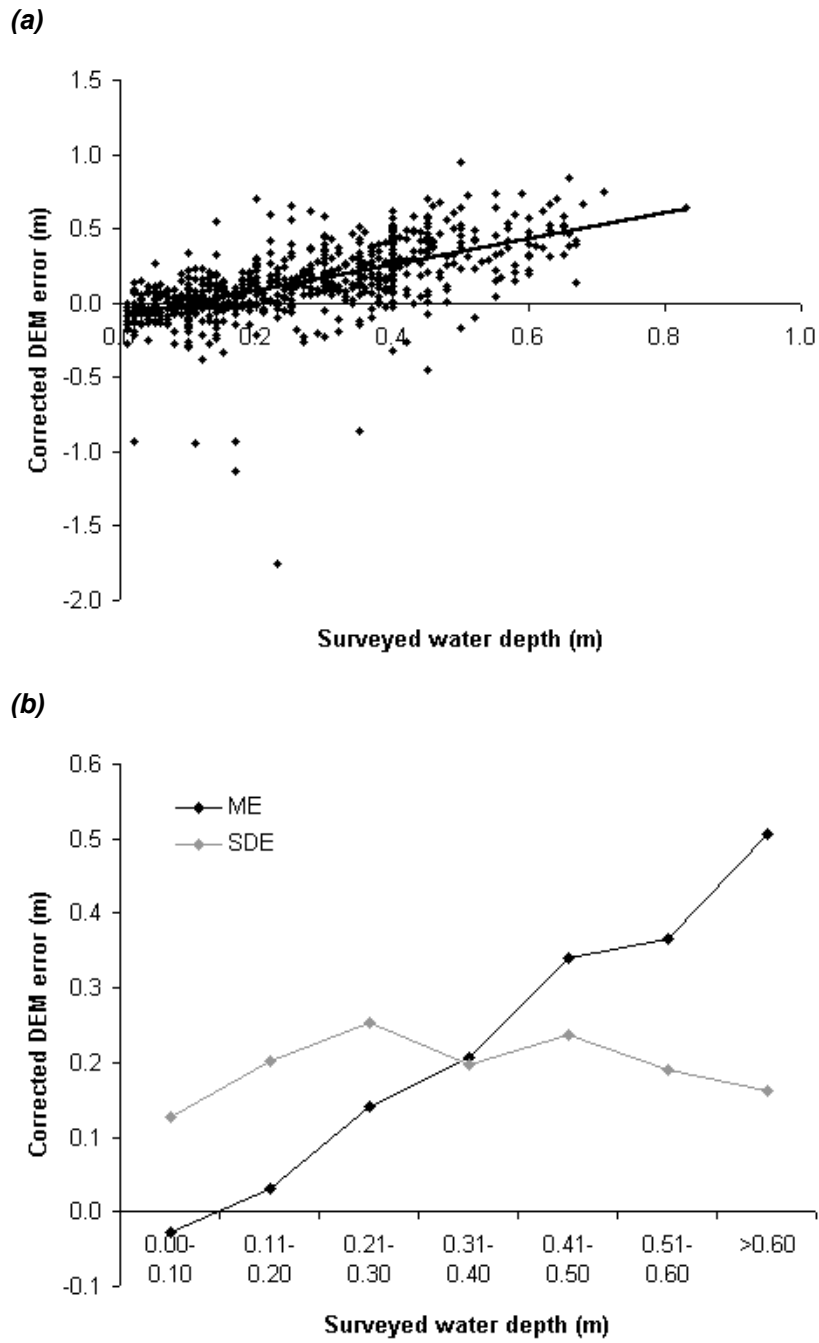


Figure 4.18 The relationship between surveyed water depth and errors from the corrected (maximum parallax = 9; $d = 0.06\text{ m}$) May 1995 whole reach DEM: (a) shows a plot of all DEM-check point pairs; (b) shows the ME and SDE for DEM points grouped according to surveyed water depth.

4.7 DEM quality assessment using derived parameters

In **Section 4.6** quantitative assessment of DEM quality was undertaken based upon independent check data collected concurrently with the imagery used for DEM

generation. The use of empirical measures of DEM quality has been criticised due to the relatively small number of point measurements that are used to interrogate a continuous surface that contains many more data points (**Section 2.3.8**; e.g. Lane *et al.*, 2000; Wise, 2000). The use of derived parameters has often been identified as a complimentary method for assessing DEM quality (e.g. Wise, 1998; Lane, 2001), due to the sensitivity of some derived parameters to relatively small DEM errors. Such errors might be missed if check data alone is used, especially if points close to the area of DEM error have not been measured. This is increasingly likely given the ease with which large topographic datasets can be produced, meaning that the disparity between the numbers of DEM independent check points becomes larger. In this study, although a relatively intensive ground survey was conducted in May 1995, the DEM quality assessment was based on only 871 dry-bed check points and 717 wet-bed check points, which corresponds to only 4.5% of the 19196 dry-bed DEM points and 5.1% of the 14132 wet-bed DEM points. For February 1999, no independent dry-bed point measurements were available, and the 231 points on which DEM quality assessment was based represented 12.1% of all 1909 wet-bed DEM points. The reliability of the subsequent measures of ME and SDE must therefore be questioned.

There are essentially two strategies for assessing DEM quality using derived parameters. The first involves the calculation of derived parameters for which independently-obtained equivalent data is available of known quality, measured to the same datum at the corresponding time. Assuming that this data is terrestrially-acquired, this commonly means that the DEM dataset must be integrated with respect to time or space in order to allow direct comparison.

In a river setting, topographic measurements often involve terrestrially-surveyed cross-sections (**Section 1.2.3**; Lane, 1998). Typically, river managers extract mean bed levels (MBL) from these cross sections (e.g. Griffiths, 1979; Reid and Poynter, 1982; Blakely and Mosley, 1987; Griffiths, 1993; Connell, 2001). Thus, MBL on a cross-sectional basis is a useful derived parameter for assessing DEM quality. Further, estimations of mean bed level for different cross-section spacings allows examination of the relationship between spacing and information loss.

The second strategy for using derived parameters is the computation of derived parameters for which no corresponding independent check data is necessarily available. Certain derived parameters have a good *a priori* theoretical basis, so geomorphological reasoning can often provide a form of DEM quality assessment. Examples of such parameters in a river environment include water depth, local bed

slope, bed shear stress distribution and flow path geometry, all of which can be derived from riverbed DEMs and water surface elevation maps.

For the North Ashburton River, both strategies were used, with mean bed level and a water depth distribution derived from the May 1995 whole reach DEM.

4.7.1 Mean bed level

Sediment storage in a reach can be represented in terms of MBL over the reach area. Mean bed level is important, as it provides an indication of aggradation and deposition rates through time, and is widely used to monitor the gravel-bed rivers of the Canterbury Plains (e.g., Griffiths, 1979; Williman and Lowe, 1988), including the North Ashburton (e.g. Connell, 2000). Although the residual biases from photogrammetric measurements of wet-bed areas are known to be larger than for dry-bed areas (**Table 4.11**), wetted channels only occupy a relatively small proportion of the North Ashburton riverbed. Consequently, the net effect of wet-bed point error is expected to be small. Calculations of MBL and MBL error take this into account, and so provide a useful test of DEM accuracy (i.e. systematic bias). The original photogrammetrically-derived DEM of the riverbed also allows an estimation of the sampling error likely to be associated with traditional surveying methods which typically determine MBL from a few, widely-spaced, cross-section surveys. An estimate of the MBL error associated with different cross-section spacings was obtained by extracting cross-sections at different spacings from the May 1995 DEM, computing MBL by the end-area method (e.g. Bannister *et al.*, 1998), and then comparing them with the “ground-truth” MBL obtained from a DEM interpolated from the independent ground survey dataset.

Figure 4.19 shows the MBL analysis undertaken for the initial DEM (uncorrected with default collection parameters; **Figure 4.15a**) and final DEM (refraction-corrected and post-processed ($d = 0.6$ m) with optimised collection parameters; **Figure 4.17a**) for the study reach for May 1995. The refraction-correction and post-processing procedure is found to reduce the whole-reach MBL error from about 0.023 m to about 0.002 m when the whole data-set is used in the MBL calculations. This does not mean that the final DEM can be measured to a precision of ± 0.002 m, but rather defines the spatially-averaged bias in the DEM surface. To put these figures into context, a spatially-averaged error of 0.001 m corresponds to a volumetric error of approximately 35 m³ over the whole reach.

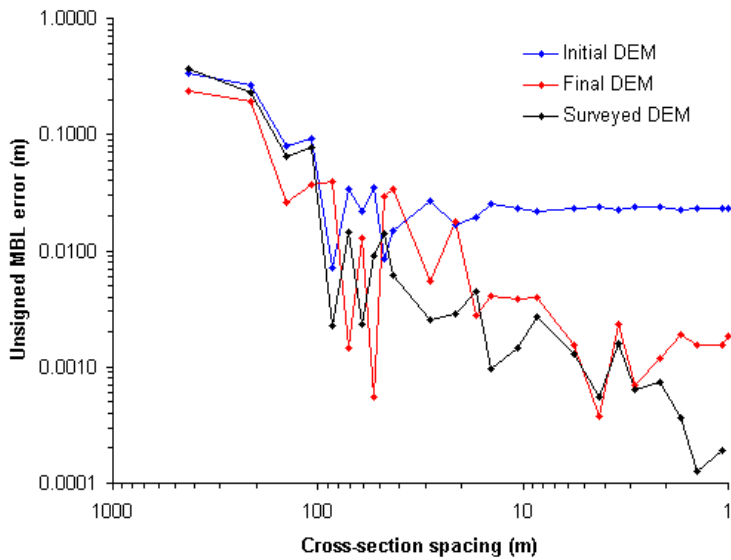


Figure 4.19 Error in mean bed level estimates for a range of cross-section spacings for the initial, final and surveyed North Ashburton DEMs. Error is defined with respect to the full resolution (1 m x 1 m) DEM derived from survey measurements.

It is also informative to compare this level of MBL bias against the error in reach MBL when the reach is represented by only a small number of cross-sections, as with a conventional monitoring programme. **Figure 4.19** shows that MBL error decreases as the number of sections is increased. However, the error associated with the survey measurements only becomes consistently less than the 0.002 m bias associated with the corrected photogrammetry when the cross-section spacing is 50 m or less, although this will vary depending on the proportion of riverbed inundated. Thus, to match the spatially-averaged accuracy of corrected photogrammetry in the study reach for the flow observed at the time of survey, a ground survey would have to use at least 10 cross-sections. However, if the percentage of wet-bed area increases, then the spatially-averaged error associated with photogrammetric measurements will increase. Conversely, at lower flows, more terrestrially-surveyed cross-sections will be needed to match the spatially-averaged photogrammetric error.

The potential inadequacy of widely-spaced cross-sections for representing riverbed topography is also highlighted in **Table 4.13**. This shows how the error in estimated reach sediment volume increases as the spacing between ground surveyed cross-sections is increased. The North Ashburton River is currently monitored using cross-sections spaced approximately 200 m apart, which represents an estimated potential error in volume of over 500000 m³ for the study reach. **Table 4.13** also demonstrates that, even before correction, digital photogrammetry produces a dataset that has a

lower volume error associated with it than with the current monitoring program. Following correction, this error is reduced further, becoming negligible as compared to the magnitude of the sediment volumes involved.

Method	Number of cross-sections	Approximate downstream spacing (m)	Reach volume above 0 datum (m ³)	Error in volume (m ³)
Ground survey (assumed true surface)	414	1	1694276	-
Photogrammetry – Initial DEM	414	1	1716356	22080
Photogrammetry – Final DEM	414	1	1693550	726
Ground survey	207	2	1691385	1096
Ground survey	84	5	1690612	1868
Ground survey	42	10	1678432	14049
Ground survey	8	50	1557461	135020
Ground survey	4	100	1312958	379523
Ground survey	2	200	1089266	603215

Table 4.13 A comparison of sediment storage volumes obtained from uncorrected and corrected photogrammetry, and from evenly-spaced cross-sections, as with a conventional monitoring programme. Error in volume is unsigned and determined with respect to the storage volume calculated from the entire ground survey data-set.

4.7.2 Water depth distribution

Corrected water depths were calculated as a by-product in the correction procedure, so it was a straight-forward task to derive a distribution of water depths from the whole reach. The advantages of the photogrammetric approach include the fact that no additional field survey measurements are required, and that the procedure can be fully automated. Some independent measurements were made of water depth (at each wet-bed point surveyed), and these can be compared with photogrammetrically-derived water depth information. **Figure 4.20** shows the distribution of water depths derived from the May 1995 North Ashburton DEM at several stages of processing: uncorrected with default collection parameters; uncorrected with optimised (increased maximum parallax) collection parameters; refraction-corrected with optimised collection parameters; and refraction-corrected and post-processed ($d = 0.06$ m) with optimised collection parameters. Also shown is the water depth distribution derived from the ground survey points.

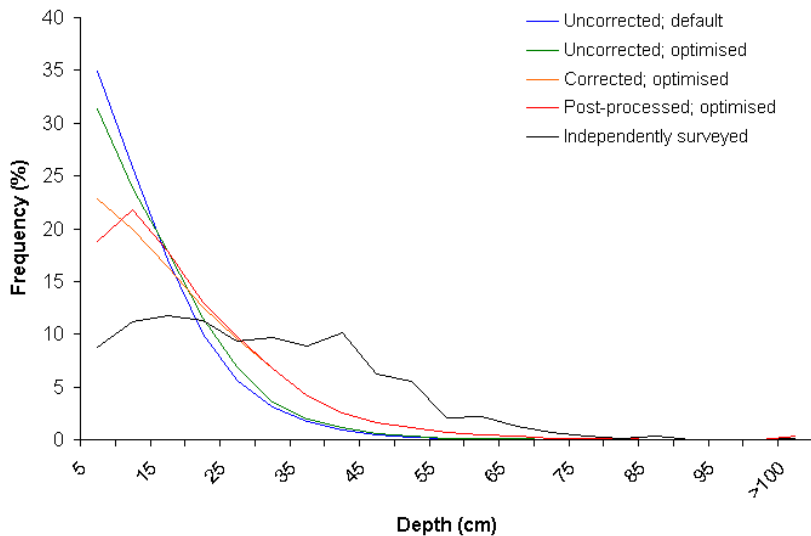


Figure 4.20 Water depth distributions derived from the May 1995 North Ashburton DEM at various stages of correction, and from independent survey measurements.

The water depth distribution information can be used to assess DEM internal and external reliability. Internal reliability relates to the effect of decisions made during the DEM collection process on DEM quality. The use of an increased maximum parallax parameter results in a small improvement in water depth representation, much smaller than the subsequent change produced by the refraction-correction algorithm. Another aspect of internal reliability highlighted by the water depth distribution calculations (though not by DEM quality assessment) is that for a small ($10\text{ m} \times 10\text{ m}$) area of submerged bed towards the upstream end of the reach, water depth calculations from the optimised (increased maximum parallax) DEM surface are too high (typically $> 2\text{ m}$; the tail in the ' $>100\text{ cm}$ ' water depth category in **Figure 4.20**). These anomalous depths are propagated through the correction process, producing a 'pit' in the final DEM surface (**Figure 4.17a**; located at [510,75]). It is not clear from the source imagery (**Figure 4.14a**) why this should be the case. Although the error is visible on the final DEM surface, use of aggregated DEM quality assessment measures (ME and SDE) does not specifically identify this region as problematic.

DEM external reliability relates to how decisions made during the refraction-correction and post-processing processes are translated into changes in DEM quality. Overall, the correction process increases water depths, which displaces the depth distribution towards that obtained from the survey measurements. Post-processing only seems to have an effect at water depths of around 0.25 m or less, suggesting that most points identified and addressed by the algorithm are in shallow water. However, it is clear that

the water depth distribution calculated from the DEM remains more heavily skewed towards shallower water than the ground survey measurements following correction. This is perhaps due to a combination of two effects. First, the photogrammetrically-derived water depths might indeed be too shallow, and the systematic error detected in corrected wet-bed elevations (**Table 4.11**) supports this assumption. Second, it might be due to the poor reliability of survey measurements in terms of representation of the true range of water depths in the study reach. The independent ground survey depth distribution is based only on those points where water depth was measured (1613 points), whereas the DEM-derived water depth distributions are based on information from every 1 m x 1 m pixel in the study reach that occurs in a wetted channel (over 10000 points). There might also be a general tendency to bias field measurements of water depth towards deeper areas of water, although this should have been prevented by the grid-based point collection strategy used (Willsman, 1995). Thus, direct comparison with surveyed depths is not necessarily helpful in this case and geomorphological reasoning about the expected range of water depths might be a more helpful method of assessing the effect of the correction process and of final DEM quality.

It is also apparent from **Figure 4.20** that the full range of water depths are being identified from the DEM surfaces. It was speculated that a maximum depth might exist whereby the underwater bed can no longer be seen with enough clarity to permit automated stereo-matching. Although this is inevitable as water depth increases, for the range of water depths in the North Ashburton study reach when surveyed in May 1995 (approximately 0-1 m), this does not seem to be an issue.

4.8 A simplified refraction-correction method

One of the key advantages of the refraction-correction algorithm developed in this chapter (hereafter labelled method A) is that it is geometrically rigorous, considering the exact position of both exposure stations. This is particularly valuable in situations where the angle of photography is not vertical and water depth is great relative to camera elevation (e.g. Butler *et al.*, 2001b), leading to potentially large variations in apparent and true depth maps calculated from each exposure station. In this case, the aerial imagery is near-vertical and the camera height is over 500 times average water depth. This raises the question of whether such a sophisticated refraction-correction is necessary. The negligible differences between water depth maps calculated from the two exposure stations (maximum difference less than 0.001 m) would suggest not.

To test this suggestion, a second refraction-correction algorithm was developed (method B). This assumed that the camera lens was directly above each image point, meaning that true water depth can be approximated by increasing the apparent depth by 134% (the Snel/Descarte Law, **Equation 4.1**). Apparent water depth was calculated as before, as the difference between modelled water surface elevation and uncorrected DEM elevation for each wet-bed DEM point. **Figure 4.21** shows the differences between refraction-corrected water depths calculated using both methods. Overall, water depths approximated using method B are less than those calculated using method A, with reach-averaged depth decreasing by 3 cm for May 1995 and 5 cm for February 1999. Nonetheless, the distribution of corrected water depths is not significantly different ($\rho < 0.05$).

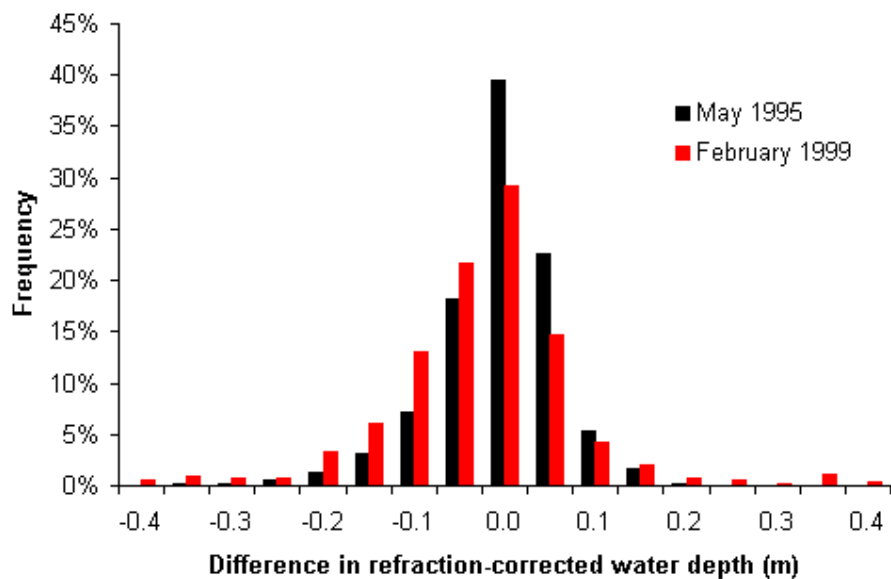


Figure 4.21 The differences in refraction-corrected water depth calculated using methods A and B of estimating refractive displacement through water.

Table 4.14 shows how these changes in corrected water depth are translated into differences in wet-bed point quality in the final refraction-corrected and post-processed DEM surface. For both May 1995 and February 1999 final DEM surfaces, there is no significant change in the quality of wet-bed point representation when method B is used ($\rho < 0.05$). This finding is potentially important as although the difference in processing time is negligible (because both methods can be automated), method B is quicker to implement.

DEM	METHOD A (OPTICAL GEOMETRY)			METHOD B (REFRACTION APPROXIMATION)		
	Points compared	ME (m)	SDE (m)	Points compared	ME (m)	SDE (m)
May 1995	717	+0.137	0.244	717	+0.139	0.240
February 1999	231	+0.128	0.222	231	+0.127	0.217

Table 4.14 DEM quality assessment of corrected DEMs using both refraction-correction methods.

4.9 Chapter summary

This chapter has described the development and implementation of an automated procedure for the clear-water case. This corrects wet-bed point DEM elevations for the effects of refraction, and post-processes the wet-bed area DEM surface to remove noise. Following an explanation of how the presence of water precludes the condition of collinearity between exposure stations and underwater points, a refraction-correction algorithm was developed based on the three-dimensional optical geometry of a camera positioned over shallow water. Potential deviations from this ideal case were identified, and post-processing methods developed to correct for them.

Next, application of this procedure was described for the North Ashburton River. Initial tests were performed for three small sub-areas, and subsequently applied to the DEMs of the whole study reach for May 1995 and February 1999. DEM quality and correction effectiveness was assessed with reference to independent check point data. Overall, it was found that digital photogrammetry can be used to obtain accurate high spatial resolution topographic information in certain fluvial environments, despite the relatively low relief and the presence of water. In dry-bed areas, despite relatively poor stereo-matching performance, feature representation in raw photogrammetric DEMs is excellent, with negligible ME and low SDE relative to the baseline photogrammetric precision based on the object-space pixel size. In wet-bed areas, initial DEM quality was lower, but it was found that the refraction-correction and post-processing both significantly improve wet-bed point quality, particularly in terms of ME (DEM accuracy). In addition, increasing the maximum parallax in the collection parameters specified prior to DEM collection improved uncorrected wet-bed point quality, and these improvements were maintained through the correction process. The derived parameters of water depth and mean bed level also illustrated the positive effect of the refraction-correction procedure.

The presence of clear water and a visible submerged bed represents an optimum case (Lane, 2001). Many braided, gravel-bed rivers have more turbid water, such that the

bed is indistinct meaning that there is insufficient bed texture to allow successful automated stereo-matching. In such a situation, photogrammetry must be abandoned in wetted channels, and alternative solutions sought. One such solution, the derivation of water depth from water colour, is described in **Chapter 5** for the Waimakariri River.

CHAPTER 5. THE TURBID WATER CASE: ESTIMATING WATER DEPTH FROM WATER COLOUR

Where water is turbid, neither digital photogrammetry nor single-frequency airborne laser scanning are suitable survey tools and alternative methods of obtaining water depth information at an equivalent spatial density must be sought (5.1). In this chapter, a method which relates water colour, as observed on digital images, to measured water depth is described (5.2) and applied to the Waimakariri study reach (5.3). Once expressions for water depth have been obtained, water depth is estimated for every visible wetted pixel (5.4). The quality of depth estimates is tested using additional, independently-acquired, water depth measurements (5.5).

5.1 Introduction

In **Chapter 4** it was demonstrated that two-media digital photogrammetry can provide high-resolution representation of submerged topography for shallow, clear water channels. However, many braided rivers are turbid, even at low flow conditions, meaning that this approach cannot be used: photogrammetry relies on line-of-sight and so elevations are calculated only for those objects or landforms visible by the sensor. This can lead to errors in the derived DEM surface, for instance where there is vegetation (when the top of vegetation is measured rather than the ground surface) or shadows which hide the true topography (e.g. Ritchie *et al.*, 1994; Lane *et al.*, 2000; Carbonneau *et al.*, in press). The presence of turbid water, which masks the riverbed, is another example of this problem. Consequently, digital photogrammetry cannot be used to estimate the bed topography of more turbid channels. Single-frequency airborne laser scanning (ALS) systems are also not able to provide topographic measurements of inundated areas.

Thus, in wet-bed areas, we must seek alternative methods to measure submerged topography. An important criteria is that the method chosen should allow data collection at a similar spatial resolution to the remote survey techniques utilised in dry areas of the riverbed. One possible approach is to use remotely-sensed pixel colour to derive an empirical relationship between water colour and water depth. This method has previously been applied successfully to a variety of rivers, and maps of estimated water depth produced (e.g. Acornley *et al.*, 1995; Winterbottom and Gilvear, 1997; Gilvear *et al.*, 1998; Marcus *et al.*, 2001). In this study, it is carried out for the Waimakariri study reach using standard colour aerial photography. Previous work has yet to translate these depth estimates into bed elevations, or incorporate them into wider riverbed topographic surfaces. In this research, the water depth information

produced will subsequently be converted into an estimated bed topography and combined with dry-bed survey using digital photogrammetry and ALS (**Chapter 6**). In this way, DEM surfaces will be produced for the Waimakariri study reach.

5.2 Theoretical background

Remotely-sensed data has been used for many years to produce bathymetric maps, but has generally been confined to estuarine and shallow coastal waters (e.g. Dietz, 1947; Lyzenga, 1981; Cracknell *et al.*, 1982; Sabins, 1987; Ibrahim and Cracknell, 1990). There are fewer applications reported in fluvial environments. However, following successful use of multi-spectral imagery and satellite data for obtaining river water depth (e.g. Lyon *et al.*, 1992; Hardy *et al.*, 1994; Acornley *et al.*, 1995; Kumar *et al.*, 1997; Winterbottom and Gilvear, 1997), Milton *et al.* (1995) suggest that standard colour or even panchromatic aerial photography may be used to provide a quantitative estimate of in-stream bathymetry under certain conditions. This has subsequently been successfully demonstrated by Winterbottom and Gilvear (1997) and Gilvear *et al.* (1998).

Water colour is a product of the behaviour of light as it passes through water. This behaviour is determined by several factors including the constituent composition of the water and suspended sediment, the nature (colour and reflectance) of the bed, and water depth. Compared to lake and ocean water (where most previous work in this area has been carried out), rivers are considered more optically complex. In particular, the colour of river water is modified by particulate matter that rivers maintain in suspension, but which tends to settle out in lakes and oceans (Davies-Colley *et al.*, 1993). Furthermore, in some rivers (such as braided, gravel-bed rivers), water is typically shallow compared to lakes and oceans. This means that the submerged riverbed is visible in all but the deepest channels, although this is controlled by both the discharge of the river and the turbidity of the water at the time of interest. Thus, the colour spectrum of river water for a given turbidity is bounded by two extreme situations. On the one hand, where there is zero water depth, all incident light will be reflected from the bed. At the other extreme, where the submerged bed can no longer be seen, all of the incident light is being reflected from the water column and a maximum predictable depth (MPD) has been reached. The magnitude of this depth will be related to the water turbidity. Its spatial extent will be governed ultimately by discharge and riverbed morphology. In between these two end-points, water colour will be determined by the relative proportion of incident light that is reflected from the submerged bed as compared to the water column.

It can be shown that the amount of light reflected from a water body decreases exponentially with depth (Lyzenga, 1981). This means that a given increase in water depth has a greater spectral response in shallower water than in deeper water (Winterbottom and Gilvear, 1997) and that shallower water will naturally be easier to segregate into depth classes than deeper water. Thus, a natural logarithmic transformation should be applied to the water colour information to obtain a linear relationship with water depth. Technically, it is pixel colour that is being related to water depth. In this study, as elsewhere, it is assumed that this is equivalent to true water colour. However, it is likely that the conversion of photographic prints to digital images will introduce some error in the form of random noise.

5.3 Acquisition and preparation of imagery

Colour aerial photography of the Waimakariri River study reach was obtained during each of the four surveys made (**Table 5.1**). For February 1999 and March 1999, the imagery that was acquired for photogrammetric analysis was suitable (**Section 3.3.3**). For the February 2000 survey, a second set of photographs were acquired at 1:8000 scale by Air Logistics (NZ) Ltd. This reduction in scale was such that the entire riverbed width could be covered by one flying line, reducing both processing time and the number of joins necessary in subsequent image analysis. For the May 2000 ALS survey, colour photographs at 1:10000 scale were taken at the time of the scanning survey, and colour prints were processed and supplied by Precision Aerial Surveys Ltd. Hardcopy photographic prints of each set of images were scanned using a standard office colour scanner with default settings. The scanning resolution for each set of images was selected to give an object-space pixel size of 1 m, to match the point spacing selected for the photogrammetric and ALS dry-bed DEMs (**Chapter 6**).

Survey date	Photograph scale	Number of flying lines required to span riverbed	Number of photos required to give total coverage	Scanning resolution (microns)
16/02/99	1:5000	2	16	200
19/03/99	1:5000	2	18	200
23/02/00	1:8000	1	7	125
25/05/00	1:10000	1	5	100

Table 5.1 Details of the aerial photographs used in this study.

Each image was rectified using a second order polynomial model in the GCPWorks module of PCI image analysis software. For the February 1999, March 1999 and February 2000 imagery, this was achieved using the PCPs that had been laid out on the riverbed prior to each session of photography as photogrammetric control. The

location of the control points had been carefully selected so that a minimum of six control points appeared on each 1:5000 image, with around double this number visible on the 1:8000 images. The position of the control points was determined using Trimble real-time kinematic (RTK) GPS survey measurements (Hicks *et al.*, 1999b).

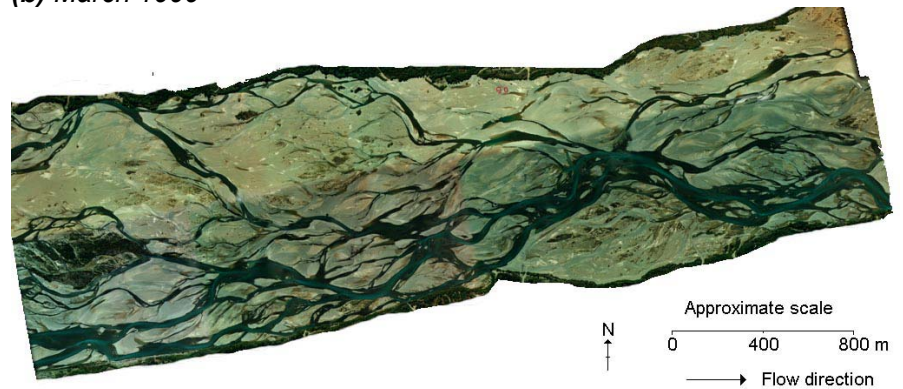
For the May 2000 survey, because ALS survey does not require ground control, PCPs were absent. These photographs were rectified using natural features common to both the rectified February 2000 and raw May 2000 images. The relative lack of relief in the study reach meant that two-dimensional rectification was considered sufficient (rather than three-dimensional ortho-rectification), with the obtained RMSE consistently less than the object-space pixel size (of 1 m). In principle, the DEMs produced by the photogrammetric and ALS surveys could have been used to ortho-rectify the imagery. However, the OrthoMax Ortho Tool module only allows ortho-rectification using one of the source images used to create a given DEM. In each case, photogrammetric measurement was performed on grey-scale imagery, whereas colour imagery was considered preferable for empirical water depth determination. As the final part of the rectification process, the individual photographs were mosaicked to form a single image of the study reach. A blending algorithm was used to minimise the appearance of seam-lines between individual images.

The rectified and mosaicked images used for water depth estimation for each survey date are shown in **Figure 5.1**. Despite the blending algorithm, a seam-line is noticeable down the centre of the riverbed in both of the epochs where two flying lines were used (February 1999 and March 1999). This reflects the fact that the time lag between two flying lines (during which time the light field must have changed) is longer than the time lag between individual images on the same flying line. However, errors due to this effect were not expected to be large. This is because the majority of water depth measurements in the affected surveys were towards the southern bank, meaning that the model would be better calibrated for the southern-most flying line. Thus, the lighting was constant in the area which covered the majority of wetted channels in the reach.

(a) February 1999



(b) March 1999



(c) February 2000



(d) May 2000

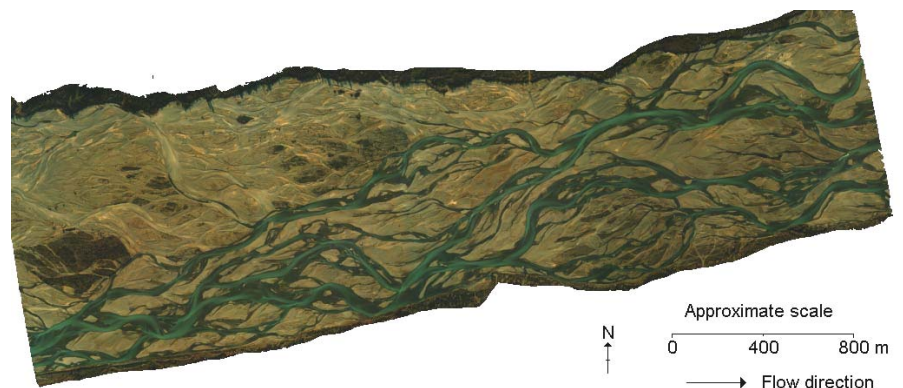


Figure 5.1 Rectified and mosaicked aerial imagery of the study reach from each photographic survey.

5.4 Development of an empirical relationship between pixel colour and water depth

To obtain the red, green and blue (RGB) values of pixels (or digital numbers, dNs) from wetted channels, the imagery was classified using a supervised maximum likelihood classification into wet and dry areas. **Table 5.2** summarises the classification accuracy statistics. For each photograph mosaic, the classification was deemed successful to the 95% confidence level. Even though colour imagery was used, vegetation had a similar spectral signature to inundated riverbed areas, and was classified as water. The images were subsequently manually-edited to re-class riverbed and bank-edge vegetated zones. The final classified images are shown in **Figure 5.2**.

Survey	Overall accuracy (from confusion matrix, %)	Kappa coefficient (mean \pm standard deviation)
February 1999	99.69	<u>0.997 \pm 0.000</u>
March 1999	98.59	<u>0.987 \pm 0.000</u>
February 2000	99.69	<u>0.998 \pm 0.000</u>
May 2000	99.44	<u>0.988 \pm 0.001</u>

Table 5.2 Classification accuracy statistics for each of the photographic surveys.

Kappa statistics that are underlined are significant at the 95% confidence level.

The classified images were used to identify and blank out dry and vegetated areas, to leave only the X,Y position and colour (in terms of RGB dN) of those pixels that fell in wetted channels. After Lyzenga (1981), the dNs were transformed using a natural logarithmic transformation to permit an empirical linear relationship between pixel colour and water depth.

To calibrate and to validate the models, a large number of water depth measurements were made by NIWA and EC field teams, concurrent with the photography (**Table 3.11**). Water depths were made using a precision sounder. This was deployed with an RTK GPS system to determine the planimetric position of each water depth sounding in the same datum system to which the photographs were georeferenced. These datasets were divided into two subsets with equal water depth distributions, one for model calibration and one for model validation. In addition, discharge (m^3/s) and turbidity were recorded at a number of locations in the study reach (**Table 5.3**) at the time of each photographic survey. Turbidity was measured using two independent methods. First, the SHMAK (Stream Health Monitoring and Assessment Kit) black disc extinction distance was measured in the field. Second, water was sampled and turbidity measured in the laboratory in Nephelometric Turbidity Units (NTU) (Hicks *et al.*, 1999b).

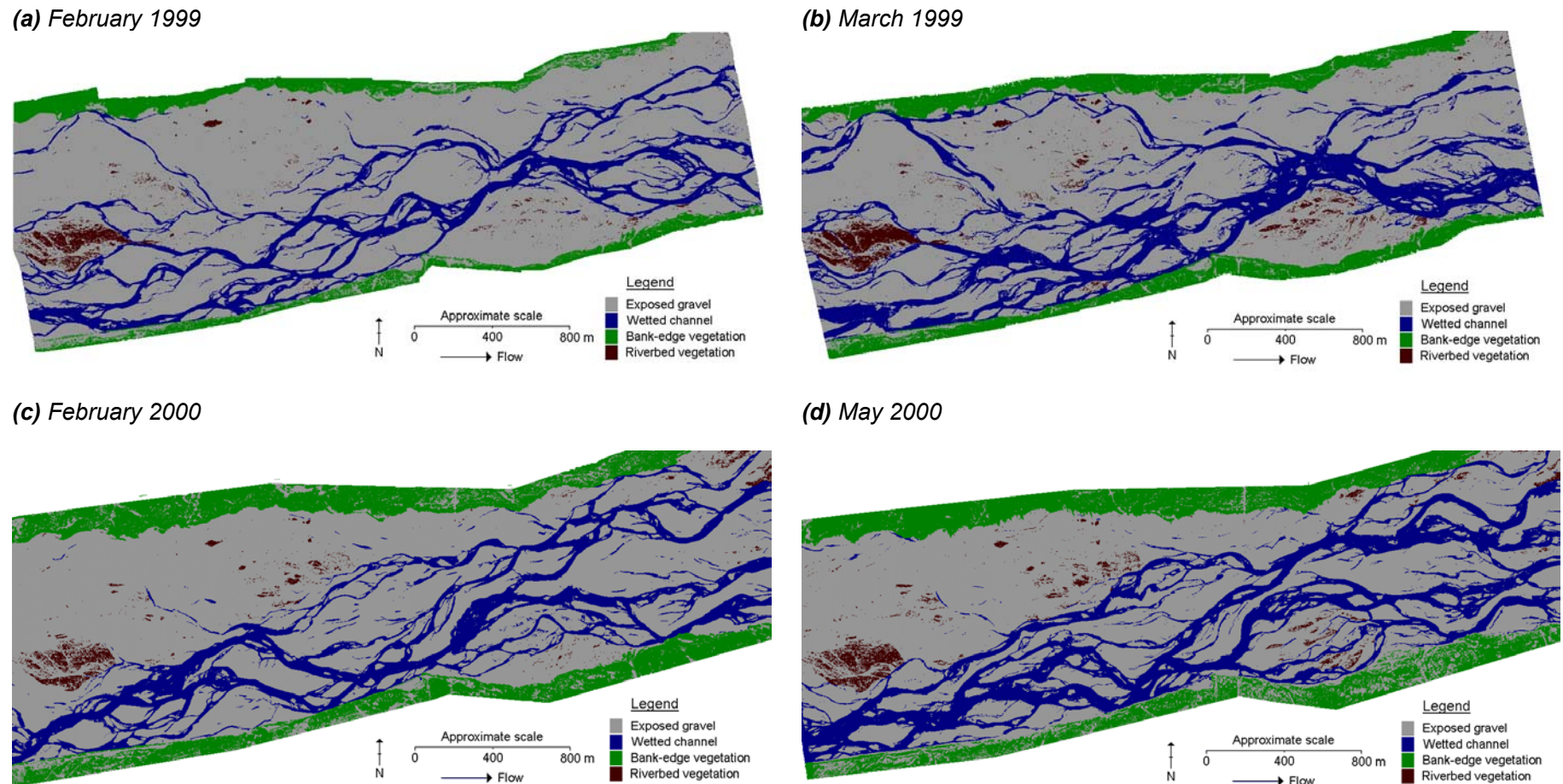


Figure 5.2 Results of maximum likelihood, manually-edited classification of mosaicked imagery (**Figure 5.1**) of the study reach.

Survey	Instantaneous river discharge (m ³ /s)	Water turbidity	
		SHMAK extinction distance (m)	NTU
February 1999	27.0	0.88	0.64
March 1999	56.0	0.84	2.65
February 2000	64.8	0.95	1.70
May 2000	73.0	0.54	9.50

Table 5.3 Details of river conditions and depth measurements at the time of photography.

Water depths were assigned to specific pixels using a simple automated spatial correspondence routine. This took each calibration water depth in turn, and calculated the average RGB values of all pixels that fell within a specified maximum search radius. The maximum search radius was set to 0.5 m (giving a diameter equal to the object-space pixel size) as this represents the best horizontal precision that can be expected from the imagery. It was found that the RGB values exhibited a large amount of noise. This was assumed to result from the spectrally non-selective scattering of light by air bubbles entrained in rapids and riffles (Davies-Colley *et al.*, 1993), as well as that introduced by the conversion of the photographs to digital form. To help counter this, a further element was added to the matching routine whereby RGB values that were significantly different (i.e. greater than 2 standard deviations) from the local average RGB value were excluded. Finally, a linear multiple regression model was fitted to the data, and an expression derived of the form $\text{depth} = f[\ln(R), \ln(G), \ln(B)]$.

Initial tests involved classifying the wetted pixels based on whether they were sand or gravel (spectrally light or dark, respectively), with a separate empirical relationship for each substrate type. Although this has been shown to improve depth estimation (e.g. Marcus *et al.*, 2001), the quality of resultant depth predictions was not significantly different to those obtained assuming only one substrate type ($p < 0.05$), so ultimately only one colour-depth relationship was used for the entire submerged bed for each survey. These expressions are shown in **Table 5.4**.

The use of empirical multivariate analysis meant that each relationship between water colour and water depth is time and place specific, although in each case the association between pixel colour and water depth was statistically significant ($p < 0.05$). However, the relationship between water depth and RGB reflectance, and hence the equations derived for each survey, vary considerably (**Table 5.4**). The reasons for the differences can, at least in part, be explained by differences in water turbidity (**Table 5.3**), reflecting the established theoretical basis on which the empirical relationship is

based. The red and blue bands were the best predictors for the February 1999 and March 1999 imagery. In each case the green band did not significantly improve the relationship ($p < 0.05$), and was removed due to a high degree of cross correlation with the blue band (R^2 of 0.59 and 0.84 for February 1999 and March 1999, respectively; both statistically significant at $p < 0.05$). The turbidity for these two epochs was relatively consistent, and the coefficients show considerable similarity.

Survey	n	Equation [Water depth (m) = ...]	SDE (m)	R^2	R^2 (using grey-scale images)
February 1999	32188	-0.24ln(R) + 0.68ln(B) - 1.02	0.191	<u>0.50</u>	0.01
March 1999	2127	-0.13ln(R) + 0.65ln(B) - 1.36	0.192	<u>0.58</u>	<u>0.12</u>
February 2000	14265	-0.77ln(R) + 1.48ln(G) - 2.64	0.169	<u>0.58</u>	0.02
May 2000	5141	0.80ln(G) - 2.47	0.182	<u>0.55</u>	<u>0.51</u>

Table 5.4 Results of the multivariate analyses between pixel colour and measured water depth for each epoch. Underlined values of R^2 are statistically significant ($p < 0.05$).

The situation was expected to be the same for February 2000, as the water had a similar turbidity. However, a problem with the blue signal on the photographic prints created a banding effect, and blue dNs were ignored in the analysis. Instead, and based on the strong correlation between the green and blue bands found in the February 1999 and March 1999 imagery, when water turbidity was comparable, only the red and green bands were used. In May 2000, the water turbidity was much higher (extinction distance was halved relative to the first three epochs). As a consequence, the nature of the relationship changes, with the green band alone providing the best predictor of depth. As opposed to the three other surveys, the level of reflectance in all three colour bands (red, green and blue) was positively related to surveyed water depth (**Figure 5.3**), meaning that black and white imagery (the average value from the red, green and blue bands) could be used with relatively little degradation of depth predictions (**Table 5.4**).

Finally, water depth maps were calculated by applying the water depth equations (**Table 5.4**) to every wet pixel in the study reach (**Figure 5.4**). The pattern of water depths appears to be geomorphologically reasonable, with the outside of bends and confluence zones (scour holes) exhibiting the deepest water. The range of water depths predicted (around 0 to 1.5 m) corresponds to experience in the field (Hicks *et al.*, 1999b).

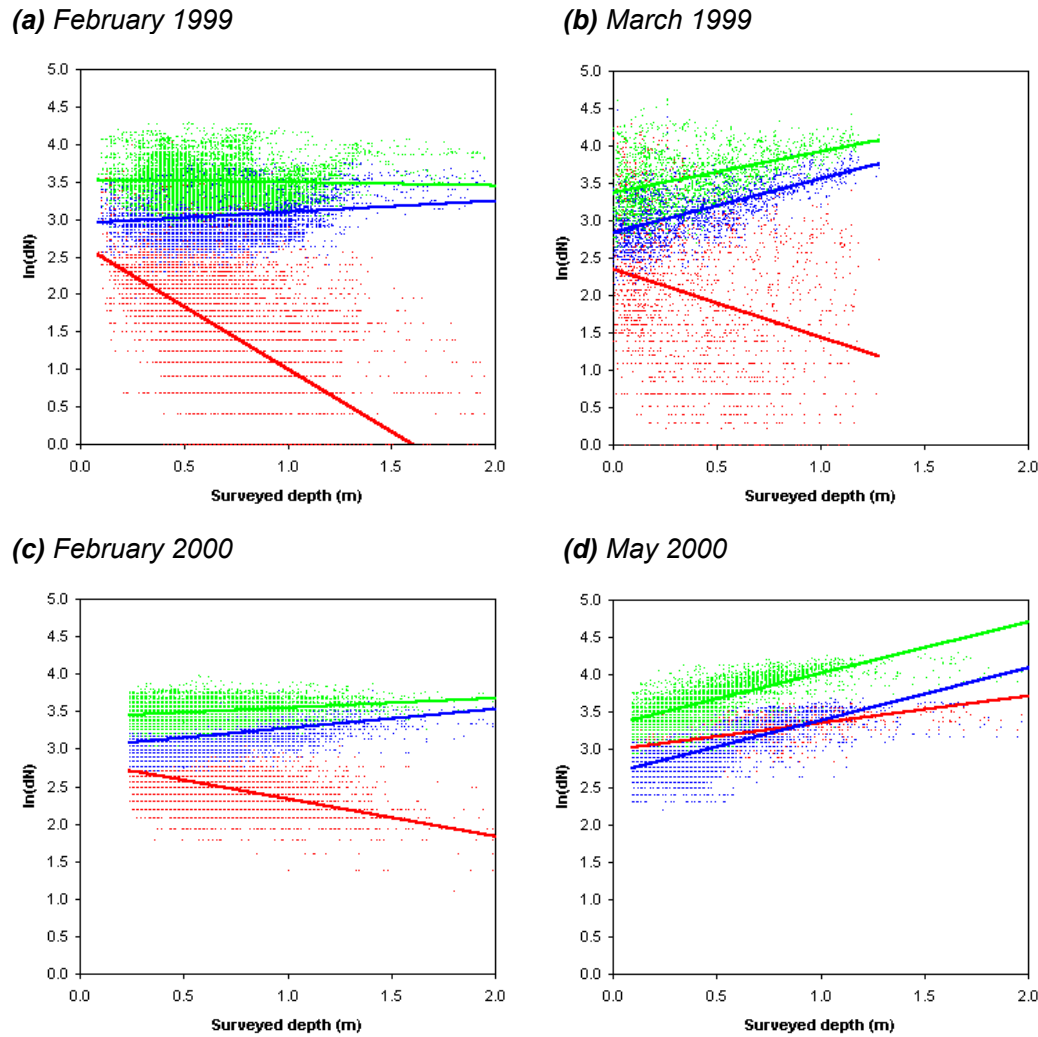
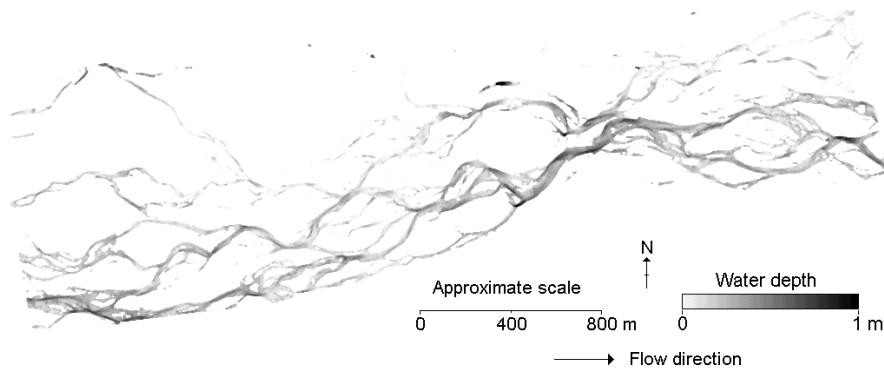


Figure 5.3 The relationship between measured depth and RGB digital numbers (dN) for each survey.

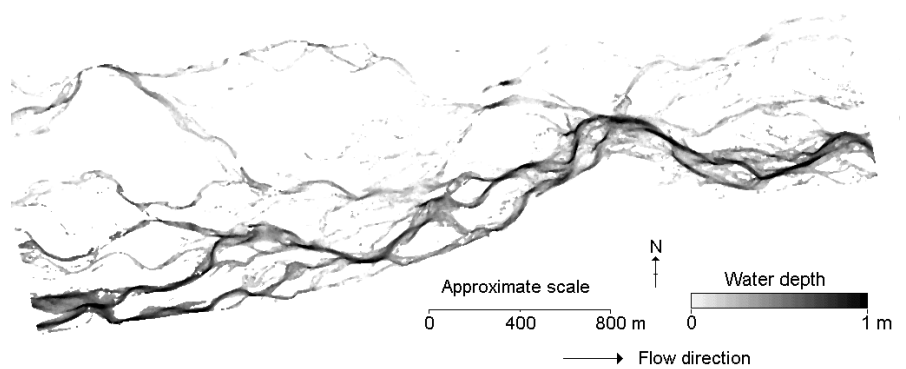
5.5 Quality assessment of depth estimates

The quality of depth predictions was assessed using the validation subsets of depth measurements (**Table 5.5**). Despite the differences in predictors used, the quality of depth estimates is remarkably consistent. Although the R^2 values are relatively low (on average about half of the variance in water depth is explained), the ME and SDE are encouraging given the range of water depths (0 m to about 1.5 m). The R^2 values are similar to values reported when standard aerial photography has been used previously in river environments (**Table 5.6**).

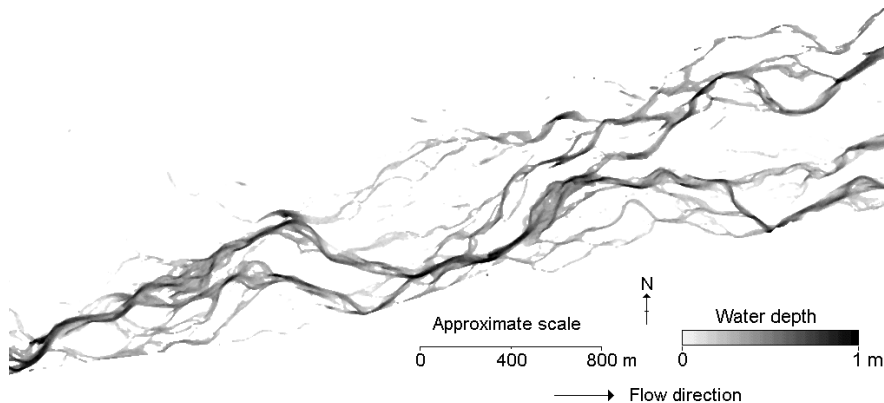
(a) February 1999



(b) March 1999



(c) February 2000



(d) May 2000

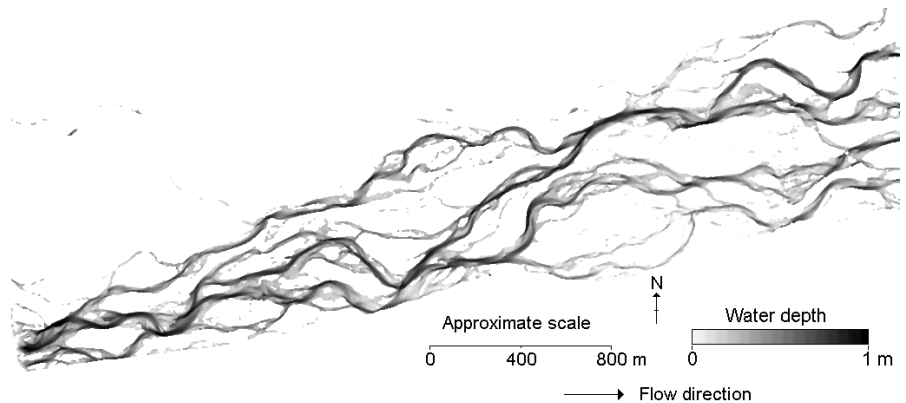


Figure 5.4 Estimated water depth maps for the study reach shown in **Figure 5.1**: (a) February 1999; (b) March 1999; (c) February 2000; and (d) May 2000.

Epoch	'Best' predictors	n	ME (m)	SDE (cm)	R^2
February 1999	RB	12996	-0.015	0.199	0.484
March 1999	RB	2059	-0.008	0.192	0.612
February 2000	RG	14302	+0.002	0.168	0.568
May 2000	G	2512	-0.002	0.178	0.561

Table 5.5 Quality assessment of the water depth estimates.

Researcher(s)	Type of imagery	Quality of depth estimate (R^2)	MPD (m)
Lyon <i>et al.</i> (1992)	Multi-spectral	0.95*	>10
Acornley <i>et al.</i> (1995)	Multi-spectral	0.73	>1
Kumar <i>et al.</i> (1997)	Single-band	Not reported	>10
Winterbottom and Gilvear (1997)	Multi-spectral Black & white	0.67 0.55	0.6
Gilvear <i>et al.</i> (1998)	Black & white / Colour	Not reported	>0.75
Marcus <i>et al.</i> (2001)	Multi-spectral	0.80-0.90	Not reported

* Class accuracy (check measurements falling within the correct 2 m depth class)

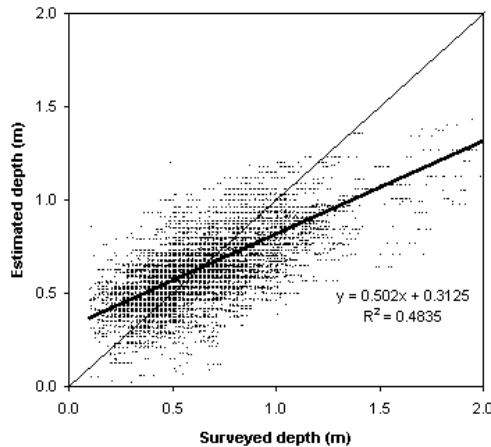
Table 5.6 Depth prediction quality and maximum predicted depth (MPD) reported in similar studies.

Direct comparison of surveyed and estimated water depths (**Figure 5.5**) shows that there is a large amount of scatter. Furthermore, these plots show that we can be less confident of the water depth estimates as actual water depth increases and tends towards the MPD (as indicated by the asymptotic trend in the points on the plots, such that the estimated depth remains constant for any given depth at higher surveyed water depths). The magnitude of the MPD appears to vary from epoch to epoch, from around 0.7 m in March 1999 and May 2000 to around 1.0 m in February 1999 and February 2000, scaling approximately with turbidity (**Table 5.3**). For comparison, a value for MPD of 0.6 m was reported by Winterbottom and Gilvear (1997) (**Table 5.6**) for the River Tay, Scotland, for a turbidity of 2 NTU.

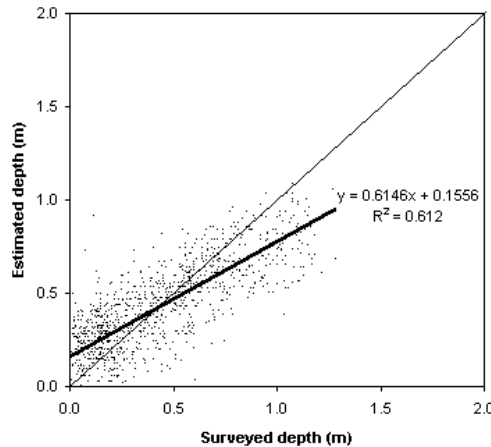
Finally, **Figure 5.6** shows the cumulative frequency distributions of corresponding surveyed and estimated depths for each epoch. For the two 1999 surveys, there appears to be a trend towards smaller depths being over-estimated and larger depths being under-estimated, leading to a compression of predictions into intermediate depths. This effect is far less pronounced for the two 2000 epochs. One explanation is

that the errors are due to the distribution of water depth measurements used for model calibration. Although a large proportion of the reach was covered during the depth surveys in February and March 1999, the majority of depth measurements were made using the jet boat-mounted echo-sounder in the deepest channels towards the centre of the study reach, leading to datasets that were biased with respect to their spatial and depth distributions.

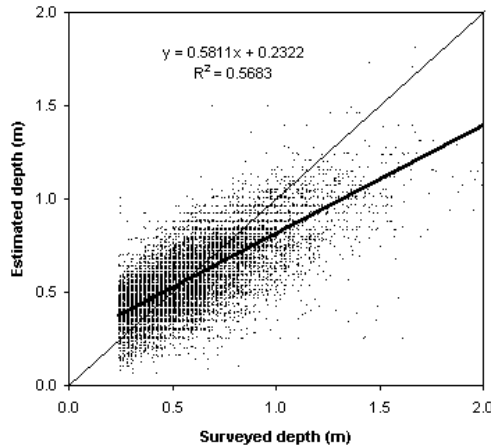
(a) February 1999



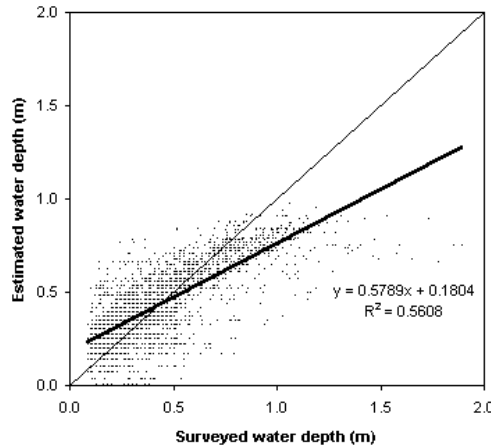
(b) March 1999



(c) February 2000



(d) May 2000

**Figure 5.5** The relationship between measured and predicted depth for each survey.

A suspicion that this was the case led to a reappraisal of survey strategy for the 2000 surveys, which utilised an aluminium dinghy. This allowed a far more representative survey of water depths to be obtained. This issue was compounded by the number of photographs taken each epoch. For the two 1999 surveys, two flying lines were used, meaning that the number of individual images was doubled, and leading to greater

colour variation between photographs. For the 2000 surveys, a single flying line was used, which minimised colour variation along the reach.

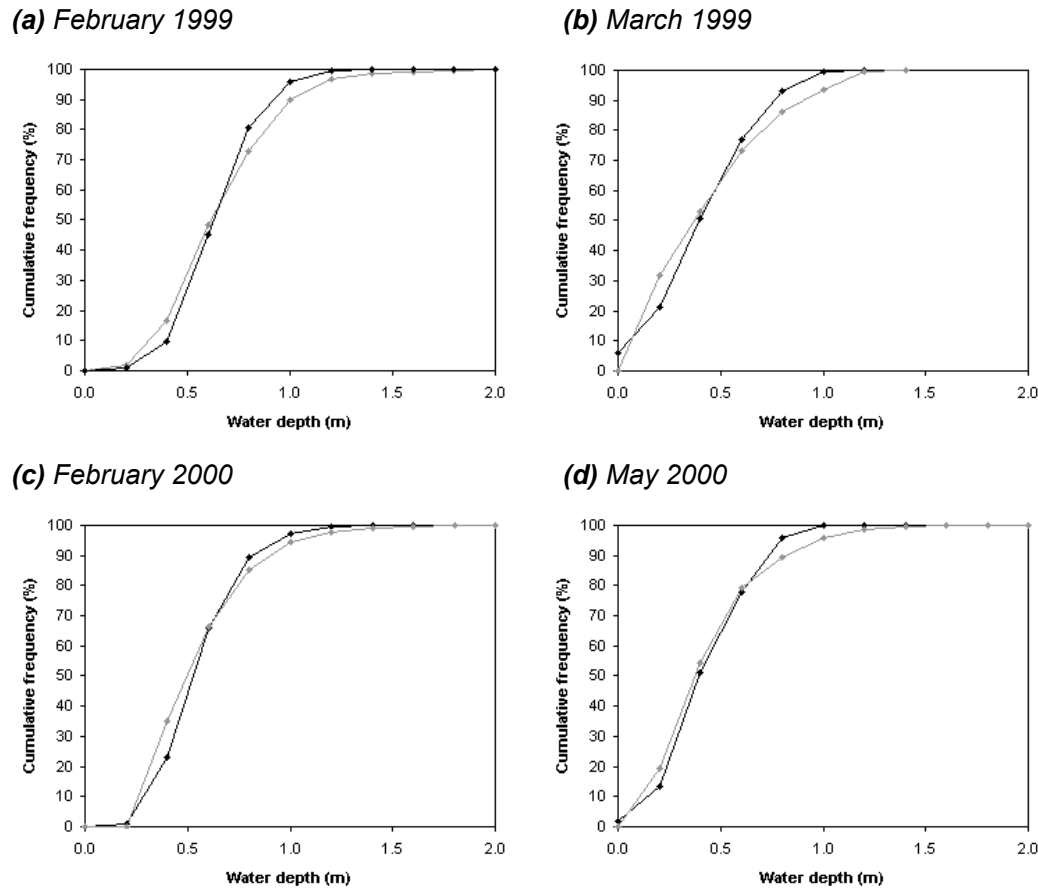


Figure 5.6 Cumulative frequency distributions of surveyed (grey) and estimated (black) water depths.

5.6 Chapter summary

Water in the Waimakariri River is normally slightly turbid, such that at low flows the bed is not clearly visible. In such a situation digital photogrammetry cannot be used, since the stereo-matching algorithm is dependent on image texture. Thus, it was necessary to reconsider data acquisition for the wet-bed areas of the Waimakariri study reach.

Image analysis was used to empirically relate water colour (in terms of red, green and blue pixel digital number) to measured water depth. The resulting multivariate expressions for water depth were used to generate maps of estimated water depth for the whole study reach. Assessment of the quality of resultant water depth maps was undertaken using additional independently-surveyed water depths. These demonstrated that around 50% of the variation in water depth was explained by

differences in pixel colour. This broadly corresponds with the results from other studies made using standard aerial photographs.

An important and novel aspect of this research was to use the water depth estimates to derive topographic information from the submerged riverbed. This involves knowledge of the water surface elevation. In **Chapter 6**, water edge points from dry-bed survey of the Waimakariri study reach will be used to model the position of the water surface, and from this the wet-bed topography will be estimated. Thus, complete DEMs of the Waimakariri study reach will be obtained. Dry-bed survey will be undertaken using both digital photogrammetry and ALS.

CHAPTER 6. THE TURBID WATER CASE: DRY-BED SURVEY USING REMOTE SENSING METHODS

In exposed riverbed areas, a high quality of topographic representation is required (6.1). In this chapter, digital photogrammetry (6.2) and airborne laser scanning (6.3) are used to survey dry-bed areas of the Waimakariri study reach. For digital photogrammetry, first the collection parameters and DEM point spacing are selected (6.2.1). Next, DEMs are generated (6.2.2) and assessed in terms of stereo-matching performance (6.2.3) and raw DEM quality (6.2.4). Based on these results, a post-processing method is developed that remove gross errors (6.2.5 to 6.2.9), and individual DEMs are joined (6.2.10). The corrected dry-bed photogrammetric DEM surfaces are used to model a water surface elevation (6.2.11). From this, estimated water depths (Chapter 5) are subtracted to give a representation of the submerged bed. Finally, reach-scale post-processing based on PCP position is used to reduce systematic error (6.2.12). For airborne laser scanning, the supplied data was used to generate a dry-bed DEM surface (6.3.1), from which water surface was modelled (6.3.2). This allows water depth information (Chapter 5) to be converted into wet-bed elevations, and a reach-scale DEM to be produced. Quality assessment (6.4) suggests that final DEM quality is acceptable both qualitatively (6.4.1), and quantitatively in terms of independent check data (6.4.2) and overlap analyses (6.4.3).

6.1 Introduction

Chapter 4 demonstrated that digital photogrammetry is capable of producing DEMs of exposed gravel riverbeds with little systematic bias and high precision. In the presence of more turbid water, direct measurement of submerged topography using digital photogrammetry is not possible. This requires that dry-bed and wet-bed areas of the Waimakariri study reach are treated separately. In Chapter 5, a method was developed that estimates water depth based on pixel colour. In this chapter, the remote survey techniques of digital photogrammetry and airborne laser scanning (ALS) are used to collect high quality topographic data from dry-bed areas.

A high quality of terrain representation is important in exposed areas for two reasons. First, much of the riverbed of a braided river at low flows is dry. This means that when aggregated over the riverbed as a whole, and depending on the end use of the DEM, dry area errors may be more significant than those in wetted channels. Second, in order to translate estimated water depth (Figure 5.4) into submerged wet-bed elevations, water surface elevation must be modelled. As previously explained with respect to the North Ashburton River (Section 4.3.2), this can be achieved by

interpolating dry channel edge points cross wetted channels. Consequently, good representation of exposed points close to wetted channels is important to ensure an accurate water surface model. In large part, this will determine the quality of subsequent wet point elevations.

6.2 Dry-bed survey using digital photogrammetry

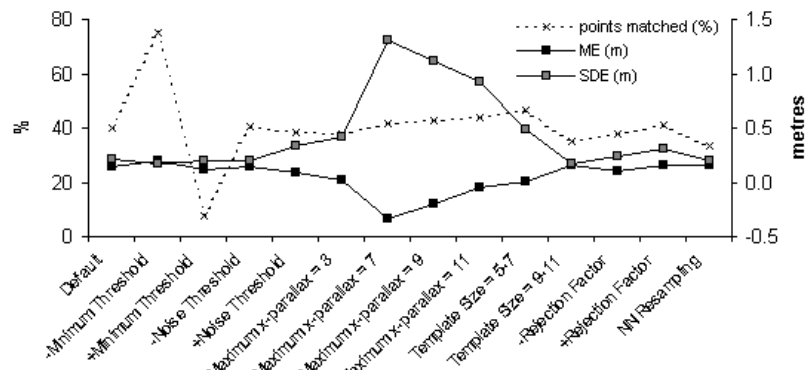
6.2.1 DEM collection strategy

Prior to DEM generation, the human operator has two areas of influence over the otherwise automated stereo-matching and DEM creation process. These are specification of DEM collection parameters and choice of DEM point spacing. The potential importance of the DEM collection parameters (**Appendix 1**) was demonstrated for the North Ashburton River, with the quality of wet-bed DEM points significantly improved ($p < 0.05$) for the whole study reach when a maximum parallax value of 9 pixels was used (**Table 4.12**). However, in dry-bed areas, the same change in collection parameters slightly reduced DEM quality. Given that there is no *a priori* basis for parameter changes in dry-bed areas, it is expected that the default parameter set should produce the best DEM quality for dry-bed areas of the Waimakariri study reach. However, this was also tested empirically using systematic perturbation of the DEM collection parameters.

Resultant DEM quality was assessed in terms of stereo-matching performance (% points matched), and ME and SDE as compared with the independently surveyed dry-bed check data (**Table 3.11**). For testing purposes, two 100 m x 100 m test areas were identified in the study reach. These comprised mostly of dry-bed points and contained a high density of check point measurements. DEMs were generated with 1 m spacing, and DEM points associated to surveyed elevations using an automated spatial correspondence algorithm. A maximum search radius of 0.5 m (half DEM spacing) was used. DEM quality results are shown in **Figure 6.1**. In the absence of any consistent improvement in both DEM dry-bed accuracy and precision, and given no theoretical basis for change, it was decided to use the default collection parameters for all subsequent DEM generation.

The same two test areas were also used to choose the optimum DEM point spacing. It was necessary to reconcile the inverse relationship between improved surface representation and increased DEM processing time (and increased volume of data), so that a specified level of DEM quality is achieved with the maximum possible DEM point spacing. To explore this, DEM were generated for both test areas using a variety of point spacings (**Table 6.1; Figure 6.2**).

(a) Test area 1



(b) Test area 2

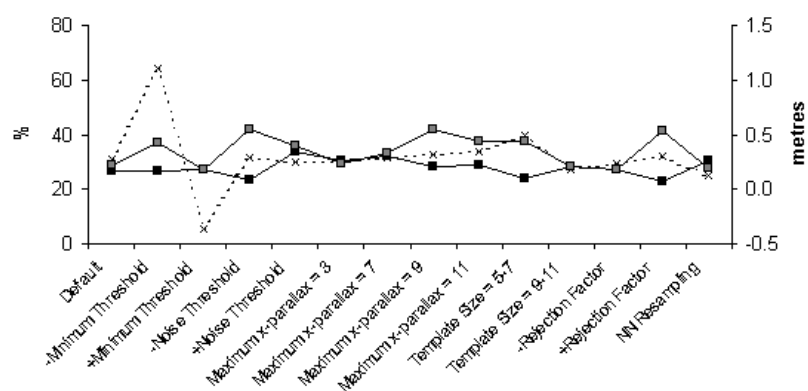


Figure 6.1 The effect of DEM collection parameter perturbation on stereo-matching matching precision and DEM quality for dry-bed points.

DEM point spacing (m)	Maximum number of points in test areas	DEM generation time (mins) ^a	DEM file size (Mb) ^b
0.37 ^c	73441	24	5.46
0.5	40401	13	3.00
1.0	10201	3	0.76
2.0	2601	0.9	0.19
3.0	1156	0.4	0.09
5.0	441	0.1	0.03
10.0	121	0.04	0.009

^a Assuming average (and readily achieved) collection rate of 50 points per second

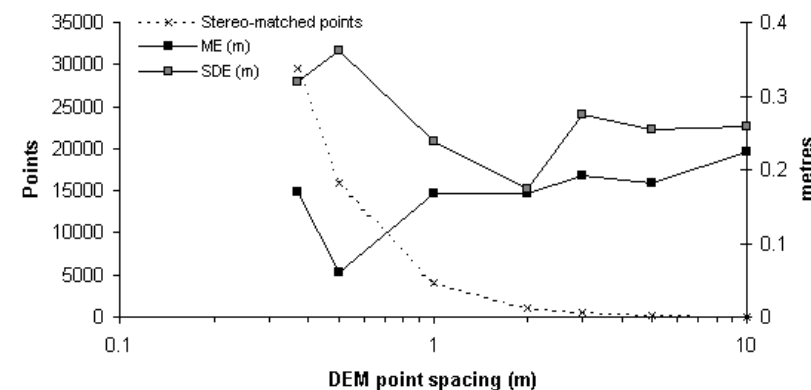
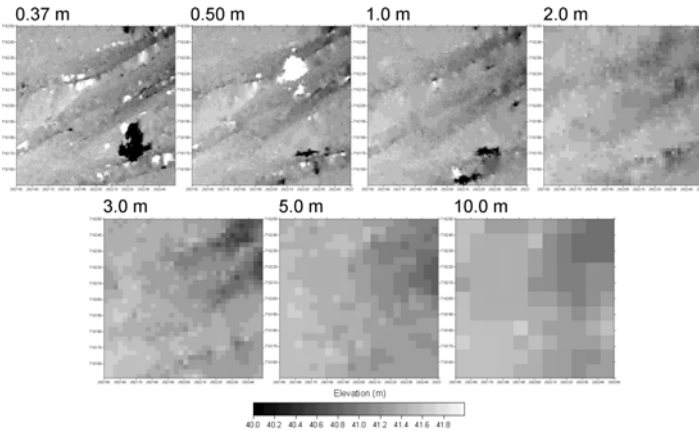
^b In x,y,z ASCII space-delimited file format

^c Smallest DEM point spacing calculated by OrthoMAX, given image scale and scanning resolution.

Table 6.1 Summary of DEM point spacings and collection details.

From visual appearance alone, it is apparent that the DEM surfaces become ‘pixelated’ above point spacings of about 3 m, and surface representation becomes increasingly poor. At small point spacings, although terrain representation is better where stereo-matching has been correct, there are more areas where gross error occurred.

(a) Test area 1



(b) Test area 2

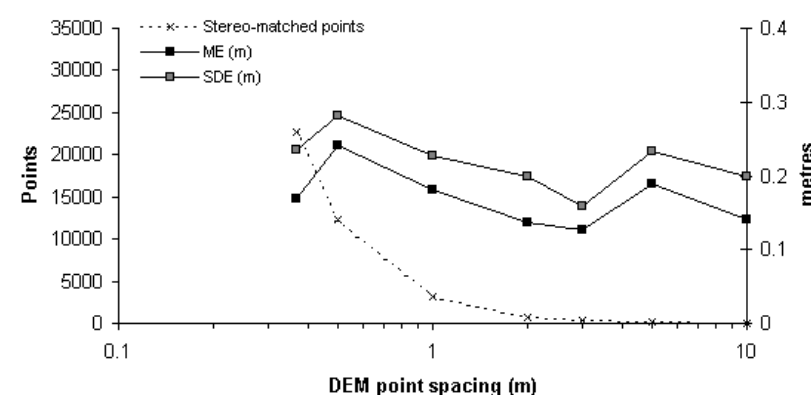
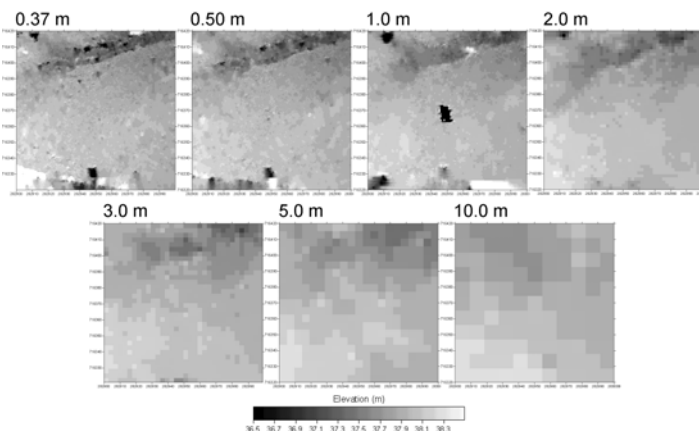


Figure 6.2 The effect of point spacing on DEM visual appearance, the number of stereo-matching points and DEM quality for both test areas.

DEM quality was tested quantitatively in terms of the number of successfully stereo-matched points (and hence the number of points used to represent the test area terrain), and ME and SDE (as compared with independently-surveyed check point elevations) (**Figure 6.2**). The maximum search radius used to associate DEM and surveyed elevations was on each occasion set to half the DEM point spacing. Where two or more surveyed points fell within the search range, their mean elevation was used.

The presence of gross error is likely to effect the reliability of the ME and SDE statistics. In order to assess its influence, points that were assumed to be gross errors were removed from their calculation. This was achieved by eliminating any DEM-check point pairs that had an elevation difference greater than the assumed maximum expected error (MEE), defined as $ME \pm 3 SDE$ (Torlegård *et al.*, 1986; Shearer, 1990). This is a global approach that allows relatively rapid identification of those DEM points, for which corresponding independently-survey check points exist, that are likely to be gross errors. Thus, gross error is only removed from the ME and SDE statistics, and not from the DEM surface itself. After corresponding points with a difference of greater than MEE had been removed, ME and SDE were recalculated. Thus, a new value of MEE was produced. This process was iterated until a value of MEE was reached such that no further points were eliminated.

From the assessment of ME and SDE, there appears to be no clear trend between point spacing and DEM dry-bed quality. The only pattern is that the number of successfully stereo-matched points from which the DEM is derived decreases rapidly at point spacings of less than 1 m, and falls more slowly thereafter. Based on this analysis, a DEM point spacing of 1 m was selected, which seemed to offer the best compromise between number of points stereo-matched and DEM quality in terms of ME and SDE. From experience in the field, it was also decided that if a point spacing greater than 1 m was used, surface representation would be lost in areas where sudden breaks of slope (i.e. channel banks) or abandoned channels occur. Good representation is particularly significant given the fundamental importance placed on channel-edge points in the modelling of water surface elevation for wetted channels (**Section 6.2.11**).

6.2.2 DEM collection

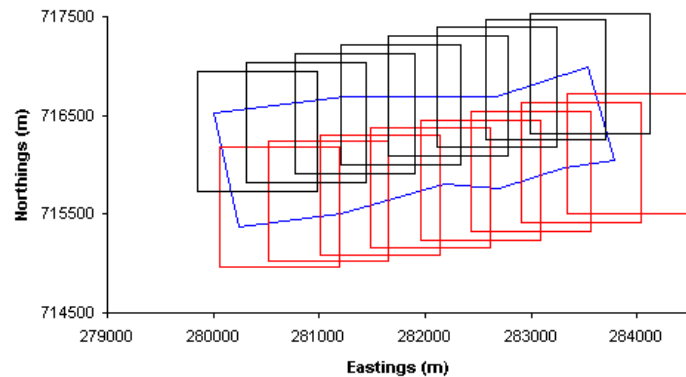
DEMs were generated for the Waimakariri River with 1 m point spacing using the February 1999, March 1999 and February 2000 images with the OrthoMAX default DEM collection parameters. Corresponding ortho-images were also generated with the same (1 m) point spacing. Unlike the North Ashburton study reach, which was covered in one photograph overlap and hence one DEM, the Waimakariri study reach consisted of many photograph overlaps (**Table 3.2; Figure 6.3**) and hence required multiple DEMs.

DEMs were produced for each overlap in the downstream direction. These are referred to as individual DEMs, to distinguish them from the reach-scale riverbed DEM surface subsequently obtained by mosaicking the individual DEM surfaces. An example of a raw individual DEM is shown in **Figure 6.4a**. Despite good topographic representation in some areas (those free of gross error), it was apparent that the individual DEM surfaces needed to be trimmed to eliminate edge effects and minimise bank-edge vegetation before further analysis. Hence, a polygon area of interest was manually defined on-screen for each individual DEM from each photographic survey, using a combination of DEM (**Figure 6.4a**) and ortho-image (**Figure 6.4b**) to identify the usable DEM area. Care was taken to ensure that adjacent areas of interest joined or overlapped such that every point of the riverbed was represented in at least one individual DEM. The area of interest defined for the raw individual DEM in **Figure 6.4a** is shown in **Figure 6.4c**, along with the bounds of neighbouring areas of interest. The trimmed individual DEM is shown in **Figure 6.4d**.

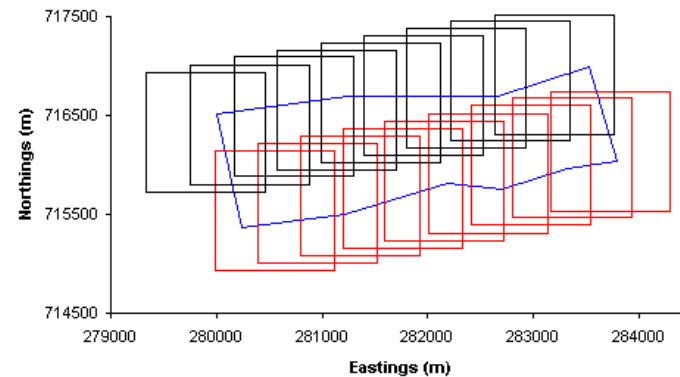
6.2.3 Stereo-matching performance

Initial DEM quality assessment was based on the stereo-matching performance statistics, calculated within the area of interest for each individual DEM. Results were restricted to dry-bed areas by using a two-way automated unsupervised minimum distance classification based on the ortho-image. Surface water and vegetation (with similar spectral signatures) were classified together, distinct from exposed areas of the riverbed. This was repeated for every trimmed individual DEM. **Figure 6.5** shows both the classified image and spatial distribution of matched points that correspond to the DEM and ortho-image presented in **Figure 6.4**.

(a) February 1999 (1:5000 scale; 2 flying lines; 16 photographs)



(b) March 1999 (1:5000 scale; 2 flying lines; 18 photographs)



(c) February 2000 (1:4000 scale; 2 flying lines; 24 photographs)

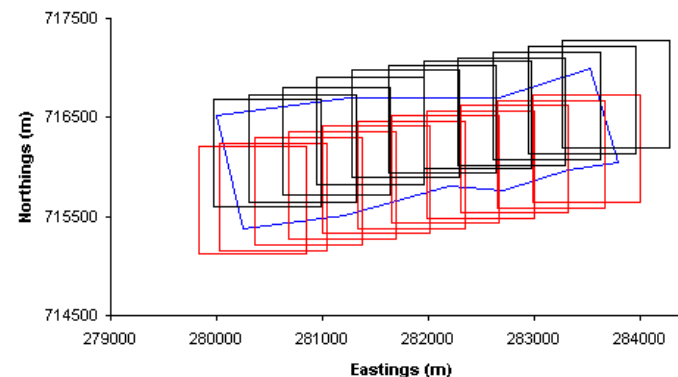


Figure 6.3 The approximate areas covered by photographs acquired during each survey. The study reach limits are outlined in blue

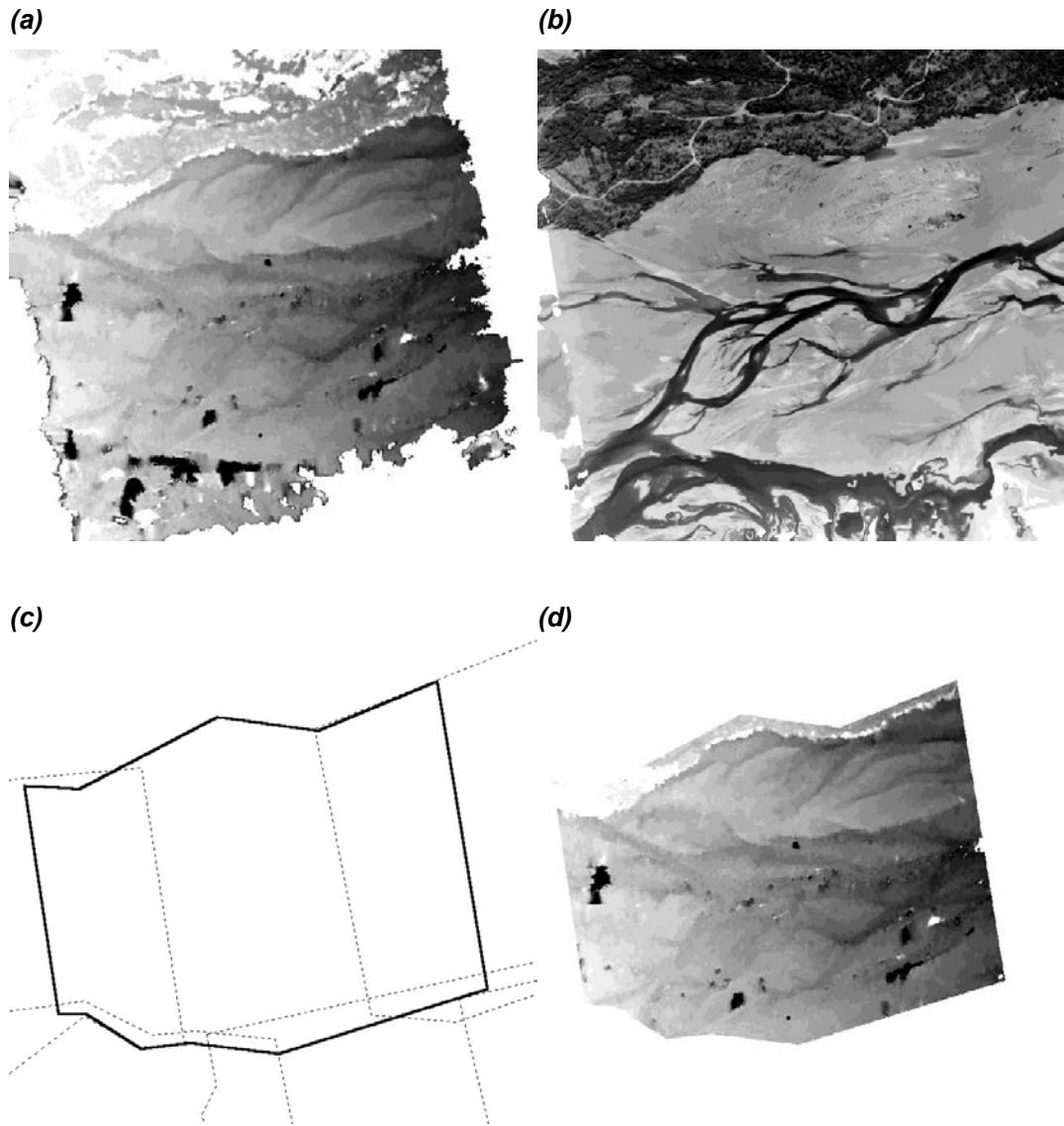


Figure 6.4 Example of a raw individual DEM (a) before and (d) after trimming based on an area of interest (c) derived manually using the raw DEM and ortho-image (b). The dashed lines in (c) represent neighbouring areas of interest.

The stereo-matching performance results for each individual DEM from each survey are shown in **Figure 6.6** and summarised in **Table 6.2**. Initially, the raw stereo-matching performance appears to be disappointing. Only a relatively small proportion of dry-bed points were successfully stereo-matched. The stereo-matching performance was considerably lower than for the North Ashburton River (around 50 % of points matched; **Table 4.10**), which perhaps reflects the smaller image scale used and its effect on image texture (**Figure 3.12**; **Table 3.5**). The February 1999 DEMs had the lowest total, with only one in five points matched, on average. The improvement in image texture (**Figure 3.12**; **Table 3.5**) associated with increase in photograph scale

from 1:5000 (February 1999 and March 1999) to 1:4000 (February 2000) appears to have had a positive effect with, on average, over a third of points matched in the later DEMs.

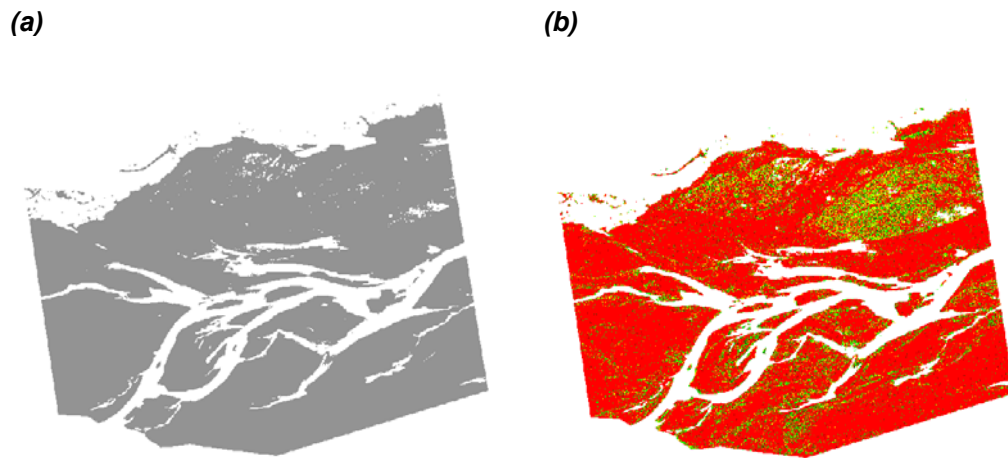


Figure 6.5: (a) the classified ortho-image, and (b) the spatial distribution of dry-bed stereo-matching performance for the individual DEM shown in **Figure 6.4**. Dark green points are ‘good’ matches, light green points are ‘fair’ matches and yellow points are ‘poor’ matches. Interpolated (non-matched) points are shown in red.

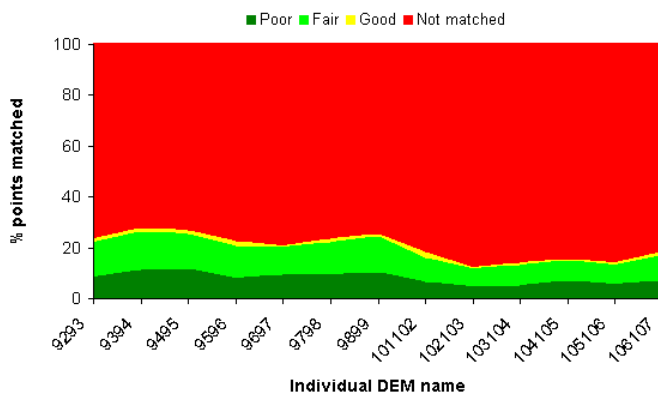
AVERAGE STEREO-MATCHED
PIXELS IN DRY-BED AREAS (%)

Survey	Number of individual DEMs	Good	Fair	Poor	Total	Average spacing of matched points (m)
February 1999	14	1.2	11.0	8.1	20.2	2.2
March 1999	16	2.0	14.9	8.9	25.8	2.0
February 2000	22	2.8	19.9	11.6	34.3	1.7

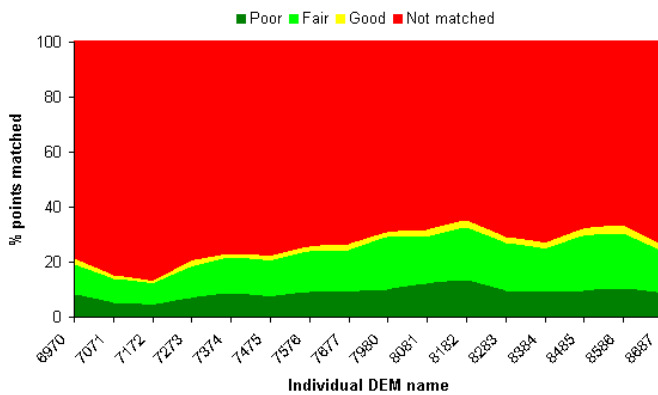
Table 6.2 Summary of stereo-matching performance for each photographic survey.

However, given an average individual DEM size of 400 m x 400 m, even 20% of points corresponds to around 32000 elevation measurements and an average point spacing of approximately 2.2 m (**Table 6.1**). This represents a large increase in the point density typically associated with terrestrial survey methods. Therefore, based on the disparity between sudden breaks of slope and large, relatively flat, and featureless bar tops associated with the Waimakariri study reach, it follows that point distribution is potentially more significant than the number of points stereo-matched.

(a) February 1999



(b) March 1999



(c) February 2000

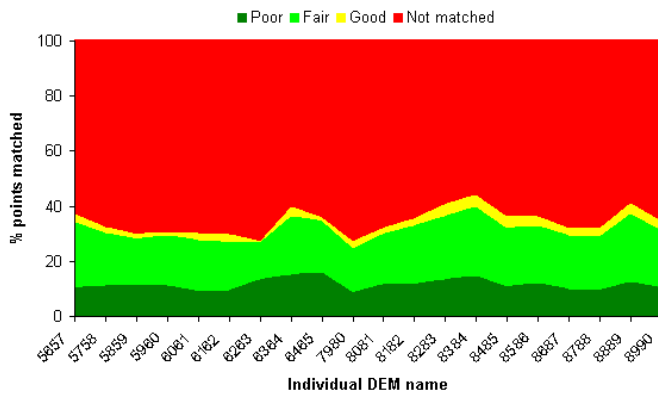
**Figure 6.6** The matching performance for individual Waimakariri riverbed DEMs.

Figure 6.5b suggests that stereo-matching has been most successful in areas of the riverbed where there is texture apparent in the source imagery (**Figure 6.4b**). This includes areas of discontinuous vegetation, breaks of slope and wetted channel margins. This is encouraging, as it is in these areas where a greater density of points is required for good surface representation (and in the case of the water edge, in order to interpolate the modelled water surface). Exposed gravel areas contain far fewer points

because the lack of image texture prevents successful correlation between corresponding points on overlapping images. This means that there will be a large amount of interpolation across gravel bars. However, given their low relative vertical relief, this may not produce a bad surface representation. This is supported by the lack of DEM quality degradation as DEM point spacing was increased, and hence the DEM surface smoothed, in the two test areas (**Figure 6.2**).

6.2.4 Raw DEM quality assessment

To produce a DEM surface of the whole study reach, the individual DEMs had to be mosaicked. This is a relatively straight-forward task since DEMs are fully rectified and geo-referenced. All that must be decided is the method of treatment of regions where two or more DEM surfaces overlap. This issue was not considered until after the individual DEMs has been post-processed, and is addressed fully in **Section 6.2.10**. However, for illustrative purposes, mosaicked raw reach-scale DEMs for each photogrammetric survey are shown in **Figure 6.7**. The surfaces have been detrended using a linear bed slope to emphasise local topographic variation.

The quality of the raw DEM surfaces was assessed quantitatively using the independent check point measurements made concurrently with photograph acquisition. Each check point measurement was associated with the closest DEM point using an automated spatial correspondence algorithm. A maximum correspondence radius of 0.5 m (half the DEM point spacing) was used. The results are summarised in **Table 6.3**.

DEM	DRY-BED			WET-BED		
	Points compared	ME (m)	SDE (m)	Points compared	ME (m)	SDE (m)
All check points						
February 1999	3699	+0.539	2.190	11297	+1.201	3.478
March 1999	253	+0.252	0.321	2461	+4.333	10.56
February 2000	1661	+0.064	0.926	6981	+0.393	2.750
With gross errors excluded						
February 1999	3320	+0.225	0.228	9848	+0.528	0.321
March 1999	249	+0.222	0.172	1910	+0.794	0.707
February 2000	1601	+0.105	0.124	6342	+0.342	0.252

Table 6.3 Quantitative DEM quality assessment of the raw reach-scale DEMs.

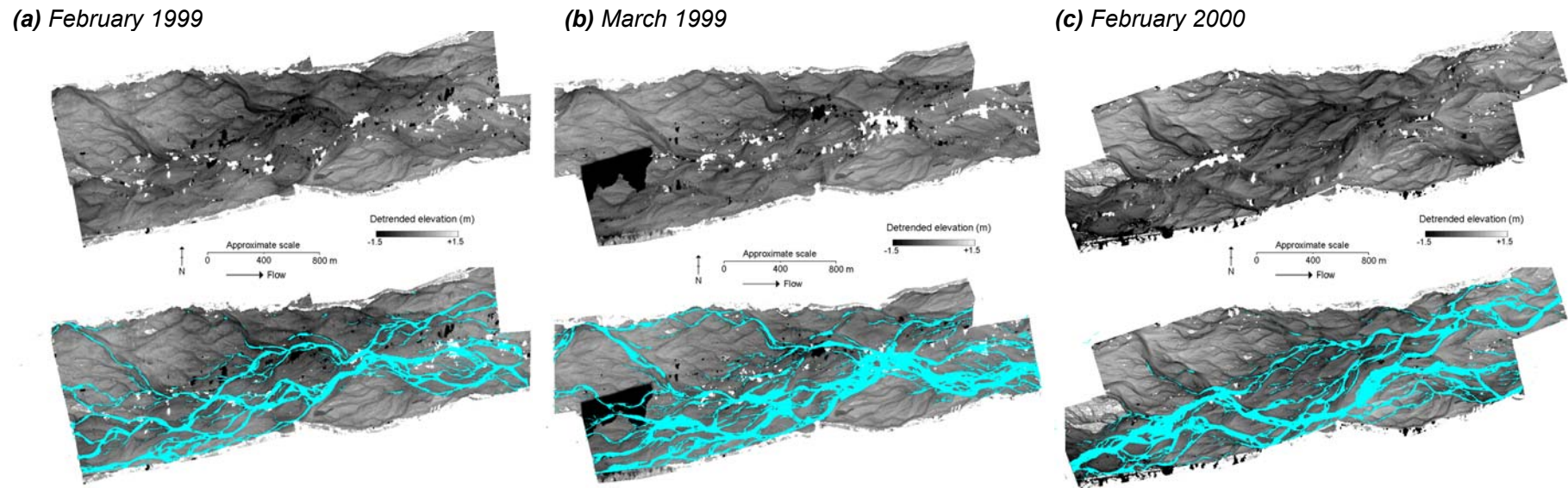


Figure 6.7 Raw DEMs of the whole study reach. For each survey, the top image shows the detrended DEM surface, and the lower image shows the same DEM but with wet-bed areas masked out.

As in the test areas (**Figure 6.2**), the presence of large gross errors (**Figure 6.13**) is likely to effect the reliability of these measures. Gross error was removed from the DEM quality statistics using the method described in **Section 6.2.1**, based on an iterative calculation of the maximum expected error (MEE), defined as $ME \pm 3 SDE$ (Torlegård *et al.*, 1986; Shearer, 1990). This was expected to reveal the true systematic and random error associated with unprocessed photogrammetric measurements. The method cannot be used for formal post-processing, as it only removes gross error from the calculated ME and SDE values, and not from the DEM surface itself. The ME and SDE statistics, following application of this method, are shown in **Table 6.3**.

The raw DEMs highlight several issues of interest. First, the dry-bed surface representation of the Waimakariri riverbed, in areas free of gross error appears visually to be excellent. Complex dendritic-type drainage networks are clearly visible over large parts of the exposed bed. This is significant as such a configuration is difficult to observe in the field due to the small vertical differences in elevation involved, relative to the large spatial extent. The quality of surface representation reflects the relatively high precision (low SDE) in dry-bed areas of the raw DEMs once the influence of gross error had been removed (**Table 6.3**).

Image scale also appears important, with visually and quantitatively improved dry-bed topographic representation in the February 2000 DEM, which was generated from larger-scale (1:4000) imagery. Following removal of gross error from the DEM quality statistics, the SDE associated with this surface is little different from that calculated for dry-bed areas of the North Ashburton study reach (**Table 4.11**) using 1:3000 imagery. Representation in the two DEMs produced from 1:5000 imagery (February 1999 and March 1999) is similar, although a hole is apparent at the upstream end of the March 1999 DEM. Here, for an unestablished reason, stereo-matching has been unsuccessful over a large area. This region is dealt with during post-processing.

Second, a positive systematic bias remains across all three DEM surfaces following removal of gross errors. In wet-bed areas, this is thought to correspond to the typical water depth in the study reach. Thus, it demonstrates how the submerged bed is not being seen, and that the photogrammetry is instead measuring some point at or near the water surface. In dry-bed areas, ME is less than in wet-bed areas. However, it remains relatively large given the small vertical relief in the study reach.

Third, it is also apparent that there are some very large gross errors in regions of the study reach, shown up by very dark and very light areas in the DEM surfaces (**Figure 6.7**). The influence of these errors is demonstrated by the large improvement in the ME

and SDE statistics when the influence of gross error was removed (**Table 6.3**). Areas of gross error are predominantly in the centre of the riverbed, and generally correspond to locations of the wetted channels. The presence of error in the wetted channels demonstrates that turbid water has caused the automated stereo-matching algorithm to produce mismatches. Subsequent interpolation where points were not successfully matched acts to exaggerate these mismatch errors. If no points had been stereo-matched in wetted channels, or points had been correctly matched on the submerged bed or water surface, such large error would not result. This supports the idea that digital photogrammetry alone is largely unsuitable for surveying submerged topography where the water is turbid. However, in areas free from gross error, it appears visually that some underwater points have been successfully stereo-matched. For instance, the small wetted channel towards the true left bank flowing south-east at the upstream end of the February 1999 and March 1999 DEMs (**Figure 6.7a,b**) appears well represented.

Finally, the DEMs clearly demonstrate that simply eliminating wet-bed areas is insufficient for removing the errors associated with the presence of turbid water, as proximal dry-bed regions are also adversely affected (i.e. some gross error remains visible when the wet-bed is blanked out; **Figure 6.7**). This reinforces the need for post-processing to be used to identify and to eliminate dry-bed points that are in error.

6.2.5 Post-processing

The development of a post-processing procedure had two main aims. The main aim of the procedure was to allow identification and elimination of gross errors from dry-bed areas of the Waimakariri photogrammetrically-derived DEM surfaces (not just from the ME and SDE statistics, as was the case with the maximum expected error method). Therefore, the procedure should improve DEM quality in dry-bed areas and in so doing improve the interpolated water surface elevation and wet-bed quality (**Section 6.2.11**). A second aim was that the post-processing procedure should be automated. Conventionally, DEM post-processing is a largely manual task, with a human operator editing DEM points where there appears to be error as compared with the corresponding stereo-photograph. Whilst this approach is still useful and necessary in some cases, it is a very slow process, with an experienced operator able to measure only 200 points per hour (Lane, 1994). With a large, high spatial resolution DEM (such as the Waimakariri study reach, which contains 4 million potential points), it is not feasible for a human operator to check every point on the DEM surface. This demonstrates the need for automated correction of raw DEMs. However, manual editing may still be necessary where highly accurate topography is desired, or where errors remain in the DEM surface.

It was decided that individual DEMs should be post-processed prior to mosaicking, due to potential difficulties joining surfaces in the presence of errors and the possibility of errors being augmented by the mosaicking process. For the Waimakariri DEMs, an automated post-processing procedure was developed in the Spatial Modeller module of ERDAS Imagine, which was used to automatically identify and remove three categories of points from the raw DEM surface: (i) points that fell in wetted and vegetated areas; (ii) points where automated stereo-matching had been unsuccessful in correlating points from both images, and where the elevation is instead interpolated from adjacent, successfully matched points; and (iii) points that fell outside a local topographic deviation criteria.

6.2.6 Basic post-processing

The removal of wetted and vegetated areas is an important first step. Digital photogrammetry was not anticipated to provide good surface representation in inundated areas because the submerged bed is poorly defined in all but the very shallowest water. Also, sun-glare from the water surface was observed to cause the stereo-matching process to fail. Thus, large errors were expected in wetted channels and observed in the raw DEM surfaces (**Figure 6.7**). Thus, wet-bed areas should be eliminated from the dataset.

Vegetation also introduces errors, as it is the top of vegetation, rather than the ground surface, that is detected by photogrammetry. One option is to correct for vegetation by estimating and subtracting average vegetation height from the DEM surface (e.g. Lane *et al.*, 2000). However, this approach is more useful where vegetation height is relatively uniform and can be estimated from height measurements made in the field. In this study, riverbed vegetation was generally sparsely distributed across the study reach, so it was decided to simply remove vegetated points.

Wet-bed and vegetated points were removed using the classified riverbed images derived from ortho-images of each individual DEMs (e.g. **Figure 6.5b**). For the purpose of the post-processing procedure, where wet-bed and vegetated points were treated in the same way (i.e. elevations in these areas were removed), a two-way classification was sufficient, as wet-bed and vegetated points were classed together.

Linked to the removal of wet-bed and vegetated points was the additional elimination of all remaining dry-bed points where the stereo-matching algorithm had been unsuccessful. Where this happens, unmatched points are interpolated by OrthoMAX using a simple bilinear interpolator from adjacent successfully stereo-matched points. In practice, this means that the importance of each matched point increases as the proportion of stereo-matched points decreases, as a greater number of neighbouring

interpolated pixels will be influenced by the elevation value of each stereo-matched point. In the case of exposed regions of large, gravel-bed rivers, interpolated elevations can be expected to be generally well-approximated by unmatched points. This is because such points tend to be in homogenous, riverbed areas and thus the interpolations are valid when based on successfully stereo-matched point elevations from the area periphery (ERDAS, 1995). However, the bilinear interpolation method used means that errors (such as those associated with wetted channels or vegetation) may be propagated across larger areas. This is illustrated for a 500 m x 400 m test area of the February 1999 DEMs in **Figure 6.8**, with large areas of gross error apparent in the raw DEM surface (**Figure 6.8a**). Consequently, anomalous points cannot simply be removed from the raw DEM surface, as the surrounding interpolated points influenced by these elevation values remain (**Figure 6.8b**). Unmatched points were identified and eliminated using the matching statistics file, produced during DEM generation (e.g. **Figure 6.8c**).

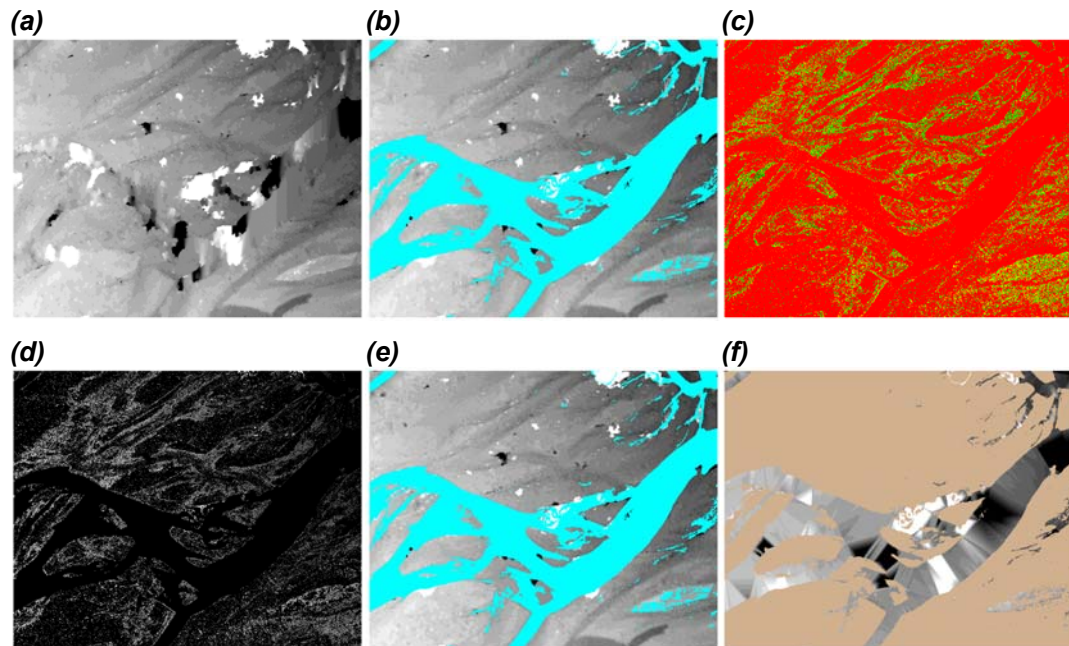


Figure 6.8 An illustration of the removal of unmatched, wet and vegetated points from the Waimakariri DEM surfaces. The raw DEM has several regions with gross errors present (**a**), which are near wetted channels, but not eliminated when wet-bed and vegetated areas are masked out (**b**). The use of the DEM stereo-matching statistics file (**c**) allows creation of a sparse DEM, comprised of only matched, dry-bed points (**d**). However, following re-interpolation gross errors remain (**e**), which are propagated into a modelled water surface elevation (**f**).

Following removal of wet-bed points, vegetated points and non-matched points, the resultant individual DEM surfaces consisted of only successfully stereo-matched dry-

bed points (**Figure 6.8d**), and are termed sparse DEMs. This approach offers two further advantages. First, it allows a more sophisticated interpolation model than bilinear interpolation to be used in subsequent surface re-interpolation. Despite this, bilinear triangulation was chosen to re-interpolate the sparse DEM surfaces in this study. More sophisticated interpolation methods would have taken much longer to process and would have required more powerful computer hardware. Furthermore, bilinear interpolation is available within the Imagine environment. Second, the sparse DEM approach dramatically reduces data storage demands, as only those pixels that are matched need to be retained in saved files.

Figure 6.8e shows a re-interpolated sparse DEM surface following removal of unsuccessful stereo-matches and wet and vegetated pixels. Despite some minor changes to the individual DEM surface (**Figure 6.8b**) there are few visible differences, and several gross errors remain which represent, therefore, mismatched points. These are located in particular near the wetted channel edges, leading to errors in subsequent interpolation, such as the modelled water surface elevation map (**Figure 6.8f**). Consequently, further post-processing was deemed necessary.

6.2.7 Individual DEM post-processing: Use of local standard deviation

Both visual evidence and empirical testing showed that errors (in the form of spikes or pits) remained following the first two stages of DEM post-processing. The small vertical relief of braided, gravel riverbeds meant that these errors are clearly visible on the DEM surface, and suggests that they are identifiable numerically. Consequently, topographic criteria were adopted in an attempt to remove the remaining gross errors. Two post-processing methods were developed and tested empirically on a 500 m x 400 m test area from the February 1999 DEMs (**Figure 6.8a**) to assess their effectiveness at gross error removal. The success of each method was judged with respect to independently surveyed check point elevations using an automated correspondence algorithm, with a maximum correspondence distance of 0.5 m (half the DEM grid spacing).

Method 1 uses local elevation values to determine the likelihood of a given elevation being in error. It is based on the assumption that the true variation in vertical relief is small. Thus, large values of local standard deviation should indicate erroneous photogrammetric measurements. Standard deviation was used as it is assumed to represent the internal precision associated with the surface. This approach is similar to that developed by Felicísmo (1994) but is not identical as irregular networks of points were being treated (sparse DEMs, e.g. **Figure 6.8d**) rather than regular grids. Using the Spatial Modeller module of Imagine, local standard deviation was calculated from

the sparse DEMs, using several search radii (5m, 10m, 15m, 20m and 25m) and all sparse DEM points for a given search radius. The resulting maps of local standard deviation are shown in **Figure 6.9**.

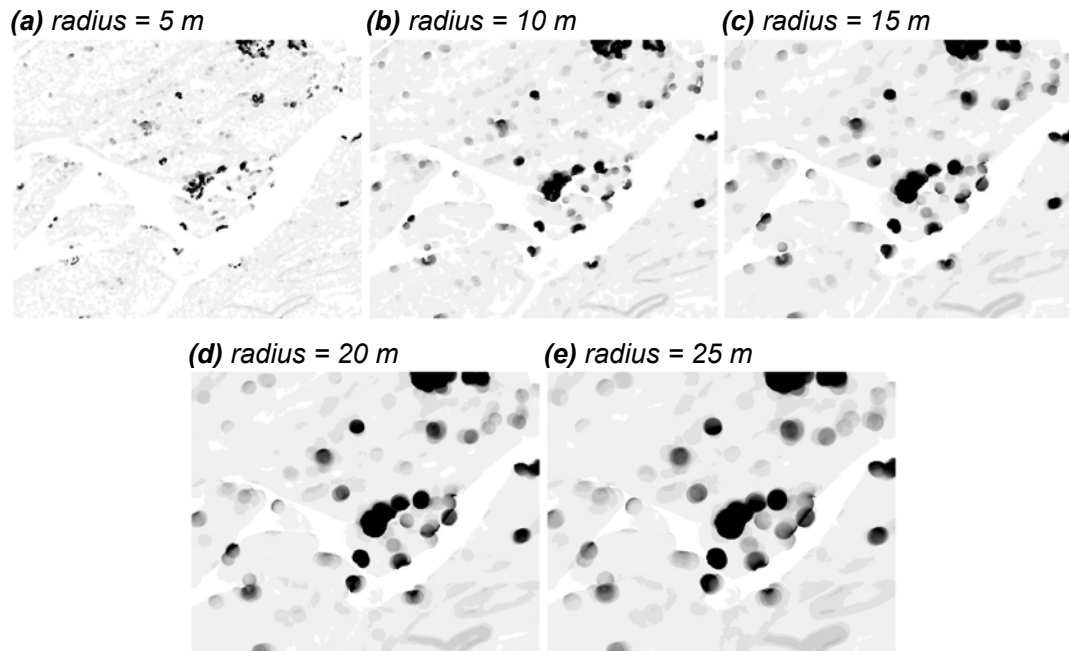


Figure 6.9 Maps of local standard deviation used to identify gross errors in the Waimakariri test areas DEM. Standard deviation is scaled from 0 (white) to 3 and above (black). Visual comparison with **Figure 6.8a** shows a good level of correspondence between standard deviation and error.

Sparse DEM points were eliminated if the corresponding point on the map of local standard deviation exceeded a given standard deviation tolerance. Three different tolerance levels were tested: 2 m; 1 m; and 0.5 m. These values correspond with the theoretical spatially-averaged standard deviation of the Waimakariri riverbed of around 1 m (Lane *et al.*, in prep.). As the tolerance level was decreased, more points were removed from the sparse DEM surface (**Figure 6.10**).

Post-processed sparse DEMs were produced for the test area using every combination of the three tolerance levels and five search radii. This gave 15 sparse DEM surfaces, plus the original unprocessed sparse DEM. Each sparse DEM was re-interpolated using bilinear interpolation because of its speed and availability within Imagine. The quality of the re-interpolated DEMs was assessed using the independent dry-bed check point measurements made concurrent with image acquisition (**Table 3.11**). The ME and SDE calculated for each re-interpolated DEM are shown in **Figure 6.10**.

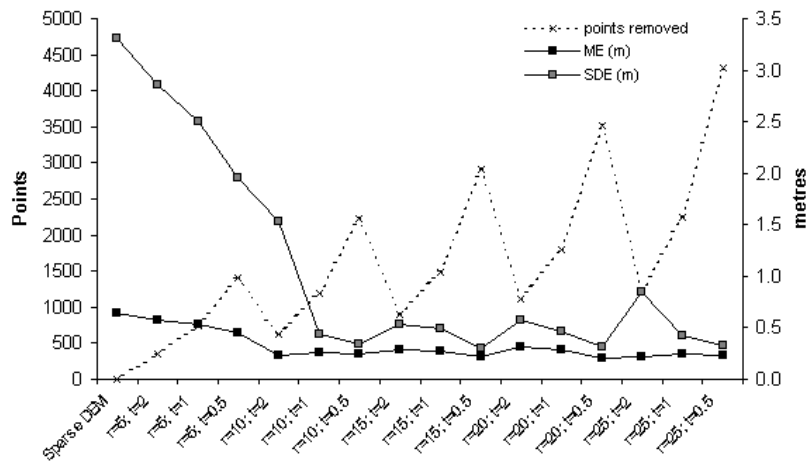


Figure 6.10 Effect of different standard deviation radius and tolerance level combinations on DEM quality using automated post-processing method 1.

Both ME and SDE fell as compared to the raw and re-interpolated sparse DEM surfaces. Generally, the ME and SDE decrease as the radius used to determine standard deviation is increased. They are at their lowest for a given radius when the tolerance level is lowest. The best combination for method 1 comprised of a standard deviation radius of 20 m and a tolerance level of 0.5 m (**Table 6.4**). Nonetheless, a ME over 0.2 m and SDE over 0.3 m remained. These values are relatively large compared to the vertical relief associated with the riverbed.

Post-processing method	Best case combination of topographic criteria	Points removed (%)	ME (m)	SDE (m)
1	Standard deviation radius = 20 m; Tolerance level = 0.5 m	75	0.208	0.308
2	Coarse DEM resolution = 5 m; Tolerance level = 1.0 m	29	0.293	0.291

Table 6.4 Summary of best case DEM quality obtained using both post-processing methods.

6.2.8 Individual DEM post-processing: Use of coarse resolution DEM

The main problem with method 1 is that it tends to impose a view of how the surface should appear (i.e. flat, hence low local standard deviation of elevation), and will also generally smooth surfaces, as sudden changes in elevation are identified as errors and removed (Hannah, 1981). Thus, an alternative method was sought. A solution to this problem followed the observation that DEMs with larger point spacings tend to smooth surface topography (**Figure 6.2**). Consequently, method 2 was developed which uses a lower resolution DEM to assess the error in elevation for a given DEM point, rather than using the elevation of neighbouring points. This method largely avoids problems

identified with method 1 by comparing two different representations of the same surface. In lower resolution DEMs, a larger image-space area is used in the calculation of the elevation of each grid cell. The main consequence is that spatial averaging occurs over a larger area which will tend to smooth individual point discrepancies. The main disadvantage is that as DEM resolution is increased, the true elevation will be more variable within each DEM grid cell, meaning that the precision of each DEM point is reduced.

To implement this post-processing method, 2 m, 5 m and 10 m resolution DEMs of the test area were also generated using OrthoMAX (**Figure 6.11**). Initially, all the DEM surfaces were subject to the basic post-processing procedure, and unmatched, wet-bed and vegetated points were removed. Next, the remaining dry-bed stereo-matched points in the high resolution (1 m) sparse DEM were subtracted from the remaining dry-bed stereo-matched points in the lower resolution DEMs. This gave maps showing difference in dry-bed elevation (**Figure 6.11**), which highlighted the likely location of gross errors in the high resolution DEM.

Points that exceeded a given elevation difference between the two DEM surfaces were removed, and the whole surface re-interpolated. Three tolerance levels were tested: 0.5 m; 1.0 m; and 2.0 m. These correspond to the same tolerance levels used during method 1. The assumed reduced precision associated with a coarser DEM surface meant that it was decided not to replace directly the eliminated 1 m DEM elevation values with the calculated lower resolution DEM values. The only exception was for the March 1999 DEM, in order to fill the large hole at the upstream end of the study reach evident in the 1 m DEM coverage (**Figure 6.7b**). The quality of post-processed DEMs was assessed using the independent check measurements (**Figure 6.12**).

Application of post-processing method 2 produced an improvement in DEM quality, with both ME and SDE reduced relative to the sparse DEM, although little additional increase in DEM quality resulted from a DEM spacing of greater than 5 m. Compared to method 1, SDE was slightly lower, indicating higher dry-bed precision, but remained above 0.25 m. However, a positive systematic bias remained (ME of at least 0.28 m), which was considerably higher than that obtained using method 1. The best combination of topographic criteria was judged to be a 5 m resolution DEM and 1 m tolerance level (**Table 6.4**), even though the use of a 0.5 m tolerance level produced a slightly higher quality DEM surface. This was because it was felt that discrepancies of just 0.5 m between 1 m and 5 m resolution DEM surfaces could occur that were not necessarily caused by errors (e.g. near steep channel banks). It was decided that such an occurrence was more unlikely with a tolerance level of 1 m, given the vertical magnitude of riverbed relief.

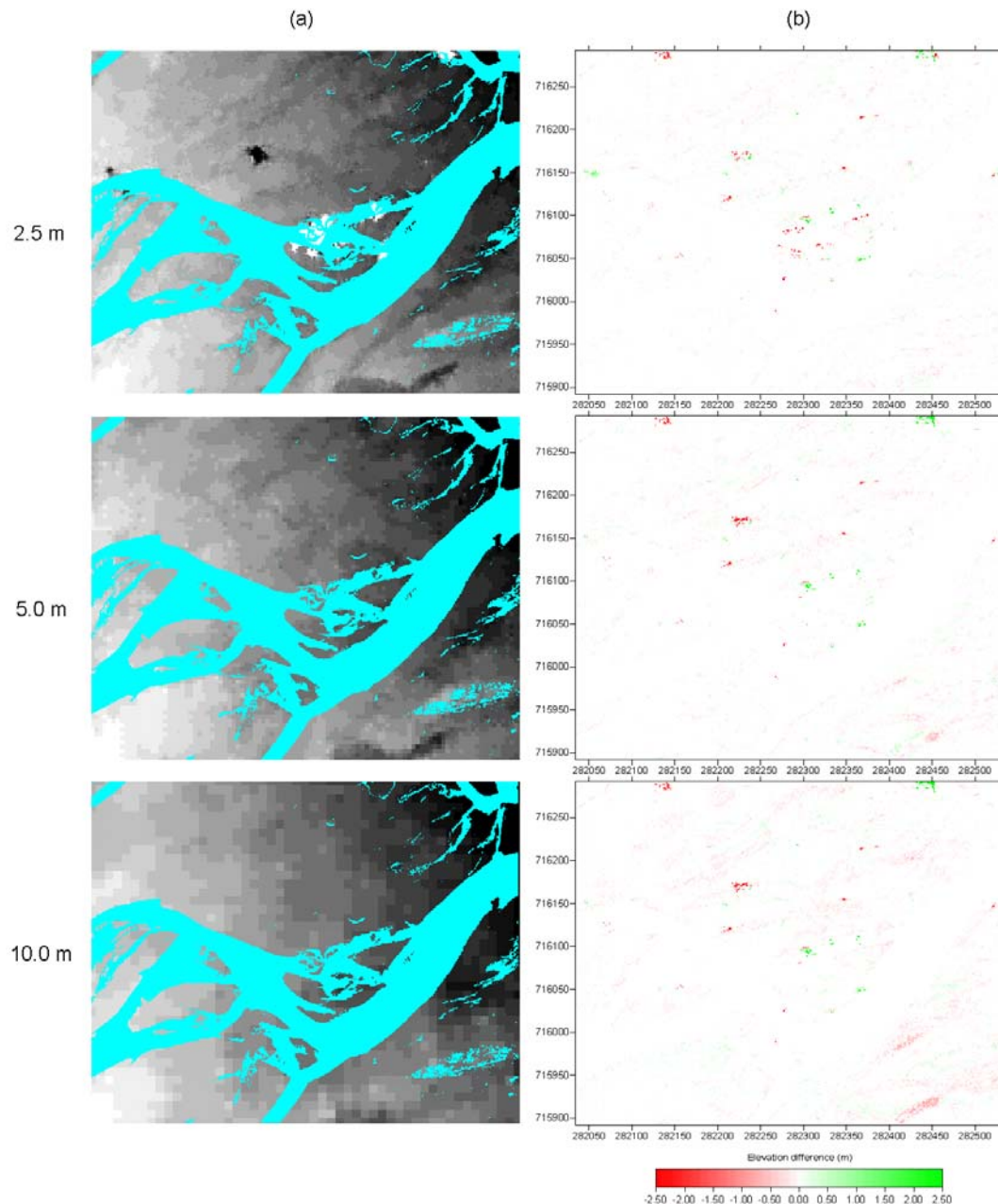


Figure 6.11 Identification of gross errors using coarser-resolution DEMs: (a) shows the three spatial resolutions tested; (b) shows the differences in elevation at dry-bed matched points relative to the test areas 1 m DEM surface.

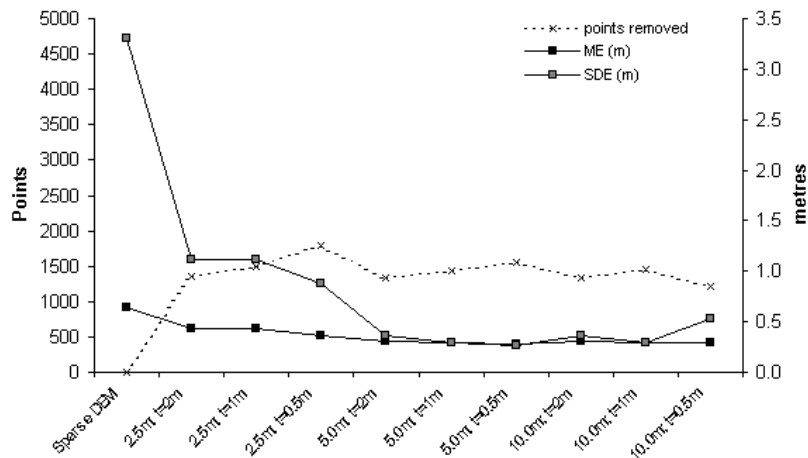


Figure 6.12 Effect of different DEM resolution and tolerance level combinations on DEM quality using automated post-processing method 2.

6.2.9 Individual DEM post-processing: Comparison of methods

Three important differences were identified between the two post-processing methods. First, visual inspection of the test area dry-bed DEM surfaces produced with the best case post-processing procedures indicated that a better surface resulted from application of method 2 (**Figure 6.13b**). Following use of method 1, some gross errors remained visible in the DEM surface (**Figure 6.13a**). However, based on the check point data alone, method 1 appears superior (with a lower ME value). This demonstrates that when relatively few check data points are used to quantify DEM quality, the assessment statistics calculated are strongly related to their distribution and do not necessarily reflect the true quality of the DEM surface as a whole (Lane *et al.*, 2000).

Second, the presence of gross errors was discovered to lead to considerable differences in the modelled water surface elevation maps (**Figures 6.13c** and **6.13d**), produced by linearly interpolating water edge dry-bed points across the wetted channels. This would be expected, since derived parameters (i.e. water surface elevation) are more sensitive to DEM quality (e.g. Ley, 1986; Wise, 1998).

Third, considerably more points are removed from the sparse DEM by method 2 (75% of points using method 1 compared to around 30% with method 2; **Table 6.4**). This is important as potential information loss due to post-processing is minimised, and it implies more efficient error identification.

Thus, method 2 was chosen as the better post-processing method for the Waimakariri individual DEMs. Consequently, OrthoMAX was used to generate 5 m-spaced DEMs

for all three photogrammetric surveys, and post-processing method 2 was applied to each individual DEM surface.

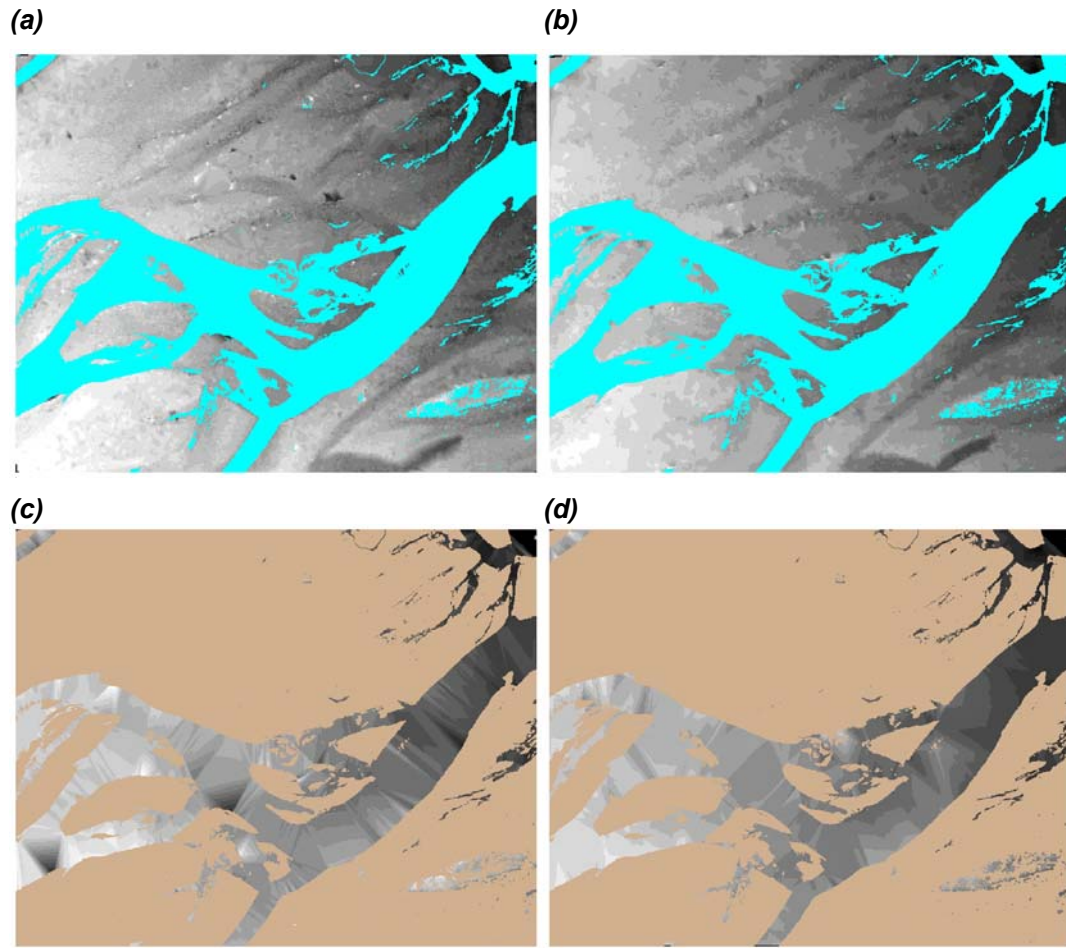


Figure 6.13 The best case test area DEMs produced using both post-processing methods: (a) the dry-bed using method 1; (b) the dry-bed using method 2; (c) the modelled water surface from the method 1 dry-bed; and (d) the modelled water surface from the method 2 dry-bed. All DEM surfaces are scaled from 38.5 m (black) to 42.5 m (white).

6.2.10 Joining of individual DEMs

Following post-processing, the individual sparse DEMs required mosaicking to form single, continuous DEM surfaces of the study reach. Two mosaicking strategies were considered. First, the sparse individual DEMs themselves (e.g. **Figure 6.8d**) were joined. This approach is preferable since only dry-bed matched points are merged and, following mosaicking, it allows the entire study reach to be re-interpolated at the same time. The ‘Mosaic Images’ module of ERDAS Imagine was used. This module allows selection of multiple raster images (including DEMs), which are then mosaicked and saved as a new Imagine image file. Several mosaicking algorithms are available, which

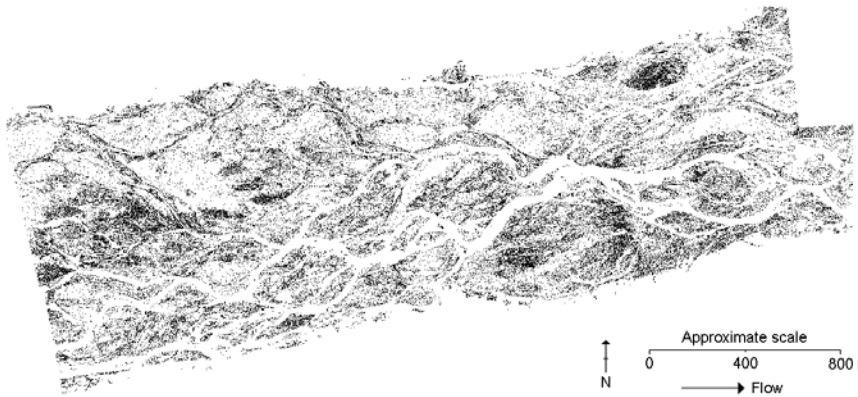
determine how overlapping areas are treated. To mosaic the sparse DEMs, the ‘average’ overlap function was used. This means that whenever two dry-bed matched points from overlapping images coincide, the mean elevation value is used. Elsewhere, all dry-bed elevation values are included in the mosaicked image. This produced whole reach sparse DEMs (**Figure 6.14**), which were then re-interpolated to form whole reach post-processed DEMs for each photogrammetric survey. Bilinear interpolation was used, since the number of data points was too large to permit a more sophisticated interpolation algorithm (e.g. kriging) given the computer resources available.

However, difficulties were experienced with this method of mosaicking. As reported in other studies that have merged multiple DEMs of relatively flat riverbed surfaces (e.g. Stojic *et al.*, 1998; Ashmore, 2001; Chandler *et al.*, 2001), joins between individual DEM tiles are apparent in the final DEM surface, particularly in dry-bed areas. These joins produce cross-stream banding for each flight line, creating a patchwork effect in the reach-scale DEM surface. This only became apparent in the detrended DEM surfaces, particularly for the March 1999 DEM (**Figure 6.15**). The bands are produced by vertical systematic differences between the elevation of overlapping sparse DEMs. Research suggests that these are caused by small random variations in PCP image-space positioning during the block triangulation phase, which can cause relatively large systematic changes in DEM edge elevation (Lane *et al.*, in prep).

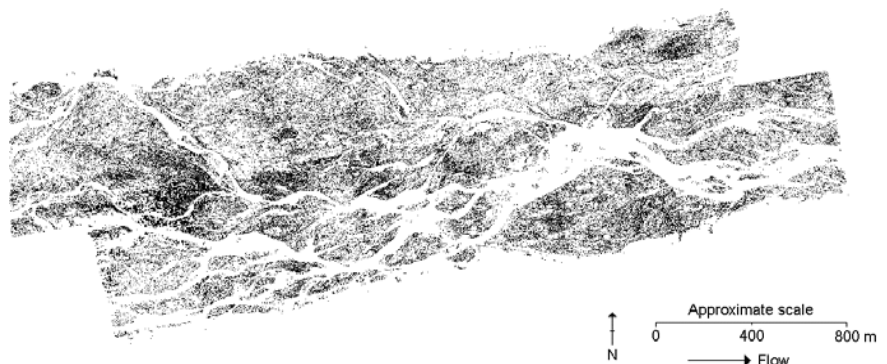
The addition of a network of tie-points during the block triangulation stage (**Section 3.3.5; Table 3.9**) reduced but did not eliminate this banding effect. Although not large in magnitude (typically less than 0.5 m or 0.1% of exposure station height), the elevation differences are significant in relation to natural topographic variation of the riverbed and relevant to the planned calculation of DEMs of difference.

To evaluate this problem, overlap analysis was performed for all three whole reach DEMs by differencing those areas where individual raw DEMs overlap. The spatial pattern of elevation discrepancies in DEM overlap areas is shown in **Figure 6.16**. There is remarkable similarity between the overlap differences in each case, with the upstream DEM too high at the upstream edge of the overlap, and too low at the downstream edge (**Figure 6.17a**). This suggests that a reasonable join can be achieved, so long as care is taken which points are incorporated from the DEMs involved in the overlap: points near the overlap centre are likely to have less systematic difference between elevations. It also implies that some sort of systematic error correction is possible.

(a) February 1999



(b) March 1999



(c) February 2000

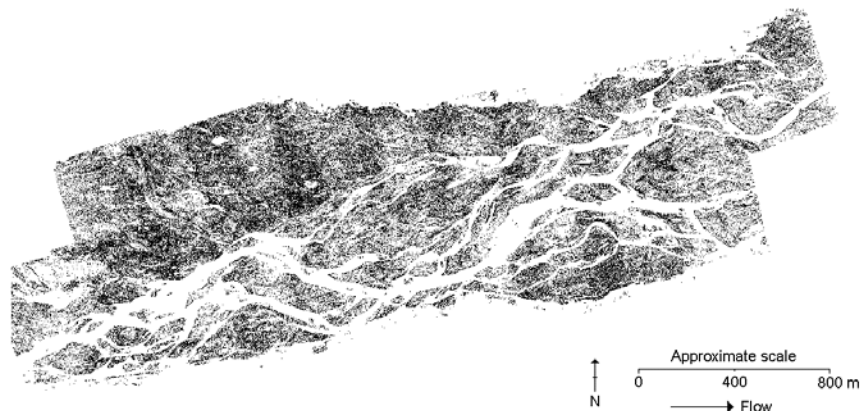


Figure 6.14 Mosaicked post-processed sparse DEMs for each photogrammetric survey.

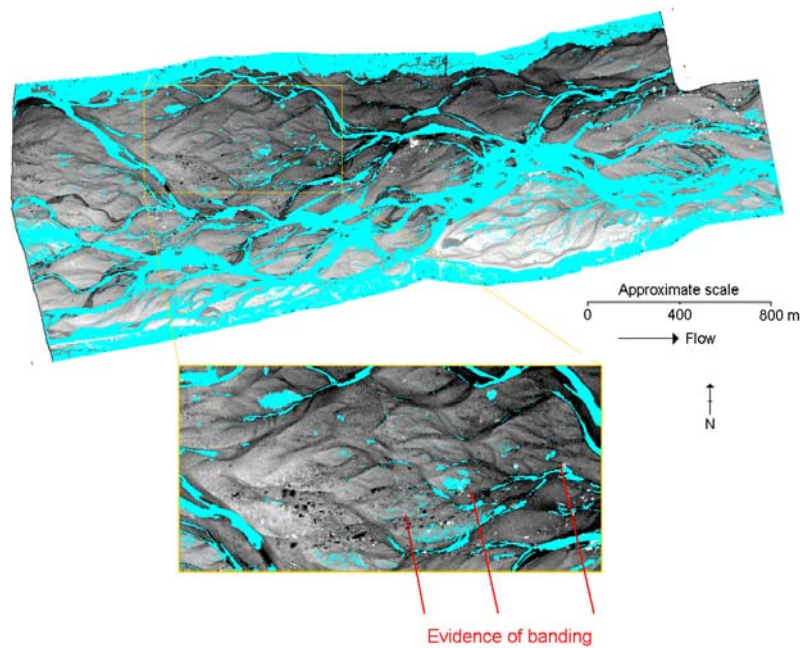


Figure 6.15 Re-interpolated whole-reach sparse DEM for March 1999. The DEM has been detrended, from -1.5 m (black) to $+1.5\text{ m}$ (white), and wet-bed and vegetated points are masked out. The banding effect caused by systematic differences between individual DEMs is visible.

The use of sparse DEMs exaggerates the problem of vertical discrepancies between overlapping DEMs by joining adjacent points regardless of elevation (**Figure 6.17b**). Points are only averaged if their planimetric position corresponds exactly. With this in mind, it was decided that a distance-weighted overlap function would improve the joins between overlapping DEMs, and would thus be a more suitable mosaicking strategy (**Figure 6.17c**). The disadvantage of such an algorithm is that it requires the post-processed sparse DEMs to be re-interpolated prior to mosaicking, increasing data volume and propagating any remaining gross errors in the post-processed individual DEM surfaces.

The individual sparse DEMs were re-interpolated using bilinear interpolation. Mosaicking was performed using the default ‘feather’ algorithm. This is a distance-weighted average algorithm which takes the average of corresponding points at the centre of an overlap, but in other areas of an overlap weights the elevation of corresponding points based on the distance from the source DEMs. Hence, the elevation of a point 1/10th of an overlap from an edge would be calculated using 90% from the nearer DEM and 10% from the more distant DEM (ERDAS, 1995). Thus, the method does not actually remove error, but rather assumes that error increases as a function of distance from a DEM.

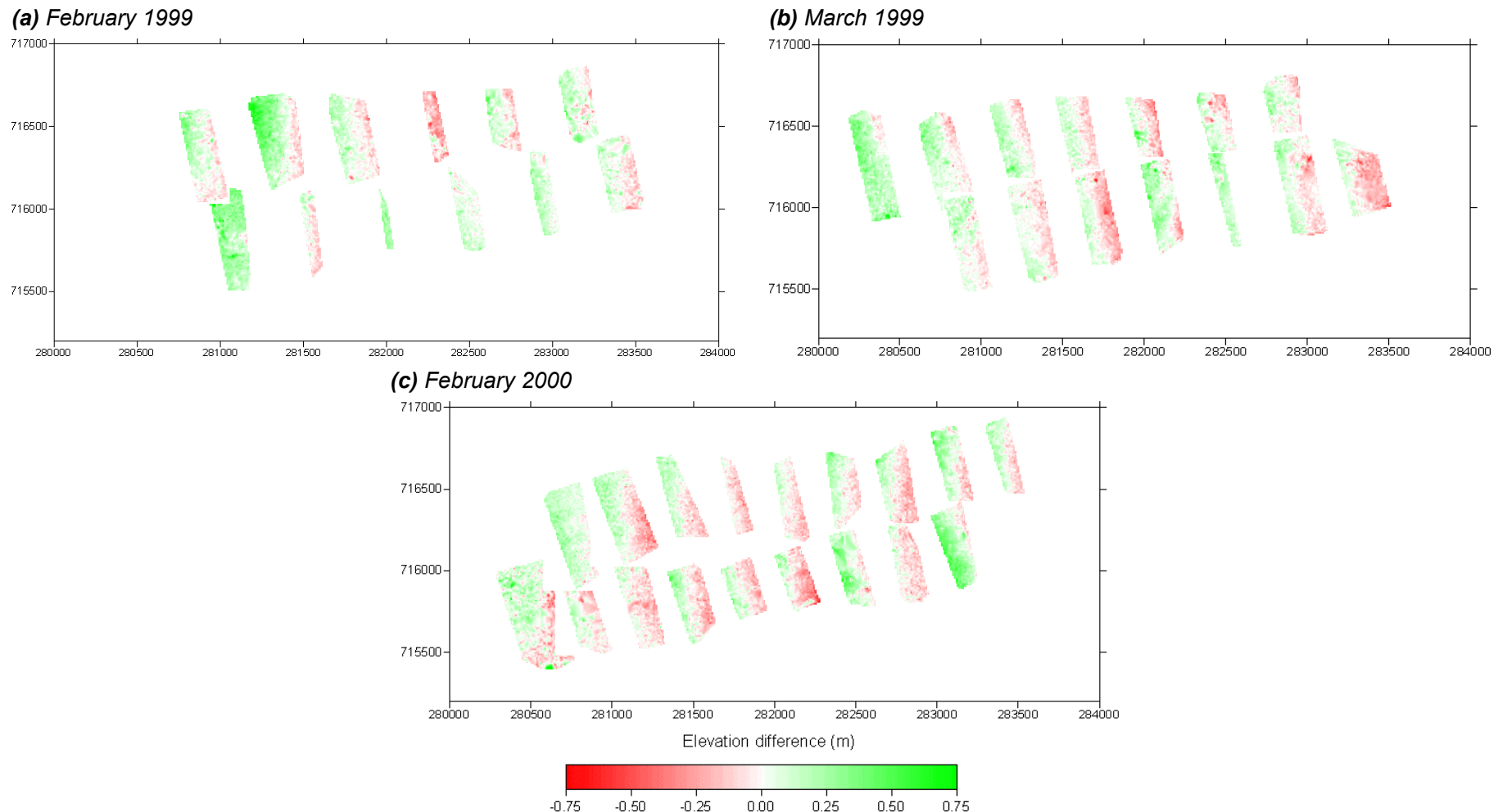


Figure 6.16 Spatial pattern of individual DEM overlap differences for each photogrammetric survey.

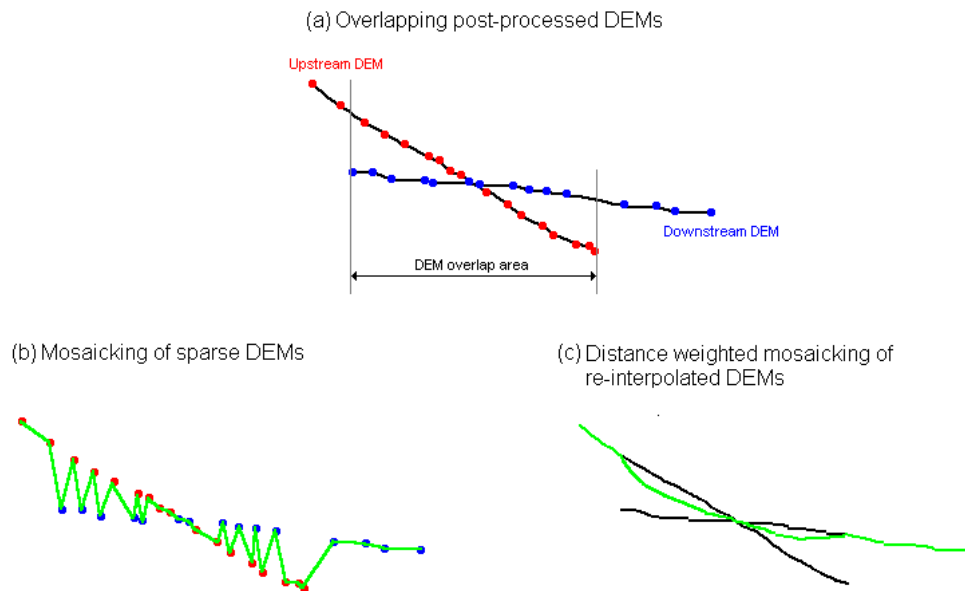


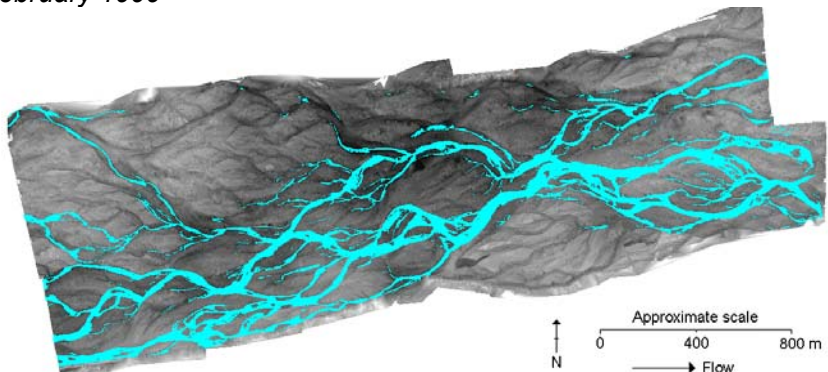
Figure 6.17 Schematic representation of the two contrasting mosaicking strategies used for joining individual overlapping DEMs (a). Mosaicking of sparse DEMs tends to reinforce elevation discrepancies (b), while distance-weighted averaging of continuous surfaces minimises elevation discontinuities (c). The green line shows the final, mosaicked, DEM surface. Vertical scale has been exaggerated.

The mosaicked, post-processed DEMs for the Waimakariri study reach for each photogrammetric survey are shown in **Figure 6.18**. Visual inspection of the detrended DEMs suggested that this second mosaicking method had, as hoped, reduced the magnitude of systematic bias between overlapping DEMs.

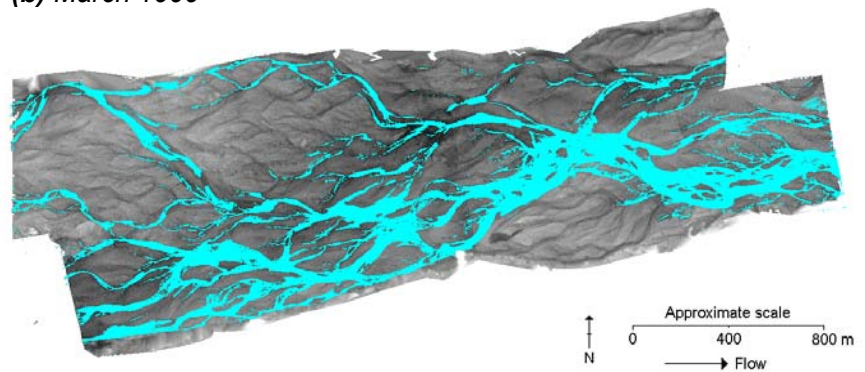
6.2.11 Integration of post-processed dry-bed DEM with water depth estimates

The next stage of DEM post-processing was the incorporation of the water depth information derived from water colour (**Figure 5.4**) to estimate the wet-bed elevation from the corrected dry-bed photogrammetric survey. Previous applications of an empirical water colour – water depth relationship in rivers environments (e.g. Acornley *et al.*, 1994; Winterbottom and Gilvear, 1997; Gilvear *et al.*, 1998) have not incorporated water depth data into a three-dimensional dry-bed topography. The key requirement for conversion of water depths into wet-bed elevations is a water surface elevation. This was modelled by interpolating water edge points obtained from dry-bed areas of the whole reach DEMs after post-processing (**Figure 6.18**).

(a) February 1999



(b) March 1999



(c) February 2000

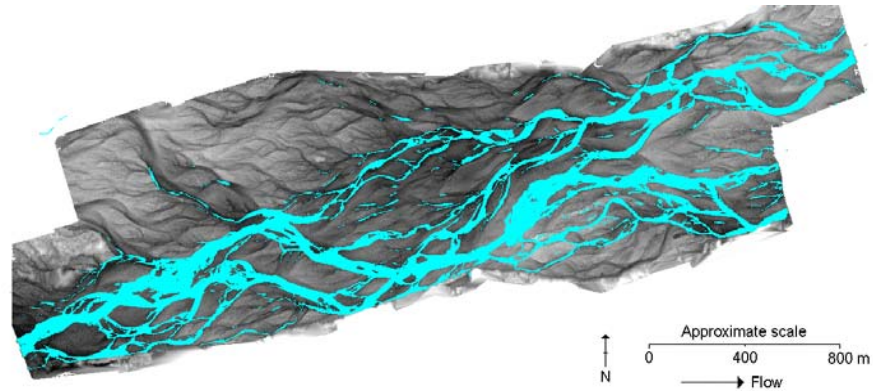


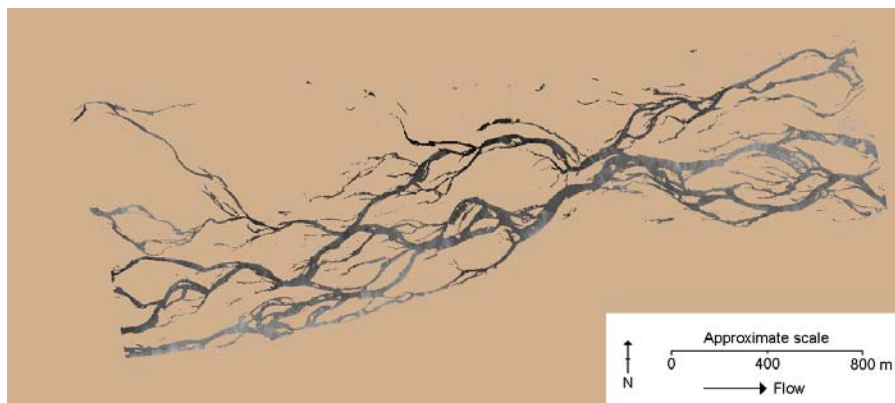
Figure 6.18 The re-interpolated whole reach post-processed DEM surfaces. Wet-bed and vegetated areas have been masked out, and the DEM surfaces have been detrended to be scaled from -1.5 m (black) to $+1.5\text{ m}$ (white). There is little visual evidence of the banding effect that previously affected the whole reach DEMs (**Figure 6.15**).

Ideally, an inexact interpolation algorithm, such as kriging, would have been used (as was used for the North Ashburton River water surface elevation maps). However, the size of the whole reach DEMs meant that this was unfeasible. Instead bilinear interpolation was used to model the water surface elevation (**Figure 6.19**). The water surface DEMs are visually encouraging with few gross errors, indicating that the automated post-processing procedure was effective at identifying and removing the gross errors that were present in the raw dry-bed DEMs (**Figure 6.7**).

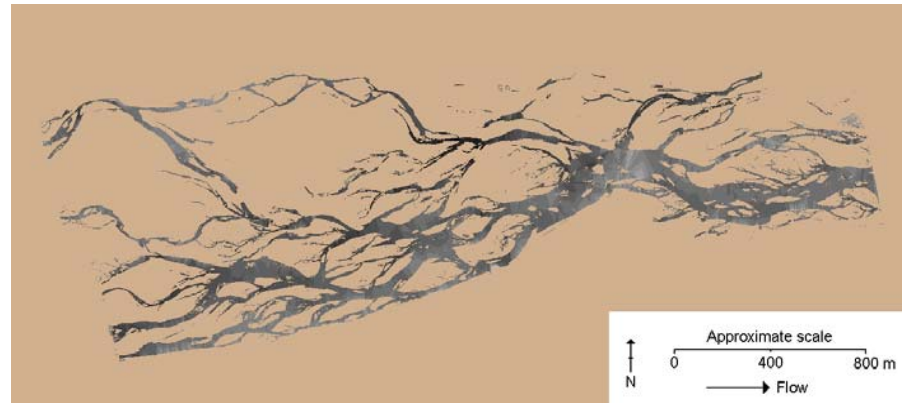
To lessen the faceted effect (produced by an exact interpolator) the water surface was smoothed using a 10 m x 10 m minimum value filter. A minimum filter was chosen because interpolation errors associated with the water surface were generally positive (i.e. the water surface was too high), probably due to opposite bank tops (rather than bank bottoms) being joined during re-interpolation. This highlights how photogrammetrically-derived elevations near the water edge are more unreliable due to mismatching effects caused by the close presence of turbid water. The selection of a 10 m x 10 m window was made based on the typical horizontal size of water surface ‘facets’. In the study reach, the average bed slope is around 0.005% (Hicks, pers. comm.). Thus, the effect of the minimum filter in areas free from error will be slight (up to 0.05 m) within a given 10 m x 10 m window.

Finally, the water depth maps (**Figure 5.4**) were subtracted from the water surface elevation maps to produce estimated wet-bed elevation maps for each photogrammetric survey. These were merged with the post-processed reach-scale dry-bed DEMs (**Figure 6.18**) to give the final DEM surfaces. These are shown in **Figure 6.20**, following subtraction of a linear bed slope to remove the downstream trend in elevation which otherwise dominates image scaling. The same linear trend surface was used in each case to aid comparison of the four DEMs. The DEMs were also trimmed to eliminate bank-edge vegetation and to leave an identical riverbed area, again to facilitate between-survey comparison.

(a) February 1999



(b) March 1999



(c) February 2000

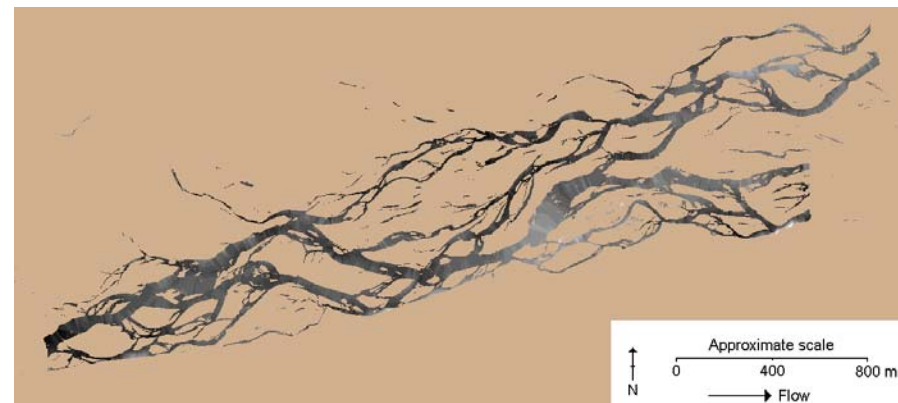
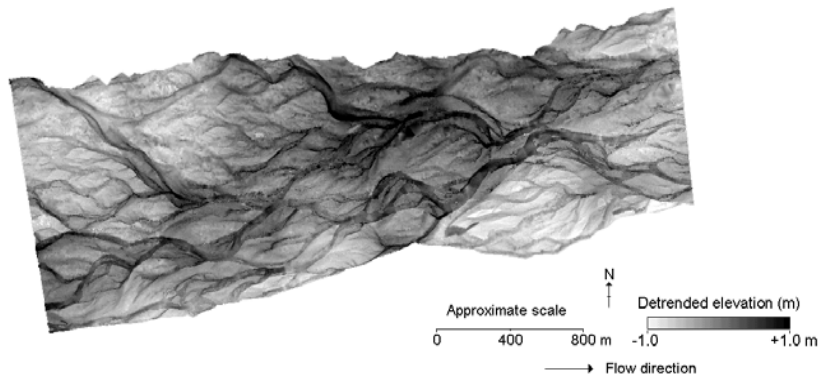
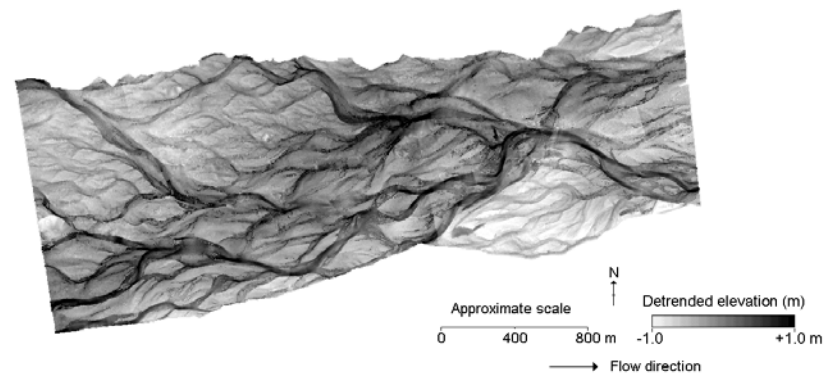


Figure 6.19 Water surface elevation maps for each whole reach DEM, modelled from the post-processed dry-bed DEMs (**Figure 6.18**). Each is detrended and scaled from -1.5 m (black) to $+1.5\text{ m}$ (white). Dry-bed and vegetated areas have been masked out.

(a) February 1999



(b) March 1999



(c) February 2000

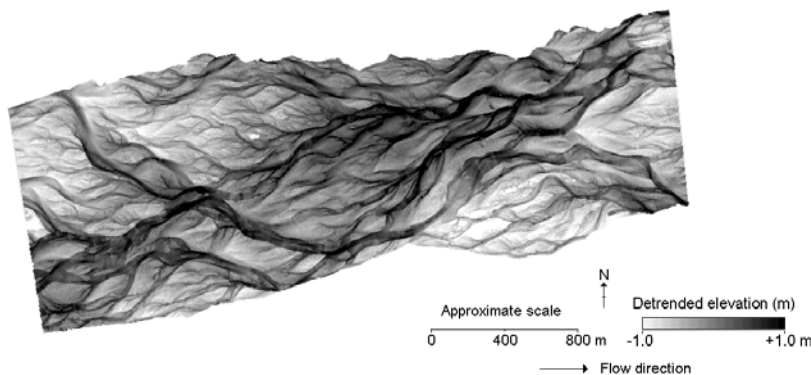


Figure 6.20 Final whole reach DEMs for the Waimakariri study reach, following post-processing, mosaicking and incorporation of estimated water depth maps. Each DEM has been detrended relative to the same linear trend surface.

6.2.12 Reach-scale post-processing: Systematic error removal

Ordinarily, when either just one stereo-pair is used, or when no post-processing is undertaken, it can be assumed that the DEM depiction of photo-control points (PCPs) locations is of high quality as the DEM surface will be most reliably calibrated at these points. Furthermore, since the DEM elevation of these points is not independent of the photogrammetric process used to create them, they can give a misleadingly favourable assessment of overall DEM quality. However, in this case, where for each photogrammetric survey multiple DEMs from a common photogrammetric block have been post-processed and mosaicked, this is not necessarily the case. Thus, an examination of the height discrepancies between the DEM surface and PCPs becomes a potentially meaningful additional post-processing method to identify and remove systematic errors.

This was performed for the three photogrammetrically-derived DEMs of the Waimakariri study reach. Photo-control points were associated to the closest DEM point using an automated spatial correspondence algorithm, and the resulting point discrepancies were interpolated into a 10 m x 10 m-spaced reach-scale surface. A minimum curvature algorithm was used in order to maximise the smoothness of this surface. The resulting maps of discrepancies are shown in **Figure 6.21**.

As would be expected, many of the PCPs are close to (less than ± 0.025 m) the post-processed DEM surface, despite the removal of points during post-processing and the subsequent re-interpolation and mosaicking. However, some PCPs show considerable deviation from the post-processed DEM surface. Areas of riverbed around these points can be assumed to be inaccurate. For example, in the test area used to evaluate post-processing methods (**Figure 6.8**), a positive systematic bias was noted, regardless of post-processing algorithm used (**Figures 6.10** and **6.12**). The test area was centred at approximately [282300,716100], and from **Figure 6.21a** it is clear that this whole region is too high relative to the nearby PCPs. Consequently, the three post-processed whole reach DEM surfaces obtained using photogrammetry (**Figure 6.20a**, **Figure 6.20b** and **Figure 6.20c**) were subject to a further correction, by subtracting the maps of deviation interpolated from PCP elevations (**Figure 6.21**).

An overview of the post-processing stages used to create reach-scale DEMs using photogrammetrically-acquired data is given in **Figure 6.22**.

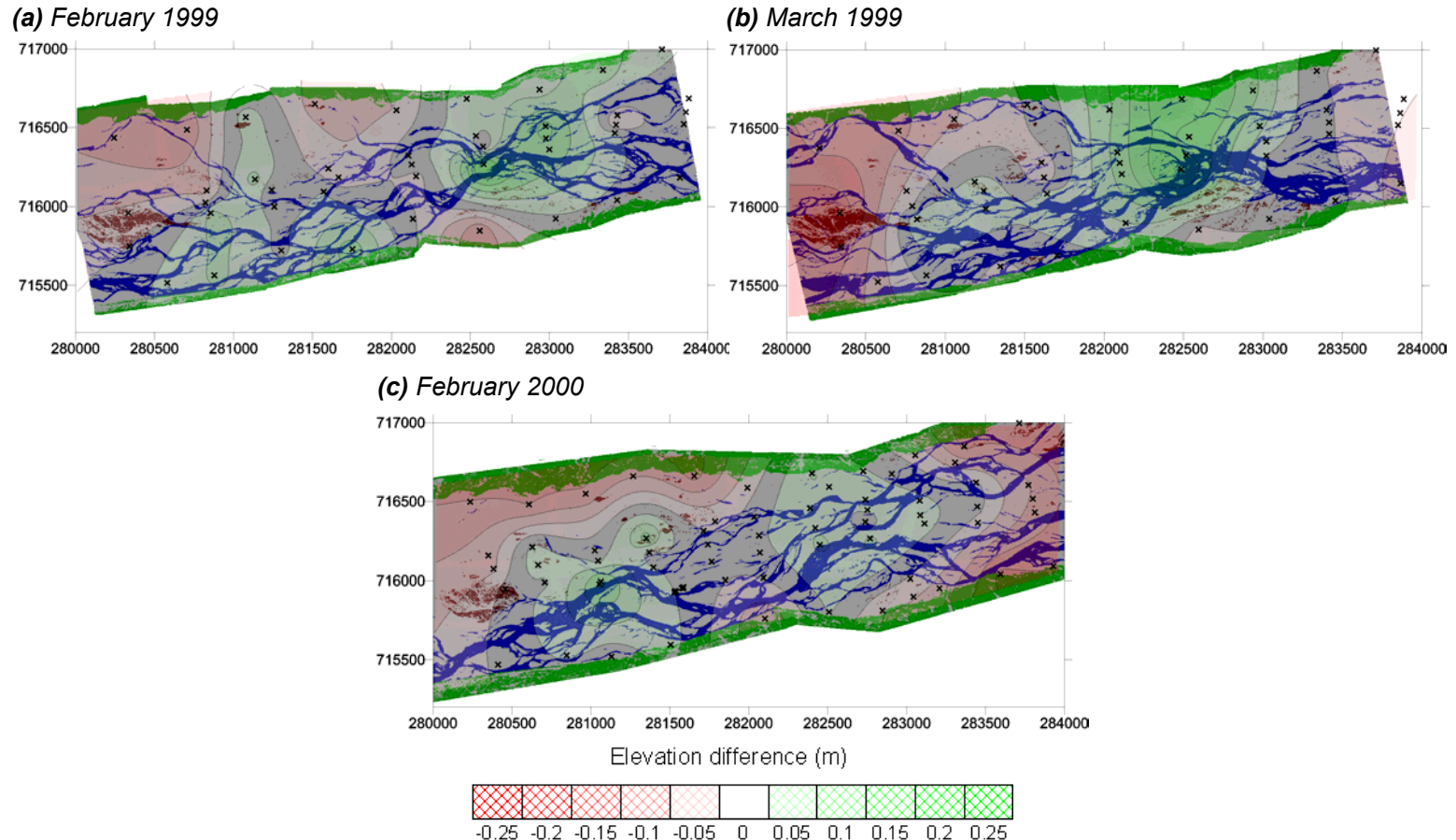


Figure 6.21 Maps of height discrepancies between the post-processed DEM surfaces and PCP elevations. Areas shaded red indicate that the final DEM surface is too low. Areas in green represent areas where final DEM elevations are too high. Zones of no shading are within ± 2.5 cm of surveyed PCP position. The location of individual PCPs is marked.

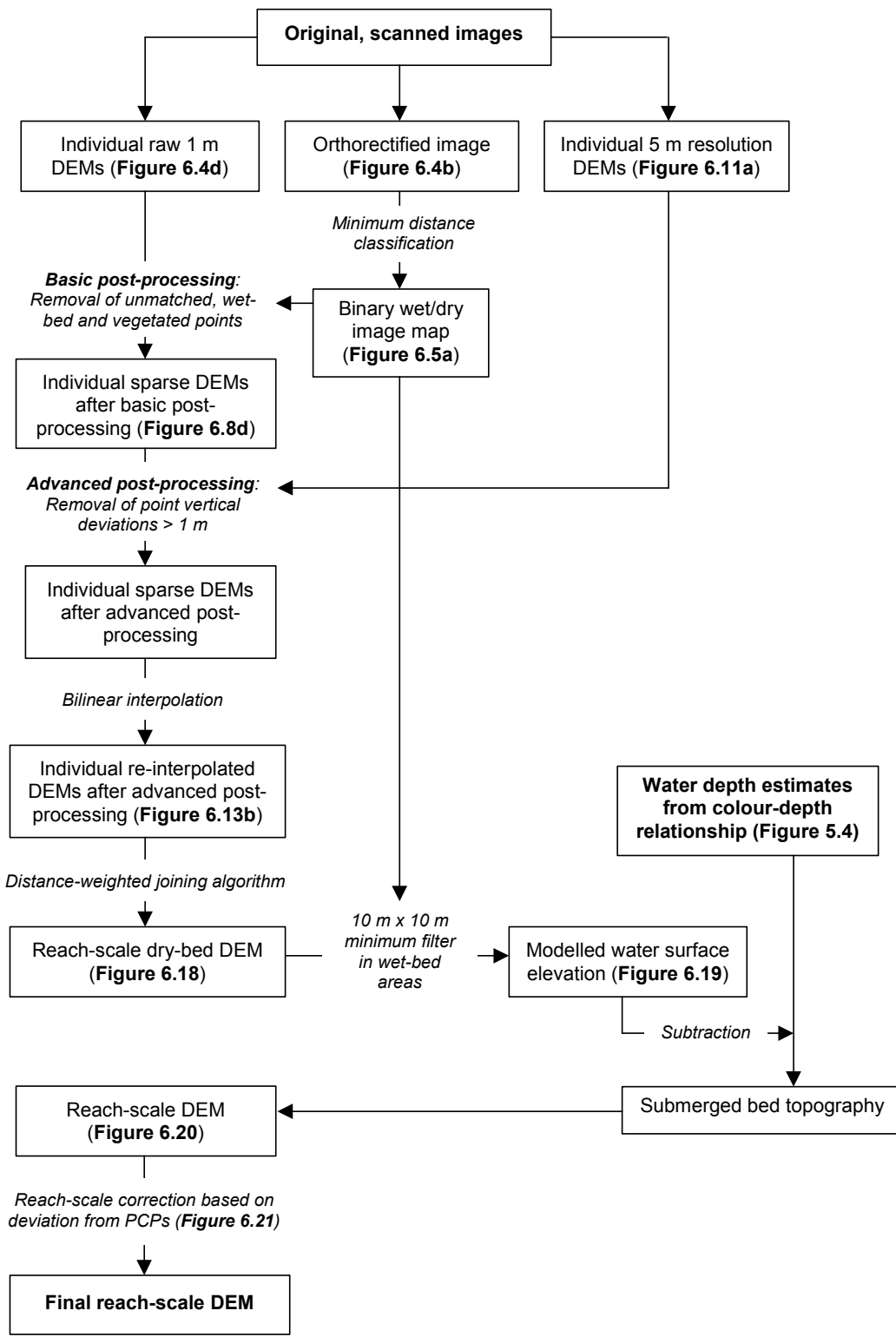


Figure 6.22 The post-processing stages used to create reach-scale photogrammetric DEMs of the Waimakariri study-reach.

6.3 Dry-bed survey using airborne laser scanning

Section 6.2 demonstrated that digital photogrammetry is able to provide dry-bed representation of large, gravel-bed rivers. However, before a final DEM surface could be produced, several stages of post-processing were necessary. Airborne laser scanning represents an alternative remote survey method to digital photogrammetry. It is suited to linear features, such as riverbeds, since topographic data can be collected continually along a flight line. By contrast, the downstream coverage of a single DEM produced using photogrammetry is constrained by the spatial coverage of overlapping photographs. Although multiple photographs can be used to span linear features, this will inevitably increase the amount of post-processing needed. Furthermore, joining individual DEM tiles may decrease the quality of the final DEM surface (**Section 6.2.10**), especially where vertical discrepancies occur.

The feasibility of using ALS to survey large, gravel-bed rivers was tested by surveying the Waimakariri study reach in May 2000. This allowed the difference in topographic data quality produced using digital photogrammetry and ALS to be examined. However, the ease of data acquisition could not be directly compared. Airborne laser scanning is largely a provided service, with data processed in-house using proprietary algorithms (Baltsavias, 1999a). This was also the case in this research, meaning that the exact nature of, and the time and resources needed for, data post-processing for the Waimakariri study reach was unclear.

6.3.1 DEM generation

Airborne laser scanning data was provided in the form of three ASCII files, one for each re-survey (**Section 3.4.3**). Each was divided into ground and non-ground subsets. The non-ground subset was understood to refer to vegetation and wet-bed areas, and was disregarded. The three ground subsets were combined and bilinear interpolation was used to create a regularly-spaced DEM of the study reach. A ground spacing of 1 m was used to correspond to the photogrammetrically-acquired DEM point spacing. As with the DEMs produced using digital photogrammetry, the removal of wet-bed and vegetated areas was necessary. The removal of wet-bed areas permits re-interpolation of a modelled water surface elevation. The removal of vegetated points should remove errors associated with detection of vegetation tops rather than the ground surface. In theory, the ground subsets used to create the ALS DEM surface should not have included either type of point. However, for consistency with the photogrammetric post-processing, all areas classified as wet-bed or vegetated in the maximum likelihood classification undertaken from the May 2000 photo-mosaic of the reach (**Figure 5.2d**) were removed. Re-interpolation was performed using bilinear interpolation.

6.3.2 Integration of dry-bed DEM with water depth estimates

The re-interpolated ALS DEM surface provided the modelled water surface that was used to convert water depth estimates (**Chapter 5**) into wet-bed elevations. The modelled water surface is shown in **Figure 6.23**. As with the water surface maps derived from digital photogrammetric dry-bed measurements (**Figure 6.19**), a faceted effect is apparent. To reduce this, the water surface was smoothed using a 10 m x 10 m minimum value filter.

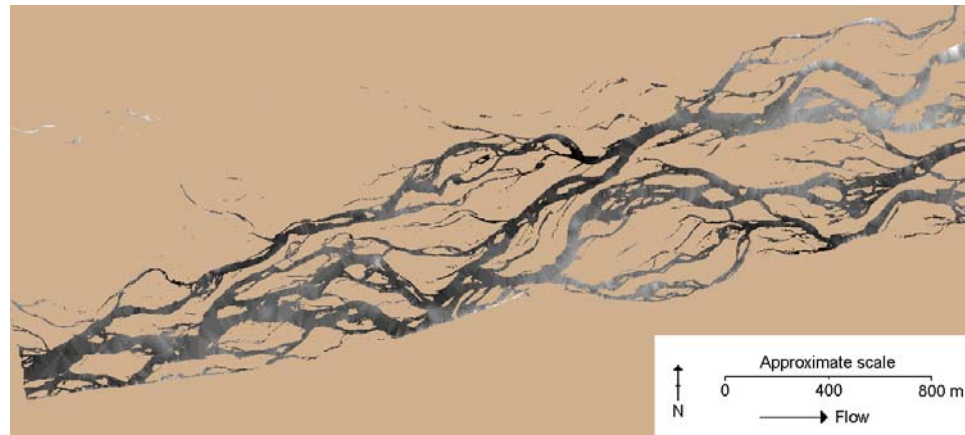


Figure 6.23 Water surface elevation map for the May 2000 ALS DEM. It has been detrended and is scaled from –1.5 m (black) to +1.5 m (white). Dry-bed and vegetated areas have been masked out.

The May 2000 water depth map (**Figure 5.4d**) was subtracted from the water surface elevation map to produce an estimated wet-bed elevation map. This was merged with the whole reach dry-bed DEM to give the final DEM surface. It is shown in **Figure 6.24** following subtraction of a linear bed slope to remove the downstream trend in elevation which otherwise dominates image scaling. The same linear trend surface used to detrend the digital photogrammetric reach-scale DEMs (**Figure 6.20**) has been used. The DEM has also been trimmed to eliminate bank-edge vegetation and to leave an identical riverbed area.

6.4 Final DEM quality assessment

Quality assessment for reach-scale DEMs produced using both digital photogrammetry and ALS was undertaken using three methods: (i) qualitative DEM assessment; (ii) comparison of DEM elevations with independently surveyed dry- and wet-bed data; and (iii) overlap analysis.

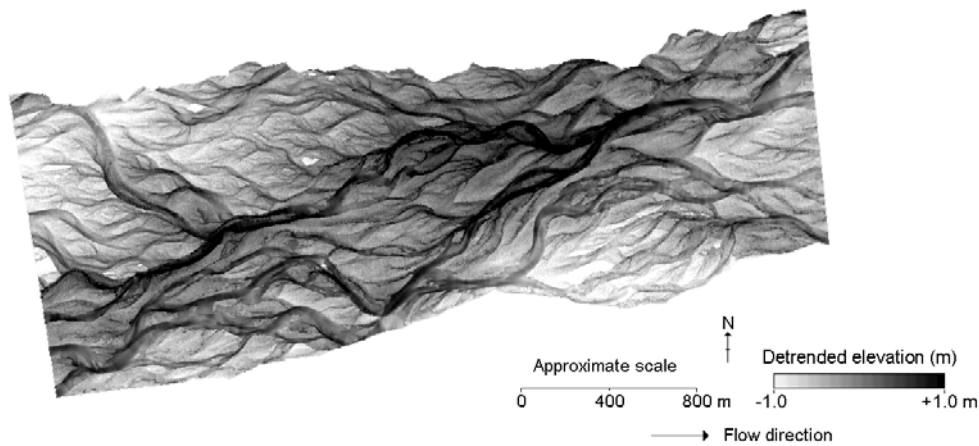


Figure 6.24 Final whole reach DEM for the Waimakariri study reach calculated using ALS. Elevations have been detrended with the same linear trend surface used in **Figure 6.20**.

6.4.1 Qualitative DEM assessment

Visually, the DEMs are extremely encouraging, and the gross error associated with the raw photogrammetric DEMs appears to have been removed successfully. Riverbed morphological structure is clearly visible in all four DEM surfaces, and allows an active braid-belt to be distinguished, flowing between large, alternating points bars with dendritic-type drainage toward their downstream margin (Hicks *et al.*, 2001). As noted for the raw DEMs, the effect of image scale appears to be significant, with visibly more topographic detail and less interpolation in the February 2000 DEM generated using 1:4000 images compared to the 1:5000 imagery used in February 1999 and March 1999.

Although collected using a completely independent method, the ALS DEM shows a remarkably similar range of detrended elevations to the photogrammetrically-derived DEMs (**Figure 6.20**). This is a valid comparison since the same linear trend surface, derived from the February 2000 DEM, was used to detrend all four DEM surfaces. The ALS surface appears to give an equivalent, or even slightly better, riverbed representation than the February 2000 photogrammetric DEM.

6.4.2 Comparison with independent check data

The second method of DEM quality assessment was comparison of DEM elevations with independently surveyed check points, acquired concurrent with the photogrammetric and ALS surveys (**Table 3.11**). Not only does this give an assessment of final DEM quality, but also an indication of the effectiveness of automated post-processing at removing errors from the DEM surface. This used an

automated spatial correspondence algorithm, with a maximum correspondence distance of 0.5 m (half the DEM grid spacing). The check elevation datasets were divided into wet-bed and dry-bed points, to allow comparison of DEM quality in both areas. In this instance, all DEM-check point pairs were used to calculate ME and SDE (i.e. not just those less than the maximum expected error). This was because an overall estimate of overall DEM quality was required.

First, the effect of post-processing on the photogrammetrically-acquired DEMs is examined (**Table 6.5** and **Figure 6.25**). Overall, the post-processing stages have reduced ME and SDE in both dry-bed and wet-bed areas, indicating that both DEM accuracy and precision have been improved. As expected, the wet-bed DEM quality is consistently lower than that associated with exposed areas of the riverbed, since it involves more potential sources of error (i.e. determination of water depths, modelling of water surface elevations).

DEM	DRY-BED			WET-BED		
	Points compared	ME (m)	SDE (m)	Points compared	ME (m)	SDE (m)
February 1999						
Raw DEM	3699	+0.539	2.190	11297	+1.201	3.478
Re-interpolated sparse DEM	3700	<u>+0.363</u>	<u>1.665</u>	11196	<u>+0.627</u>	<u>2.346</u>
Post-processed DEM	3700	<u>+0.174</u>	<u>0.265</u>	11202	<u>+0.356</u>	<u>0.302</u>
PCP-corrected DEM	3700	<u>+0.084</u>	<u>0.261</u>	11202	<u>+0.260</u>	<u>0.318</u>
March 1999						
Raw DEM	253	+0.252	0.321	2461	+4.333	10.56
Re-interpolated sparse DEM	241	<u>+0.168</u>	<u>0.360</u>	2427	<u>2.882</u>	<u>7.407</u>
Post-processed DEM	241	+0.154	0.260	2431	<u>+0.323</u>	<u>0.249</u>
PCP-corrected DEM	241	<u>+0.013</u>	<u>0.257</u>	2431	<u>+0.145</u>	<u>0.256</u>
February 2000						
Raw DEM	1661	+0.064	0.926	6981	+0.393	2.750
Re-interpolated sparse DEM	1665	+0.084	0.345	6981	<u>+0.015</u>	<u>2.632</u>
Post-processed DEM	1661	<u>+0.110</u>	<u>0.141</u>	6980	<u>+0.145</u>	<u>0.219</u>
PCP-corrected DEM	1661	<u>+0.088</u>	<u>0.131</u>	6981	<u>+0.101</u>	<u>0.219</u>

Table 6.5 The effect of the post-processing procedure on dry-bed and wet-bed DEM quality for the whole reach photogrammetric DEMs of the Waimakariri River.

Underlined values represent significant decreases in error from the previous stage of correction at 95% confidence level.

In both wet-bed and dry-bed areas, the raw photogrammetric DEMs contained large areas of gross error (**Figure 6.3**). These were concentrated in areas close to surface

water. Consequently, DEM precision is low indicated by high SDE values. For these DEMs, the ME statistic is relatively meaningless, since it is disproportionately influenced by the extreme error values introduced by the areas of gross error. Removal of unmatched, wet-bed and vegetated points, and automated post-processing using a coarser resolution DEM improved DEM quality significantly ($p < 0.05$), and SDE fell to more acceptable values in both wet-bed and dry-bed zones.

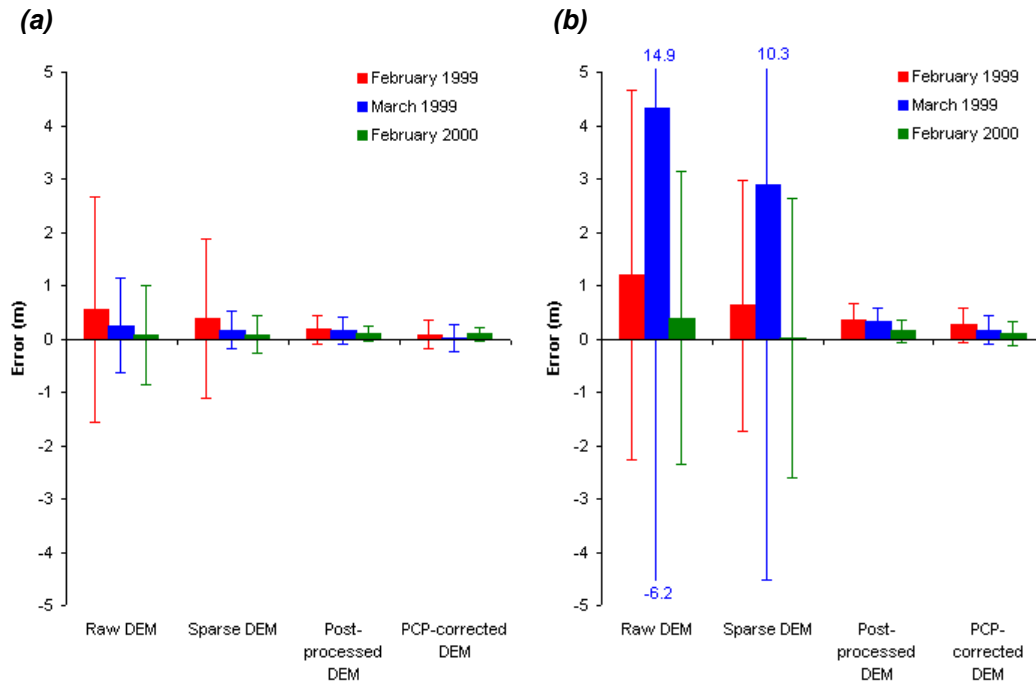


Figure 6.25 The effect of the post-processing procedure on dry-bed and wet-bed DEM quality for the whole reach DEMs of the Waimakariri River. The bars represent ME (DEM accuracy) with the vertical error bars indicating \pm SDE (DEM precision). Approximately two-thirds of errors fall within the bounds of each error bar.

However, a positive systematic bias remained in the post-processed photogrammetrically-acquired DEMs of between 0.1 and 0.2 m. Implementation of the DEM surface correction based on discrepancies from the surveyed PCP positions (**Figure 6.20**) reduces the residual ME (and so improves DEM accuracy) in the final DEM surface. Systematic error in dry-bed areas is reduced to an acceptable level given the vertical relief in the study reach. The final values of dry-bed DEM precision are similar, though slightly higher, to those calculated for the raw DEM surfaces when gross errors were disregarded (**Table 6.3**). This is not surprising since gross error removal meant that the final DEM surface was produced using fewer points. Thus, interpolation will have introduced a greater level of random error in parts of the DEM

surface, reflected by the increase in SDE. By contrast, post-processing has greatly improved overall DEM accuracy (in terms of ME).

Next, the quality of the four final DEM surfaces was compared (**Table 6.6**). This indicates that for the photogrammetrically-acquired DEMs, source image scale is a critical control upon photogrammetric precision. The dry-bed precision (indicated by SDE) for the two DEMs generated using 1:5000 photographs is similar (around ± 0.26 m), but is roughly halved when 1:4000 imagery is used. The quality of dry-bed points is still slightly higher than obtained using the 1:3000 imagery of the North Ashburton River (**Table 4.11**). The dry-bed quality of the ALS survey is excellent, and only the February 2000 DEM approaches the level of accuracy and precision it achieved in dry-bed areas.

DEM	DRY-BED			WET-BED		
	Points compared	ME (m)	SDE (m)	Points compared	ME (m)	SDE (m)
DEM acquired using digital photogrammetry						
February 1999	3700	+0.084	0.261	11202	+0.260	0.318
March 1999	241	+0.013	0.257	2431	+0.145	0.256
February 2000	1661	+0.088	0.131	6981	+0.101	0.219
DEM acquired using airborne laser scanning						
May 2000	338	-0.019	0.100	1060	+0.037	0.250

Table 6.6 Final DEM quality for all four reach-scale DEM surfaces of the Waimakariri River.

The SDE calculated for wet-bed points is higher than for dry-bed points, and is more consistent between surveys. This is expected because the same methodology (estimated water depth map subtracted from modelled water surface elevation) was used for both photogrammetric and ALS surfaces. The negligible ME of wet-bed points obtained using ALS suggests that the systematic bias observed in the equivalent photogrammetric measurements result from difficulties in reliably specifying water edge elevations using automated stereo-matching. This is supported by the findings of Reid (2001) who showed that the error associated with photogrammetric measurements is highest near water edges. For a small sub-area of the February 1999 unprocessed DEM, error based on check point measurements fell from -0.197 ± 0.313 m to -0.014 ± 0.195 m when points within 1 m of wetted channels were excluded. Thus, although the post-processing procedure developed in **Section 6.2** has improved DEM quality, errors remain near wetted channels. Such problems are not experienced with the ALS survey.

Although formal MBL analysis (as computed for the North Ashburton; **Section 4.7.1**) was not calculated for the Waimakariri due to the absence of sufficiently-spaced ground survey data, an estimate of net riverbed error can be estimated by weighting the dry-bed and wet-bed errors based on the relative proportions of exposed and submerged topography. The estimated reach-averaged riverbed error statistics are presented in **Table 6.7**. They show that the net systematic bias is less than ± 0.011 m or less in all cases, and as low as -0.004 m for the May 2000 DEM surface. Reach-averaged SDE is considerably lower for the February 2000 and May 2000 DEMs, reflecting their superior dry-bed precision (**Table 6.6**).

DEM	DRY-BED		WET-BED		
	ME \pm SDE	Proportion of riverbed area (%)	ME \pm SDE	Proportion of riverbed area (%)	Reach-averaged ME \pm SDE (m)
February 1999	$+0.084 \pm 0.261$	83	$+0.260 \pm 0.318$	17	$+0.114 \pm 0.271$
March 1999	$+0.013 \pm 0.257$	76	$+0.145 \pm 0.256$	24	$+0.045 \pm 0.257$
February 2000	$+0.088 \pm 0.131$	80	$+0.101 \pm 0.219$	20	$+0.091 \pm 0.149$
May 2000	-0.019 ± 0.100	74	$+0.037 \pm 0.250$	26	-0.004 ± 0.139

Table 6.7 Estimation of reach-averaged DEM quality based on the relative proportion of dry-bed and wet-bed area.

The use of check measurements has attracted criticism for only considering a small number of points relative to an entire DEM, and so giving an unrepresentative assessment of surface quality (Wise, 2000). In the case of the Waimakariri, there are around 2.9 million points in the final DEM surfaces (**Figure 6.20**), yet the number of check points measured was only in the order of hundreds or thousands (**Table 6.6**). Thus, the proportion of DEM points assessed, particularly in dry-bed areas, is very low, despite the number of points measured in some cases being relatively large by terrestrial survey standards (**Table 6.8**). Consequently, the reliability of calculated DEM quality statistics should be questioned. This is reinforced by consideration of the spatial distribution of check elevation measurements, which is another important consideration when point data is used to assess the quality of a continuous surface. The spatial positioning of the check points used in this study is shown in **Figure 6.26**.

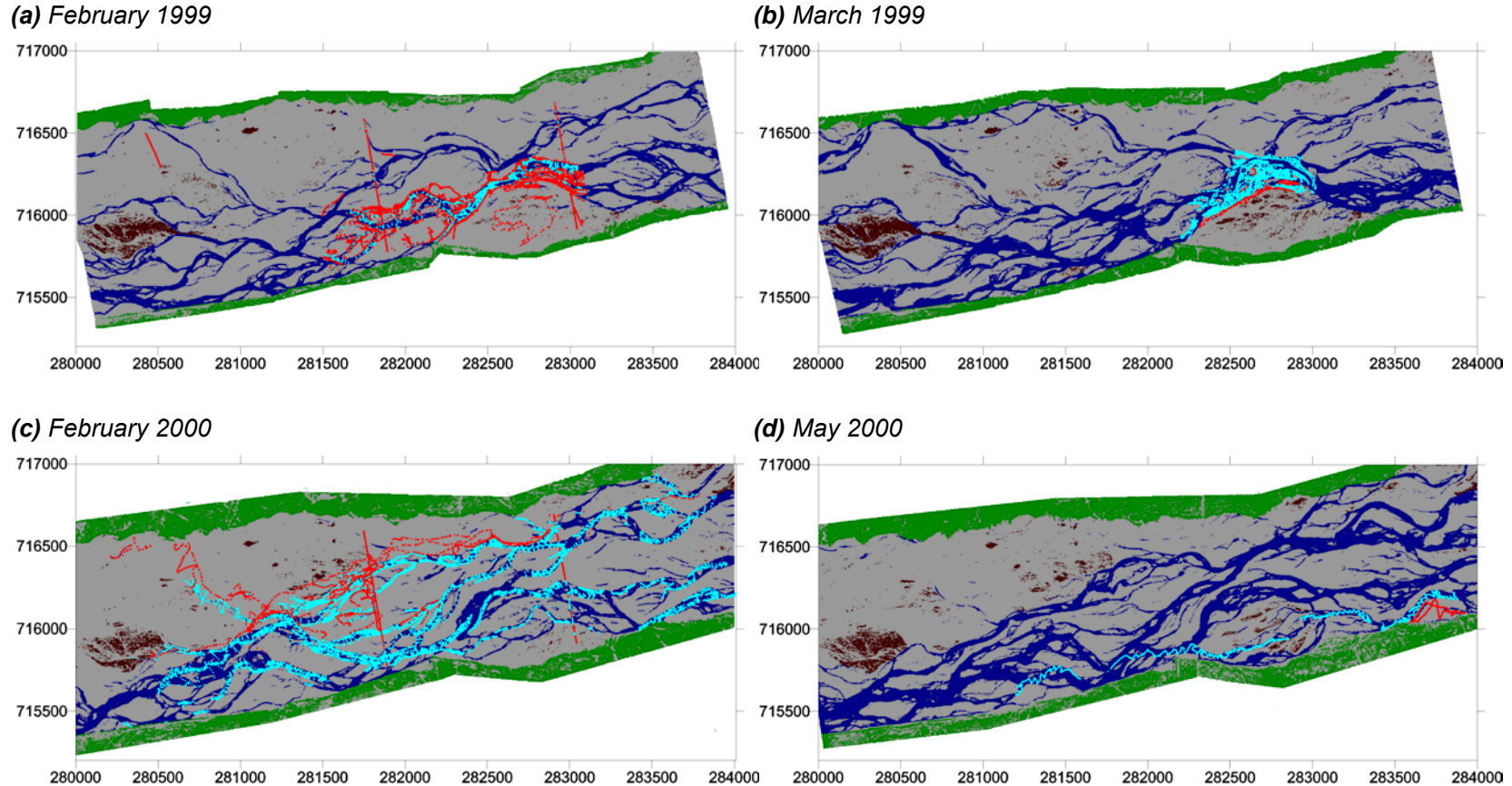


Figure 6.26 The spatial distribution of dry-bed (red) and wet-bed (blue) independent check point measurements. They have been superimposed on the classified images of the riverbed shown in **Figure 5.2**.

DEM	DRY-BED			WET-BED		
	Points compared	Total DEM points	Proportion (%)	Points compared	Total DEM points	Proportion (%)
February 1999	3700	3269829	0.11	11202	648211	1.73
March 1999	241	2879449	0.01	2431	905063	0.27
February 2000	1661	3231137	0.05	6981	808846	0.86
May 2000	338	2995083	0.01	1060	1024273	0.10

Table 6.8 Comparison between number of DEM points in dry- and wet-bed areas and the number of surveyed check points used to assess DEM quality.

This highlights two issues. First, with the exception of the February 2000 ground survey, the check points are restricted to a relatively small area of the study reach. Second, the dry-bed points are generally located near wetted channels. Although such points are critical to DEM representation (since these determine the modelled water surface and hence the quality of wet-bed points), they tell us little about the inherent quality of the dry-bed DEMs (i.e. those areas unaffected by the presence of surface water). Given the gross errors observed in the raw DEMs near the wet-bed, we would expect dry-bed check points at or near these locations to represent a worst case dry-bed DEM quality (*cf.* Reid, 2001).

6.4.3 Overlap analysis

To overcome these problems, overlap analysis was used. This involves the comparison of DEM surfaces where redundant topographic data exists: where elevations at the same planform location have been measured more than once. While this can never give a wholly independent indication of DEM quality, it does compliment the DEM quality statistics acquired using check point measurements, particularly in areas not containing any ground survey points. It has been used previously in the context of both photogrammetric and ALS surveys (e.g. Pyle *et al.*, 1997; Stojic *et al.*, 1998; Fraser *et al.*, 1999; Hofton *et al.*, 2000; Huang, 2000). Redundant data exists in the Waimakairi photogrammetrically-acquired datasets through the generation of overlapping individual DEMs (February 1999, March 1999, February 2000). For the ALS data, redundant data exists because the reach was re-surveyed three times in order to decrease average point spacing. Visual analysis of DEM overlaps has previously been used to evaluate the optimum mosaicking technique for minimising photogrammetric DEM joins (**Figure 6.16**). However, quantitative overlap analysis allows an indication of DEM precision in terms of the variation between two DEM representations of the same terrain. A good degree of correspondence suggests a high level of DEM precision. DEM accuracy cannot be estimated, since neither overlapping DEM necessarily represents the true surface, although the vertical bias is nevertheless an interesting additional statistic.

For the photogrammetrically-derived data, overlap analysis was performed by differencing the sparse, post-processed, individual DEM (i.e. no unmatched, wet-bed or vegetated points). This meant that only dry-bed, stereo-matched points, and importantly no interpolated points, were compared. Despite this, some difference between overlapping DEM surfaces is expected. The systematic difference between the elevation of adjacent DEM tiles (**Figure 6.17**) will introduce systematic error into overlap analysis. This should be reflected in the mean difference between overlapping DEM points. Random error is also expected, due to two main factors. First, there will be that associated with the differencing of two surfaces that contain random error (**Section 2.3.9**). Even if the DEM surfaces contain no additional error, overlap analysis would have a background level of random error equivalent to the root of the sum in quadrature of their theoretical precision (**Equation 2.12**). Second, the slightly different view angle of the photographs used to generate the overlapping DEMs will also introduce random error. The total random error associated with overlapping DEM points is indicated by the standard deviation of difference. The results from overlap analysis of the photogrammetric DEMs are summarised in **Table 6.9** and **Figure 6.27**.

DEM	Points compared	Mean difference (m)	Standard deviation of difference (m)
February 1999	59535	+0.075	0.192
March 1999	121975	+0.040	0.174
February 2000	190513	+0.015	0.177

Table 6.9 Aggregated overlap analysis statistics for the photogrammetrically-derived DEMs.

As expected, the mean difference between overlapping individual DEMs are small (less than 0.08 m), although the mean values are somewhat misleading given the spatial pattern of overlap errors observed in **Figure 6.16**. It is perhaps significant that the mean vertical bias associated with the February 2000 DEM is lowest, as this suggests that increased image scale also improves the vertical alignment of neighbouring DEM tiles. The simple explanation for this is that the increased image scale means that PCP positioning will be more precise in object-space terms.

The standard deviation of overlap difference is remarkably consistent between the three DEMs, despite the higher precision of the February 2000 DEM suggested by DEM quality assessment based on the check point measurements (**Table 6.6**). At first, the SDE values seem relatively high. However, they must be viewed with respect to the maximum theoretical precision attainable given the image scale and scanning resolution used to create the DEM surfaces. Given a theoretical photogrammetric

precision of around ± 0.07 m (depending on image scale; **Table 3.4**), the theoretical precision associated with differencing two dry-bed DEM surfaces will be approximately ± 0.10 m (the root of the sum in quadrature of the photogrammetric theoretical precision; **Equation 2.12**). In this context, the observed overlap precision (0.15–0.17 m) is relatively encouraging, suggesting that the major component of this value is composed of (unavoidable) random errors, inherent to the photogrammetric process, and therefore that most gross errors have been successfully removed.

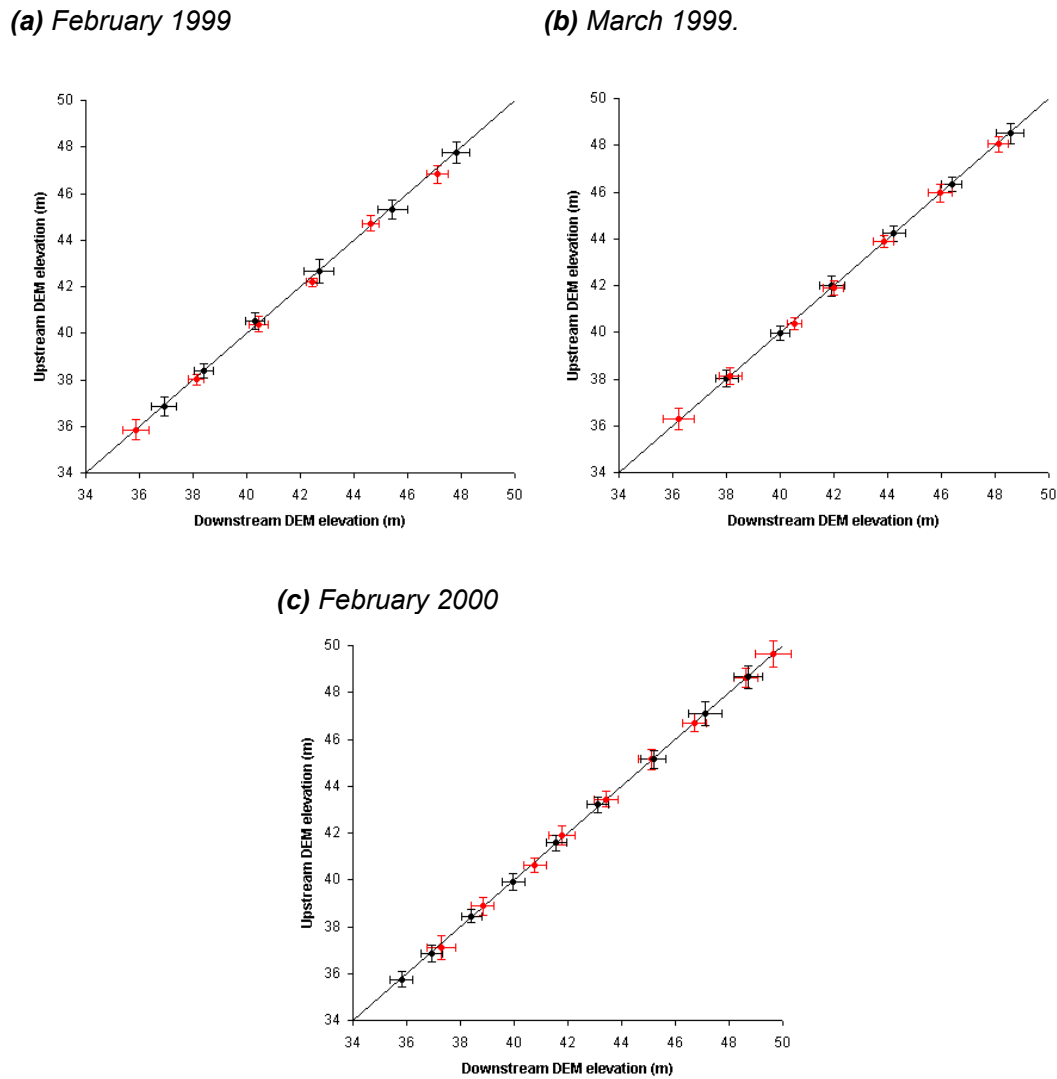


Figure 6.27 The relationship between upstream and downstream elevations for individual DEM overlaps shown in **Figure 6.16**. The mean elevations in the overlap area are shown, with error bars representing the standard deviation of individual DEM elevations. The overlaps are colour-coded to reflect the DEM outlines in **Figure 6.3**.

For the dry-bed ALS dataset, the situation was complicated by irregularly spaced raw ground-strike data, which meant that few points had exactly the same planimetric

position. Consequently, an automated spatial correspondence algorithm was used which compared the elevation of two points if they fell within 0.5 m horizontal distance of each other (half the point spacing used to interpolate the randomly-spaced raw data into a regularly-spaced DEM).

The results from the overlap analysis for the ALS data are shown in **Figure 6.28** and **Table 6.10**. There appears to be considerable variation in the spatial distribution of elevation differences between successive ALS passes. Overlap 1 shows little spatial pattern, and the mean elevation difference between the first and second ALS passes is small (less than 0.002 m). However, the positive bias shown by overlap 2 and the negative bias shown by overlap 3 suggest that the elevation measurements made by the third ALS pass were too low (compared to passes 1 and 2) by around 0.4 m. The SDE associated with the ALS overlaps are relatively consistent, with an average of just over ± 0.20 m. This is slightly higher than the precision estimated from overlap analysis of the photogrammetric DEMs (**Table 6.9**), which is perhaps relatively surprising given the superior ALS DEM precision suggested by comparison with independent check point data (**Table 6.6**). However, it can explained by two factors.

Overlap	Points compared	ME (m)	SDE (m)
1 (Pass 1 – Pass 2)	52528	+0.017	0.210
2 (Pass 2 – Pass 3)	50369	+0.037	0.216
3 (Pass 3 – Pass 1)	50265	-0.050	0.227
Average	51054	+0.001	0.218

Table 6.10 Overlap analysis statistics for the ALS-derived DEM.

First, ALS survey has a lower inherent precision (usually put between 0.10 and 0.15 m; Baltsavias, 1999a) than the digital photogrammetry used in this study. Thus, differencing of two independently-acquired ALS surfaces will produce a total random error of approximately 0.14-0.21 m, due entirely to random error in the two source datasets (the root of the sum in quadrature, **Equation 2.12**).

Second, the ALS elevation data is randomly-distributed. This means that points used in overlap analysis are up to 0.5 m horizontal distance apart, which will introduce some random differences between re-surveys. In contrast, the photogrammetric overlap analysis, because it is raster-based, only used points with directly corresponding planimetric position. Based on these factors, it would appear that the dry-bed ALS data for the Waimakariri contains very few additional errors.

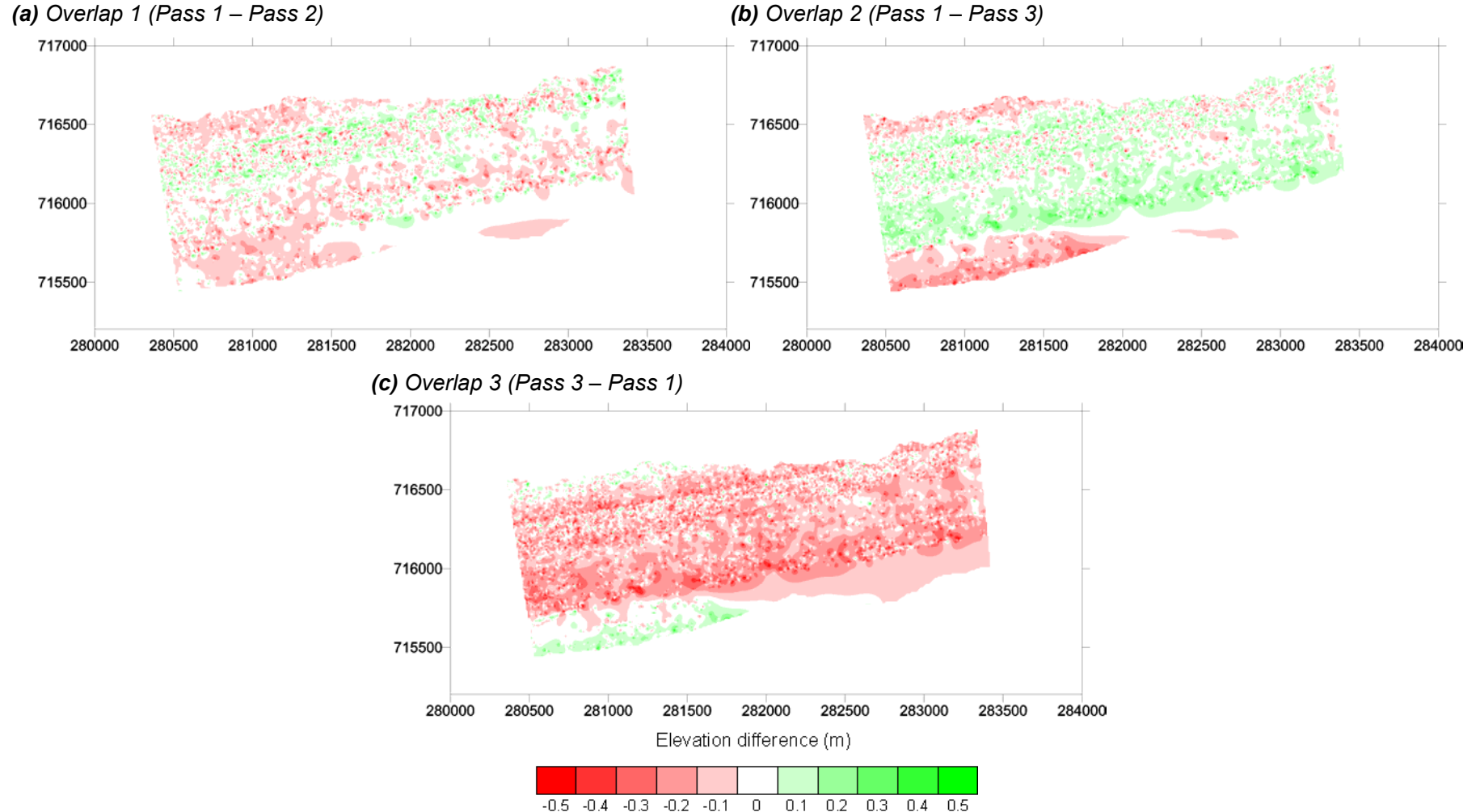


Figure 6.28 Overlap analysis for the three flight passes used in the ALS survey.

6.5 Chapter summary

This chapter has demonstrated that both digital photogrammetry and airborne laser scanning (ALS) can be used to obtain topographic information for dry-bed areas of a large, braided, gravel-bed river.

As compared to the North Ashburton study reach, the main challenge posed by the photogrammetric measurement of the Waimakariri study reach was its spatial extent. At around 100 times the area of the North Ashburton study reach, smaller scale imagery and multiple DEMs were required to cover the entire area of interest. The use of smaller scale imagery caused a decrease in image texture (**Figure 3.12**). This led to a reduction in stereo-matching performance, compared to the North Ashburton results, although far more points were successfully matched than usually associated with terrestrial survey methods. As a result, point distribution became important, though in areas where higher point density was required (such as breaks of slope and wetted channel edges), increased image texture led to a disproportionately higher number of matched points.

Following testing of a number of DEM collection parameter sets and DEM point spacings, DEMs were generated for the study reach using digital photogrammetry for February 1999, March 1999 and February 2000. The raw DEM surfaces had several areas of gross errors, and an automated post-processing routine was developed which removed: (i) unmatched points; (ii) points in inundated and vegetated areas; and (iii) using topographic criteria based on elevation deviation from a coarser DEM surface. Following post-processing of the individual DEM surfaces, methods of joining them into a reach-scale DEM were considered. The presence of systematic elevation differences between overlapping DEMs meant that a distance-weighted algorithm was preferable to join adjacent DEM tiles.

For reach-scale DEMs produced using both digital photogrammetry and ALS, the water surface was modelled by interpolating bank edge points across wetted channels, and the estimated water depths were subtracted to give an estimated wet-bed topography. When merged with the dry-bed DEMs, final DEMs were produced with complete topographic representation of the study reach.

Finally, reach-scale post-processing was undertaken to remove systematic error in the final photogrammetric DEM surfaces. Comparison with PCP positions suggested the presence of systematic errors, most likely introduced by post-processing and mosaicking. Subtraction of a surface extrapolated from these discrepancies reduced

reach ME to levels more acceptable given the small vertical relief associated with gravel-bed rivers.

DEM quality assessment results suggested that both digital photogrammetry and ALS represent feasible methods of surveying large, braided, gravel-bed rivers. However, considerable post-processing was needed for the photogrammetrically-derived measurements to obtain the quality of DEM necessary to portray the relatively low relief associated with large, gravel riverbeds. Even then, problems remained with reliable specification of water edge elevations. DEM quality assessment also suggested that DEM quality is closely linked to image scale, with retention of image content a key requirement for successful digital photogrammetric survey. Based on independent check point measurements, the quality of dry-bed representation in the ALS DEMs was superior to that produced in the best photogrammetric DEM surface. However, overlap analyses suggested that the difference in quality between the surfaces produced using the two remote sensing methods was less than was suggested by comparison of DEM points with independent check measurements.

The increase in topographic data volume permitted by remote sensing methods such as digital photogrammetry and ALS offers to further our understanding of gravel-bed rivers. One particular area of progress is the use of time-series DEMs of riverbeds to allow visualisation and quantification of morphological change (e.g. Lane *et al.*, 1994; Lapointe *et al.*, 1998; Stojic *et al.*, 1998; Chandler and Ashmore, 2001; Smart and Brasington, 2001). DEMs of difference, produced by subtracting successive DEM surfaces, provide all of the necessary input data to infer average sediment transport rate between the two survey times (e.g. Lane *et al.*, 1995a; Lane, 1998). However, it is not yet known whether airborne remote survey methods can produce DEMs of sufficient quality to allow significant morphological change to be detected. This will be tested in **Chapter 7** using both the North Ashburton and Waimakariri DEMs. Furthermore, by subtracting DEM surfaces, the relative error associated with the resultant DEM of difference will inevitably be large (**Table 2.7**). Consequently, DEMs of difference also represent a derived surface which may be used to provide another useful assessment of DEM quality itself.

CHAPTER 7. THE FEASIBILITY OF USING THE MORPHOLOGICAL METHOD TO INFER BEDLOAD TRANSPORT RATES IN LARGE, BRAIDED, GRAVEL-BED RIVERS

In this chapter, the feasibility of using the derived riverbed DEM surfaces to quantify morphological change will be examined. Initially, the morphological method is briefly explained and sources of error discussed (7.1). The DEMs of difference (7.2) are analysed in three ways. First, the quality of post-processed DEMs of difference is assessed (7.3) in terms of reach-averaged elevation (7.3.1) and volumetric (7.3.2) changes, and in terms of the three components of error (7.3.3): gross (7.3.4); systematic (7.3.5); and random (7.3.6 to 7.3.9). Each of these is expected to have a particular error signature in the DEMs of difference. Recalculation of volumetric change following identification and/or removal of these errors allows assessment of information loss and hence evaluation of their significance in the DEMs of difference. Second, the same methods of error assessment are applied to DEMs at various stages of post-processing (7.4) to demonstrate the value of the post-processing procedures developed in Chapters 4 and 6. Hence, reach-averaged volume change (7.4.1), gross errors (7.4.2), systematic error (7.4.3) and random error (7.4.4) are all examined, and compared to the levels found in the corresponding post-processed DEMs of difference. Third, the effect of cross-section spacing on morphological change information obtained is examined, by simulating cross-sectional surveys at a range of spacings (7.5) in order to evaluate remote sensing techniques in relation to traditional survey methods.

7.1 Introduction

For many geomorphological systems, morphological change is hard to document due to large spatial and temporal variations in the magnitude and rate of landform modification. Selection of a small study area (as is common for conventional geomorphological investigation) implies *a priori* assessment of where and when system change will occur, but this is not always successful (e.g. Nicholas and Sambrook-Smith, 1998). Even if landform change is observed, it often remains difficult to describe or to isolate the effect of any one event because very few systems are adequately instrumented or monitored (Brunsden and Chandler, 1996). Consequently, one of the most important benefits offered by the use of remotely-sensed topographic data in geomorphological study is the scope for employing time-series of DEMs of the same area to visualise and to quantify morphological change. The high spatial resolution, large spatial area and high degree of temporal control associated with technologies

such as digital photogrammetry (where archive photography may also be used; Chandler and Cooper, 1989) and airborne laser scanning (ALS), permit long-term morphological changes to be monitored for entire geomorphological systems.

7.1.1 *Rationale*

In fluvial geomorphology, the importance of high quality measurement of morphological change is increased by the suggestion that better estimates of certain river channel processes may result from the measurement of river channel form and its change through time than from direct measurement of the processes themselves (Carson and Griffiths, 1989). In particular, spatially-distributed measurement of bedload transport rates remains hindered by the problems of adequately measuring or modelling transport rates and fluctuations at single points (Gomez *et al.*, 1990). One solution to this problem is the estimation of time-integrated bedload transport rates from observed changes in river form (Lane, 1998). Braided rivers are particularly suitable candidates for application of morphological methods because of their complex and transient riverbed morphology (Ashmore and Church, 1998).

7.1.2 *Theoretical basis*

The theoretical basis for estimating sediment transport rates from morphological change in the channel is the sediment continuity equation (Lane, 1997; Ashmore and Church, 1998). In one-dimensional, steady-state, finite difference form, this is given as

$$\frac{\Delta i_{bY}}{\Delta Y} + \frac{\rho(1-\varepsilon) \Delta Z}{\Delta t} = 0 \quad (7.1)$$

where Δi_{bY} is the mass transport rate (kg/m/s) in the downstream direction, ΔZ is the change in elevation, Δt is the length of time over which the calculation is being made, ρ is sediment density, ε is sediment porosity and Y is downstream distance. In two-dimensional form, this is given as

$$\frac{\Delta i_{bx}}{\Delta X} + \frac{\Delta i_{bY}}{\Delta Y} + \frac{\rho(1-\varepsilon) \Delta Z}{\Delta t} = 0 \quad (7.2)$$

where X is the cross-stream distance. One-dimensional application allows the estimation of temporal fluctuations in bed material transport rate in a series of river reaches (e.g. Goff and Ashmore, 1994; Martin and Church, 1996; McLean and Church, 1999). Two-dimensional application allows estimation of spatial variation in bedload transport rates from within a river reach (e.g. Lane *et al.*, 1995a; Lane, 1998). However, both applications are dependent on high quality estimates of ΔZ .

7.1.3 DEMs of difference

Data output from remote sensing techniques is commonly in the form of high spatial resolution, regularly-spaced DEMs. Differencing of successive DEM surfaces permits rapid visualisation of channel changes (Lane, 1998). Furthermore, DEMs of difference (digital elevation models representing change between successive DEM surfaces) provide the necessary information required for morphological methods to be operationalised (Lane, 1998). For one-dimensional channel changes (**Equation 7.1**), Δz may be obtained by calculating the net volume of difference between the two DEM surfaces and dividing by the area of surface common to both DEMs. For two-dimensional channel changes (**Equation 7.2**), the value of ΔZ at each DEM point can be used to determine the net contribution of the grid cell to the transport rate in the time between the DEMs were acquired. For a regularly-spaced grid, the change in bedload transport rate between successive DEMs at a particular location is given by (Lane, 1998)

$$\Delta i_{bij} = \frac{\rho(1-\varepsilon)\Delta Z_j \Delta X}{\Delta t} \quad (7.3)$$

7.1.4 Boundary conditions and sediment routing

To obtain estimates of sediment transport rate from DEMs of difference, two further inputs are required: (i) boundary conditions (i.e. specification of the sediment transport at a reference cross-section); and (ii) sediment routing conditions (i.e. specification of the path(s) taken by sediment within the study reach).

Four methods have been used to specify boundary conditions for input to the morphological method. First, boundary conditions can be obtained by using traditional methods to measure transport rate (e.g. Lane *et al.*, 1995a). Apart from the problems associated with most methods for direct measurement of sediment transport rate (e.g. Gomez *et al.*, 1990), there is also a methodological problem of integrating instantaneous direct samples of sediment transport rate within a time-averaged sediment budget obtained using the morphological method (Ashmore and Church, 1998). Successive samples must be time-integrated using some simple temporal averaging routine (e.g. Lane *et al.*, 1995a) that requires frequent sampling during the period of study. If the morphological method is to be applied in two dimensions, then point direct samples must be made at several locations across the channel (e.g. Lane *et al.*, 1995a).

Second, a downstream limit on the occurrence of sediment transport can be used as a zero gravel transport boundary. The calculated budget then proceeds upstream based on volume change at each surveyed cross-section or grid-cell (e.g. Goff and Ashmore,

1994; Lane *et al.*, 1995a; Martin and Church, 1995; McLean and Church, 1999; Ham and Church, 2000). Third, a non-negative transport condition may be assumed throughout the reach (e.g. Ferguson *et al.*, 1992; Goff and Ashmore, 1995; Nicholas and Sambrook-Smith, 1998). Given that this assumption always produces at least one cross-section with zero transport rate, this method is likely to introduce negative bias into estimates of sediment transport and under-estimate average transport rate (Ashmore and Church, 1998).

Fourth, in the absence of a known transport rate, an estimate of sediment transport may be derived as the product of bed material mobilised per unit length of channel, multiplied by the distance of travel. Estimation of the distance of travel requires identification of particle step length. In gravel-bed rivers, this can be achieved by assuming that the average distance of transport is from the centroid of an erosion zone to the centroid of an accretion zone (Carson and Griffiths, 1989; Ferguson *et al.*, 1992). This has also been interpreted as the riffle spacing (e.g. Church *et al.*, 1987; Goff and Ashmore, 1994).

The method for specifying the sediment routing condition depends on whether the morphological method is applied in one or two dimensions. In one dimension, the situation is considerably simpler, as sediment transport is assumed to be uni-directional (i.e. downstream only). Thus, sediment is assumed to move downstream, past successive cross-sections until deposited within a reach. In two-dimensional analysis, sediment movement is bi-directional (i.e. downstream and cross-stream). In this case, sediment routing must be modelled using a flow-driven sediment routing model (Lane, 1998), which simulates sediment movement for each cell based on observed erosion and deposition in upstream cells and local flow direction. Flow direction may be obtained from spatially-distributed point measurements of flow velocity (Lane *et al.*, 1995a) or from a depth-averaged flow model (Lane *et al.*, 1995b). At larger spatial scales, such as that of the rivers studied in this research, the modelling of sediment routing is considerably more complex.

7.1.5 Limitations of the morphological method

There are two groups of limitations associated using calculated volumes of change to estimate process rates (Lindsay *et al.*, in review): (i) process-related; and (ii) data quality-related. Process-related errors are caused by three groups of uncertainties. First, **Equations 7.1** and **7.2** only consider change in transport rate. Thus, accurate specification of boundary conditions and sediment routing (**Section 7.1.4**) is required. Second, there is a temporal resolution issue. As Δt tends to zero in **Equations 7.1** and **7.2**, the magnitude of ΔZ for a given Δt will change. Third, there is a possibility of local

compensation of scour and fill between surveys, which will negatively bias volumes of change, and which will increase as Δt increases. (Lindsay and Ashmore, in review).

The second group of errors correspond to the quality of the topographic data collected and affect all applications of the morphological method. Adequate quantification of channel topography and topographic change represents a fundamental constraint over the success of the morphological method (Lane, 1997; Ashmore and Church, 1998). Survey density, distribution, frequency and quality will all influence the pattern of channel change observed, and consequently the magnitude of sediment transport rates estimated.

Ground survey of cross-sections has been the most common source of topographic data for channel change calculations (e.g. Neill, 1969; Griffiths, 1979; Ferguson and Ashworth, 1992; Goff and Ashmore, 1994; Hoey, 1994; Martin and Church, 1995; McLean and Church, 1999). The individual data points obtained are likely to be of high quality. However, the relatively coarse cross-section spacing and re-survey frequency associated with terrestrial survey methods (**Section 1.2.3; Table 1.1**) may introduce uncertainty into channel representation (Lane *et al.*, 1994). These issues are intensified as the size of the reach under study is increased.

A second source of channel change information is planimetric data, often from aerial photographs (e.g. Popov, 1962; Neil, 1971; Church *et al.*, 1987; Carson and Griffiths, 1989; Ham and Church, 2000). Although primarily two-dimensional in scope, when supplemented with estimated or surveyed bank height information, this approach allows an approximate three-dimensional description of channel changes between successive photographs to be made, and sediment transport rates to be estimated without need for spatial integration. Nonetheless, the assumption that a representative depth of erosion can be defined is clearly a weakness with this approach (Ham and Church, 2000).

The adoption of automated remote sensing survey methods has permitted topographic data to be acquired at far greater spatial densities and temporal frequencies than was allowed by conventional survey techniques. This has meant that factors such as data quality, data distribution, interpolation error and the effects of bed roughness have become increasing relevant to application of the morphological method (e.g. Lane, 1998; Brasington *et al.*, 2000; Ham and Church, 2000; Lindsay *et al.*, in review). In addition, differencing of DEMs produced using automated methods has allowed simulation of the effects of different spatial and temporal resolutions on the topographic change detected (e.g. Lane, 1998; Lindsay and Ashmore, in review).

A key issue that emerges is whether remote sensing techniques are able to produce DEMs of sufficient quality to allow morphological methods to estimate sediment transport reliably in gravel-bed river environments. This issue is particularly important given the small relative relief associated with gravel riverbeds, and the rapid propagation of error that can occur when multiple DEMs are combined (Burrough and McDonnell, 1998). Initial applications of analytical photogrammetry (Lane *et al.*, 1995a) and intensive GPS survey (Brasington *et al.*, 2000) to generate DEMs of difference for gravel-bed river reaches have produced encouraging results. However, DEMs acquired using fully-automated data acquisition methods, including data collection from both exposed and inundated riverbed areas, have yet to be treated in this manner. Similarly, research to date has generally been confined to relatively small river channels.

In this chapter, three particular issues are explored: (i) the quality of DEMs of difference produced using the final, post-processed, DEMs of the North Ashburton and Waimakariri study reaches is evaluated (**Section 7.3**); (ii) the role of the post-processing procedures is considered, including incorporation of submerged topography, in improving DEM of difference quality (**Section 7.4**); and (iii) the quality of DEMs of difference produced from automated remote sensing survey methods is addressed, as compared with conventional, terrestrial, survey techniques (**Section 7.5**).

7.2 DEMs of difference

The DEM of difference is a critical component when applying two-dimensional morphological methods. Errors or uncertainties that exist in the difference surface will inevitably be propagated into estimates of sediment transport rate. However, little research has been conducted to assess the quality and reliability of DEMs of difference, given the errors that will inevitably be present in the DEM surfaces used in their calculation. Furthermore, if the issue is reversed, DEMs of difference are also a potentially critical test of DEM quality, highlighting areas of large vertical elevation difference between two DEM surfaces where little or no change was expected. It has been suggested that derived parameters might be a more rigorous method of assessing DEM quality (e.g. Wise, 2000; Lane, 2000), as they can consider DEM quality over an entire DEM surface. They may also be more useful measures, as they can give information about parameters that are geomorphologically-significant (Lane, 2000). In many ways, the DEM of difference may be seen as the ultimate derived parameter, and so a very useful assessment of DEM quality.

In this research, six riverbed DEM surfaces have been obtained: two for the North Ashburton River; and four for the Waimakariri River. From these, four epochs were

identified (**Table 7.1**). The epochs were selected to examine riverbed change at a range of spatial and temporal scales. The North Ashburton River is a medium-sized gravel-bed river (active width less than 100 m in the study reach), and the time-step of four years spans several bankfull flood events (**Figure 3.8**). The Waimakariri River is much larger, with the area of the study reach approximately two orders of magnitude greater than that of the North Ashburton (**Table 7.1**). The three photogrammetric surveys of the Waimakariri were chosen to provide information on the morphological impact of a single flood event (occurring late-February 1999; **Figure 3.9**) and typical annual change (February 1999 to February 2000; **Figure 3.10**). The ALS survey in May 2000 also allowed the effect of a second large flood event (occurring early-April 2000; **Figure 3.16**) to be assessed.

Prior to generation of the DEMs of difference, the area surrounding the DEMs was eliminated (elevation values set to equal zero) so that each DEM surface showed the same riverbed area. This was done for three reasons. First, the area of interest boundary was defined to exclude any bank-edge vegetation from the DEM surfaces. Invasion or disappearance of vegetation during an epoch would introduce erroneous volumes of apparent cut and fill into the DEM of difference (e.g. Derose *et al.*, 1998; Brown and Arbogast, 1999), which would potentially be large in magnitude relative to the typical morphological change of the riverbed. Second, the area of interest was set to bound exactly the same area of riverbed for each DEM. This eliminated potential edge problems where one DEM surface extends further upstream or downstream than another. This would also be expected to produce large positive or negative errors into the DEM of difference. Third, the identical areal extent of the final DEMs of difference allows justifiable inter-comparison between difference surfaces as it is the same riverbed area that is being considered on each occasion.

Calculation of DEMs of difference was relatively straight-forward, as both the North Ashburton and Waimakariri DEMs had equal object-space pixel spacing of 1 m, and were collected to an equal datum using the same grid scheme. This meant that no point re-sampling, datum transformation or grid correction was necessary.

7.3 Quality assessment of DEMs of difference from post-processed DEMs

Initially, DEMs of difference were calculated from the final, post-processed, riverbed DEMs (**Figure 4.17**; **Figure 6.20**). These are shown in **Figure 7.1**, and are hereafter referred to as the post-processed DEMs of difference. In a DEM of difference, the magnitude of each pixel represents the vertical elevation change between the two DEM surfaces used in its construction at that point on the riverbed. Negative changes (shaded red) indicate a decrease in elevation and positive changes (shaded green)

indicate an increase in elevation. White areas have experienced no net vertical elevation change. Visually, the DEMs of difference are extremely encouraging. There appears to be a high degree of spatial organisation in the patterns of cut and fill observed, with a tendency for discrete zones of erosion and deposition.

River	Code (used hereafter)	Initial DEM survey date	Final DEM survey date	Epoch length (days)	Area of difference DEM (m ²)	Number of flood events ^a
North Ashburton	NA	19/05/1995	16/02/1999	1369	28451	5
Waimakariri	W1	16/02/1999	19/03/1999	31	2913427	1
Waimakariri	W2	16/02/1999	23/02/2000	372	2913427	8
Waimakariri	W3	23/02/2000	07/04/2000	44	2913427	2

^a Defined as the number of events recorded during the epoch where near-total floodplain inundation results. Floodplain inundation occurs at instantaneous flows of around 100 m³/sec for the North Ashburton (Duncan, pers. comm.) and around 800 m³/sec for the Waimakariri (Hicks *et al.*, 2001) for the respective study reaches.

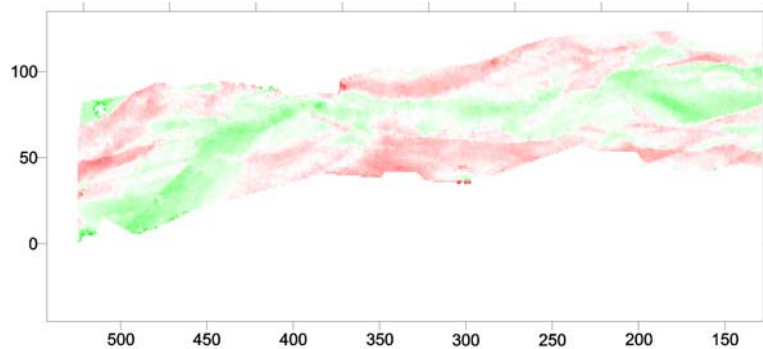
Table 7.1 Details of the four epochs for which DEMs of difference were calculated for the North Ashburton and Waimakariri study reaches.

7.3.1 Reach-averaged elevation change statistics

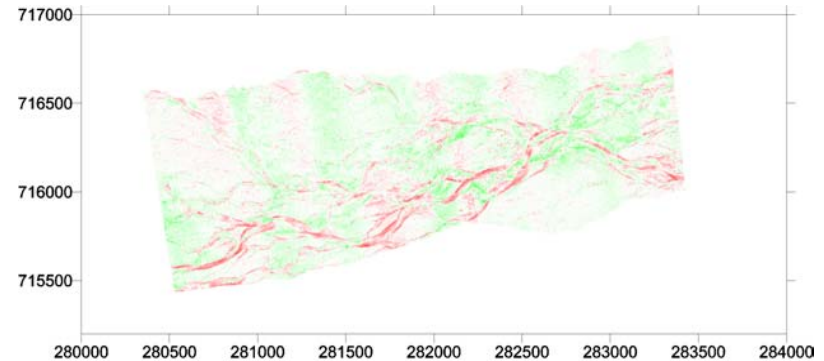
The simplest statistics that can be obtained from a DEM of difference describe the global, reach-averaged, elevation change. The mean difference (MD_{global}) between two DEM surfaces is expected to be small when spatially-averaging reach-scale channel bed level changes determined over such relatively small time-steps. However, a MD_{global} of zero would only occur if net aggradation exactly equalled net degradation in the reach, which is an unlikely scenario. The global standard deviation of difference (SDD_{global}) indicates the range of differences ($\pm 1 SDD_{global}$) that are observed over the majority (68%) of the riverbed area, assuming a normal distribution of elevation differences.

Table 7.2 summarises the reach-averaged elevation change statistics associated with each post-processed DEM of difference (**Figure 7.1**). The global mean difference (MD_{global}) is less than 0.1 m for each post-processed DEM of difference. The maximum and minimum global differences are also broadly comparable for each post-processed DEM of difference, suggesting that large gross errors are not present at the reach scale. The SDD_{global} is less than 0.5 m in each case.

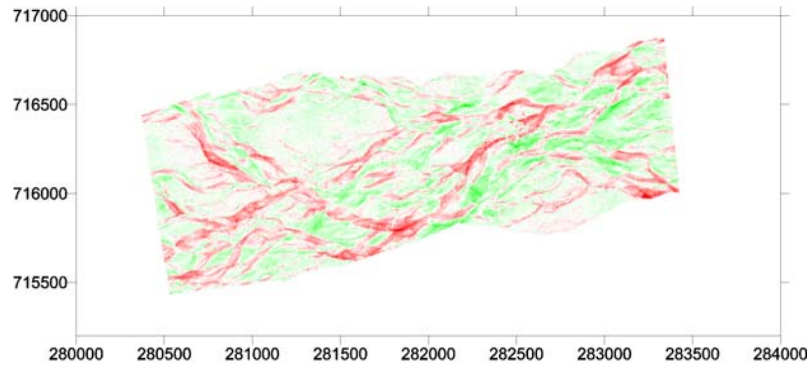
(a) North Ashburton – May 1995 to February 1999 (NA)



(b) Waimakariri – February 1999 to March 1999 (W1)



(c) Waimakariri – February 1999 to February 2000 (W2)



(d) Waimakariri – February 2000 to May 2000 (W3)

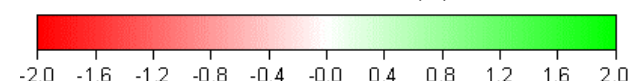
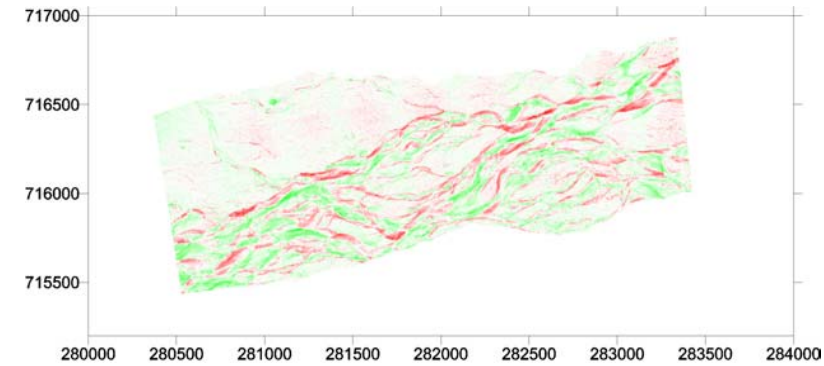


Figure 7.1 Post-processed DEMs of difference for the North Ashburton and Waimakariri study reaches

From the Kolmogorov-Smirnov goodness of fit statistic, the difference distributions associated with the post-processed DEMs of difference (**Figure 7.2**) are not normally distributed ($p < 0.05$). Statistically, they are too peaked (coefficient of kurtosis > 0 ; $p < 0.05$), although not significantly skewed (coefficient of skewness ≈ 0 ; $p < 0.05$), meaning that greater than 68% of observations would be expected to be within ± 1 SDD of the mean. Thus, over 68% of point elevation differences in each DEM of difference are expected to be less than the corresponding SDD_{global} value.

DEM of difference	Global mean difference (m)	Global standard deviation of difference (m)	Minimum difference (m)	Maximum difference (m)
NA (May 95 – Feb 99)	+0.024	0.324	-1.704	+1.959
W1 (Feb 99 – Mar 99)	+0.058	0.270	-1.665	+1.783
W2 (Feb 99 – Feb 00)	+0.013	0.433	-2.478	+2.544
W3 (Feb 00 – May 00)	+0.033	0.369	-1.994	+1.997

Table 7.2 Reach-averaged elevation change statistics derived from the post-processed DEMs of difference.

In the context of the reliability of the DEMs of difference, and in particular their capacity to indicate errors in the individual surfaces used to create them, the results are encouraging. The small MD_{global} values suggest that large vertical discrepancies do not exist between the various DEM surfaces used to calculate the DEMs of difference. This implies a degree of consistency between post-processed DEM surfaces, despite the different photograph scales (1:3000 for the North Ashburton; 1:4000 and 1:5000 for the Waimakariri) and remote survey techniques (digital photogrammetry and ALS) being employed. The maximum and minimum values of difference are commensurate to the approximate maximum water depth observed in the study reaches (**Figures 4.20** and **5.6**), which to a large degree determine the largest vertical change in elevation that it is reasonable to expect. Differences between SDD_{global} values can perhaps be explained by the number of flood events spanned by each DEM of difference (**Table 7.1**). It appears that a direct relationship exists between the number of flood events during which floodplain inundation was expected and the distribution of elevation differences at the reach-scale.

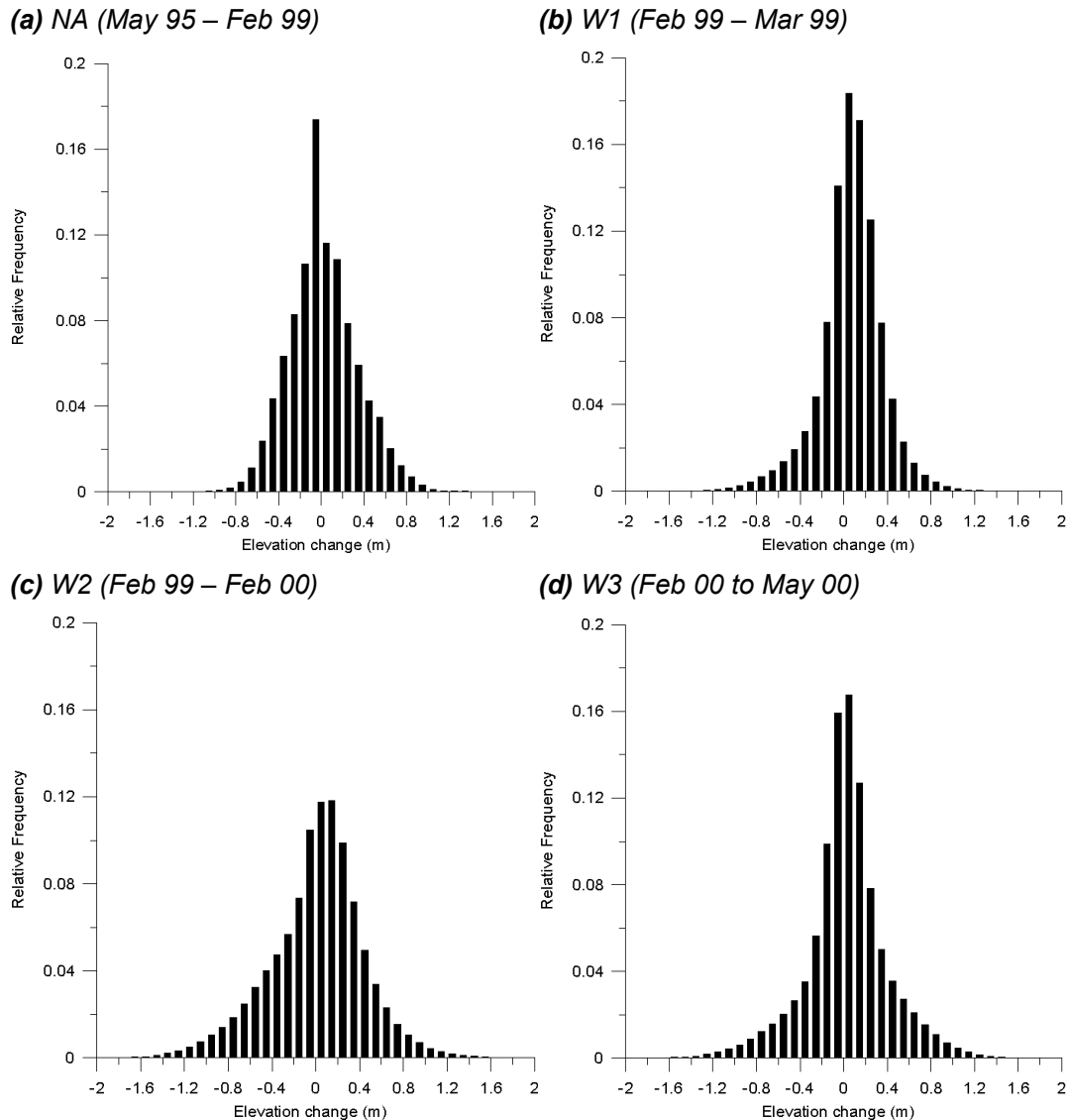


Figure 7.2 Distribution of elevation differences that comprise the post-processed DEMs of difference.

7.3.2 Reach-averaged volume change statistics

The reach-averaged volume change statistics for each post-processed DEM of difference are shown in **Table 7.3**. Changes in the post-processed DEMs of difference (**Figure 7.1**) have been grouped according to whether they are positive (fill) or negative (cut), and the areas, volumes and spatially-averaged volumes (volume per unit riverbed area) of each have been calculated.

DEM of difference	CUT			FILL			NET CHANGE	
	Area (m ²)	Volume (m ³)	Reach-averaged (m ³ /m ²)	Area (m ²)	Volume (m ³)	Reach-averaged (m ³ /m ²)	Volume (m ³)	Reach-averaged (m ³ /m ²)
NA (May 95 – Feb 99)	12824	3130	0.119	13382	3745	0.143	+614	+0.023
W1 (Feb 99 – Mar 99)	1027033	211118	0.072	1885830	381408	0.131	+170290	+0.058
W2 (Feb 99 – Feb 00)	1266587	458581	0.157	1625786	496253	0.170	+37672	+0.013
W3 (Feb 00 – May 00)	1285326	335255	0.115	1607054	430079	0.148	+94824	+0.033

Table 7.3 Reach-averaged volume change statistics derived from the post-processed DEMs of difference.

It is apparent from **Table 7.3** that despite considerable differences in the absolute volumes and areas of cut and fill, reach-averaged cut and reach-averaged fill for each post-processed DEM of difference are of similar magnitudes. The clearest exception to this is the cut volume calculated for W1 of only 0.072 m, which explains the larger net volume change per unit area (or mean difference) that is associated with that DEM of difference (**Table 7.2**). All four DEMs of difference exhibit net positive change (i.e. aggradation). For the North Ashburton DEM of difference, this could be evidence of the accumulation of a wedge of bed material reported in the study reach (Laronne and Duncan, 1992). For the Waimakariri DEMs of difference, this may reflect the long term aggradation downstream of Crossbank (spanned by the study reach), linked to its location at the current-day hinge-point location (Griffiths, 1979, 1991; Reid and Poynter, 1982).

7.3.3 *Error detection*

All the post-processed DEM of difference statistics presented to this point have been ‘raw’ (i.e. calculated using **Equation 2.5**), meaning that no recognition has been given to the uncertainties associated with the DEM surfaces used to generate them. However, **Tables 4.11** and **6.6** suggest that errors do remain in the post-processed DEMs. These will reduce the accuracy, precision and reliability of the final difference surface. The combined error of the two DEMs used in the calculation of a DEM of difference relative to the true surfaces determines the quality of the volumetric calculation (Ashmore and Church, 1998). Thus, we need to be confident that the changes observed and quantified in the DEMs of difference are real and not produced by errors in each surface.

Identification and quantification of errors in the post-processed DEMs of difference was carried out based on the three types of error discussed in **Section 2.3.1**: gross error; systematic error; and random error. The strategies required to detect each type of error reflect how their various effects are manifest in DEMs of difference: gross error tends to produce spikes or pits in the DEM of difference surface; systematic error causes systematic bias; and random error produces background noise. The type of error also determines whether or not the errors detected may be reduced or removed: gross and systematic error may both (theoretically) be eliminated; random error cannot. Both of these factors reinforce the importance of recognising different components of error.

7.3.4 *Gross error*

Gross error, in the form of outliers, can be identified in DEM of difference surfaces both visually and statistically as points which deviate from the local DEM characteristics. Once identified, these points are easy to remove. Visually, neither the DEMs of

difference (**Figure 7.1**) nor the histograms of elevation differences derived from them (**Figure 7.2**) show any large outlying points, indicating little readily visualised gross error.

Gross error was assessed by adapting the method of error detection developed by Felisicimo (1994). The test is based on calculating the difference between a DEM point and the value estimated from the mean value of the eight neighbouring DEM points. By applying the process to every point in the post-processed DEMs of difference, a population of local elevation differences was defined for which a mean difference (MD_{local}) and standard deviation of differences (SDD_{local}) were calculated. Statistically, gross error was identified using the notion of maximum expected difference (MED_{local}) introduced as maximum expected error (MEE) in **Section 2.3.8** (e.g. Torlegård *et al.*, 1986; Shearer, 1990). This is usually defined as $\pm 3 SDE$, or in this case $\pm 3 SDD_{local}$. Only around 0.27% of measurements should fall outside this value. **Table 7.4** shows the MED_{local} exceedance statistics for each of the post-processed DEMs of difference calculated in this research.

DEM of difference	SDD_{local} (m)	MED_{local} (m)	Points < minimum MED_{local}	Points > maximum MED_{local}	Total exceedance (%)
NA (May 95 – Feb 99)	± 0.098	± 0.294	94	129	0.78
W1 (Feb 99 – Mar 99)	± 0.093	± 0.279	32145	28653	2.15
W2 (Feb 99 – Feb 00)	± 0.076	± 0.228	17123	28122	1.55
W3 (Feb 00 – May 00)	± 0.092	± 0.276	23284	17049	1.38

Table 7.4 Detection of gross errors in the post-processed DEMs of difference based on maximum expected local elevation difference.

The MED_{local} exceedance statistics show that gross errors persist in all four post-processed DEMs of difference. Each has greater than 0.27% of the points that would be theoretically expected to exceed three standard deviations from the mean. The effect of these predicted gross errors on the total volume change for the study areas was tested by eliminating from the post-processed DEMs of difference all points that exceeded MED_{local} . The reach-averaged volume change statistics were recalculated and are presented in **Table 7.5**. These show how the largest difference from the raw reach-averaged volume change statistics (**Table 7.3**) is only $0.006 \text{ m}^3/\text{m}^2$ (fill observed for W2). Nonetheless, if these differences are considered relative to the net change in volume for each DEM of difference, they become more important. This reflects the fact that error is always amplified in net change calculations.

DEM of difference	CUT			FILL			NET CHANGE		
	Area (m ²)	Volume (m ³)	Reach-averaged (m ³ /m ²)	Area (m ²)	Volume (m ³)	Reach-averaged (m ³ /m ²)	Volume (m ³)	Reach-averaged (m ³ /m ²)	Relative difference (%)
NA (May 95 – Feb 99)	14685	3069 (-61)	0.117 (-0.001)	13328	3632 (-113)	0.139 (-0.004)	+666 (+52)	+0.025 (+0.002)	(+9)
W1 (Feb 99 – Mar 99)	1012352	195753 (-15365)	0.067 (-0.005)	1900277	367441 (-13967)	0.126 (-0.005)	+168892 (-1398)	+0.058 (+0.000)	(0)
W2 (Feb 99 – Feb 00)	1266587	450353 (-8228)	0.155 (-0.002)	1625786	479178 (-17075)	0.164 (-0.006)	+46113 (+8441)	+0.016 (+0.003)	(+23)
W3 (Feb 00 – May 00)	1285326	323282 (-11973)	0.111 (-0.004)	1607054	421987 (-8092)	0.145 (-0.003)	+90943 (-3881)	+0.031 (-0.002)	(-6)

Table 7.5 Revised reach-averaged volume change statistics derived from the post-processed DEMs of difference with gross errors removed. The figures in brackets represent the change from the raw reach-averaged volume changes (**Table 7.3**).

Given these observations, it was decided that removal of points assumed to be gross error using this method could not be justified, and was ultimately not beneficial to the post-processed DEM of difference surfaces. The use of local elevation difference to detect and remove gross errors only gives an indication of which points are deemed gross errors based on the statistical characteristics of the DEM surface. Moreover, the effect on volume changes following removal of such points was negligible. In addition, the high level of consistency within and between the global elevation change statistics for the post-processed DEMs of difference (**Table 7.2**), suggests that the extreme differences observed may reflect process-controls and represent real morphological changes. If this is the case, the removal of such points may in fact reduce the useful information content that can be derived.

7.3.5 *Systematic error*

Systematic error in a DEM of difference will be made up of the total systematic error in the DEM surfaces used in its creation, and will cause systematic deviation from the true value of elevation change at any given point. Unlike gross or random error, systematic error cannot be analysed statistically, but its presence may be detected, quantified and removed if independent calibration information is available. This may be in the form of areas which are recognised to have experienced no morphological change (in which case the DEM of difference should equal zero) or areas of independently-established morphological change. For the DEMs of difference derived in this study, no formal calibration data for the expected morphological change was available. Instead, elevation change assumptions developed from geomorphological reasoning were used to inform assessment of systematic errors.

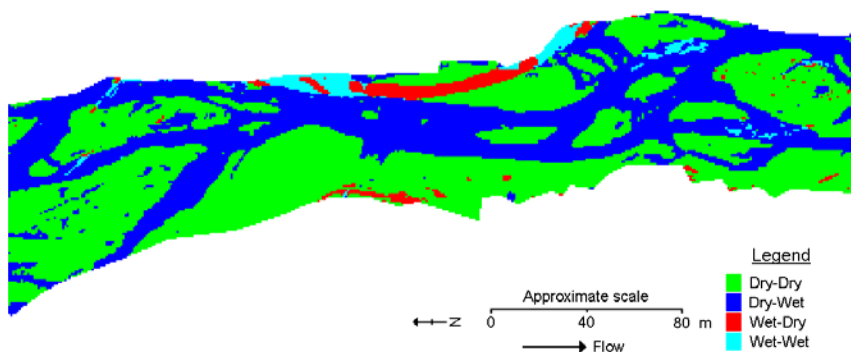
Three assumptions were proposed, based on the postulated nature of riverbed change during the epoch spanned by the DEM of difference. These were: (1) that areas that changed from exposed (dry-bed) to inundated (wet-bed) would experience predominantly erosion and little deposition (net negative elevation change); (2) that areas that changed from wet-bed to dry-bed would experience mainly deposition and little erosion (net positive elevation change); and (3) that the more stable bar-top zones, away from wetted channels, would experience relatively little elevation change. Large deviations from these assumed ideal situations would be taken to indicate the presence of systematic error. No assumptions were made in areas that were inundated during both surveys due to the uncertain nature of topographic change in this case.

Initially, systematic error was assessed for the whole study reaches. First, it was necessary to determine the type of change experienced. This used the classified images acquired using unsupervised maximum likelihood classification (e.g. **Figure 5.2**). Vegetated areas were manually re-classified as dry-bed areas. Spatial Modeller was used to combine the classified images to create maps showing the estimated wet-dry history of every riverbed grid cell for each post-processed DEM of difference (**Figure 7.3**). Four classes of points were identified based on the position of wet and dry pixels at the start and end of each epoch: dry-dry; dry-wet; wet-dry; and wet-wet.

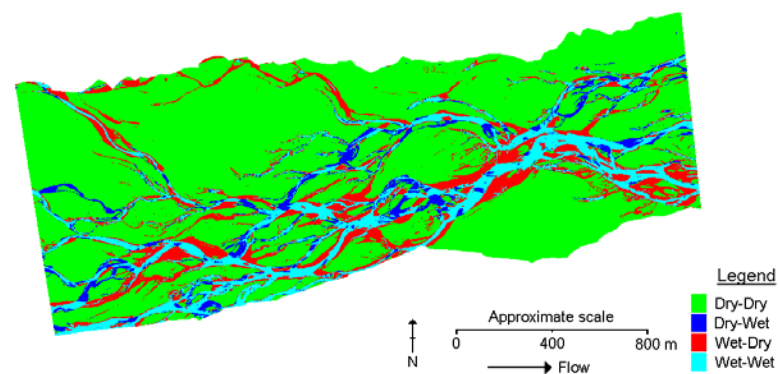
This scheme of classifying riverbed changes has several recognised weaknesses. First, given the occurrence of at least one bankfull flood during the time period represented by each DEM of difference, no areas remained completely dry. Second, intra-epoch changes in the configuration of wetted channels are not considered, which may be particularly significant for the DEMs of difference that span longer time periods (e.g. NA, W2; **Table 7.1**), depending on the dynamism of the river in that time. Finally, the configuration of wetted channels at any given time based on aerial imagery alone is related to river stage. Although discharge was broadly comparable between photographic surveys (**Tables 3.1** and **3.2**), which were all performed at low flows, some of the wet-dry history pattern discovered is likely to be due to river stage alone. Despite these potential difficulties, the zone maps shown in **Figure 7.3** were still believed to show the essential change in wetted channel configuration required to test for systematic error based upon the geomorphological assumptions.

The second stage involved recalculation of the volume change statistics for each wet-dry history zone for each post-processed DEM of difference (**Table 7.6**). Each assumption was addressed in turn. Assumption 1 related to areas which changed from dry-bed to wet-bed (**Figure 7.3**). Theoretically, erosion should dominate in these zones. This was supported by the calculated volume change statistics, with the volume of material lost significantly greater than the volume of material deposited (**Figure 7.4a**). Assumption 2 was the inverse condition, involving areas that altered from wet-bed to dry-bed during the time period spanned by the DEMs of difference, and where deposition would be expected to be more important. Again, the calculated volume change supported this, with net aggradation observed in the wet-dry zone in all four post-processed DEMs of difference.

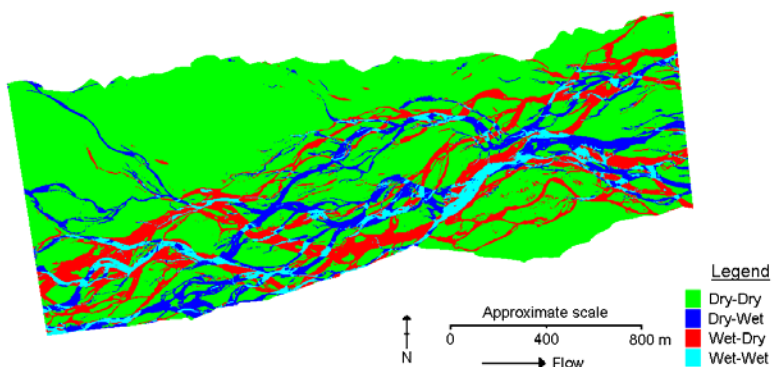
(a) North Ashburton – May 1995 to February 1999 (NA)



(b) Waimakariri – February 1999 to March 1999 (W1)



(c) Waimakariri – February 1999 to February 2000 (W2)



(d) Waimakariri – February 2000 to May 2000 (W3)

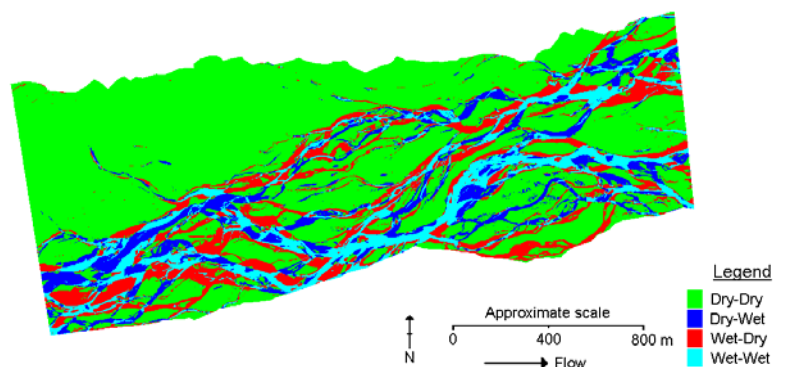


Figure 7.3 Classified maps of the assumed wet-dry history of riverbed pixels, created by comparing binary classified images of wet-bed and dry-bed areas from the start and end of each epoch spanned by the post-processed DEMs of difference.

Zone	DEM of difference	CUT			FILL			NET CHANGE	
		Area (m ²)	Volume (m ³)	Zone-averaged (m ³ /m ²)	Area (m ²)	Volume (m ³)	Reach-averaged (m ³ /m ²)	Volume (m ³)	Zone-averaged (m ³ /m ²)
Dry-Dry	NA (May 95 – Feb 99)	7623	1780	0.126	6551	1637	0.115	-144	-0.010
	W1 (Feb 99 – Mar 99)	575081	56724	0.027	1513401	262081	0.125	+205356	+0.098
	W2 (Feb 99 – Feb 00)	752717	189902	0.095	1232778	304062	0.152	+114160	+0.057
	W3 (Feb 00 – May 00)	786090	113406	0.060	1069760	185136	0.099	+71731	+0.038
Dry-Wet	NA (May 95 – Feb 99)	623	273	0.396	65	17	0.024	-256	-0.372
	W1 (Feb 99 – Mar 99)	288890	110291	0.304	73812	12110	0.033	-98181	-0.271
	W2 (Feb 99 – Feb 00)	412345	240161	0.537	34730	6549	0.015	-233612	-0.523
	W3 (Feb 00 – May 00)	372987	192234	0.444	59287	11129	0.026	-181105	-0.418
Wet-Dry	NA (May 95 – Feb 99)	4023	898	0.084	6612	2056	0.193	+1159	+0.109
	W1 (Feb 99 – Mar 99)	11974	1769	0.012	131749	59271	0.412	+57502	+0.400
	W2 (Feb 99 – Feb 00)	24391	3672	0.012	278252	159785	0.525	+156113	+0.513
	W3 (Feb 00 – May 00)	11848	1797	0.006	287823	170473	0.569	+168676	+0.563

Table 7.6 Volume change statistics derived from the post-processed DEMs of difference divided by wet-dry history zone. Data have been colour-coded to reflect the geomorphological assumption (identified above) to which they most closely relate: assumption 1 in blue; assumption 2 in red; and assumption 3 in green.

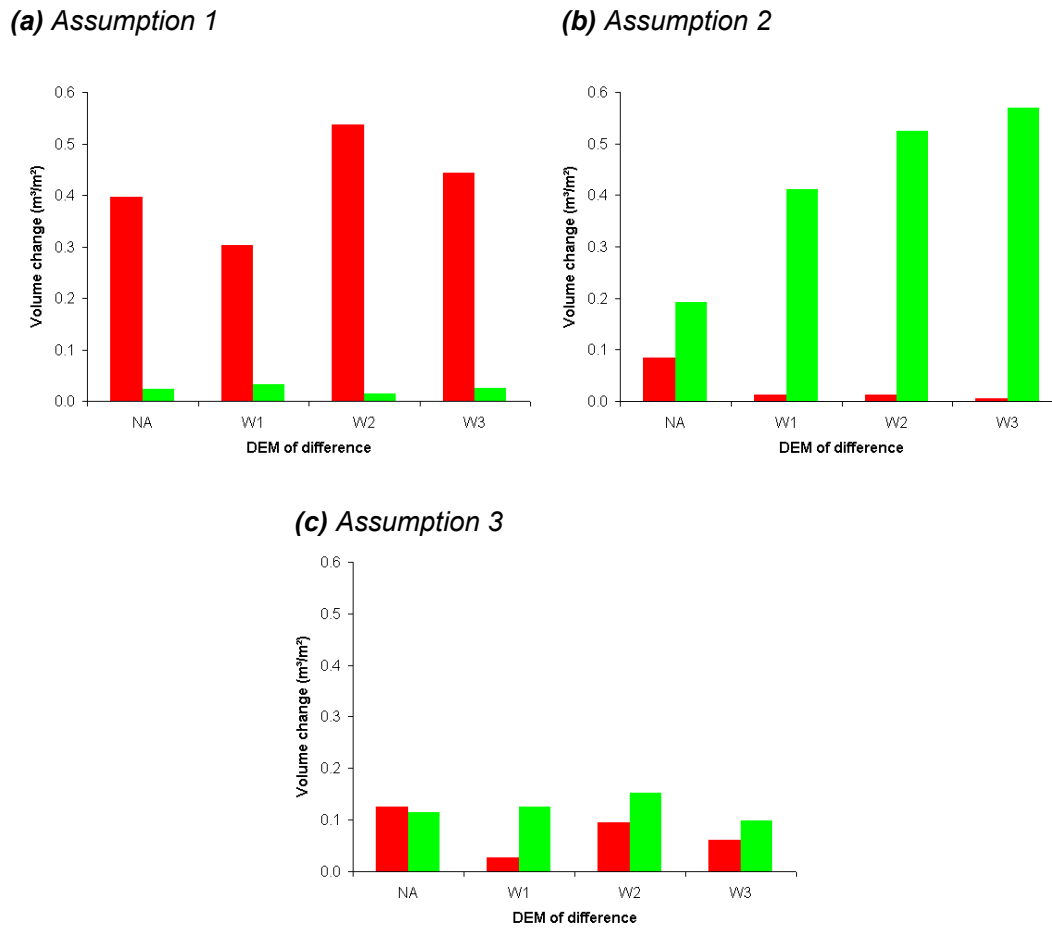


Figure 7.4 Comparison of cut (red) and fill (green) volumes for the whole study reaches, with respect to the three geomorphological assumptions. NA is North Ashburton May 95 – Feb 99; W1 is Waimakariri Feb 99 – Mar 99; W2 is Waimakariri Feb 99 – Feb 00; and W3 is Waimakariri Feb 00 – May 00.

For the Waimakariri post-processed DEMs of difference, fill volumes exceeded cut volumes by an order of magnitude. The difference was less marked for the North Ashburton (**Figure 7.4b**). Assumption 3 suggested that dry areas in both images would have little vertical elevation change. The vertical magnitude of change in dry-dry zones was considerably less than in either dry-wet or wet-dry zones (**Figure 7.4c**), totalling $0.15 \text{ m}^3/\text{m}^2$ at most (fill in W2; **Table 7.6**). Furthermore, volumes of erosion and deposition were found to be broadly similar in three of the post-processed DEMs of difference (NA, W2 and W3), yielding a net volume change per unit riverbed area of less than $0.06 \text{ m}^3/\text{m}^2$ in each case (**Table 7.6**). However, dry-dry regions in DEM of difference W1 experienced a net increase in zone-averaged volume of almost $0.10 \text{ m}^3/\text{m}^2$, suggesting the presence of a systematic error.

Examining all three assumptions together, it appears that systematic errors are not especially detectable in the post-processed DEMs of difference at the reach scale, on the basis of expected volume changes. However, the identification of expected changes from the classified images (**Figure 7.3**) is likely to be least reliable at the reach-scale. For example, assumption 3 relates to bar-top areas away from wetted channels, whereas zones which are classified as dry-dry also include parts of the active braid-belt which are close to wetted channels. Consequently, the presence of systematic error was further investigated for the Waimakariri study reach by using smaller sub-areas which allowed tighter control over the type of morphological change that was assumed to have occurred. Four 500 m x 200 m sub-areas were defined (**Figure 7.5**): two within the active braid-belt (BB1 and BB2); and two from bar-top areas (BT1 and BT2). The volume change statistics were then recalculated for each sub-area. The results relevant to the assessment of systematic errors are summarised in **Table 7.7** and **Figure 7.6**. It was felt that equivalent sub-areas could not be identified with any confidence for the North Ashburton due to the smaller spatial extent of the riverbed coupled with the longer time spanned by the DEM of difference. Consequently, this analysis was only performed for the Waimakariri post-processed DEMs of difference.

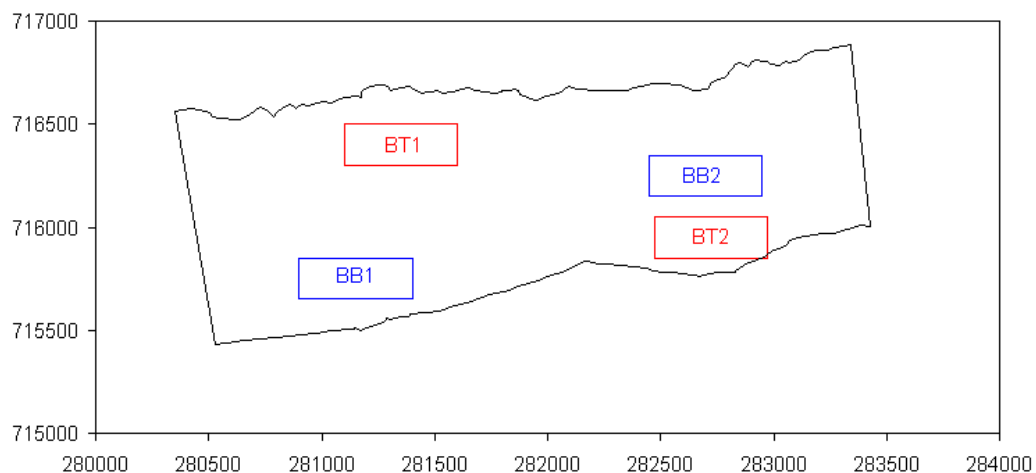


Figure 7.5 The positions of the four sub-areas in bar-top (BT) and braid-belt (BB) locations.

Zone	Sub-area (DEM of difference)	CUT			FILL			NET CHANGE	
		Area (m ²)	Volume (m ³)	Zone- averaged (m ³ /m ²)	Area (m ²)	Volume (m ³)	Zone- averaged (m ³ /m ²)	Volume (m ³)	Zone- averaged (m ³ /m ²)
Dry-Dry	BT1(W1)	32522	3622	0.036	67752	12202	0.122	+8579	+0.086
	BT1(W2)	8946	891	0.027	24476	3695	0.111	+2805	+0.084
	BT1(W3)	56998	7066	0.071	43221	4916	0.049	-2151	-0.021
	BT2(W1)	17507	1078	0.011	81340	9206	0.093	+8128	+0.082
	BT2(W2)	12335	1834	0.058	19458	2602	0.082	+768	+0.024
	BT2(W3)	24386	4423	0.062	46780	8436	0.119	+4013	+0.056
Dry-Wet	BB1(W1)	29362	12397	0.383	3013	394	0.012	-12003	-0.371
	BB1(W2)	6041	2827	0.464	57	5	0.001	-2822	-0.463
	BB1(W3)	30418	11261	0.316	5214	674	0.019	-10587	-0.297
	BB2(W1)	22754	6975	0.207	10992	2046	0.061	-4929	-0.146
	BB2(W2)	9977	4399	0.394	1181	172	0.015	-4227	-0.379
	BB2(W3)	18220	9680	0.516	534	42	0.002	-9638	-0.514
Wet-Dry	BB1(W1)	79	9	0.001	7816	3440	0.436	+3431	+0.435
	BB1(W2)	751	141	0.022	5817	2688	0.409	+2546	+0.388
	BB1(W3)	3	0	0.000	16451	12396	0.753	+12396	+0.753
	BB2(W1)	31	3	0.001	5031	3369	0.665	+3366	+0.665
	BB2(W2)	60	5	0.001	4086	3541	0.854	+3536	+0.853
	BB2(W3)	161	14	0.001	16323	10552	0.640	+10538	+0.639

Table 7.7 Volume change statistics for the four sub-areas divided by wet-dry history zone. Data have been coloured-coded to reflect the geomorphological assumption (identified above) to which they most closely relate: assumption 1 in blue; assumption 2 in red; and assumption 3 in green. W1 is Waimakariri Feb 99 – Mar 99; W2 is Waimakariri Feb 99 – Feb 00; and W3 is Waimakariri Feb 00 – May 00.

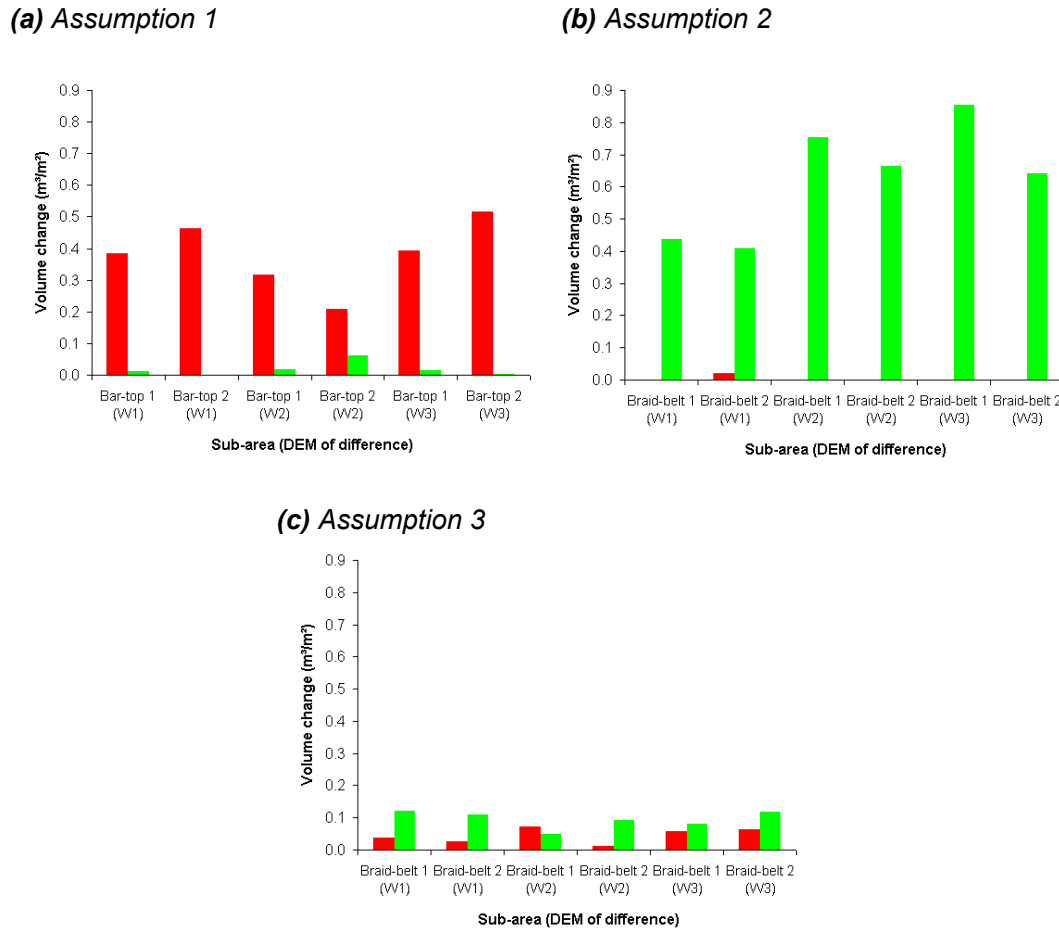


Figure 7.6 Comparison of cut (red) and fill (green) volumes for the Waimakariri sub-areas, with respect to the three geomorphological assumptions. W1 is Waimakariri Feb 99 – Mar 99; W2 is Waimakariri Feb 99 – Feb 00; and W3 is Waimakariri Feb 00 – May 00.

The sub-area volume change statistics generally correspond with the results that would be expected given each of the three assumptions (Figure 7.6). In areas that changed from dry-bed to wet-bed, erosion was dominant (assumption 1; Figure 7.6a). For both braid-belt sub-areas, spatially-averaged erosion was at least $0.20 \text{ m}^3/\text{m}^2$, while spatially-averaged deposition was less than $0.02 \text{ m}^3/\text{m}^2$ in all but one case (sub-area BB2 in W2, which experienced fill of $0.061 \text{ m}^3/\text{m}^2$). Consequently net cut was experienced, and the magnitudes are commensurate with channel depth (assuming that bank erosion is the major source of cut material). In areas that changed from wet-bed to dry-bed, deposition was characteristic (assumption 2; Figure 7.6b). For both braid-belt sub-areas, spatially-averaged deposition was greater than $0.40 \text{ m}^3/\text{m}^2$, with spatially-averaged erosion of $0.02 \text{ m}^3/\text{m}^2$ or less. As a result, there was net deposition,

with a vertical magnitude commensurate with what would be expected if active channels were in-filled with sediment.

Finally, in bar-top areas which are assumed to have remained largely dry (dry-dry zones), little net elevation change was observed (assumption 3; **Figure 7.6c**). Both spatially-average erosion and deposition, and hence net elevation change, were generally less than $0.10 \text{ m}^3/\text{m}^2$ (so considerably less than the magnitude of change associated with the braid-belt). Two of the largest net elevation changes were calculated for W1, reinforcing the notion established at the reach scale (**Figure 7.4c**) that this post-processed DEM of difference may contain the largest systematic error. However, since this method of systematic error appraisal only gives an indication of its presence (i.e. the net volume changes observed might represent real morphological changes), it was decided that this could not be proven conclusively. As a result, the DEMs of difference calculated from the post-processed DEMs were deemed to be essentially free of systematic error.

7.3.6 *Random error: Theory*

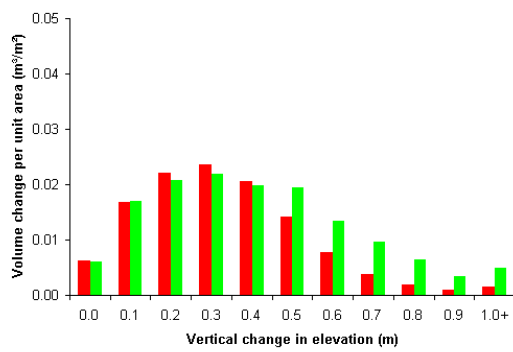
Random errors in a DEM of difference correspond to the random noise that inevitably results when two DEM surfaces containing uncertainties are differenced. However, the distinction of real morphological change from artefacts caused by background noise is clearly important for the subsequent calculation of volumes of change. In **Section 2.3.9**, the total uncertainty due to random error when two measurements are differenced was shown to be the root of the sum in quadrature of the precision of each measurement (**Equation 2.12**). In the context of DEMs of difference, this corresponds to the precision associated with the DEM surfaces used in its creation, and will define the precision for a given DEM of difference. Since random error in a DEM of difference cannot be removed nor reduced without modification of the input DEM surfaces, it controls the minimum level of detection (Brasington *et al.*, 2000). Given that vertical elevation changes in gravel riverbed environments are small relative to riverbed extent, this places great significance on riverbed DEM quality, and is likely to be a critical control over the ability of remote sensing to provide topographic input to morphological calculation of sediment movement.

The main effect of random errors on DEMs of difference is to reduce the useful information content, as there can be less confidence that smaller point elevation changes represent real morphological change. This will depend upon both the estimated precision of the DEM of difference (and hence on the precision of the DEM surfaces used to calculate the DEM of difference) and on the distribution of morphological changes observed. For example, if all observed morphological change

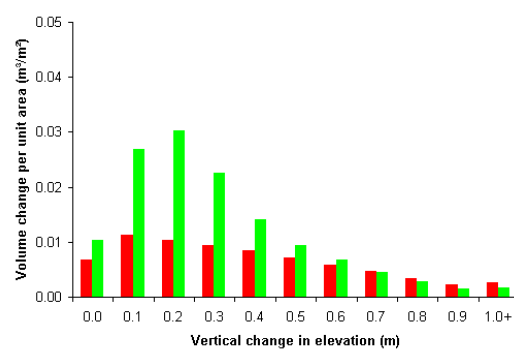
exceeds the estimated minimum level of precision, then random errors would not be expected to alter the magnitude of change detected. However, in order to use the change information to infer sediment transport rates (using **Equations 7.1** and **7.2**), volumes of change are of most interest. These will be influenced by random error, regardless of its magnitude, although the relative importance of random errors will fall as either the volumes of change increase or the minimum level of precision decreases.

To test the potential sensitivity of the North Ashburton and Waimakariri post-processed DEMs of difference to a minimum level of detection, the distribution of morphological change was calculated for the entire study reaches. The resulting plots (**Figure 7.7**) show the contribution of different elevation change magnitudes to total volumes of cut and fill for each reach. These calculations are only meaningful if systematic error is absent. This was demonstrated to be the case for the DEMs of difference considered here in Section 7.3.5.

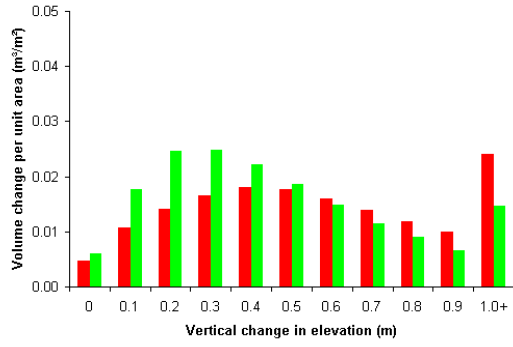
(a) NA (May 95 – Feb 99)



(b) W1 (Feb 99 – Mar 99)



(c) W2 (Feb 99 – Feb 00)



(d) W3 (Feb 00 – May 00)

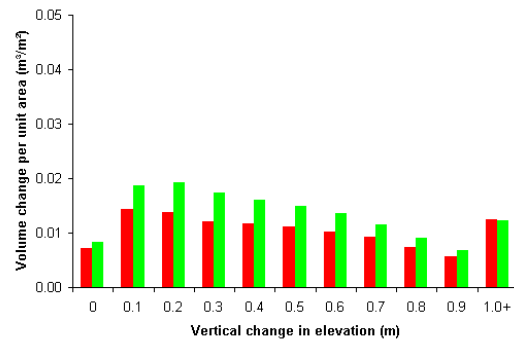


Figure 7.7 Distributions of morphological change in terms of cut (red) and fill (green) volumes for the post-processed DEMs of difference (Figure 7.1**).**

Despite the differences in the length of time spanned by each DEM of difference, there is considerable similarity between the derived distributions of morphological change in

both shape and magnitude of volume change. Furthermore, in each case, a magnitude-frequency effect can be detected, with the most morphological change associated with intermediate magnitudes of elevation change (0.10-0.30 m). This is encouraging because it implies that the effect of random errors, which will render less confidence in smaller elevation changes (i.e. those less than the precision of the DEM of difference), is not necessarily large.

In order to estimate the effect of random errors upon detection of morphological change, the precision associated with each post-processed DEM of difference must be calculated. From **Equation 2.12**, this requires parameterisation of the precision of the DEM surfaces used in their creation. As discussed in **Section 2.3.8**, there are several ways of conceptualising and quantifying the precision of a DEM surface. In this study, at least four measures have been used: theoretical precision (**Equation 2.1** for digital photogrammetry; $\pm 0.10\text{--}0.15$ m (**Section 2.3.3**) for ALS; mean Z-direction standard deviation of PCP residuals calculated during block triangulation (for digital photogrammetry only; **Table 3.9**); SDE calculated from comparison with independent check point measurements (**Equation 2.3**) for both dry-bed and wet-bed areas; and the standard deviation of elevation differences calculated from overlap analysis (**Tables 6.9 and 6.10**). These are summarised in **Table 7.8**. Using **Equation 2.12**, five values of estimated precision may be assigned to each post-processed DEM of difference (**Table 7.9**).

DEM	Theoretical precision (m)	PCP-based precision (m)	Check point precision (m)		Overlap analysis precision (m)
			Dry-bed	Wet-bed	
North Ashburton – May 95	± 0.075	± 0.070	± 0.116	± 0.244	n/a
North Ashburton – Feb 99	± 0.042	± 0.031	n/a	± 0.222	n/a
Waimakariri – Feb 99	± 0.070	± 0.052	± 0.261	± 0.318	± 0.192
Waimakariri – Mar 99	± 0.070	± 0.051	± 0.257	± 0.256	± 0.174
Waimakariri – Feb. 00	± 0.056	± 0.049	± 0.131	± 0.219	± 0.177
Waimakariri – May 00	c. ± 0.10	n/a	± 0.100	± 0.250	± 0.218

Table 7.8 Parameterisation of the precision associated with the post-processed DEMs.

The effect of these estimates of random error upon the maximum morphological change information obtained from the post-processed DEMs of difference may be addressed either deterministically or probabilistically. Both were examined in this study.

The first approach was deterministic (**Section 7.3.7**) and treated the estimated precision value as a fixed minimum level of detection (LOD_{min}). Consequently, morphological changes of a vertical magnitude less than LOD_{min} are assumed not to be

statistically distinguishable from the random noise associated with subtracting two surfaces containing random errors and were disregarded in volume estimates. This allowed information loss to be calculated for a given LOD_{min}.

DEM of difference	Theoretical precision (m)	PCP-based precision (m)	Check point precision (m)		Overlap analysis precision (m)
			Dry-bed	Wet-bed	
NA (May 95 – Feb 99)	±0.086	±0.077	±0.164 ^a	±0.330	n/a
W1 (Feb 99 – Mar 99)	±0.090	±0.078	±0.366	±0.408	±0.259
W2 (Feb 99 – Feb 00)	±0.090	±0.071	±0.292	±0.386	±0.261
W3 (Feb 00 – May 00)	±0.115	n/a	±0.165	±0.332	±0.281

^a Assumes a dry-bed SDE of ±0.116 m for the February 1999 DEM (for when no dry-bed independent check point measurements were available).

Table 7.9 Parameterisation of the precision estimated for the post-processed DEMs of difference (from **Equation 2.12**).

The second approach to estimating the effect of random error on calculations of morphological change was probabilistic (**Section 7.3.8**), based upon assessing the likelihood that a given elevation change is significant and hence real. Thus, each point elevation change was converted to a *t* statistic by considering its magnitude relative to the precision of the DEM surfaces used:

$$t = \frac{Z_1 - Z_2}{\sqrt{\hat{s}_1^2 + \hat{s}_2^2}} = \frac{\Delta Z}{LOD_{min}} \quad (7.4)$$

where *Z* is the elevation of a corresponding point and \hat{s} is the standard deviation of DEM surfaces 1 and 2. A requirement of this method is that random error in the input DEM (\hat{s}_1 and \hat{s}_2) for both surfaces is normally distributed. Statistically, this could not be demonstrated for the post-processed DEMs of difference produced in this research ($p < 0.05$; **Section 7.2.1**). However, the *t* test is relatively robust in the case of deviation from a Gaussian distribution (Norcliffe, 1977; Blalock, 1979).

In the context of a DEM of difference, the elevation change is represented as the *Z*-coordinate (ΔZ) and the sum in quadrature of standard deviation values is the DEM of difference precision or minimum level of detection (LOD_{min}) (**Equation 7.4**). Once the *t* statistic is calculated, elevation changes are weighted based on the assumed probability that the observed change at that point is correct. Hence, this approach uses all values in the DEM of difference, rather than just those that exceed the LOD_{min} (as with the deterministic approach). Smaller elevation changes carry less weight since we can be less confident that they represent real morphological change. For example, a

vertical elevation change that is double the magnitude of LOD_{min} would be assigned a t value of 2.0, and hence a two-tailed probability of the change being significant of 95.5%. For an elevation change half the value of LOD_{min} , the t value would become 0.5, giving only a 38.3% probability that the change is significant. Above the 95% confidence interval ($t = 1.96$), a weight of 1.0 was assigned as it was assumed that above this threshold all observed morphological change reflected real riverbed elevation changes. **Table 7.10** summarises the relationship between elevation change, LOD_{min} , t value and probability and weight.

Vertical elevation change, Z, in terms of LOD_{min}	t statistic	Two-tailed probability of significance (%)	Weight
0.10 x LOD_{min}	0.10	8.0	0.080
0.25 x LOD_{min}	0.25	19.7	0.197
0.50 x LOD_{min}	0.50	38.3	0.383
0.75 x LOD_{min}	0.75	54.7	0.547
1.00 x LOD_{min}	1.00	68.3	0.683
1.96 x LOD_{min}	1.96	95.0	1.000
2.00 x LOD_{min}	2.00	95.5	1.000
3.00 x LOD_{min}	3.00	97.3	1.000
4.00 x LOD_{min}	4.00	99.99	1.000
5.00 x LOD_{min}	5.00	99.9999	1.000

Table 7.10 Examples of t values, probabilities and weights calculated from given elevation changes and LOD_{min} values

7.3.7 Random error: Deterministic approach

The deterministic method of assessing random error was applied to all four riverbed post-processed DEMs of difference for each value of precision estimated in **Table 7.8**. For the theoretical, PCP-based and overlap analysis precision, this was relatively straightforward as the precision values relate to the riverbed as a whole. However, the precision calculated from comparison of remotely-sensed data with the independent check point measurements is divided into wet-bed and dry-bed areas and, therefore, the process is more complex. From **Figure 7.3**, four types of morphological change were identified (dry-dry; dry-wet; wet-dry and wet-wet) based on comparison of the wet-dry classified images at the start and end of the epochs spanned by the DEMs of difference. This means that four different values of DEM of difference precision (or LOD_{min}) were produced (**Table 7.11**). The information loss calculation was then made for each morphological change type using the correct LOD_{min} value for that zone, and summed to give the total information loss for the whole study reach (**Table 7.12**).

DEM of difference	DRY-DRY			DRY-WET		
	DEM 1 Dry-bed SDE (m)	DEM 2 Dry-bed SDE (m)	LOD _{min} (m)	DEM 1 Dry-bed SDE (m)	DEM 2 Wet-bed SDE (m)	LOD _{min} (m)
NA (May 95 – Feb 99)	±0.116	n/a	±0.164 ^a	±0.116	±0.222	±0.250
W1 (Feb 99 – Mar 99)	±0.261	±0.257	±0.366	±0.261	±0.256	±0.366
W2 (Feb 99 – Feb 00)	±0.261	±0.131	±0.292	±0.261	±0.219	±0.341
W3 (Feb 00 – May 00)	±0.131	±0.100	±0.165	±0.131	±0.250	±0.282

DEM of difference	WET-DRY			WET-WET		
	DEM 1 Wet-bed SDE (m)	DEM 2 Dry-bed SDE (m)	LOD _{min} (m)	DEM 1 Wet-bed SDE (m)	DEM 2 Wet-bed SDE (m)	LOD _{min} (m)
NA (May 95 – Feb 99)	±0.244	n/a	±0.270 ^a	±0.244	±0.222	±0.330
W1 (Feb 99 – Mar 99)	±0.318	±0.257	±0.409	±0.318	±0.256	±0.408
W2 (Feb 99 – Feb 00)	±0.318	±0.131	±0.344	±0.318	±0.219	±0.386
W3 (Feb 00 – May 00)	±0.219	±0.100	±0.241	±0.219	±0.250	±0.332

^a Assumes a dry-bed SDE of ±0.116 m for the February 1999 DEM (for when no dry-bed independent check point measurements were available).

Table 7.11 Estimated LOD_{min} for the four types of morphological change defined in **Figure 7.3.**

DEM of difference	MORPHOLOGICAL CHANGE < LOD _{min}				TOTAL INFORMATION LOSS	
	Dry-Dry (m ³)	Dry-Wet (m ³)	Wet-Dry (m ³)	Wet-Wet (m ³)	Volume (m ³)	Reach-averaged (m ³ /m ²)
NA – Cut	267	10	351	33	661	0.023
NA – Fill	234	5	461	4	704	0.025
W1 – Cut	52431	29494	1449	20620	103994	0.036
W1 – Fill	202969	9161	14558	23061	249749	0.086
W2 – Cut	60125	20898	2705	9295	93023	0.032
W2 – Fill	115302	3494	15104	9584	143484	0.050
W3 – Cut	38665	14915	872	12159	66611	0.023
W3 – Fill	49161	5339	5007	17258	76765	0.026

Table 7.12 Calculation of morphological change less than LOD_{min} for each type of morphological change and summation of total information loss for the entire study reaches. NA is North Ashburton May 95 – Feb 99; W1 is Waimakariri Feb 99 – Mar 99; W2 is Waimakariri Feb 99 – Feb 00; and W3 is Waimakariri Feb 00 – May 00.

The information loss statistics for both cut and fill volumes are summarised in **Table 7.13**. Information losses are expressed as percentages relative to the total volume of negative or positive morphological change (**Table 7.3**).

7.3.8 Random error: Probabilistic approach

Probabilistic assessment of random error in the post-processed DEMs of difference was carried out for the four riverbed post-processed DEMs, using each of the LOD_{min} values (**Table 7.9**), based on different parameterisations of post-processed DEM precision (**Table 7.8**). A t value was calculated for each post-processed DEM of difference point, and its probability and hence weight was derived using an automated algorithm adapted from Cody (1993). Next, the raw elevation change at that point was multiplied by its calculated weight. Finally, the weighted morphological change was totalled and compared to the raw morphological change (**Table 7.3**) to determine the information loss in terms of total cut and fill volumes. The situation was more complicated for the precision derived from independent check measurements, as different zones of morphological change (**Figure 7.3**) contain unique values of LOD_{min} . As before, each zone was treated separately, and the reach-scale information loss totalled for each post-processed DEM of difference (**Table 7.14**). The final information loss totals, using the probabilistic method of evaluating systematic error, are presented in **Table 7.15**.

7.3.9 Random error: Comparison and discussion

The information loss calculated using both the deterministic (**Table 7.13**) and probabilistic approaches (**Table 7.15**) are summarised and compared in **Figure 7.8**. As would be expected, the relative importance of information loss is largest for higher values of LOD_{min} . It is also significant that the estimation of the effect of systematic error using the probabilistic method retains a higher proportion of morphological change information, with the difference between the two approaches directly proportional to the magnitude of information lost.

Figure 7.9 shows the W2 (Waimakariri; Feb 99 to Mar 99) DEM of difference recalculated using both approaches, to illustrate the effect of imposing a minimum level of detection. Two different examples of LOD_{min} have been used: that based on the theoretical precision (± 0.090 m; **Figure 7.9a,b**); and that based on precision calculated from overlap analysis (± 0.261 m; **Figure 7.9c,d**). Comparison with **Figure 7.1c** shows those areas where information content has been lost due to the assumed presence of random error. It is visually apparent that the probabilistic approach retains more elevation change information for a given level of detection, but that the difference is not large.

	LOD _{MIN} PREDICTED FROM THEORETICAL PRECISION		LOD _{MIN} PREDICTED FROM PCP RESIDUALS		LOD _{MIN} PREDICTED FROM INDEPENDENT CHECK SURVEY		LOD _{MIN} PREDICTED FROM OVERLAP ANALYSIS	
DEM of difference	Loss of cut volume (%)	Loss of fill volume (%)	Loss of cut volume (%)	Loss of fill volume (%)	Loss of cut volume (%)	Loss of fill volume (%)	Loss of cut volume (%)	Loss of fill volume (%)
NA (May 95 – Feb 99)	5.0	4.2	4.2	2.8	19	17	n/a	n/a
W1 (Feb 99 – Mar 99)	7.8	6.4	6.2	4.8	49	65	33	42
W2 (Feb 99 – Feb 00)	2.4	2.8	1.6	1.7	20	29	24	22
W3 (Feb 00 – May 00)	8.0	7.2	N/a	n/a	20	18	29	29

Table 7.13 Calculation of information loss relative to total cut and fill volumes (**Table 7.3**) for each predicted LOD_{min} value using a deterministic approach.

DEM of difference	MORPHOLOGICAL CHANGE LOST					TOTAL INFORMATION LOSS	
	Dry-Dry (m ³)	Dry-Wet (m ³)	Wet-Dry (m ³)	Wet-Wet (m ³)	Volume (m ³)	Reach-averaged (m ³ /m ²)	
NA – Cut	216	22	253	27	518	0.018	
NA – Fill	183	4	364	4	555	0.020	
W1 – Cut	36511	23390	973	14409	75283	0.026	
W1 – Fill	129552	5998	12539	16199	164288	0.056	
W2 – Cut	45258	21251	1793	6819	75121	0.026	
W2 – Fill	83707	2479	14811	7149	108146	0.037	
W3 – Cut	27972	14457	601	8692	51722	0.018	
W3 – Fill	36848	3739	5770	13687	60044	0.021	

Table 7.14 Calculation of morphological information loss due to probability-weighting for each type of morphological change and summation of total information loss for the entire study reaches. NA is North Ashburton May 95 – Feb 99; W1 is Waimakariri Feb 99 – Mar 99; W2 is Waimakariri Feb 99 – Feb 00; and W3 is Waimakariri Feb 00 – May 00.

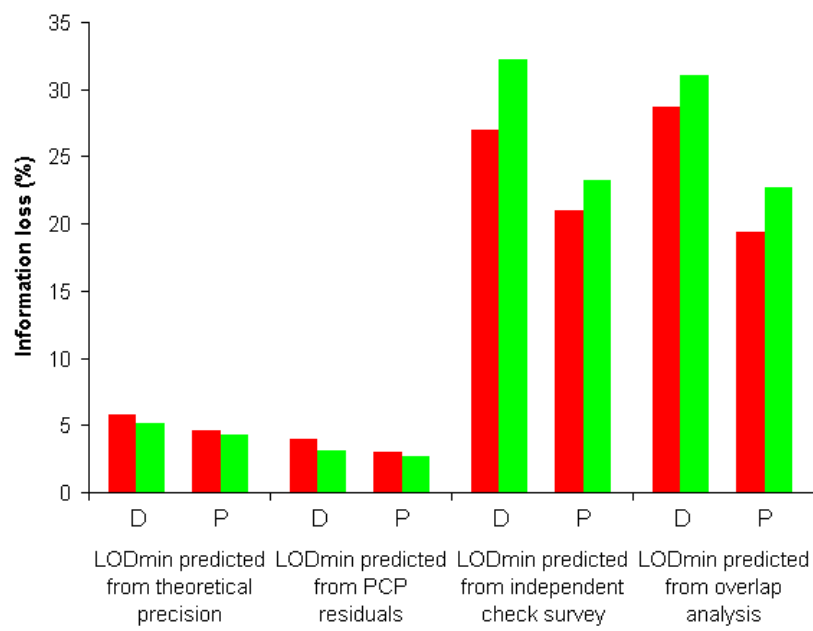


Figure 7.8 Mean estimated information loss in terms of cut (red) and fill (green) volumes due to random error for each predicted LOD_{min} value using both deterministic (D) and probabilistic (P) approaches.

	LOD _{MIN} PREDICTED FROM THEORETICAL PRECISION		LOD _{MIN} PREDICTED FROM PCP RESIDUALS		LOD _{MIN} PREDICTED FROM INDEPENDENT CHECK SURVEY		LOD _{MIN} PREDICTED FROM OVERLAP ANALYSIS	
DEM of difference	Loss of cut volume (%)	Loss of fill volume (%)	Loss of cut volume (%)	Loss of fill volume (%)	Loss of cut volume (%)	Loss of fill volume (%)	Loss of cut volume (%)	Loss of fill volume (%)
NA (May 95 – Feb 99)	3.4	2.8	2.5	2.1	15	14	n/a	n/a
W1 (Feb 99 – Mar 99)	6.3	5.7	5.0	4.4	36	43	25	30
W2 (Feb 99 – Feb 00)	2.1	2.6	1.4	1.6	17	22	12	17
W3 (Feb 00 – May 00)	6.4	6.0	n/a	n/a	16	14	21	21

Table 7.15 Calculation of information loss relative to total cut and fill volumes (**Table 7.3**) for each predicted LOD_{min} value using a probabilistic approach.

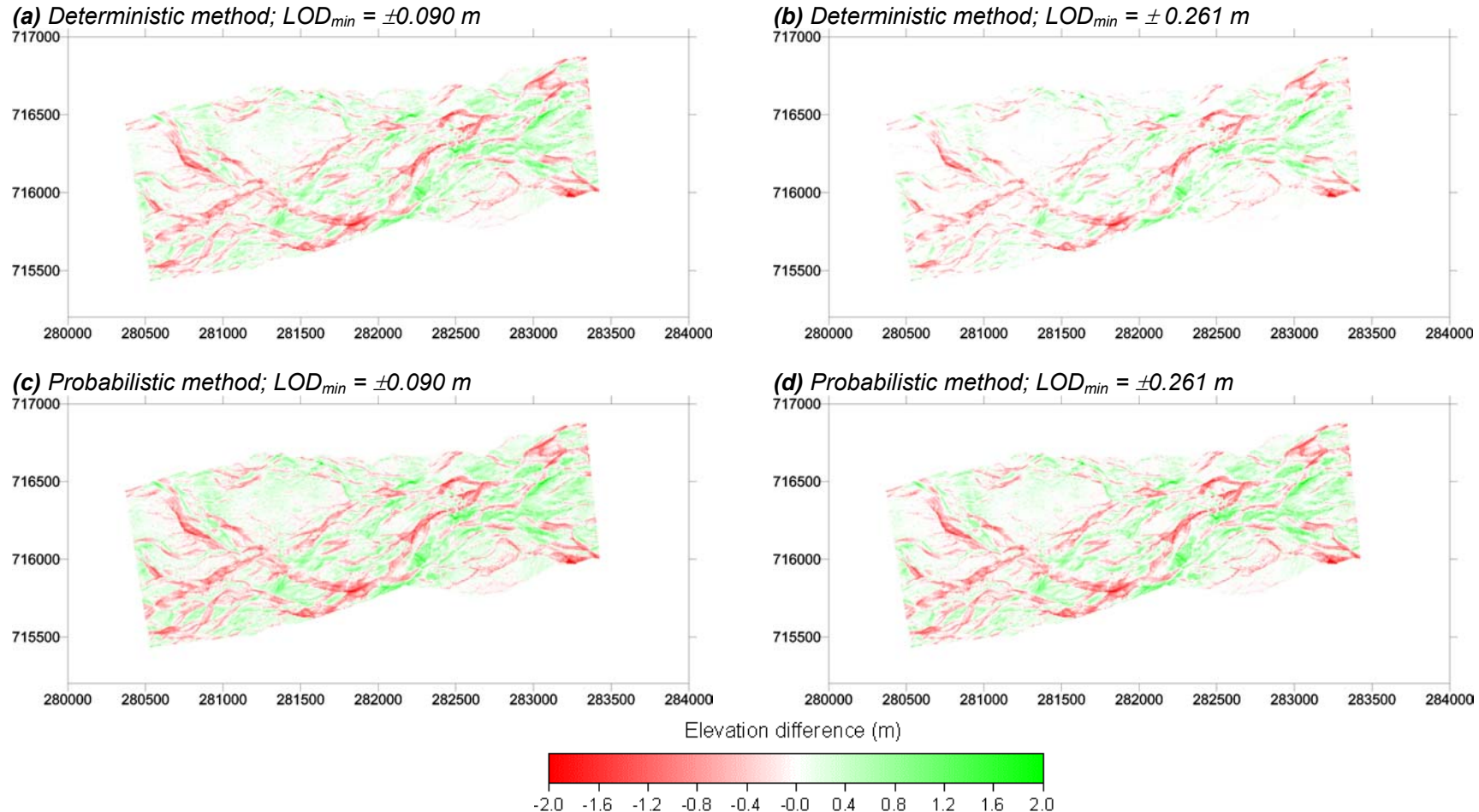


Figure 7.9 Recalculation of the W2 (Waimakariri; Feb 99 – Feb 00) post-processed DEM of difference (**Figure 7.1c**) to illustrate the effect of random error elimination using both deterministic and probabilistic methods. Two levels of detection are illustrated both each approach.

Based on the probabilistic approach to assessing the effect of random error, for LOD_{min} values predicted from both theoretical precision and PCP precision, only around 6% or less of morphological change information is not statistically distinguishable from background noise. This is extremely encouraging as it suggests, in theory at least, that digital photogrammetry and ALS can be used successfully to quantify morphological change in gravel-bed river environments. However, the theoretical levels of precision possible are rarely achieved, so the LOD_{min} predicted from the overlap analysis and independent check point measurements are perhaps more realistic indicators of the practical feasibility of the morphological method. Using these values, between 10% and 25% of morphological change information is lost, meaning that at least three quarters of riverbed change can be detected statistically.

Furthermore, the magnitude of cut and fill volume information lost for a given LOD_{min} and given DEM of difference are broadly similar. This is important because it means that although the total and net morphological change volumes derived from the post-processed DEMs of difference will inevitably be underestimated, the relative morphological change (i.e. the ratio between cut and fill) will be retained, making estimates of average sediment transport rate more reliable. If erosion had been found to be a significantly more spatially-concentrated process than deposition (e.g. Ashmore and Church, 1998), then proportionally more depositional information would have been lost, introducing a negative bias into subsequent DEM of difference applications.

The main anomalies are the information loss calculated for post-processed DEM of difference W1 with a precision based on the check point measurements. These are considerably larger, with 35% of cut volume and 40% of fill volume lost. The higher information loss observed here is due to a combination of a relatively high value of LOD_{min} (ranging from ± 0.369 to ± 0.413 m depending on wet-dry history; **Table 7.9**) coupled with the relatively small morphological changes that occurred (around two-thirds of vertical point changes were less than 0.30 m; **Table 7.2**).

From this discussion, it becomes apparent that the effect of random errors depends on four factors: (i) how precision is parameterised (and, therefore, what value of LOD_{min} is used); (ii) how the LOD_{min} value is used (i.e. deterministically or probabilistically); (iii) the magnitude of information loss that is deemed acceptable; and (iv) the magnitude of morphological change that occurs.

First, and assuming that the precision of a continuous surface can be adequately and accurately quantified, the proportion of volume change information that is required to be retained defines the baseline level of DEM of difference precision (or LOD_{min}) needed. Since this is related to the precision of the post-processed DEM surfaces used

in its creation (**Equation 2.12**), this should also inform the initial survey design. This is illustrated in **Figure 7.10** and **Table 7.16** for the post-processed DEMs of difference acquired in this study. The consistency between the cumulative information loss curves in **Figure 7.10**, even for small magnitude elevation changes, suggests that for the post-processed DEMs of difference in this study, the importance of random errors at the reach-scale is not large.

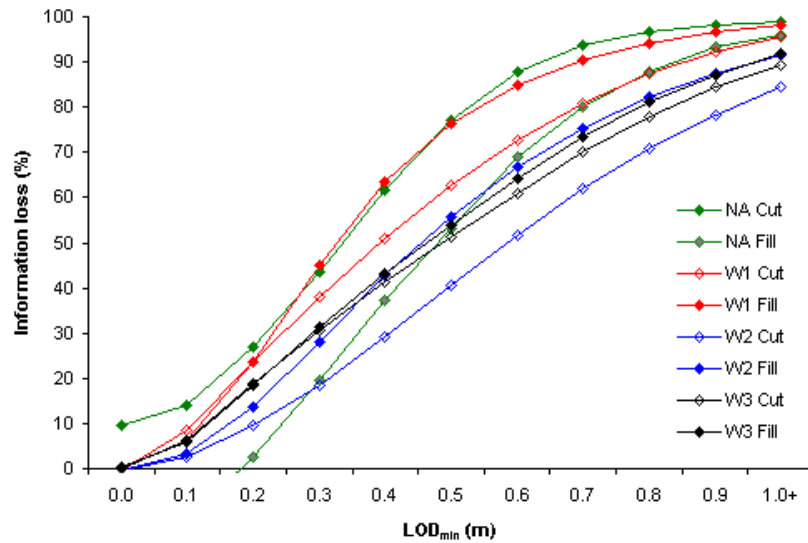


Figure 7.10 Cumulative information loss totals (relative to total volumes of cut and fill) derived from the post-processed DEMs of difference. NA is North Ashburton May 95 – Feb 99; W1 is Waimakariri Feb 99 – Mar 99; W2 is Waimakariri Feb 99 – Feb 00; and W3 is Waimakariri Feb 00 – May 00.

Information loss (%)	Approximate DEM of difference precision (LOD_{min}) required (m) ^a	Approximate DEM precision required (m) (from Equation 2.12) ^b
1	± 0.01	± 0.01
5	± 0.08	± 0.06
10	± 0.15	± 0.11
25	± 0.25	± 0.18
50	± 0.45	± 0.32

^a Based on visual inspection of **Figure 7.10**.

^b Assuming two DEMs of equal precision, such that DEM precision = $\sqrt{(LOD_{min}^2 / 2)}$

Table 7.16 Estimated DEM of difference precision and DEM precision required to fulfil given information loss tolerances.

In practice, the parameterisation of surface precision remains problematic, meaning that choice of precision statistic is also important. In this chapter, four measures of

surface precision were analysed. Two of these (theoretical and PCP-based) are commensurate with the DEM precision required to recover 95% of morphological change (around ± 0.06 m from **Table 7.16**). The other two (based on independent check measurements and overlap analysis) suggest the final riverbed DEMs are less precise, and are commensurate with the DEM of precision required to recover 75% of morphological change (around ± 0.20 m from **Table 7.16**). However, there is a general problem with using check point measurements to define a minimum level of detection in a derived DEM of difference. Any measure of precision calculated for a DEM surface using independent check data will contain a component of error associated with the check measurements themselves. For gravel beds, the error associated with conventional survey techniques may be relatively large, due to the high local bed roughness (Lindsay *et al.*, *in review*). Thus, the survey measurements will have a natural variance, related to the grain size that constrains check point quality. Thus, estimates of LOD_{min} calculated from independent check points will generally overestimate the level of precision in a DEM of difference surface solely due to the survey methods used.

The second factor which influences the effect of random error is the way in which the LOD_{min} value is used. The deterministic and probabilistic approaches differentiate between detection of point elevation changes *per se* and their quantification in terms of volumes of erosion and deposition. The deterministic approach primarily addresses the detection of change. Where vertical elevation change is less than LOD_{min} , the change is deemed as insignificant as compared to random background noise. Thus, the volume change at that point is set to zero, even if some volume of change did occur. The probabilistic approach is more explicit in its consideration of volumes of change, in that detection of change is not separated from the volume of change it represents. Thus, point elevation changes that are small relative to LOD_{min} are still assumed to signify a volume change, but one which we can be less confident is correct. Hence, the volume change at that point is given relatively little weight in the final volumetric calculation.

The final two factors that determine the importance of random error are the information loss that is deemed acceptable, and the magnitude of morphological change observed. These factors are very closely inter-related and cannot be considered independently of each other. The decision about what level of information loss is acceptable must be based on expected morphological changes, since in relative terms small elevation changes are more influenced by random errors. Using the deterministic approach, elevation changes smaller than LOD_{min} will translate as zero volume change. Using the probabilistic approach, the relative information loss will be larger for smaller elevation changes. Where actual morphological change is expected to be small (for example,

gravel riverbeds), the relative importance of information loss due to random error calculated using both methods will be larger. This has important implications for specifying the temporal frequency of re-survey. At shorter time intervals, the magnitude of change will typically decrease (perhaps linked to the number of near-bankfull flood events; **Table 7.1**). This implies that the ability to detect change using remote sensing methods will also decrease, not because LOD_{min} is downgraded, but rather because the ratio of ΔZ to LOD_{min} is decreased.

7.3.10 Conclusions

This section has examined the quality of post-processed DEMs of difference of the North Ashburton and Waimakariri study reaches. Data quality was investigated in terms of the three components of error identified in **Section 2.3.1**, since it was recognised that gross, systematic and random error would each be manifest in different ways.

Gross error was assessed by examining the prevalence and magnitude of local elevation differences that were greater than an expected maximum expected error. Following elimination of predicted gross error, volumes of cut and fill were recalculated to examine the effect of these extreme elevation change values. Their net effect upon volumetric change was not found to be great, so gross error was not identified as an important error source in the DEMs of difference.

Systematic error was assessed with reference to three geomorphological assumptions that were made regarding the expected nature of morphological change in the study reach. The DEMs of difference were examined for systematic error both at the reach-scale and at the scale of four small sub-areas that were chosen with respect to the geomorphological assumptions used. In both cases, it was concluded that systematic error did not seem to be a significant problem in the DEMs of difference.

Random error was assessed in terms of the minimum level of detection (LOD_{min}) that can be predicted based on the precision of the DEM surfaces used to create a given DEM of difference. From the recognition that the main effect of random error is to reduce the useful (or statistically significant) information content of a DEM of difference surface, two approaches to quantifying this information loss were tested. The deterministic approach assumed that only elevation changes with magnitudes greater than LOD_{min} could be distinguished from the background noise signal. The probabilistic approach used the minimum level of detection to assign probabilities that a given vertical elevation change was real, and weighted point volume changes accordingly. Recalculation of the volumes of cut and fill following application of both methods showed that the importance of random errors depended on the measure of precision used, magnitude of morphological change observed and maximum tolerated

information loss. Overall, random error did not appear to effect the DEMs of difference significantly at the reach-scale.

From this assessment, two key question emerge. First, what has been the effect of post-processing in terms of the quality of DEM of difference produced? Second, how does the error that remains in the post-processed DEM of difference compare with that associated with conventional, terrestrial survey methods? These two issues are addressed in the following two sections.

7.4 Effect of post-processing on DEM of difference quality

First, the effect of DEM post-processing on the quality of the resultant DEMs of difference was assessed. This was achieved by repeating the quality assessment procedure, previously undertaken for the post-processed DEMs of difference, for DEMs of difference produced from riverbed DEMs at various stages of post-processing. These are summarised in **Table 7.17**. Two additional DEMs of difference were calculated for the North Ashburton study reach. For the Feb 99 – Mar 99 (W1) and Feb 99 – Feb 00 (W2) Waimakariri DEMs of difference, four additional surfaces were produced. For the Feb 00 – May 00 (W3) DEM of difference, only one additional surface was created. This was because the ALS data was not available for prior (in-house) stages of post-processing. The DEMs of difference are displayed in **Figure 7.11** (NA), **Figure 7.12** (W1), **Figure 7.13** (W2) and **Figure 7.14** (W3). For the Waimakariri DEMs of difference, the improvement in DEM of difference quality as a result of increasing levels of DEM post-processing is visually obvious in terms of a decrease and/or elimination of erroneous elevation changes. For the North Ashburton DEMs of difference, the change is more subtle.

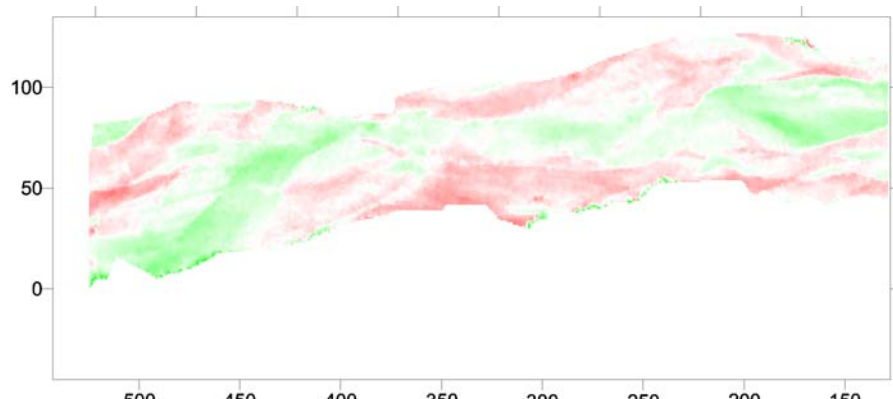
7.4.1 Reach-averaged elevation change statistics

The reach-averaged elevation change statistics associated with each DEM of difference are summarised in **Table 7.18**. The improvement in DEM of difference quality is most apparent in the Waimakariri DEMs of difference. As DEM processing progresses, DEM quality improves, in terms of both the global standard deviation of difference (SDD_{global}) and the minimum and maximum global differences. It is by the fourth level of processing (W1-4; W2-4) that these measures have been reduced to sensible values, given the typical vertical relief in the reach. For the North Ashburton reach, refraction-correction and the use of an optimised maximum parallax has relatively little effect upon the reach-averaged elevation change statistics. The results also demonstrate how the global mean difference may not be a very reliable quality assessment statistic in the presence of extreme values.

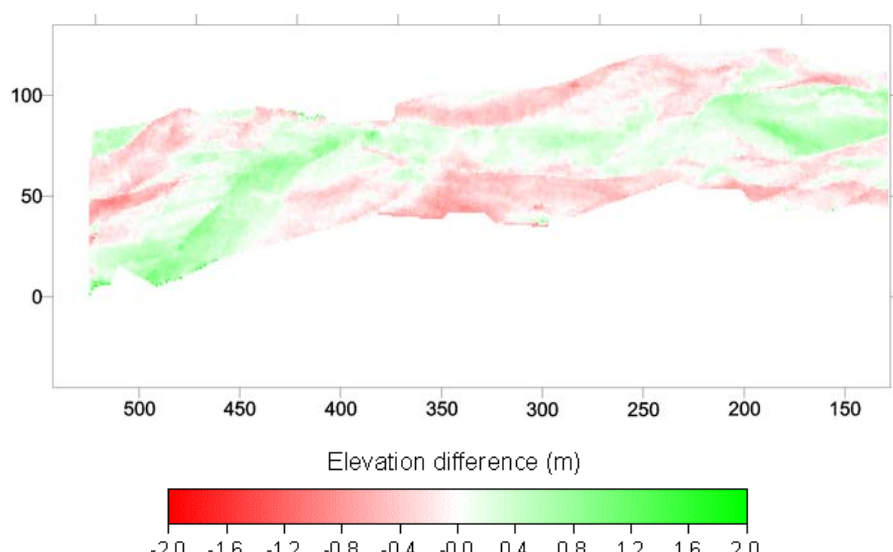
DEM of difference	Code (used hereafter)	Level of post-processing in input DEMs	Figure
NA (May 95 – Feb 99)	NA-1	Uncorrected with default collection parameters	7.11a
	NA-2	Corrected with default collection parameters	7.11b
	NA-3	Corrected with optimised collection parameters	7.1a
W1 (Feb 99 – Mar 99)	W1-1	Unprocessed	7.12a
	W1-2	Unprocessed with estimated water depths subtracted	7.12b
	W1-3	Following removal of unmatched, wet-bed and vegetated points, interpolation of water surface and subtraction of estimated water depths	7.12c
	W1-4	Following removal of local elevation deviations based on coarse DEM surface, re-interpolation of water surface and subtraction of estimated water depths	7.12d
	W1-5	Following PCP-based correction for systematic error	7.1b
W2 (Feb 99 – Feb 00)	W2-1	Unprocessed	7.13a
	W2-2	Unprocessed with estimated water depths subtracted	7.13b
	W2-3	Following removal of unmatched, wet-bed and vegetated points, interpolation of water surface and subtraction of estimated water depths	7.13c
	W2-4	Following removal of local elevation deviations based on coarse DEM surface, re-interpolation of water surface and subtraction of estimated water depths	7.13d
	W2-5	Following PCP-based correction for systematic error	7.1c
W3 (Feb 00 – May 00)	W3-1	Unprocessed	7.14
	W3-5	Following PCP-based correction for systematic error for photogrammetric DEM. Following removal of wet-bed and vegetated points, interpolation of water surface and subtraction of estimated water depths for ALS DEM.	7.1d

Table 7.17 Summary of all of the DEMs of difference assessed for errors. Those in bold are the final, post-processed DEMs that were analysed in 7.3.

(a) NA-1



(b) NA-2



Elevation difference (m)

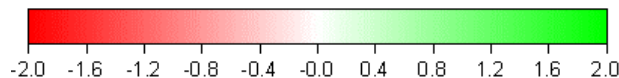


Figure 7.11 The North Ashburton (May 95 – Feb 99) DEMs of difference produced from DEMs at various stages of post-processing.

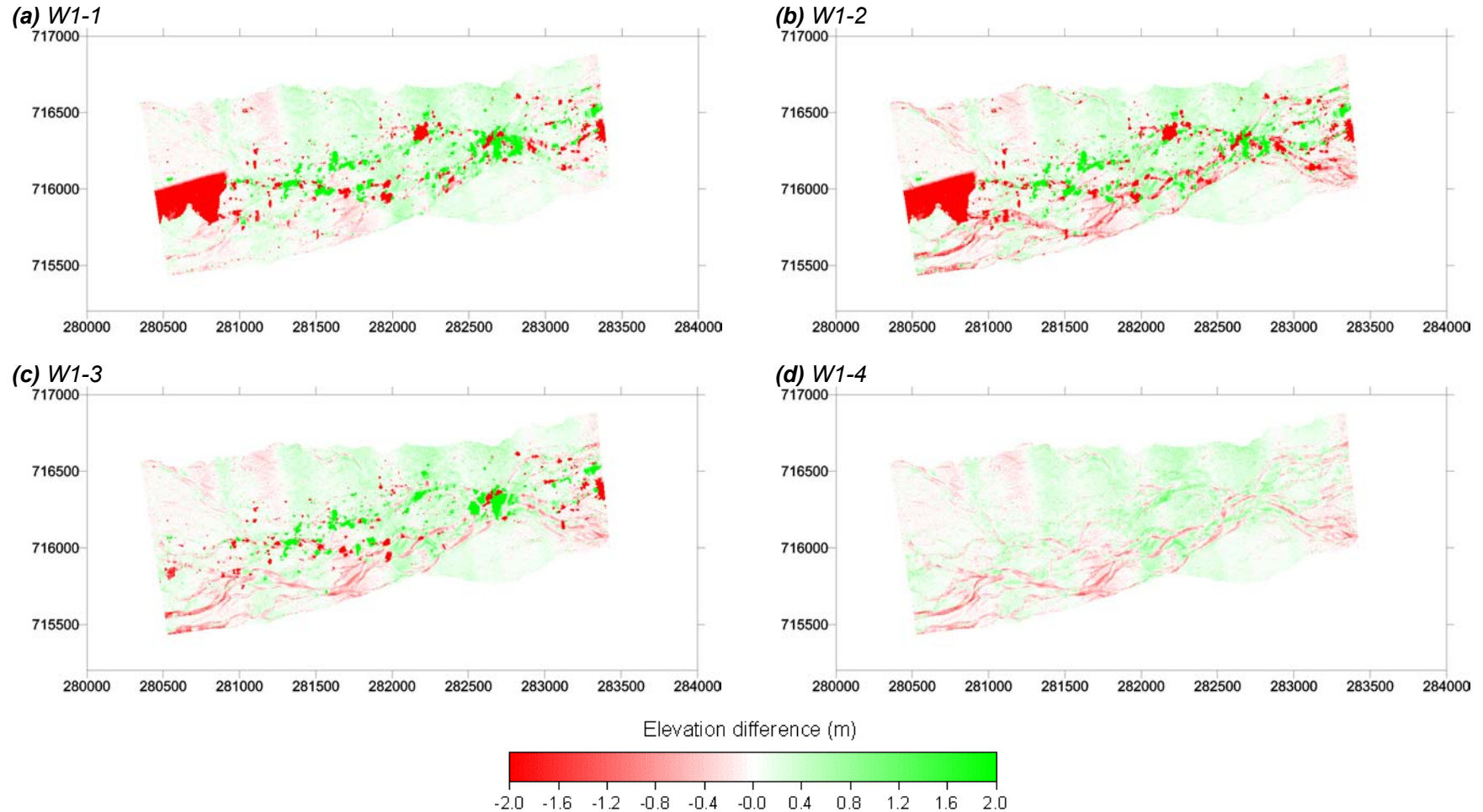


Figure 7.12 The W1 (Feb 99 – Mar 99) DEMs of difference produced from DEMs at various stages of post-processing.

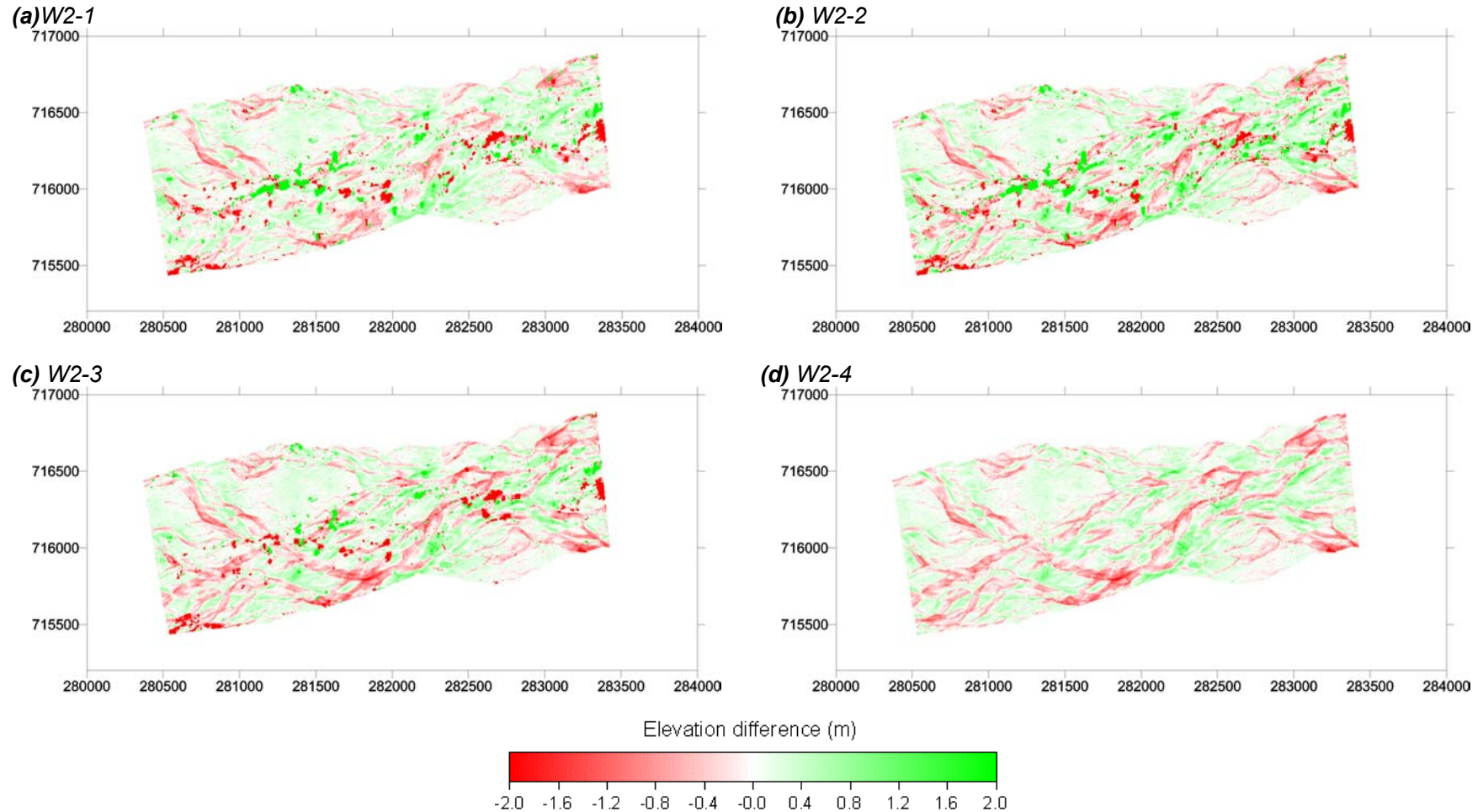


Figure 7.13 The W2 (Feb 99 – Feb 00) DEMs of difference produced from DEMs at various stages of post-processing.

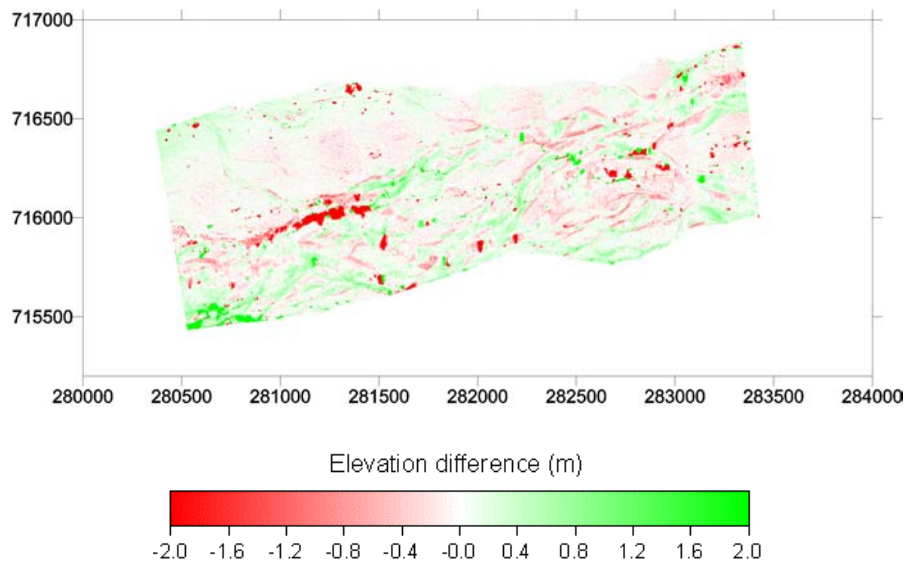


Figure 7.14 The W3-1 (Feb 00 – May 00) DEM of difference produced from unprocessed DEMs.

The effects of post-processing on the reach-aggregated volumetric estimates of cut and fill that can be derived from the DEM of difference surfaces are shown in **Table 7.19** and **Figure 7.15**. Again, the effect of post-processing on the North Ashburton DEM of difference is relatively small, although the volume of net aggradation observed is considerably increased. The effect of post-processing is much larger on the Waimakariri DEMs of difference, with the magnitude and direction of net change altered. The direction of change is particularly important if the DEM of difference is to be used to estimate sediment transport rate. From W1, the removal of unmatched, wet-bed and vegetated points (stage 3) and gross error removal (stage 4) produce the largest improvements in the quality of volume change information, relative to the post-processed DEM of difference surfaces. The same pattern is repeated for W2, although the relative improvement is smaller.

To assess the effect of post-processing on the quality of DEMs of difference more closely, the tests for gross error (**Section 7.3.4**), systematic error (**Section 7.3.5**) and random error (**Section 7.3.6**) were repeated for each of the DEMs of difference.

7.4.2 Gross error

First, gross error was identified using a variation of the error detection method developed by Felisicimo (1994). The results are presented in **Table 7.20**. For consistency, the local maximum expected error (MED_{local}) calculated from the post-processed DEMs (**Table 7.4**) were used for each DEM of difference at each stage of post-processing. The corresponding changes in volumes of cut and fill as a result of removal of the gross errors identified are summarised in **Table 7.21**.

DEM of difference	Global mean difference (m)	Global standard deviation of difference (m)	Minimum difference (m)	Maximum difference (m)
NA-1 (May 95 – Feb 99)	+0.012	0.325	-1.684	+2.316
NA-2 (May 95 – Feb 99)	+0.019	0.315	-1.133	+1.975
NA-3 (May 95 – Feb 99)	+0.024	0.324	-1.704	+1.959
W1-1 (Feb 99 – Mar 99)	-0.866	7.302	-105.800	114.670
W1-2 (Feb 99 – Mar 99)	-0.981	7.234	-105.800	114.670
W1-3 (Feb 99 – Mar 99)	+0.155	2.321	-63.483	+56.164
W1-4 (Feb 99 – Mar 99)	+0.072	0.286	-1.773	+1.876
W1-5 (Feb 99 – Mar 99)	+0.058	0.270	-1.665	+1.783
W2-1 (Feb 99 – Feb 00)	-0.017	3.343	-87.475	+95.450
W2-2 (Feb 99 – Feb 00)	+0.058	3.199	-87.475	+95.450
W2-3 (Feb 99 – Feb 00)	-0.010	2.083	-63.362	+75.703
W2-4 (Feb 99 – Feb 00)	-0.003	0.435	-2.622	2.476
W2-5 (Feb 99 – Feb 00)	+0.013	0.433	-2.478	+2.544
W3-1 (Feb 00 – May 00)	-0.022	2.147	-94.729	+88.054
W3-5 (Feb 00 – May 00)	+0.033	0.369	-1.994	+1.997

Table 7.18 Reach-averaged elevation change statistics for the post-processed DEMs of difference. Post-processed DEMs of difference are displayed in bold.

DEM of difference	CUT			FILL			NET CHANGE	
	Area (m ²)	Volume (m ³)	Reach-averaged (m ³ /m ²)	Area (m ²)	Volume (m ³)	Reach-averaged (m ³ /m ²)	Volume (m ³)	Reach-averaged (m ³ /m ²)
NA-1 (May 95 – Feb 99)	13957	3354	0.122	13610	3619	0.131	+265	+0.010
NA-2 (May 95 – Feb 99)	12952	3136	0.120	13272	3606	0.138	+471	+0.018
NA-3 (May 95 – Feb 99)	12824	3130	0.119	13382	3745	0.143	+614	+0.023
W1-1 (Feb 99 – Mar 99)	978386	3768358	1.294	1934606	1254255	0.431	-2514103	-0.863
W1-2 (Feb 99 – Mar 99)	1149378	3958911	1.359	1763479	1109381	0.381	-2849530	-0.978
W1-3 (Feb 99 – Mar 99)	1035333	556333	0.191	1877354	1008154	0.346	+451821	0.155
W1-4 (Feb 99 – Mar 99)	1012352	216198	0.074	1900277	425420	0.146	+209222	+0.072
W1-5 (Feb 99 – Mar 99)	1027033	21118	0.072	1885830	381408	0.131	+170290	+0.058
W1-1 (Feb 99 – Feb 00)	1192770	1153687	0.399	1699662	1105278	0.382	-48409	-0.017
W1-2 (Feb 99 – Feb 00)	1218863	1086792	0.376	1673571	1256227	0.434	169434	0.059
W1-3 (Feb 99 – Feb 00)	1310789	984961	0.341	1581513	693910	0.240	-291051	-0.101
W1-4 (Feb 99 – Feb 00)	1279046	482843	0.167	1613219	474467	0.164	-8377	-0.003
W1-5 (Feb 99 – Feb 00)	1266587	458581	0.157	1625786	496253	0.170	+37672	+0.013
W3-1 (Feb 00 – May 00)	1318654	653606	0.226	1573789	588459	0.203	-65147	-0.023
W3-5 (Feb 00 – May 00)	1285326	335255	0.115	1607054	430079	0.148	+94824	+0.033

Table 7.19 Reach-averaged volume change statistics derived from the DEMs of difference calculated from DEMs at various levels of post-processing (**Table 7.17**). Post-processed DEMs of difference are displayed in bold.

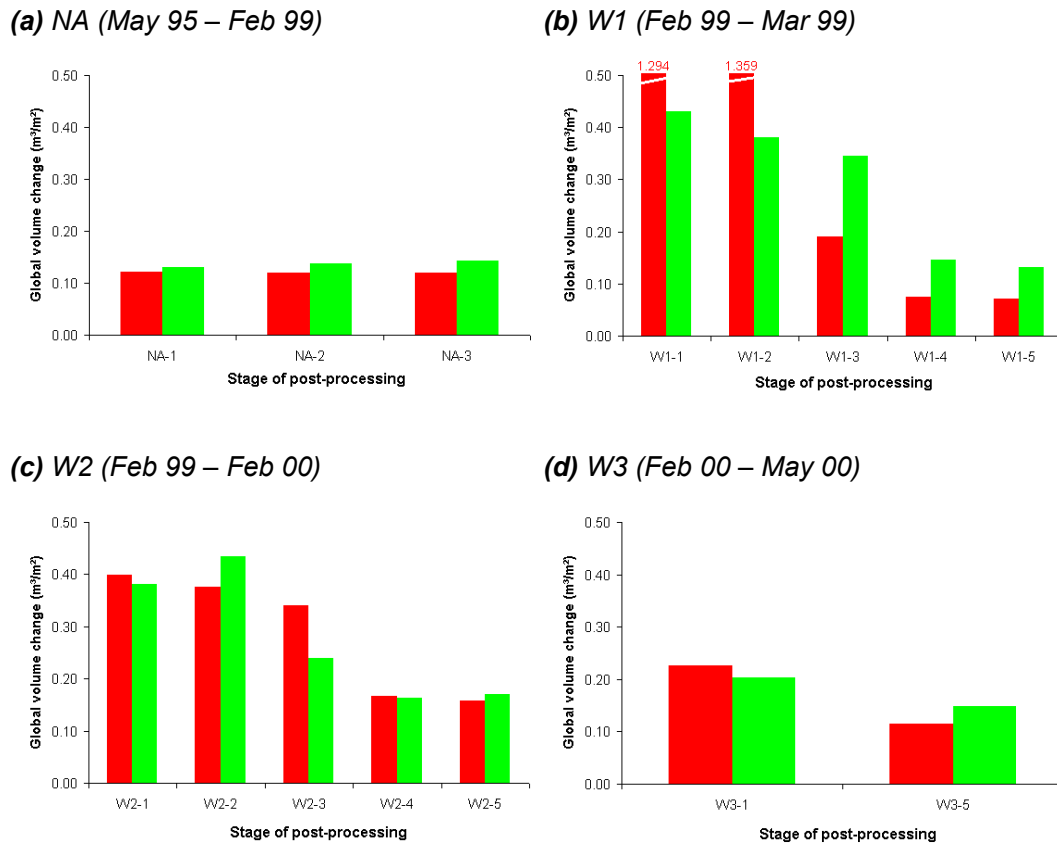


Figure 7.15 The effect of post-processing on the resultant DEMs of difference. Cut volumes are in red and fill volumes in green. Both are reach-averaged.

For the North Ashburton study reach, the improvements made to the riverbed DEMs have little effect in terms of both the number and volume of gross errors in the DEMs of difference. The number of points statistically identified as gross errors decreases following use of the refraction correction with default collection parameters, as does the volume of these errors. However, both values are increased when the refraction-correction is applied to DEMs generated using an increased maximum parallax parameter. Thus, this measure of the effect of using different DEM collection parameters suggests that the optimised parameter set actually decreases the reliability of resultant DEMs of difference with respect to gross errors. Nevertheless, the volumetric significance of the gross errors identified in the North Ashburton DEMs of difference is small, corresponding to less than 5% of the reach-averaged cut, fill and net change volumes (Table 7.21; Figure 7.16).

For the Waimakariri study reach, the positive effect of post-processing is far more apparent, with both the number (Table 7.20) and volume (Table 7.21) of gross errors considerably decreased. It is encouraging that the stage of post-processing which

aimed to identify and remove of gross errors in the riverbed DEMs (stage 4; **Table 7.17**) also produces the largest reduction in gross errors in the DEMs of difference. As expected, the post-processing stage which attempted to reduce systematic error (stage 5; **Table 7.17**) has little effect on gross error. The improvement in Waimakariri DEM of difference quality is highlighted by the decrease in the relative importance of gross errors in terms of total cut, fill and net change volumes (**Figure 7.16**). In the post-processed DEMs of difference, little more than 5% of total cut and fill volumes are attributable to gross errors.

For both reaches, the number of points that exceed the maximum expected error, relative to the total number of DEM points, is less than 6% even prior to post-processing (**Table 7.20**). This reinforces how the number of points effected by gross errors is small, and consequently how difficult their detection can be, particularly using manual methods.

7.4.3 Systematic error

The presence of systematic error in the DEMs of difference was assessed with reference to the three geomorphological assumptions detailed in **Section 7.3.5**. These make use of assumed wet-dry histories for the North Ashburton and Waimakariri study reaches (**Figure 7.2**) to designate areas where mainly erosion (dry-wet zones), mainly deposition (wet-dry zones) or little elevation change (dry-dry) is expected. Prior to the calculation of volumes of morphological change in each zone, gross error identified in **Section 7.4.2** was subtracted from the totals of cut and fill. This was done to remove the effects of gross error from those associated with systematic bias. As the aim of the analysis was to compare changes in cut and fill volumes between post-processing stages, rather than examine absolute values of cut and fill, the analysis was performed for the whole study reaches, despite the potential problems of applying the geomorphological assumptions at the reach-scale (**Section 7.1.5**). The calculated zone-averaged volumes of cut and fill for each DEM of difference are summarised in **Table 7.22** and **Figure 7.17**.

Overall, post-processing appears to have removed most systematic error from the DEMs of difference, particularly in the case of the Waimakariri DEMs of difference. For the North Ashburton, the changes brought about by post-processing are relatively small, although there is a net increase in cut volume in dry-wet zones (where erosion is assumed to be dominant; assumption 1) and a net increase in fill volume in wet-dry zones (where deposition is assumed to be dominant; assumption 2).

DEM of difference	MED_{local} (m)	Points < minimum MED_{local}	Points > maximum MED_{local}	Total exceedance (%)
NA-1 (May 95 – Feb 99)	±0.294	109	93	0.71
NA-2 (May 95 – Feb 99)	±0.294	70	94	0.58
NA-3 (May 95 – Feb 99)	±0.294	94	129	0.78
W1-1 (Feb 99 – Mar 99)	±0.279	46592	44185	3.12
W1-2 (Feb 99 – Mar 99)	±0.279	94004	78992	5.94
W1-3 (Feb 99 – Mar 99)	±0.279	54089	53057	3.68
W1-4 (Feb 99 – Mar 99)	±0.279	34307	29411	2.16
W1-5 (Feb 99 – Mar 99)	±0.279	32145	28653	2.15
W1-1 (Feb 99 – Feb 00)	±0.228	57540	52709	3.78
W1-2 (Feb 99 – Feb 00)	±0.228	67436	84060	5.20
W1-3 (Feb 99 – Feb 00)	±0.228	44731	46672	3.14
W1-4 (Feb 99 – Feb 00)	±0.228	17726	27564	1.55
W1-5 (Feb 99 – Feb 00)	±0.228	17123	28122	1.55
W3-1 (Feb 00 – May 00)	±0.276	28669	27965	1.94
W3-5 (Feb 00 – May 00)	±0.276	23284	17049	1.38

Table 7.20 Detection of gross errors in the DEMs of difference based on maximum expected local elevation difference.

DEM of difference	CUT		FILL		NET CHANGE	
	Volume loss (m ³)	Reach-averaged (m ³ /m ²)	Volume loss (m ³)	Reach-averaged (m ³ /m ²)	Volume (m ³)	Reach-averaged (m ³ /m ²)
NA-1 (May 95 – Feb 99)	66	0.002	78	0.003	+12	+0.001
NA-2 (May 95 – Feb 99)	41	0.002	73	0.003	+32	+0.001
NA-3 (May 95 – Feb 99)	61	0.002	113	0.004	+52	+0.002
W1-1 (Feb 99 – Mar 99)	584558	0.201	294498	0.101	-290060	-0.100
W1-2 (Feb 99 – Mar 99)	704461	0.242	294898	0.101	-409563	-0.141
W1-3 (Feb 99 – Mar 99)	119886	0.041	185406	0.064	+65520	+0.022
W1-4 (Feb 99 – Mar 99)	15532	0.005	14446	0.005	-1086	-0.000
W1-5 (Feb 99 – Mar 99)	15365	0.005	13967	0.005	-1398	-0.000
W1-1 (Feb 99 – Feb 00)	361212	0.124	253718	0.087	-107494	-0.037
W1-2 (Feb 99 – Feb 00)	315780	0.108	306059	0.105	-9721	0.003
W1-3 (Feb 99 – Feb 00)	173924	0.060	85871	0.029	-88053	-0.030
W1-4 (Feb 99 – Feb 00)	8915	0.003	16079	0.006	+7164	+0.002
W1-5 (Feb 99 – Feb 00)	8228	0.002	17075	0.006	+8441	+0.003
W3-1 (Feb 00 – May 00)	154664	0.053	122635	0.042	-32029	-0.011
W3-5 (Feb 00 – May 00)	11973	0.004	8092	0.003	-3881	-0.001

Table 7.21 Decrease in volumes of cut and fill following the removal of gross error and the effect on net volume change for DEMs of difference at various stages of post-processing (**Table 7.17**).

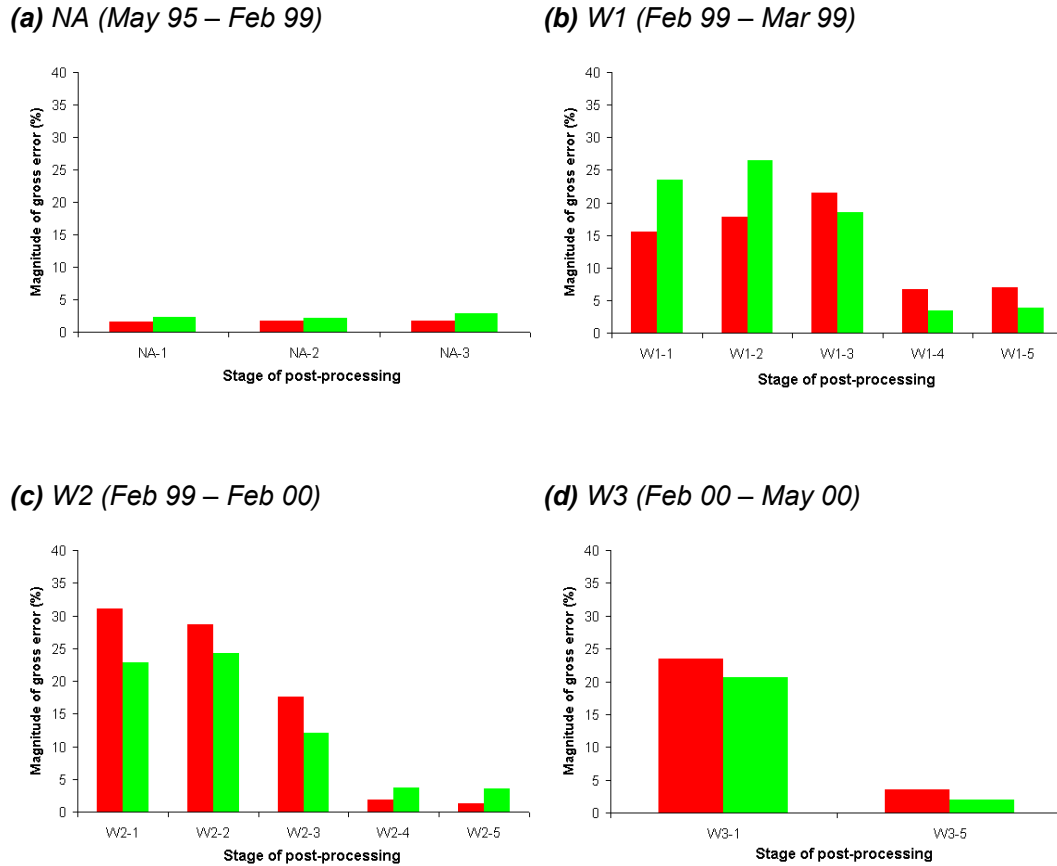


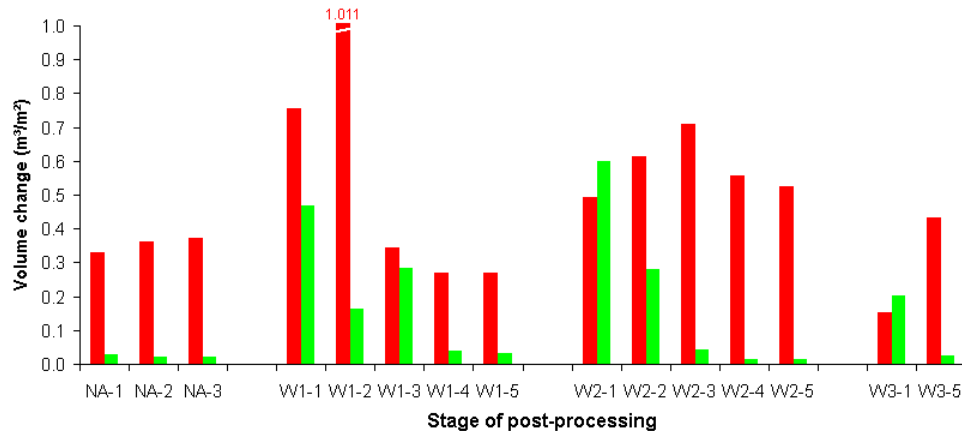
Figure 7.16 The volume of change associated with statistically-identified gross errors in the DEMs of difference at various stages of post-processing. Values are expressed relative to the total volumes of cut, fill and net change calculated from the corresponding DEM of difference surfaces (**Table 7.21**). Cut volumes are in red and fill volumes in green.

For the Waimakariri study reach, large systematic errors are present in unprocessed DEMs of difference with respect to all three assumptions: there is considerable fill in dry-wet zones (where erosion is assumed to be dominant; assumption 1); there is considerable cut in wet-dry zones (where deposition is assumed to be dominant; assumption 2); and there are relatively large volumes of both cut and fill in dry-dry zones (where little change is expected; assumption 3). Each deviation from the assumed state is reduced by post-processing.

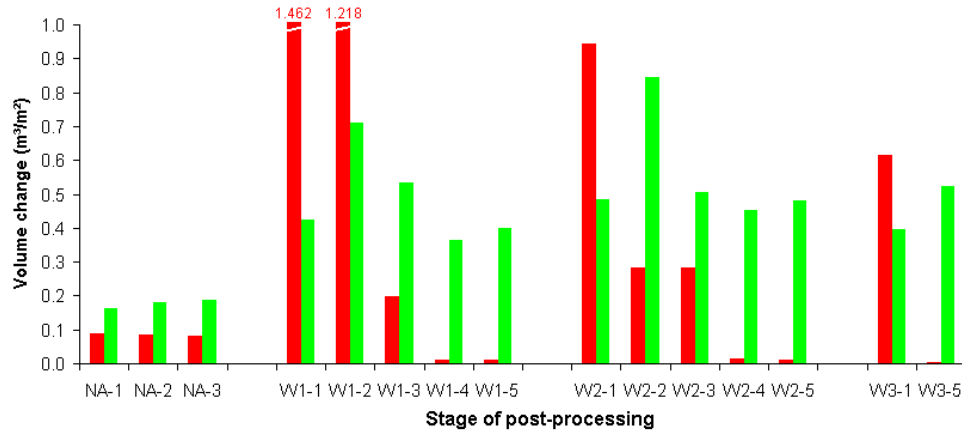
	DRY-DRY (ASSUMPTION 3)		DRY-WET (ASSUMPTION 1)		WET-DRY (ASSUMPTION 2)	
DEM of difference	Zone-averaged cut (m ³ /m ²)	Zone-averaged fill (m ³ /m ²)	Zone-averaged cut (m ³ /m ²)	Zone-averaged fill (m ³ /m ²)	Zone-averaged cut (m ³ /m ²)	Zone-averaged fill (m ³ /m ²)
NA-1 (May 95 – Feb 99)	0.126	0.109	0.331	0.029	0.089	0.162
NA-2 (May 95 – Feb 99)	0.125	0.113	0.362	0.022	0.084	0.179
NA-3 (May 95 – Feb 99)	0.125	0.112	0.374	0.022	0.083	0.188
W1-1 (Feb 99 – Mar 99)	1.034	0.217	0.757	0.469	1.462	0.423
W1-2 (Feb 99 – Mar 99)	1.034	0.214	1.011	0.163	1.218	0.711
W1-3 (Feb 99 – Mar 99)	0.073	0.213	0.345	0.283	0.199	0.532
W1-4 (Feb 99 – Mar 99)	0.028	0.144	0.271	0.038	0.012	0.365
W1-5 (Feb 99 – Mar 99)	0.027	0.124	0.271	0.032	0.011	0.401
W1-1 (Feb 99 – Feb 00)	0.219	0.277	0.494	0.600	0.943	0.486
W1-2 (Feb 99 – Feb 00)	0.153	0.214	0.612	0.279	0.283	0.844
W1-3 (Feb 99 – Feb 00)	0.150	0.191	0.807	-0.053	0.291	0.499
W1-4 (Feb 99 – Feb 00)	0.098	0.148	0.555	0.013	0.013	0.453
W1-5 (Feb 99 – Feb 00)	0.094	0.151	0.526	0.015	0.011	0.481
W3-1 (Feb 00 – May 00)	0.140	0.134	0.153	0.202	0.615	0.397
W3-5 (Feb 00 – May 00)	0.059	0.098	0.433	0.026	0.005	0.525

Table 7.22 Volume change statistics derived from the DEMs of difference at various stages of post-processing divided by wet-dry history zone. Data have been colour-coded to reflect the geomorphological assumption to which they most closely relate.

(a) NA (May 95 – Feb 99)



(b) W1 (Feb 99 – Mar 99)



(c) W2 (Feb 99 – Feb 00)

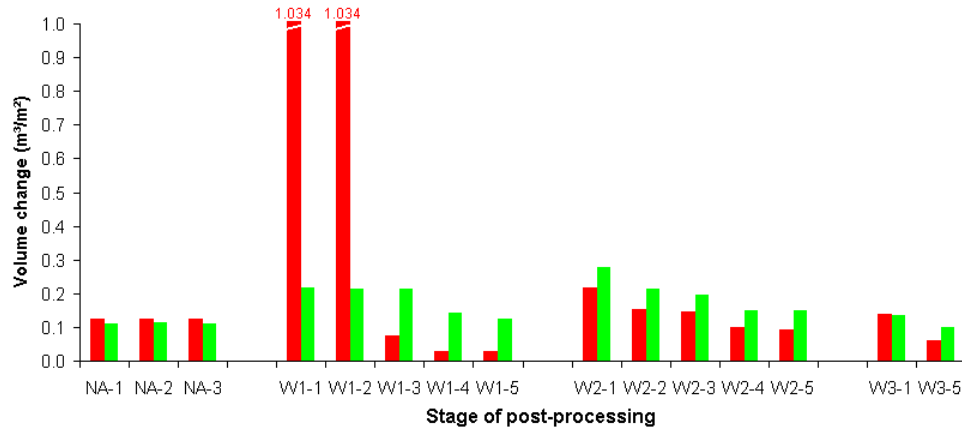


Figure 7.17 Comparison of cut (red) and fill (green) volumes for the reach-scale DEMs of difference at various stages of post-processing with respect to the three geomorphological assumptions.

This analysis also highlights an interesting theoretical issue. The main difference between the unprocessed (**Figures 7.12, 7.13 and 7.14**) and post-processed (**Figure 7.1**) Waimakariri DEMs of difference is the presence of relatively small areas of erroneously high elevation change. Given that the background change in the DEMs of difference at all stages of post-processing is little different from that observed in the post-processed DEMs of difference, the large discrepancies in observed volumes of change suggests that these erroneous values are influencing calculation, despite the prior elimination of gross errors from the cut and fill volumes. Thus, the distinction between point or small-area gross error (as detected by the gross error assessment method; **Section 7.3.4**) and relatively small areas of systematic error has started to break down.

7.4.4 Random error

As before, the importance of random error in the DEMs of difference was assessed using the concept of a minimum level of detection (LOD_{min}). The probabilistic approach was chosen but, because the main aim of the analysis was to compare the effects of different stages of post-processing on a given DEM of difference rather than to examine actual information loss, this choice is not significant. The method used was identical to that employed for the post-processed DEMs of difference (**Section 7.3.6**), with a t statistic calculated from the ratio of elevation change at a point and LOD_{min} value (**Equation 7.4**). This was then used to define the confidence with which the elevation change could be assumed to be real, and the elevation change value was scaled accordingly. For t values greater than 1.96 ($\rho < 0.05$), morphological change was assumed to be real and values were scaled by 1.0 (**Table 7.23**). As compared to analysis of the post-processed DEMs of difference, we can have less confidence in the identification of random error, due to the possible presence of systematic error in some of the DEMs of difference (**Figure 7.17**). As some systematic errors are thought to be linked to areas of erroneously high elevation change, absolute values of cut and fill information lost should not be affected, because these focus on small elevation changes. However, it could lead to under-estimation of the relative effect of random error as compared to total volumes of change.

The estimation of information loss due to random error was carried out on the DEMs of difference at various stages of post-processing using two values of LOD_{min} : those obtained from the theoretical precision of the DEM surfaces; and those calculated from overlap analysis. For consistency, the LOD_{min} values calculated from the post-processed DEMs of difference were used in each case (**Table 7.23**). These represent

the best estimate of the true precision of the DEMs of difference, and so should give the best indication of information loss due to random error.

DEM of difference	Theoretical precision (m)	Overlap analysis precision (m)
NA (May 95 – Feb 99)	±0.086	±0.260 ^a
W1 (Feb 99 – Mar 99)	±0.090	±0.259
W2 (Feb 99 – Feb 00)	±0.090	±0.261
W3 (Feb 00 – May 00)	±0.115	±0.281

^a Assumed value based on Waimakariri overlap analysis.

Table 7.23 Values of LOD_{min} used to examine information loss due to random error in the DEMs of difference at various stages of post-processing.

The results, in terms of absolute information loss for each DEM of difference, are summarised in **Table 7.24** and **Figure 7.18**. As compared with gross and systematic error, post-processing appears to have relatively little effect on the importance of random error in the resultant DEMs of difference. This is not surprising, since random error is inherent in the data acquisition methods used, and this cannot be reduced by *post priori* manipulation of the datasets. For the Waimakariri DEMs of difference, the information loss due to random error slightly increases as a result of post-processing. This is thought to result directly from the elimination of gross errors. Where gross errors are identified and removed (as local elevation deviation from a coarser DEM surface; **Section 6.2.8**), the resulting gaps in the digital riverbed surface are filled by interpolation. This will introduce random error in the form of interpolation uncertainties. Thus, although the level of gross error is reduced, it is likely to be at the expense of an increase in random error. However, the increase in reach-averaged information loss due to post-processing is small, totalling less than $0.005 \text{ m}^3/\text{m}^2$ in each case.

7.4.5 Conclusions

In this section, the error assessment methods developed in **Section 7.3** were used to determine the effect of the post-processing procedures developed in previous chapters upon gross errors, systematic error and random error in the resultant DEMs of difference. For the North Ashburton DEM of difference, correction for refraction and subsequent post-processing had relatively little effect on the quality of DEMs of difference. For the Waimakariri DEMs of difference, it was found that the gross and systematic error were present in unprocessed DEM of difference surfaces. However, the post-processing procedures did successfully identify and eliminate these errors. As

a result, the information loss due to random error slightly increased, since the process of gross error removal led to uncertainties introduced by the interpolation required to fill in gaps in terrain.

DEM of difference	LOD _{min} PREDICTED FROM THEORETICAL PRECISION		LOD _{min} PREDICTED FROM OVERLAP ANALYSIS	
	Reach-averaged loss of cut volume (m ³ /m ²)	Reach-averaged loss of fill volume (m ³ /m ²)	Reach-averaged loss of cut volume (m ³ /m ²)	Reach-averaged loss of fill volume (m ³ /m ²)
NA-1 (May 95 – Feb 99)	0.004	0.004	0.029	0.026
NA-2 (May 95 – Feb 99)	0.004	0.004	0.028	0.027
NA-3 (May 95 – Feb 99)	0.004	0.004	0.028	0.027
W1-1 (Feb 99 – Mar 99)	0.003	0.007	0.015	0.038
W1-2 (Feb 99 – Mar 99)	0.003	0.007	0.015	0.034
W1-3 (Feb 99 – Mar 99)	0.004	0.007	0.017	0.036
W1-4 (Feb 99 – Mar 99)	0.004	0.007	0.018	0.039
W1-5 (Feb 99 – Mar 99)	0.005	0.007	0.018	0.039
W1-1 (Feb 99 – Feb 00)	0.003	0.005	0.019	0.031
W1-2 (Feb 99 – Feb 00)	0.003	0.004	0.017	0.029
W1-3 (Feb 99 – Feb 00)	0.003	0.004	0.018	0.029
W1-4 (Feb 99 – Feb 00)	0.003	0.005	0.019	0.030
W1-5 (Feb 99 – Feb 00)	0.003	0.004	0.019	0.030
W3-1 (Feb 00 – May 00)	0.008	0.009	0.027	0.033
W3-5 (Feb 00 – May 00)	0.007	0.009	0.024	0.031

Table 7.24 Calculation of information loss relative to total cut and fill volumes for the corresponding DEM of difference (**Table 7.17**) for each predicted LOD_{min} value, using a probabilistic approach.

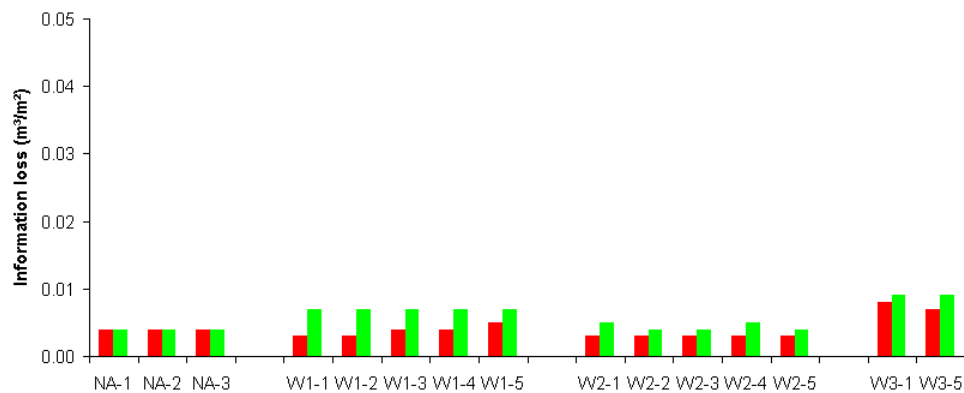
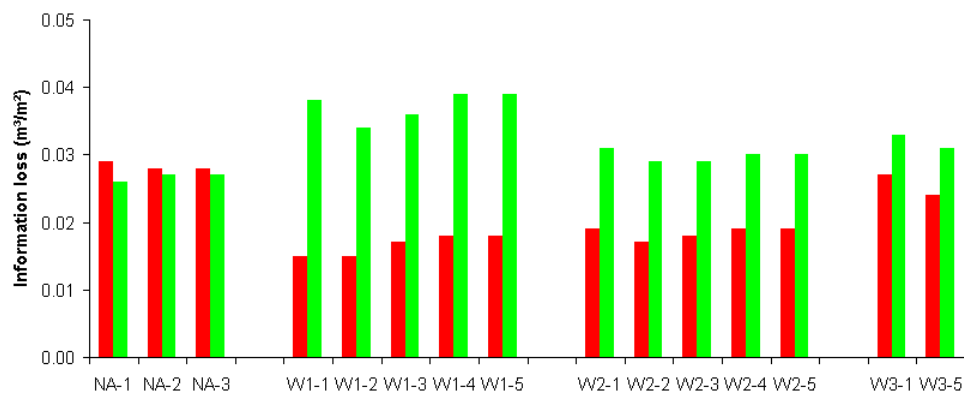
(a) LOD_{min} calculated from theoretical precision(b) LOD_{min} calculated from overlap analysis

Figure 7.18 Loss of cut (red) and fill (green) volumes for DEMs of difference at various stages of post-processing for different LOD_{min} values.

7.5 Comparison with conventional survey methods

7.5.1 Rationale

Section 7.4 has demonstrated that the automated post-processing methods developed and applied in Chapters 4 and 6 appear to produce a reduction in gross and systematic error, with only marginal increase in random error. However, in terms of comparing the utility of terrestrial and remote sensing methods, the magnitude of these errors is less important than the extent to which they are propagated into useful derived parameters (Lane, 2000; Wise 2000). In the case of river monitoring, a commonly-used parameter is mean bed level and bed level change. This is traditionally obtained using terrestrially-surveyed cross-sections of gravel-bed rivers, and is used as the basis for river management of the Waimakariri and North Ashburton Rivers (e.g. Griffiths, 1979; Reid and Poynter, 1982; Blakely and Mosley, 1987; Griffiths, 1993; Connell, 2001). Given a relatively wide spacing between successive cross-sections (successive profiles

are typically positioned at least two active riverbed widths apart; Blakely and Mosley, 1987), it is uncertain how reliably morphological change can be measured using this survey strategy.

Thus, the DEMs of difference obtained using digital photogrammetry and ALS were analysed to estimate the effect of cross-section spacing on the morphological change that can be recovered from the study reaches. This allows two issues to be investigated. First, it gives an indication of the relative quality of morphological information derived using remote sensing methods compared to that which might be expected from a traditional cross-section based survey strategy. Second, it allows a method of assessing the effect of post-processing on the quality of parameters derived from the DEM of difference surfaces.

7.5.2 Method

For a regularly-gridded DEM of a riverbed, the average elevation (\bar{z}_i) for a given cross-section (i) is given as

$$\bar{z}_i = \frac{\sum_{j=1}^n z_j}{n} \quad (7.5)$$

where j is the cross-sectional position and n is the number of points measured in the cross-stream direction. Thus, the mean bed level for an entire reach (MBL) is given as

$$\text{MBL} = \frac{\sum_{i=1}^m \bar{z}_i}{m} \quad (7.6)$$

where m represents the number of cross-sections used. To determine morphological change from a DEM of difference, the same method is used. Hence, average cross-sectional elevation change ($\Delta\bar{z}_i$) for cross-section i is given as

$$\Delta\bar{z}_i = \frac{\sum_{j=1}^n \Delta z_j}{n} \quad (7.7)$$

and the change in mean bed level (ΔMBL) is given as

$$\Delta\text{MBL} = \frac{\sum_{i=1}^m \Delta\bar{z}_i}{m} \quad (7.8)$$

This method was used to sample the unprocessed and post-processed DEMs of difference. It was implemented in two stages: calculation of cross-stream averaged bed

level change (**Equation 7.7**); and simulation of the effect of different cross-section spacings (**Equation 7.8**).

The first step involved calculation of average elevation change ($\Delta\bar{z}$; **Equation 7.7**) for each cross-section of the DEMs of difference using the Spatial Modeller module of Imagine. At each cross-section (i.e. each row of cells in the raster image), the elevation change was summed and divided by the number of cells in the image. As Spatial Modeller is primarily designed for use in a raster environment, cross-stream averaging could only be performed in the X- or Y-direction. This required the Waimakariri DEMs of difference to be re-oriented, such that flow was orthogonal to one of these directions. This was achieved by using the geometric correction process available in Imagine to effect a clockwise rotation of 9.5° which oriented the riverbed in an east-west direction. Data was re-sampled to a regular grid using bilinear interpolation. A consequence of this was that the (X, Y) datum information was lost. The North Ashburton DEM of difference was already oriented due north-south so needed no further treatment.

The second stage was the simulation of the effect of different cross-section spacings upon the detected change in mean bed level (ΔMBL ; **Equation 7.8**). This was performed using an automated routine which used the cross-section average elevation change data series to calculate the reach-averaged change in mean bed level that would be calculated for the reaches for a given cross-section spacing. First, the cross-section average elevation change data series were detrended, as analysis of this kind requires stationary data (Davis, 1986). The minimum cross-section spacing (and maximum number of cross-sections, m_{\max}) was defined by the DEM point spacing (i.e. 1 m). The maximum cross-section spacing (and minimum number of cross-sections, m_{\min}) was set as half of the DEM of difference downstream length: 198 m for the North Ashburton; and 1507 m for the Waimakariri.

Calculation of change in mean bed level proceeded within a downstream window equal in length to the maximum cross-section spacing. This was placed at a random location within the DEM of difference cross-section elevation change data series. This process was repeated multiple times for each cross-section spacing in order to reduce and to quantify the effects of sampling error. For consistency, the same number of repetitions were used for each reach, despite their vastly different sizes. Thus, 150 repetitions were used (set as around ten times less than the Waimakariri maximum cross-section spacing).

The results of this analysis allow two particular issues to be investigated. First, by applying the analysis to post-processed DEMs of difference, it permits determination of the influence of cross-section spacing on mean bed level changes. Second, by

performing the analysis on unprocessed and post-processed DEMs of difference, it allows further visualisation and quantification of the effect of the post-processing methods used.

7.5.3 *Effect of cross-section spacing*

First, the post-processed DEMs of difference were analysed. Two results are produced by the simulation. The first is the change in mean bed level (ΔMBL), which represents the spatially-averaged elevation change determined from a given cross-section spacing. It is presented in **Figure 7.19** as the difference from the mean bed level change calculated from the minimum cross-section spacing of 1 m. This is analogous to systematic error, and so indicates the relative accuracy (or bias) of the bed level change measurement made using a given cross-section spacing. The second result is the standard deviation of reach-averaged change in mean bed level calculated from the repetitions made for each cross-section spacing. It is presented in **Figure 7.19** as the difference from the standard deviation calculated from the minimum cross-section spacing of 1 m. This represents sampling error (or sensitivity) associated with the choice of cross-section location for a given cross-section spacing.

The simulation of the effect of cross-section spacing shows how the systematic error generally increases as the cross-section spacing is increased. For the Waimakariri River, the post-processed DEMs of difference show a consistent pattern (which in itself suggests that the post-processing has been successful). In each case both the systematic error and sensitivity due to sampling is low and tends to zero. However, above cross-section spacings of around 100 m, large deviations become clear. The deviations are particularly large for the calculated standard deviation value, suggesting that the detected change in mean bed level becomes increasingly sensitive to the choice of cross-section location at spacings of 100 m or more. Thus, for the typical cross-section spacing used for long term river monitoring (500-800 m; Griffiths, 1993; Hicks *et al.*, 1999b), significant differences start to be produced between the detected and true pattern of bed level change. These correspond to relatively large values of reach-aggregated volumetric error (**Table 7.25**).

For the North Ashburton River, deviation from zero error occurs at a cross-section spacing of only 10 m. This is interesting, as it suggests that the cross-section spacing required to detect mean bed level change accurately (less than 10 m) is less than that required to depict static mean bed level accurately (less than 50 m; calculated in the mean bed level analysis in **Section 4.7.1**). At wider spacings, the relative systematic error increases, producing large aggregated volumetric errors (**Table 7.25**). The standard deviation value associated with the North Ashburton River actually decreases

to a minimum at a cross-section spacing of around 80 m. This suggests that the calculation of change in mean bed level is least sensitive to cross-section location for cross-sections spaced this distance apart. This is perhaps linked to a typical length scale of morphological change in the reach, which potentially has very important implications for river monitoring strategy.

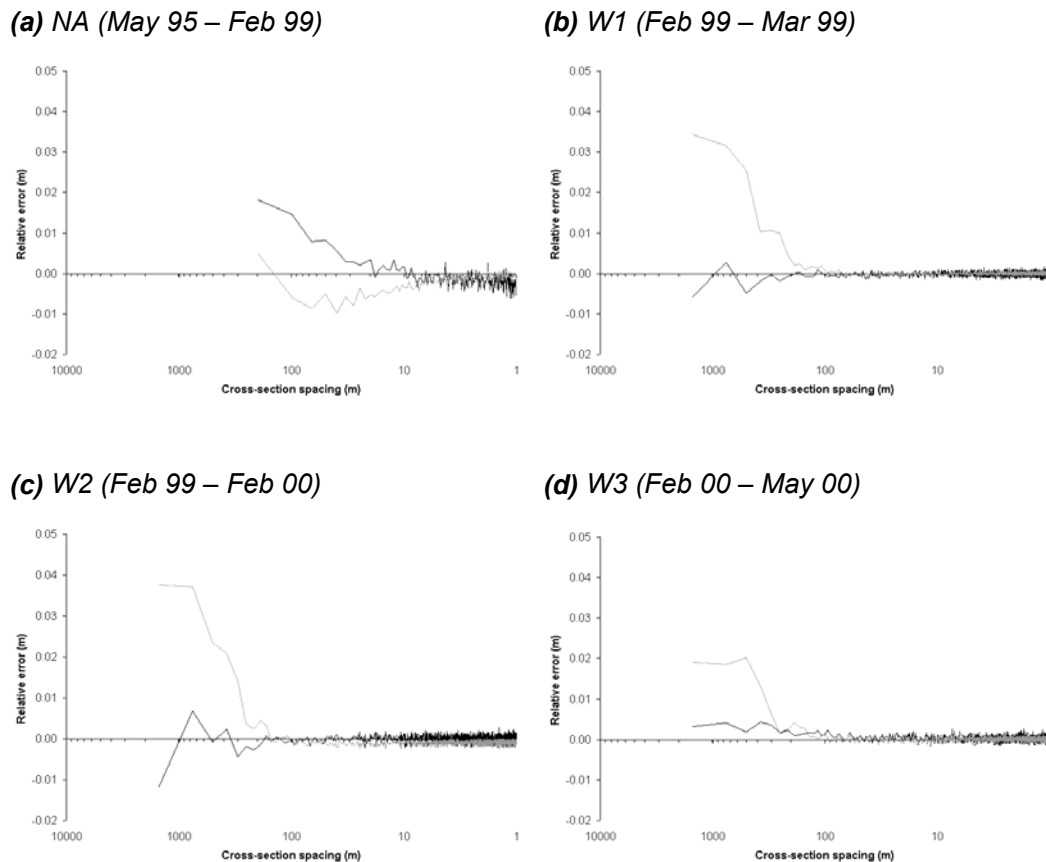


Figure 7.19 The results of mean bed level change analysis using various cross-section spacings for each post-processed DEM of difference. Mean bed level change is plotted in black. The standard deviation of mean bed level change calculations for a given cross-section spacing are plotted in grey. Both are relative to the value calculated using the minimum (1 m) cross-section spacing.

Furthermore, for both study reaches, widely-spaced cross-sections may actually change the direction of morphological change observed. For two post-processed DEMs of difference (W1 and W2), at certain cross-section spacings, the reaches are perceived to experience net degradation, although smaller cross-section spacings suggest net aggradation (Table 7.25). The reverse is true for DEM of difference NA. This is also significant with respect to the management of gravel-bed rivers based on conventionally surveyed (and widely-spaced) cross-sections.

	NA (May 95 – Feb 99)	W1 (Feb 99 – Mar 99)	W2 (Feb 99 – Feb 00)	W3 (Feb 00 – May 00)				
Approximate downstream spacing (m)	Reach-aggregated volume change (m^3)	Relative error in volume (m^3)	Reach-aggregated volume change (m^3)	Relative error in volume (m^3)	Reach-aggregated volume change (m^3)	Relative error in volume (m^3)	Reach-aggregated volume change (m^3)	Relative error in volume (m^3)
1	-1252	-	+9710	-	+25638	-	-37583	-
2	-1323	-71	+9090	-620	+26066	+428	-37787	-204
5	-1313	-61	+11907	-2197	+25192	-446	-33126	+4457
10	-1264	-12	+7129	-2581	+28997	+3359	-37845	-262
50	-926	+326	+9536	-174	+21501	-4137	-36185	+1398
100	-797	+455	+10022	+312	+23074	-2564	-34670	+2913
200	+129	+1381	+7691	-2019	+17888	-7750	-30649	+6934
500	n/a	n/a	+17364	+7654	+45196	+19558	-25609	+11974
750	n/a	n/a	-6934	-16644	-8332	-33970	-28173	+9410
1500	n/a	n/a	+12236	+2526	-10751	-36389	-3991	+33592

Table 7.25 A comparison of sediment storage volumes obtained from uncorrected and corrected photogrammetry, and from evenly-spaced cross-sections, as with a conventional monitoring programme. Error in volume is unsigned and determined with respect to the storage volume calculated from the entire ground survey data-set.

7.5.4 Effect of post-processing

The final aspect of the bed level change analysis was an examination of the effect of post-processing. **Figure 7.20** shows a comparison of the same cross-section spacing simulation results for both unprocessed and post-processed DEMs of difference. For the Waimakariri, the post-processing reduces both the magnitude of mean bed level change and its sensitivity to location of cross-sections used in its calculation, particularly for W1. The post-processed values are negligible in comparison, especially at small cross-section spacings. For the North Ashburton, post-processing has little effect on either mean bed level change or its sensitivity. The results from both study reaches support the quality assessment of DEMs of difference at different stages of post-processing undertaken in **Section 7.4**.

7.6 Chapter summary

This chapter has investigated the feasibility of employing riverbed DEMs derived using digital photogrammetry and ALS (**Chapters 4 and 6**), to calculate morphological change in the study reaches. This calculation is required as a fundamental step in the estimation of sediment transport rate, which is the ultimate aim of the morphological method. In this chapter, morphological change information was used in three ways.

First, the feasibility of using sequential DEMs acquired using remote sensing methods to quantify morphological change for large, gravel-bed rivers was assessed. Based on the assessment of gross, systematic and random error, it appears that the remote sensing methods tested (digital photogrammetry and ALS) do allow collection of sequential DEMs of sufficient quality to permit measurement of morphological change in gravel-bed river environments. However, consideration of the potential effect of random error showed that initial survey design must be informed by the required minimum elevation changes that must be detected so that information loss due to random error can be minimised.

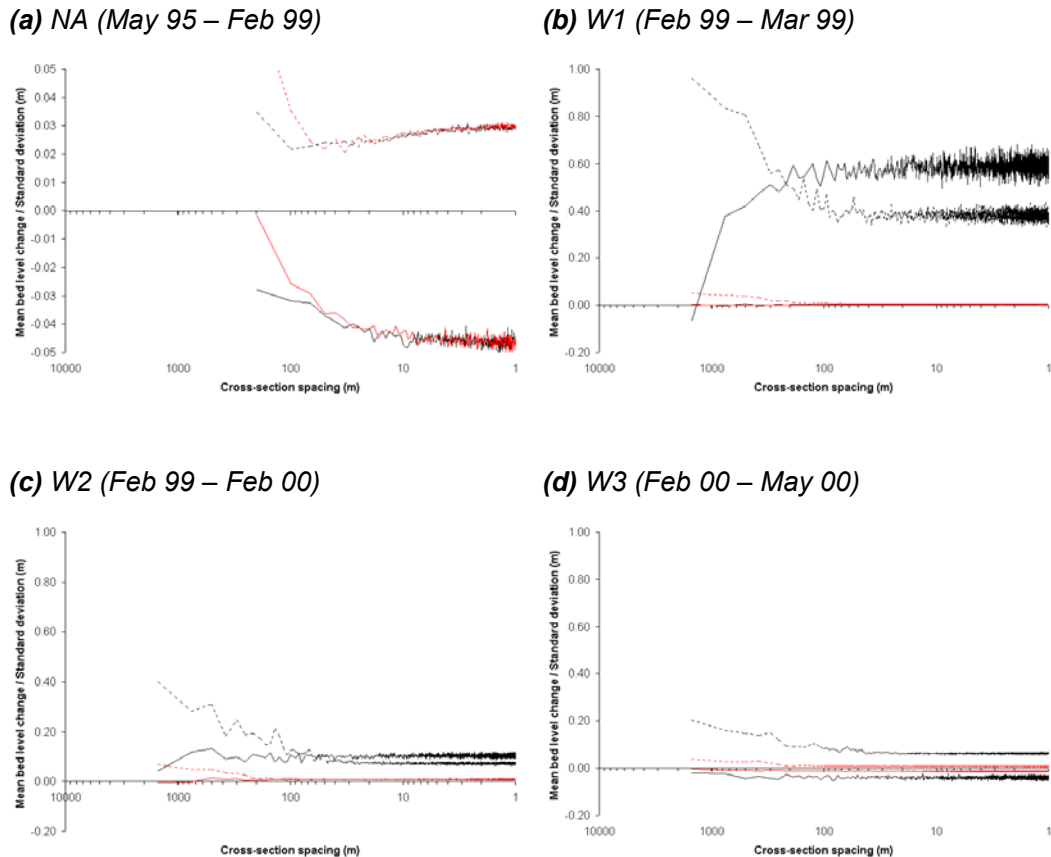


Figure 7.20 The results of mean bed level change analysis using various cross-sections spacings for each unprocessed (black) and post-processed (red) DEM of difference. Mean bed level change is plotted in solid lines. The standard deviation of mean bed level change calculations for a given cross-section spacing are plotted in dashed lines.

Second, the effect of post-processing was examined. Assessment of gross, systematic and random error suggested that considerable improvements were made to the DEM of difference surfaces by post-processing, particularly in terms of gross error removal. A consequence of this was a slight, but inevitable, increase in random error. The refraction-correction developed for the North Ashburton River made little difference to the quality of DEMs of difference, suggesting that for shallow, clear-water rivers, morphological change can be detected from unprocessed digital photogrammetry.

Third, the morphological change information was used to simulate the error arising from the use of cross-sectional surveys, as are currently used to monitor the North Ashburton and Waimakariri Rivers. For the Waimakariri River it was found that systematic error and sensitivity to choice of cross-section location both tended to zero below cross-section spacings of around 100 m. At wider spacings, relatively large

errors were found to occur. For the North Ashburton River, the critical cross-section spacing was around 10 m, although the sensitivity was minimised with a cross-section spacing of around 80 m. Mean bed level change analysis also provided an additional method for assessing the effect of post-processing. This supported the earlier findings that in the case of the Waimakariri River, post-processing is essential to remove errors in the DEM surfaces derived using digital photogrammetry and ALS.

CHAPTER 8. CONCLUSIONS

*Based on the results achieved and experience gained from application of digital photogrammetry and airborne laser scanning to two large, gravel-bed rivers, this chapter concludes this thesis. Following a brief summary of the thesis structure (8.1), the research objectives presented **Chapter 1** are re-visited (8.2). Next, the overall project aim - to assess the ability of remote sensing techniques to measure the riverbed morphology of large, gravel-bed rivers - is re-addressed (8.3). Finally, the research is critically evaluated and possible directions for further work are identified (8.4).*

8.1 Introduction

The importance of topographic representation in many areas of contemporary fluvial geomorphology and river management places great importance on the quality of morphological data acquired. Limitations associated with conventional terrestrial survey techniques have prompted alternative methods to be sought. Remote sensing technologies now permit automated collection of high spatial resolution topographic data over large spatial areas at relatively low financial cost. However, there has been uncertainty as to whether remote sensing data collection methods are suitable for large, gravel-bed river environments, due to the unique characteristics of these areas. These include small vertical relief relative to spatial extent and the presence of distributed, shallow, surface water.

The overall aim of this study was to investigate whether two remote sensing techniques, digital photogrammetry and airborne laser scanning (ALS), can be used to survey large, gravel-bed rivers, by their application to two study reaches located on the Canterbury Plains, New Zealand. **Chapter 2** placed this research in context by reviewing data acquisition and data quality issues. Past applications of aerial imagery, photogrammetry and ALS in river environments were reviewed, and consideration was given to remote measurement of submerged topography using image analysis and through-water photogrammetry methods. Three types of error were introduced: systematic, random and gross. These were subsequently related to potential sources of error and assessment of DEM quality.

The substantive findings of this work were presented in **Chapters 3 to 7**. **Chapter 3** was primarily concerned with the project design necessary for both digital photogrammetric and ALS survey of large, gravel riverbeds. **Chapter 4** described the application of digital photogrammetric survey to the North Ashburton study reach, and the development of an automated refraction correction algorithm and post-processing

routine to increase DEM quality. **Chapter 5** described the estimation of water depth where water is more turbid, using an empirically-derived relationship between pixel colour and water depth. In **Chapter 6**, the depth estimates made for the much larger Waimakariri study reach were incorporated within dry-bed surveys made using digital photogrammetry and ALS. For digital photogrammetric survey, the importance of post-processing was demonstrated, which allowed an increase in DEM quality in both dry-bed and wet-bed areas. **Chapter 7** was concerned with assessing the feasibility of using the post-processed riverbed DEMs of the North Ashburton and Waimakariri study reaches to determine volumetric change.

8.2 Research objectives re-visited

Following the results presented in previous chapters, and based on wider experience gained while undertaking this work, the research objectives explained in **Section 1.3** are now re-visited.

8.2.1 Objective (i): to establish the research design necessary to yield topographic information from large, gravel riverbeds with a quality that allows channel morphology and morphological change to be determined;

Project design is a critical aspect of any topographic survey. Large, gravel riverbeds, where there is typically a marked disparity between spatial area and vertical relief, represent an extreme case. Project design is crucial to ensure data is collected with sufficient density and quality to allow recovery of the key riverbed features. Conventional terrestrial survey methods often allow a reactive research design, with a survey strategy that is able to be changed during data collection (e.g. point density varied to reflect field experience of surface features). This may not be the case for repeat monitoring where uncertainties may arise if the same points are not re-surveyed (Ashmore and Church, 1998). However, the use of remote sensing methods to obtain topographic data, particularly when data is to be acquired from specially-commissioned flights, has highlighted the importance for *a priori* mission planning (Wolf and Dewitt, 2000; Lane, 2001). Acquisition of data using digital photogrammetric or ALS survey usually requires a large initial outlay (i.e. the financial cost of the flight) which it is often impractical or impossible to repeat. Consequently, the flight specifications must be correct given the aims of the project, as these will define the maximum level of data quality obtained. For both digital photogrammetry and ALS, survey planning is centred around the inevitable trade-off that occurs between the lower flying heights desirable for maximising point density, and hence optimising feature representation, and the

higher flying heights preferable for reducing data volume and financial cost (Lane, 2000).

In terms of digital photogrammetry, survey strategy should be informed by the level of precision desired (Lane, 2001), both for static DEM surfaces and based on the propagation of random errors if sequential DEMs are to differenced. The theoretical vertical precision of photogrammetrically-derived elevations is equivalent to the object-space pixel size, and is dependent on both image scale (and hence flying height) and the scanning resolution used to convert hard-copy photographs in to digital images (**Equation 2.1**). For a given vertical precision, the flying height and scanning resolution should be set so as to minimise data volume and financial cost.

The North Ashburton study reach is small enough to permit total coverage in one photograph overlap at a scale of 1:3000, which was sufficient to give the desired theoretical precision (**Section 3.3.2**). For study reaches of similar area, this situation is considered preferable. Not only did this reduce the financial cost associated with acquiring digital images (i.e. purchasing the diapositives and paying for scanning to convert them to digital form), but it also reduced data volume, decreased block triangulation time and removed the need to merge multiple DEMs.

The Waimakariri study reach is much larger, necessitating the acquisition of multiple photographs (**Section 3.3.2**). With an image scale of 1:5000, 16-18 photographs were required to cover the study reach. Using an image scale of 1:4000, 24 were needed. The increased data volume is potentially problematic, as each digital image must be loaded in turn to define the image-space position of the fiducials and photo-control points during the block triangulation phase. In the case of the 1:4000 images, given a single image digital file size of around 255 Mb, and a corresponding reduced resolution image (RRDS) of 85 Mb, this required upwards of 8000 Mb (around 8 gigabytes) of storage space if all images were to be held on a hard drive simultaneously. In practice, the least squares bundle adjustment solution only requires the RRDS files to be present, but this still required around 2000 Mb (around 2 gigabytes) of storage space. Increasing the image scale also meant that more DEM joins were necessary in the final reach-scale DEM surface. Furthermore, based on the banding effect identified in **Section 6.2.10**, increasing the number of joins may potentially reduce overall DEM quality, even if the theoretical precision of each individual DEM tile is improved.

Perhaps the most significant conclusion in relation to survey design for acquiring topographic data from gravel riverbeds using digital photogrammetry is the importance of retaining image texture in the source imagery. Conventionally, the change in

expected photogrammetric precision for a given change in object-space pixel size can be readily quantified (using **Equation 2.1**). However, if image texture is reduced or lost, the automated stereo-matching algorithm will match fewer points, and DEM precision will decrease by a greater and unknown amount. In the case of gravel riverbeds, image texture is present in the form of individual cobbles. If the source imagery is at a scale such that this texture is not clearly visible, final DEM quality will inevitably be reduced by a greater amount than would be predicted from consideration of image scale and scanning resolution alone. This effect was clearly noticeable with regard to the North Ashburton and Waimakariri digital photogrammetric surveys (**Figure 3.12**). From the theoretical precision estimates (**Equation 2.1**), the North Ashburton May 1995 survey was approximately equal to that associated with the February 1999 and March 1999 Waimakariri photogrammetric surveys (**Table 3.4**). However, the far superior image texture of the North Ashburton May 1995 images, meant that around twice as many dry-bed points were successfully stereo-matched (**Tables 4.10** and **6.2**), relative to riverbed area. Consequently, based on comparison with independent check points, the final dry-bed SDE for the May 1995 North Ashburton DEM was less than half that calculated for the February 1999 and March 1999 Waimakariri DEMs (**Tables 4.11** and **6.6**). Likewise, from calculation of theoretical precision alone, the February 2000 Waimakariri DEM should have been around 20% more precise than either the February 1999 or March 1999 Waimakariri photogrammetric analyses (**Table 3.4**). However, the increase in scale improved image texture sufficiently such that final dry-bed SDE was halved. The improvement in dry-bed precision is particularly important if the DEMs are to be differenced, as it will determine the minimum level of detection of derived DEMs of difference (Brasington *et al.*, 2000) and hence the information loss that may occur.

From this discussion, it would appear that image scale alone is the most important determinant of photogrammetric precision. However, the North Ashburton aerial photographs from February 1999, obtained at the same scale as the May 1995 imagery and scanned at around two times the resolution, produced images with much less texture (**Figure 3.12**). The effect on final DEM precision cannot be assessed because no independent check-point measurements were made in dry-bed areas, although 10% fewer dry-bed points were successfully stereo-matched (**Table 4.10**) and wet-bed precision was considerably higher than its May 1995 value (**Table 4.11**). This implies that lighting conditions at the time of exposure and the scanning process itself are also potentially important factors. The sensitivity of image texture also suggests the presence of a threshold, above which image texture is rapidly lost. The magnitude of such a threshold will be dependent on gravel size, but for the grain size distributions

measured for the North Ashburton and Waimakariri study reaches (d_{50} of approximately 0.03 m; Laronne and Duncan, 1992; Carson and Griffiths, 1989), it would appear to fall somewhere around an image scale of 1:4000.

For the ALS survey of the Waimakariri study reach, the desired average point spacing of 1 m was achieved by using a swathe width of 575 m (meaning three flight lines were necessary to span the riverbed) and by repeating the survey three times (**Section 3.4.3**). This gave around 1.8 million dry-bed points in the study reach, and a final average dry-bed point spacing of 1.6 m. As a comparison, using digital photogrammetric survey of the same study reach, dry-bed points were successfully stereo-matched with an average spacing of 2.2 m (February 1999), 2.0 m (March 1999) and 1.7 m (February 2000). During the North Ashburton photogrammetric analysis, dry-bed points were successfully stereo-matched with an average spacing of 1.4 m (May 1995) and 1.5 m (February 1999). The direct relationship between point spacing and DEM precision (from comparison with independent check data; **Tables 4.11** and **6.6**) suggests that the density and distribution of points used to generate the DEM surface is an important factor behind differences in overall DEM quality. There appears to be a threshold above which DEM precision rapidly deteriorates, presumably as a specific scale of morphological detail is lost (*cf.* Lane, 1998). For the study reaches examined here, this appears to occur at and above point spacings of 2 m.

Another feature of the ALS survey was the difference between riverbed surfaces generated from each of the three repeat surveys. Overlap analysis demonstrated considerable variation in point elevations, with a systematic negative bias in the third survey and an average standard deviation of difference of over 0.20 m (**Table 6.9** and **Figure 6.10**). Thus, although a decrease in average point spacing was achieved, it was only achieved with a potential loss in precision (due to intra-survey variations) in the reach-scale final DEM surface.

Project design has clearly been demonstrated to be important in the case of remote measurement of larger gravel-bed rivers. Following a decrease in surface quality above average point spacings of 2 m, this is proposed as a an important recommendation for topographic surveys of large, gravel-bed rivers. Thus, future digital photogrammetric and ALS surveys should ideally be designed so as to provide measurements spaced less than 2 m apart. In the case of digital photogrammetry, this point spacing could traditionally be achieved by setting the image scale and scanning resolution to suitable values. However, this research has shown that a third parameter, image texture, is also important. As image scale is decreased, the texture visible from exposed gravel surfaces decreases, and is eventually lost. Thus, the automated stereo-matching

algorithm successfully matches fewer points, and the actual point spacing is increased from its theoretical value. Thus, it is likely that the precision of the resultant DEM surface is also decreased, relative to its theoretical value, due to interpolation uncertainties associated with the creation of a continuous raster DEM surface from fewer point elevations.

8.2.2 Objective (ii): to develop and to apply procedures for dealing with the presence of water on the riverbed

Two approaches have been developed and applied to recover submerged topography. For the North Ashburton River, the water is clear and the bed is clearly visible on vertical aerial photographs at low flows. In the clear-water case, through-water photogrammetry was used (e.g. Fryer, 1982; Butler *et al.*, 2001b), with an automated *post priori* method developed to geometrically-correct elevation based on assumed refraction at an air-water interface (**Figure 4.3**). Although the quality of wet-bed points was improved by the refraction-correction, particularly for the May 1995 survey when river stage was higher, wet-bed representation in the final DEM surfaces contained systematic error and had a SDE around half that of dry-bed areas (**Table 4.11**).

The quality of photogrammetrically-measured underwater points seemed to be critically related to the depth of water (**Figure 4.18**). Where there was no water or where water was very shallow (less than about 0.2 m), the mean errors associated with refraction-corrected and post-processed photogrammetric DEMs were low and not that different to those in exposed parts of the riverbed (**Table 4.11**). As water depth increased, ME tended to increase. Consequently, the application of through-water digital photogrammetry in river environments depends on both the range of water depths at the time of photography and on the point quality required. Braided, gravel-bed rivers tend to have shallow, distributed flow, making them ideal for two-media photogrammetric survey, particularly at low flows.

The more-turbid water common at low flows in the Waimakariri River obscures the submerged bed in vertical aerial photographs, and meant that remote sensing technologies had to be abandoned in wetted areas. Instead, empirical water colour – water depth relationships (e.g. Winterbottom and Gilvear, 1997; Gilvear *et al.*, 1998) were successfully adopted to obtain estimates of water depth (**Figure 5.4**). The accuracy of depth estimates (in terms of ME) was found to be high (as would be expected from an empirical relationship), while the precision of depth estimates (in terms of SDE) was little different to that obtained from digital photogrammetric measurements of the exposed areas of riverbed. The nature of the multivariate

equation and the range of depths for which the method can be used were both found to be determined by water turbidity at the time of photography. The maximum predictable depth and the success of the method (in terms of R^2) are similar to those obtained in other studies that have estimated water depth from standard aerial photographs (e.g. Winterbottom and Gilvear, 1997). Paradoxically, a higher turbidity appeared to give more reliable results, particularly where black and white imagery was used (**Table 5.4**), although this clearly limits the range of depths that can be estimated.

A systematic trend was detected for the two 1999 Waimakariri estimated depth maps cases: the depth of shallow water was consistently over-estimated and the depth of deep water consistently under-estimated (**Figure 5.5**). At the reach-scale, these errors largely cancel out (giving a low global ME). At channel-scales, they may lead to considerable discrepancies in water volume. It is suggested that this is due to a combination of a biased surveyed depth data-set, in terms of spatial and depth distribution, and the use of two flying lines. For the February and May 2000 photographic surveys, when a more representative calibration water depth dataset and single flying line were used, the effect was much less pronounced.

A novel aspect of this work was the subsequent conversion of water depths to submerged topography by modelling a water surface elevation map based on water edge elevations derived from digital photogrammetric (**Section 6.2.11**) and ALS (**Section 6.3.2**) measurements in dry-bed areas. Assessment of final wet-bed quality suggested that a systematic error remains in wet-bed elevations for all Waimakariri DEMs except the May 2000 survey (**Table 6.6**), suggesting that the ALS survey better represents water edge zones (from which the water surface is interpolated). The precision with which underwater elevations are estimated is relatively low compared to the riverbed relief, although it is similar to that associated with remote survey of dry-bed areas in the February 1999 and March 1999 DEMs.

The ability to remotely survey water depths at a high spatial resolution over large spatial scales is potentially a very powerful tool. However, the real utility associated with these methods is that they provide synoptic water depth information at a comparable spatial scale and density as can already be obtained using other dry-bed remote survey methods (e.g. digital photogrammetry and ALS). This brings much closer the prospect of remote survey of entire large, gravel riverbeds. Using both approaches, the quality of single depth estimates using remote survey is less than would be obtained using conventional depth measurement techniques. However, the spatial area that can be covered is potentially much greater. Thus, the total uncertainty may be similar or even less than that associated with conventional depth mapping of

large braided rivers at the reach-scale. Furthermore, by integrating elevation errors across the whole riverbed, the weighting associated with wet-bed point errors is decreased (e.g. **Figure 4.19** and **Table 6.8**), since relatively little of the riverbed is inundated at the time of image acquisition.

8.2.3 Objective (iii): to evaluate the quality of surface representation of digital terrain models of braided, gravel riverbeds produced using digital photogrammetry and airborne laser scanning.

Surface quality was assessed using a variety of methods. The most common and only truly independent method is to compare DEM elevations with ground survey measurements (Torlegard *et al.*, 1986). Thus, the collection of elevation data using a method with a known higher order of quality should form an integral aspect of any study that develops remote sensing for topographic data acquisition.

The ground survey of check point measurements was critical to this research, since it permitted an independent assessment of DEM quality. Nonetheless, difficulties were encountered in terms of the spatial distribution of data collected for the Waimakariri study reach: data was spatially clustered both at the bar-scale (predominantly along the water edge) and reach-scale (concentrated in particular areas of the reach) (**Figure 6.26**). Consequently, the confidence that the observed discrepancies between surveyed and DEM points are representative of the whole DEM surface is reduced (**Wise, 2000**).

In terms of identifying errors in a DEM surface, an optimum check point survey strategy could aim for an even distribution of check points across the entire area of interest, with greater concentration of points in areas where higher DEM quality is required (i.e. in this case, water edge locations). The potential importance of being able to assess spatially-varying systematic error was highlighted by the improvements in DEM quality that were achieved by adjusting the final Waimakariri DEM surface based on elevation discrepancies identified from photo-control points (PCPs) (**Section 6.2.12**). Similar assessments using independent check measurements were not possible, for either the digital photogrammetric or ALS dry-bed surveys.

To identify gross error and larger-scale random error, independent check point measurements are less suitable. This was highlighted in **Section 4.7.2**, where an area of erroneously low elevation was produced when the DEM collection parameters were changed from their default values. Identification of this area was only achieved using the derived parameter of water depth. Similarly, in the case of the Waimakariri River, gross error was also more readily identified though a derived parameter: interpolation

of water surface elevation. In this case, the modelled water surface elevation highlighted gross error (**Figure 6.13**), which had not been indicated by comparison with check point data (**Table 6.4**).

The potential utility of overlap analysis was also demonstrated (**6.4.3**) for both digital photogrammetric and ALS survey. The results of overlap analyses suggested that the random error associated with ALS survey was larger than that associated with digital photogrammetry (**Tables 6.9** and **6.10**). This would be expected from the theoretical precision calculated for each survey method. However, it was the opposite of the pattern suggested by independent check measurements (**Table 6.6**).

8.2.4 Objective (iv): to develop and to apply automated post-processing procedures to identify and eliminate errors from topographic surfaces obtained using remote sensing methods, and to assess their effectiveness at improving final DEM quality.

Following digital photogrammetric survey of both the North Ashburton and Waimakariri study reaches, gross error was present in the raw DEM surfaces (**Figures 4.15** and **6.7**). In the case of the North Ashburton, this error corresponded to areas where the ideal geometry of through-water photogrammetry broke down due to its application in a field setting and the associated lack of control over factors such as water surface and lighting conditions. Previous close-range applications have been able to exercise far greater control over the conditions at the time of exposure (e.g. Fryer, 1982; Fryer and Kniest, 1984; Butler *et al.*, 2001b). Thus, post-processing was developed as an integral part of the automated refraction correction procedure (**Figure 4.3**), identifying points where it was assumed that the submerged bed had not been seen, based on elevation deviation from the modelled water surface and lateral distance from the wetted channel edge. This correction improved the wet-bed representation of both photogrammetric surveys of the North Ashburton study reach (**Table 4.11**), particularly for February 1999 when river discharge was especially low. In dry-bed areas, the North Ashburton raw DEMs did not require post-processing.

For the Waimakariri digital photogrammetric DEMs, a greater amount of post-processing was required to deal with frequent gross errors in the raw DEMs. Given the spatial extent and number of points involved, it was important that this should be automated as far as possible. Areas of gross error were found to correspond broadly to the location of wetted channels (**Figure 6.7**), although their influence extended beyond the bounds of the channels themselves. This supports the findings of Reid (2001) that the quality of riverbed DEM surfaces is reduced close to wetted channels. Yet, it is

particularly important that the areas proximal to wetted channels were well represented in the DEM surface, since these areas were used to derive the modelled water surface elevation map, and so in part determined the quality of the entire wet-bed. An automated post-processing routine was developed which removed points that: (i) were not successfully stereo-matched; (ii) were classified as either wet-bed or vegetation; and (iii) were greater than a given tolerance level different to a coarser-resolution DEM of the same area (**Figure 6.22**). In terms of visual appearance (**Section 6.4.1**), comparison with independent check data (**Table 6.5**), and based on assessment of error in the DEMs of difference (**Table 7.16** and **Figure 7.20**), the post-processing routine was judged to have successfully removed most gross error from the Waimakariri DEM surfaces.

Subsequently, a further correction based on the known positions of the PCPs was applied to the photogrammetrically-derived DEMs of the Waimakariri study reach. This was found to reduce systematic bias in the final DEM surface (**Table 6.5**), and also appeared to reduce the apparent banding effect (**6.2.10**) found in this study and elsewhere (e.g. Stojic *et al.*, 1998; Ashmore, 2001) when multiple low-relief DEMs are joined (Lane *et al.*, in prep). The magnitude of banding was also reduced by the *a priori* addition of tie-points during the exterior orientation phase of photogrammetric block creation (**Table 3.9**). In addition, there appears to be a relationship between the quality of vertical correspondence between overlapping individual DEM and the image scale used in the photogrammetric analysis. From overlap analysis of the Waimakariri photogrammetric surveys, the potential magnitude of banding was reduced when image scale was increased from 1:4000 to 1:3000 (**Table 6.9**).

8.2.5 Objective (v): to evaluate the reliability of estimates of volumes of erosion and deposition inferred from remotely-sensed digital elevation models of large, gravel-bed rivers, and hence to assess the feasibility of using morphological methods to estimate sediment transport rate.

One of the largest potential benefits of using remote sensing methods to obtain high spatial resolution topographic data is the ability to produce sequential DEMs in order to visualise and quantify morphological change (Lane, 1998). In river environments, this permits the employment of morphological methods of estimating sediment transport from channel change (Ashmore and Church, 1998). However, in common with other derived parameters (Ley, 1986; Wise, 1998; Lane, 2000), calculation of morphological change is sensitive to errors in the DEM surfaces used. Thus, DEM quality determines both the quality of DEMs of difference produced, and the subsequent quality of volumetric change and sediment transport calculations.

Despite the sensitivity of DEMs of difference to errors in the DEM surfaces used to create them, the difficulty in obtaining independent check data relating to morphological change makes rigorous testing problematic. Thus, in order to assess the feasibility of the North Ashburton and Waimakariri DEMs of difference, new approaches needed to be developed. The reliability of the DEMs of difference was assessed with reference to gross error (Cooper and Cross, 1988). These were defined by point deviation from the elevation change value expected given the morphological observed in surrounding DEM points (Felicísmo, 1994; **Section 7.3.4**). The accuracy of the DEMs of difference was assessed in terms of systematic bias (Cooper and Cross, 1988). This was achieved by making geomorphological assumptions regarding the expected nature of morphological change in certain zones of the study reaches (**Section 7.3.5**). Deviation from the three expected cases of dominant erosion, dominant deposition and no change indicated systematic error. The precision of the DEMs of difference, or the magnitude of random error (Cooper and Cross, 1988), was examined in terms of the minimum level of detection (LOD_{min}) possible given the precision of the input DEM surfaces (Brasington *et al.*, 2000). Unlike gross and systematic error, random error cannot be removed from a DEM surface. This meant that the information loss as a result of random error was an important consideration. This was quantified using two approaches: (i) deterministic (**Section 7.3.7**), which only considered elevation changes greater than the minimum level of detection in volumetric calculations; and (ii) probabilistic (**Section 7.3.8**), which considered all elevation changes, but gave less weight to smaller elevation changes in volumetric calculations.

From the error assessment, the detection of morphological change from the post-processed DEMs of difference was found to be feasible. The volumetric significance of gross error was unimportant (**Table 7.5**), little systematic bias was found at either reach (**Figure 7.4**) or local (**Figure 7.6**) scales, and the information loss associated with random error at the reach scale was relatively small using both approaches (**Figure 7.8**), depending on the LOD_{min} value used. However, the analysis also highlighted the importance of post-processing, without which meaningful morphological change calculations were not possible for the Waimakariri DEMs of difference (**Figure 7.12** and **Figure 7.13**). For the North Ashburton DEM of difference, refraction-correction and post-processing had little effect in terms of the quality of DEMs of difference.

Calculation of DEMs of difference also allowed the change in mean bed level to be calculated (**Figure 7.19**), which represents a second derivative of the initial DEM surfaces. Based on random sampling of the DEMs of difference using different cross-section spacings, it was demonstrated that the reliability morphological change inferred

from widely-spaced cross-sectional surveys is poor, and could lead to potentially large volumetric discrepancies at the reach-scale (**Table 7.25**).

8.3 Research aim revisited

The overall aim of this research was:

to assess the ability of remote sensing, based upon digital photogrammetry and airborne laser scanning, to measure the morphology of large, braided, gravel-bed rivers with sufficient quality to allow changes in bed morphology in space and time to be detected.

Both digital photogrammetry and ALS have been shown to be capable of producing high spatial resolution DEMs of large, gravel-bed rivers. The riverbed DEMs demonstrate complex braidplain morphology not readily observable using traditional, terrestrial, survey techniques (**Figures 4.17** and **6.20**). Furthermore, the quality of the DEMs was sufficient to allow morphological changes to be detected with enough reliability, accuracy and precision to allow volumetric calculations to be made. This suggests that sediment transport rates may also be estimated.

The amount of post-processing required for each technology varied considerably. The ALS data provided for the Waimakariri study reach required no further post-processing, other than the incorporation of the estimated submerged bed. However, it was unclear how much post-processing had taken place before the taken was provided. The level of post-processing required for digital photogrammetric data varied between the two study reaches. For the North Ashburton River, dry-bed areas needed no post-processing, although some was undertaken in wetted areas. For the Waimakariri River, gross error was present in the raw DEM surfaces, which was only removed following significant post-processing.

An important aspect of this research has been the integration of dry-bed and wet-bed surveys. For clear-water, through-water digital photogrammetry was shown to have much potential for direct remote measurement of submerged topography. For more turbid water, water depths estimated using image analysis were successfully integrated with dry-bed survey data to provide a DEM of the entire study reach. In both cases, knowledge of the water surface was required. This was achieved by interpolating water edge points, measured as part of the dry-bed survey, across wetted channels. This clearly places great importance on the accuracy of water edge points, and on the ability of post-processing to remove errors in these areas.

8.4 Wider implications

Ultimately, the quality of individual point measurements made using both digital photogrammetry and ALS is likely to be less than that associated with conventional surveying techniques such as levelling or Total Station survey. In part, this is because the inherent data quality of remote sensing methods remains lower, although this is likely to change as technological developments occur (e.g. large format digital cameras, improved ALS hardware, superior stereo-matching and post-processing algorithms, combined digital photogrammetric-ALS survey). However, it is also because remote measurements lead to an inevitable loss of direct human evaluation of each measurement that is made (Lane, 2001). This may also be significant in terms of the location of each measurement, as remotely-sensed data collection is not informed by topographic features.

In river environments, the most important consideration in terms of the current quality of remote measurements is how the reduced point quality associated with digital photogrammetry and ALS compare with the bias imparted by traditional, terrestrial survey of widely-spaced cross-sections. The movement from traditional cross-sectional survey to remote survey using digital photogrammetry and ALS dramatically increases the spatial density of points measured. Thus, it is important to assess whether the gains in terms of data coverage and density outweigh the losses in data quality associated with each point measurement. This situation is more complex in the case of gravel riverbeds, due to the further reduction in data quality associated with submerged topography. Thus, the relative proportions of wet-bed and dry-bed areas also become significant (although the quality associated with traditional survey of underwater points is also likely to be reduced). This suggests that to obtain the maximum benefit associated with remote measurement, surveys should take place at low flows.

In this context, the analysis of mean bed level for the North Ashburton study reach (**Figure 4.19**) and the simulation of mean bed level change from the DEMs of difference (**Figure 7.19**) perhaps represent the most important results of the research. In the case of mean bed level, the net error of conventional survey methods and digital photogrammetry were found to be approximately equal at cross-section spacings of around 50 m. Thus, at cross-section spacings smaller than this, conventional survey would be expected to give higher quality mean bed level calculations. At wider cross-section spacings, digital photogrammetry with refraction-correction in wetted channels, should give better results.

In the case of mean bed level change, large deviations from the mean bed level change calculated from the DEM of difference occur at cross-section spacings of 10 m

(for the North Ashburton) and 100 m (for the Waimakariri). This suggests the cross-sectional spacing required to indicate change in mean bed level is around five times less than that required to represent static bed morphology. Thus, despite the additional uncertainties related to the differencing of DEM surfaces, conventionally-surveyed cross-sections would need to be even more closely-spaced to give the same net error as associated with digital photogrammetry and ALS.

It is also important to consider the wider applicability of the methods used to derive DEM surfaces in this research. In dry-bed areas, the post-processing routines that were developed for the Wiamakariri riverbed DEMs (**Figure 6.22**) were designed specifically for large, relatively flat, gravel-bed rivers. Thus, it is unlikely that they will be as effective in other environments. For example, comparison of different resolution DEM surfaces to highlight the presence of gross error (**Section 6.2.8**) presupposes that natural local topographic variation will be less than the tolerance level used to detect erroneous elevations. In environments with larger local variation (i.e. roughness), this approach is unlikely to be suitable, even if the tolerance level is increased. In this case, elevation highs and lows would both be highlighted as areas of error and subsequently smoothed. Thus, these post-processing methods may not be as suitable in areas where topographic variation is higher (e.g. Deroose *et al.*, 1998; Lane *et al.*, 2000) or where relative vertical relief is greater (e.g. Butler *et al.*, 1998).

In wet-bed areas, the methods of deriving submerged topography are also landform-specific. Both through-water photogrammetry and image-analysis methods, require relatively clear, shallow water such that the bed is visible. Furthermore, the interpolation of water surface elevation will only be successful where there are correct dry-bed points at or near the water surface elevation on both sides of wetted channels. Where there are vertical channel banks, the water surface may be incorrectly modelled from the bank-tops, leading to systematic positive bias of water surface and submerged bed elevations. In some areas of the Waimakariri study reach, this was a potential weakness. One possible solution is the manual addition of breaklines at the water edge to constrain the interpolated water surface elevation surface. Attempts were made towards achieving this by using the stereo-viewing capabilities of the Professional version of OrthoMAX (available at the University of Leeds) to interrogate the individual sparse DEM surfaces manually, and to modify the elevation of points which appeared incorrect. Based on a small sub-area of the Waimakariri February 1999 DEM surface, the benefits of this approach, as compared with the automated post-processing routine, were minimal. This is because the stereo-viewer only allows the scanned images to be viewed in stereo. These typically contain a image-space pixel size that is up to two

orders of magnitude greater than the grain size of the source hard-copy photographs. Thus, it becomes relatively difficult for a human operator to correctly position the elevation of corresponding image points, particularly in areas of poor photographic contrast. The use of analytical photogrammetry (which is based on stereo-viewing of original hard-copy images) might improve this situation, but would dramatically reduce the speed with which DEMs could be generated (Chandler, 1999).

8.5 Critical review and future research

This research has represented a first attempt at using digital photogrammetry and ALS to survey large, braided, gravel-bed rivers. Consequently, there are a number of aspects of this work that could have been carried out differently, and which now represent potential future avenues of research.

First, project design has been shown to exert a critical control over the quality of terrain representation obtained. This is particularly important with regard to digital photogrammetric survey. The theoretical precision of digital photogrammetry is determined by the image scale and scanning resolution used (**Equation 2.1**). Thus, given a standard scanning resolution, a relatively stable relationship should be obtained between image scale used and the derived DEM stereo-matching performance and precision. However, in the case of gravel riverbeds, this was not the case due to variable image texture (**Figure 3.12**), mainly due to the outline of individual particles becoming indistinct. The point at which this occurs will be affected by image scale, scanning resolution and the gravel particle size distribution. Thus, more work is needed to assess the relationship between image scale, scanning resolution, image texture and DEM quality for photographs of coarse gravels.

Second, the effect of different interpolation schemes on the representation of gravel riverbeds was not fully investigated. In this study, digital photogrammetric and ALS data was processed in terms of randomly-distributed point elevations, and then interpolated to give a continuous surface. Furthermore, in the post-processing routines for both the North Ashburton and Waimakariri study reaches, interpolation was required to cover gaps in the terrain that resulted from the elimination of points that were assumed to be in error. Thus, interpolation was a key aspect of the digital elevation modelling process. The small local relief of large, gravel riverbeds means that elevation differences that result from the interpolation method chosen, although perhaps small in absolute terms, can be significant in terms of relative relief. For digital photogrammetric measurement of large, gravel riverbeds, the quality of interpolation in bar-top areas is of key importance. In these areas, the stereo-matching performance was poor,

meaning that relatively few points were successfully stereo-matched. This places greater importance on the interpolation between those bar-top points that were successfully-matched. Preliminary investigation by Reid (2001) suggests that important differences may result from the use of different interpolation algorithms. It is likely that the optimum interpolator is landform-specific, and the method most preferable for gravel riverbeds requires further investigation, as does the whole issue of the effect of interpolation on surface quality.

Third, the independent check data collection strategy could have been improved. Despite the criticisms that have been made regarding the assessment of DEM surfaces using point elevation data, independent check data remain an essential method of assessing the quality of DEM surfaces. However, the validity of using check data to quantify DEM quality relies on the check data meeting several criteria regarding their spatial distribution and its representation of the area of interest. The North Ashburton May 1995 ground survey represented an ideal situation, whereby the whole study reach was surveyed at a point spacing of 7 m in dry-bed areas and 2 m in wet-bed areas. Thus, the spatial distribution of points was equal across the DEM, and valid conclusions could be made regarding both the magnitude and spatial pattern of error. The Waimakariri, mainly because of its larger spatial extent, had a poor distribution of check measurements, particularly in dry-bed areas. However, to an extent, the acquisition of check data is retrogressive in that it uses the very survey methods that remote measurement is supposed to replace. Therefore, it is also important that the quality of remote sensing measurements is assessed internally, such that independent check measurements are no longer required. This research has made a start in this direction, using methods such as overlap analysis (**Section 6.4.3**) and automated assessment of error in DEMs of difference (**Section 7.3**). Both approaches attempt to quantify DEM quality without the need for independent check data measurements.

Fourth, linked to internal DEM quality assessment, is the need for automated methods of identifying and correcting point errors (Lane, 2001). The post-processing methods developed in this work, particularly in the case of the Waimakariri River, where a coarse resolution DEM was used to identify and remove gross error (**Section 6.2.8**), represent an important and potentially very productive line of research. However, further developments are needed to permit reliable detection and *post priori* removal of point errors. These need to be grounded in measures of data quality that differ from those commonly used in surveying (Cooper, 1998). Point inaccuracies are not a serious problem if they have only a small effect upon the derived parameters we wish to obtain (Lane, 2001). Thus, methods should also be developed which begin to

recognise the spatially-variable and spatially-dependent nature of point quality. Error in many DEM surfaces is spatially-dependent on the surface features represented in the DEM (Carboneau *et al.*, 2001). In the case of gravel riverbeds, the largest errors generally occurred close to wetted channels. Errors in these areas have critical importance in the DEM surface as a whole as they could potentially be propagated across large areas of the riverbed through interpolation of an incorrect water surface. Thus, there is a greater need to ensure a high degree of surface quality in these regions, and intelligent error detection algorithms may be required which focus on wetted channel edges.

Finally, substantive issues associated with high spatial resolution DEM datasets of large, gravel-bed rivers are largely yet to be addressed. In many ways, the methodological and technological aspects of gravel-bed rivers research are relatively straight-forward. A much larger and potentially more challenging issue is to use these new methods to inform both fluvial geomorphological research activities and river management strategies (Lane, 2001). First, this allows new approaches to be utilised in order to address old and existing research questions. For example, braided river flow and sediment transport can be investigated using high spatial resolution DEMs of gravel riverbeds as the topographic boundary conditions for numerical simulations (e.g. Lane and Richards, 1998; Bradbrook *et al.*, 2000; Hicks *et al.*, 2001). Also, sediment transport can be estimated by using sequential riverbed DEMs to allow utilisation of the morphological method (e.g. Lane *et al.*, 1995a). Second, these new methods also open up the possibility of developing new and innovative methods for studying large, gravel-bed rivers. For example, the spatial and dynamic scaling associated with braided rivers appears an exciting area for future research. Recent years have seen the development of numerical methods for assessing fractal scaling of the planform geometry of braided rivers (e.g. Sapozhnikov and Foufoula-Georgiou, 1996, 1997, 1999). However, approaches are required which evaluate the both multi-dimensional scaling associated static channel morphology, and also the dynamic scaling associated with bedload transport and channel change. Such results are important because they would allow three-dimensional validation of numerical of large, braided rivers of flow and sediment transport. Also, the incorporation of riverbed morphological information within a wider remote sensing and GIS framework may allow reach-scale assessment of important geomorphological and ecological parameters, such as the spatial distribution of grain-scale roughness (e.g. Butler *et al.*, 2001a) and habitat availability (e.g. Marcus *et al.*, 2001; Carboneau *et al.*, in press). The adoption of remote measurement of riverbed topography should allow such developments to be made.

APPENDIX 1. THE ORTHOMAX DEM COLLECTION PARAMETERS

The parameters which control the OrthoMAX Vision automated stereo-matching algorithm.

Parameter	Description of parameter	Default value
Minimum threshold	The minimum acceptable correlation coefficient used to consider (noise threshold) and consider (minimum threshold) at each point. Lower values mean more points are considered and accepted as successful matches, respectively, which may result in a larger number of false matches. The default value is thought to reflect the average correlation for points matched by the human eye. Decisions over appropriate value should be made with reference to local topography and image quality. Where terrain is rugged or image quality poor, it may be necessary to lower these thresholds.	0.6
Noise threshold		0.4
Maximum parallax	The maximum vertical search range (in pixels of x-parallax) below and above a predicted elevation for a given point. The predicted elevation is either taken from the previous RRDS, or in the case of the coarsest RRDS, from an average of points used in block triangulation. Higher values of maximum parallax will cause DEM generation to be slower, since a greater elevation range is interrogated at each point. This parameter is directly related to elevation changes in the imagery, and should be increased if these are large.	5
Minimum template size	The smallest initial and largest final template size (in pixels) used by the area correlator. A value of a represents a 'window' shape of $a \times a$ pixels and means a^2 pixels will be used in the correlation calculation. Matching begins using the minimum template size and continues to larger templates if the matching fails for a given template size. Smaller templates will increase the precision of a given match, but also increase the number of unsuccessful matches. Larger template sizes are usually needed if image content is low, but will generally smooth terrain and dramatically increase processing time.	7
Maximum template size		9

Minimum precision	The minimum acceptable estimated precision (in pixels) for a point passing the minimum threshold test. This parameter determines the precision label attached to each successfully matched point. Lower values of precision are more likely to indicate a correct match. All matched points are labelled as good, fair or poor, with precision bandwidths of one-third of the minimum precision value. Reducing the minimum precision value makes the process more selective, although changing this parameter only changes the criterion used to accept points and not the actual precision of the match.	0.5
Rejection factor	A smoothing factor for rejecting anomalous spikes and pits during post-processing. During post-processing after each RRDS, the correlated elevation is compared against the elevation estimated from neighbouring pixels in an attempt to remove false highs and lows in the dataset. A point is rejected if its elevation value is more than the rejection factor times the standard deviation of neighbouring points different from the average value of surrounding points. Larger values reduce the number of points rejected.	1.5
Skip factor	The minimum spacing of points used at a given RRDS (apart from the finest resolution RRDS), increased to accelerate the generation of large DEMs.	2
Edge factor	A parameter which helps to control ambiguous correlations which may result in false fixes. The edge factor describes the ratio between the major and minor axis of the error ellipsoid, computed using the estimated precision of each correlated pair of image points. A ratio higher than the edge factor suggests an elongated error ellipse and an unreliable correlation. Such points are removed and an interpolated elevation used.	2.5
Start RRDS	The start and end RRDS values dictate the range of resolutions the Vision algorithm works through in the stereo-matching process. Block triangulation results are used to determine the initial elevation of the model, such that when elevation range is large, the start RRDS should be increased. The end RRDS should be set to zero to obtain the highest precision from the process.	4
End RRDS		0
Y parallax allowance	The Y parallax allowance is designed to enable successful DEM generation when the block triangulation results suggest that perfect collinearity has not been achieved. If this is the case, the epipolar constraint may be less effective at identifying search areas for stereo-matching. Increasing this parameter allows greater variation in search window location. Given a robust bundle adjustment solution, lowering this parameter will allow more precise stereo-matching.	0

Re-sampling	Governs whether bilinear interpolation (on) or nearest neighbour interpolation (off) is used during orthorectification of image patches.	On
Post processing	An option to determine whether post-processing (including both interpolation and blunder editing) is performed after completion of correlation at each RRDS.	On

(Sources: *Tateishi and Akutsu, 1992; ERDAS, 1995; Smith, 1997; Gooch et al., 1999; Lane et al., 2000*).

REFERENCES

- AAM Geodan 2000, Waimakariri riverbed at Crossbank: digital data documentation, AAM Surveys, Brisbane, Queensland. Unpublished report.
- Ackermann, F. 1978, 'Experimental investigation into the accuracy of contouring from DTM', *Photogrammetric Engineering and Remote Sensing*, 44, 1537-1548.
- Ackermann, F. 1996, 'Digital photogrammetry: challenge and potential', *Photogrammetric Engineering and Remote Sensing*, 62(6), 679.
- Ackermann, F. 1999, 'Airborne laser scanning - present status and future expectations', *ISPRS Journal of Photogrammetry and Remote Sensing*, 54, 64-67.
- Acornley, R. M., Cutler, M. E. J., Milton, E. J. and Sear, D. A. 1995, 'Detection and mapping of salmonid spawning habitat in chalk streams using airborne remote sensing'. In: *Remote Sensing in Action, Proceedings of the 21st Annual Conference of the Remote Sensing Society*, Southampton, 267-274.
- Adams, J. 1979, 'Gravel size analysis from photographs', *ASCE Journal of the Hydraulics Division*, 104, 1247-1255.
- Andrews, E. D. 1993, 'Entrainment of gravel from naturally sorted riverbed material', *Bulletin of the Geological Society of America*, 94(10), 1225-1231.
- Ashmore, P. E. 1991, 'How do gravel-bed rivers braid?', *Canadian Journal of Earth Science*, 28, 326-341.
- Ashmore, P. E. and Church, M. A. 1998, 'Sediment transport and river morphology: a paradigm for study'. In: *Gravel bed rivers in the environment* (eds. Klingeman, P. C., Beschta, R. L., Komar, P. D. and Bradley, J. B.), Water Resources Publications, Highlands Ranch, Colorado, USA, 115-148.
- Ashmore, P. E., Ferguson, R. I., Prestegaard, K. L., Ashworth, P. J. and Paola, C. 1992, 'Secondary flow in anabranch confluences of a braided gravel-bed stream', *Earth Surface Processes and Landforms*, 17, 299-311.
- Ashworth, P. J. and Ferguson, R. I. 1986, 'Interrelationships of channel processes, changes and sediments in a proglacial braided river', *Geographiska Annaler*, 68(4), 361-371.
- Atkinson, P. M. 1999, 'Geographical information science: geostatistics and uncertainty', *Progress in Physical Geography*, 23(1), 134-142.
- Bak, P. 1997, *How nature works*, Oxford University Press, Oxford.
- Baltsavias, E. P. 1999a, 'A comparison between photogrammetry and laser scanning', *ISPRS Journal of Photogrammetry and Remote Sensing*, 54, 83-94.
- Baltsavias, E. P. 1999b, 'Airborne laser scanning: basic relations and formulas', *ISPRS Journal of Photogrammetry and Remote Sensing*, 54, 199-214.

- Bannister, A., Raymond, S. and Baker, R. 1998, Surveying, 7th edition, Longman, Harlow.
- Barker, R., Dixon, L. and Hooke, J. 1997, 'Use of terrestrial photogrammetry for monitoring and measuring bank erosion', *Earth Surface Processes and Landforms*, 22(13), 1217-1227.
- Bates, P. D., Anderson, M. G. and Horritt, M. 1998, 'Terrain information in geomorphological models: stability, resolution and sensitivity'. In: *Landform monitoring, modelling and analysis* (eds. Lane, S. N., Richards, K. S. and Chandler, J. H.), Wiley, Chichester, 279-309.
- Bates, P. D., Horritt, M. S., Smith, C. N. and Mason, D. 1997, 'Integrating remote sensing observations of flood hydrology and hydraulic modelling', *Hydrological Processes*, 11(14), 1777-1795.
- Beschta, R. L. 1983, 'Long-term changes in channel widths of the Kowai River, Torlesse Range, New Zealand', *Journal of Hydrology (New Zealand)*, 22(2), 112-122.
- Blakely, R. J. and Mosley, M. P. 1987, Impact of the Waimakariri River Control Scheme on the River and its Environment, National Water and Soil Conservation Authority, New Zealand, Wellington. Water and Soil Miscellaneous Publication 102.
- Blalock, H. M. 1979, Social statistics, 2nd edition, McGraw-Hill, New York.
- Blasco, F., Bellan, M. F. and Chaudhury, M. U. 1992, 'Estimating the extent of floods in Bangladesh using SPOT data', *Remote Sensing of Environment*, 39(3), 167-178.
- Bollweg, A. E. 1999, 'Water management of the river Rhine: water level from laser altimetry', *Geomatics*, 13(11), 30-44.
- Bolstad, P. V. and Stowe, T. 1994, 'An evaluation of DEM accuracy: elevation, slope and aspect', *Photogrammetric Engineering and Remote Sensing*, 60(11), 1327-1332.
- Bradbrook, K. F., Lane, S. N. and Richards, K. S. 2000, 'Numerical simulation of three-dimensional, time-averaged flow structure at river channel confluences', *Water Resources Research*, 36(9), 2731-2746.
- Brasington, J., Rumsby, B. T. and McVey, R. A. 2000, 'Monitoring and modelling morphological change in a braided gravel-bed river using high resolution GPS-based survey', *Earth Surface Processes and Landforms*, 25, 973-990.
- Brown, D. G. and Arbogast, A. F. 1999, 'Digital photogrammetric change analysis as applied to active coastal dunes in Michigan', *Photogrammetric Engineering and Remote Sensing*, 65(4), 467-474.
- Brown, D. G. and Bara, T. J. 1994, 'Recognition and reduction of systematic error in elevation and derivative surfaces from 7½-minute DEMs', *Photogrammetric Engineering and Remote Sensing*, 60(2), 189-194.

- Brunsden, D. and Chandler, J. H. 1996, 'Development of an episodic landform change model based upon the Black Ven Mudslide, 1946-1995'. In: *Advances in hillslope processes* (eds. Anderson, M. G. and Brooks, S. M.), Wiley, Chichester, 869-896.
- Bryant, R. G. and Gilvear, D. J. 1999, 'Quantifying geomorphic and riparian land cover changes either side of a large flood event using remote sensing: River Tay, Scotland', *Geomorphology*, 29(3-4), 307-321.
- Burrough, P. A. and McDonnell, R. A. 1998, *Principles of geographical information systems*, Oxford University Press, Oxford.
- Butler, J. B., Lane, S. N. and Chandler, J. H. 1998, 'Assessment of DEM quality characterising surface roughness using close range digital photogrammetry', *Photogrammetric Record*, 19(92), 271-291.
- Butler, J. B., Lane, S. N. and Chandler, J. H. 2001a, 'Automated extraction of grain-size data from gravel surfaces using digital image processing', *ASCE Journal of Hydraulic Engineering*.
- Butler, J. B., Lane, S. N., Chandler, J. H. and Porfiri, K. 2001b, 'Through-water close-range digital photogrammetry in flume and field environments', *Photogrammetric Record*.
- Carboneau, P. E., Lane, S. N. and Bergeron, N. 2001, 'Automated correction of DEMs using edge detection based on conditional filtering'. Paper presented to the First Annual Meeting of the Remote Sensing and Photogrammetry Society, 12-14 September 2001, London.
- Carboneau, P. E., Lane, S. N. and Bergeron, N. in press, 'Cost-effective non-metric photogrammetry and its application to a study of coarse gravel riverbeds', *International Journal of Remote Sensing*.
- Carrara, A., Bitelli, G. and Carla, R. 1997, 'Comparison of techniques for generating digital terrain models from contour lines', *International Journal of Geographical Information Science*, 11(5), 451-473.
- Carson, M. A. 1986, 'Characteristics of high-energy "meandering" rivers: the Canterbury Plains, New Zealand', *Geological Society of America Bulletin*, 97, 886-895.
- Carson, M. A. and Griffiths, G. A. 1987, 'Bedload transport in gravel channels', *Journal of Hydrology (New Zealand)*, 26(1), 1-151.
- Carson, M. A. and Griffiths, G. A. 1989, 'Gravel transport in the braided Waimakariri River - transport mechanisms, measurements and applications', *Journal of Hydrology*, 109, 201-220.
- Carter, G. S. and Shankar, U. 1997, 'Creating rectangular bathymetry grids for environmental numerical modelling of gravel-bed rivers', *Applied Mathematical Modelling*, 21, 699-708.
- Chandler, J. H. 1999, 'Effective application of automated digital photogrammetry for geomorphological research', *Earth Surface Processes and Landforms*, 24, 51-63.

- Chandler, J. H. and Ashmore, P. 2001, 'Detecting braided river channel change using terrestrial oblique digital imagery and automated digital photogrammetry'. In: Geomatics, Earth Observation and the Information Society, Proceedings of the First Annual Conference of the Remote Sensing and Photogrammetric Society, Remote Sensing and Photogrammetric Society, London, 12-14 September 2001.
- Chandler, J. H. and Clark, J. S. 1992, 'The archival photogrammetric technique: further application and development', *Photogrammetric Record*, 14(80), 241-247.
- Chandler, J. H. and Cooper, M. 1988, 'Monitoring the development of landslides using archival photography and analytical photogrammetry', *Land and Minerals Surveying*, 6, 576-584.
- Chandler, J. H. and Moore, R. 1989, 'Analytical photogrammetry: a method for monitoring slope instability', *Quarterly Journal of Engineering Geology*, 22, 97-110.
- Chandler, J. H. and Padfield, C. J. 1996, 'Automated digital photogrammetry on a shoestring', *Photogrammetric Record*, 15, 545-560.
- Chandler, J. H., Shiono, K., Rameshwaren, P. and Lane, S. N. 2001, 'Measuring flume surfaces for hydraulics research using a Kodak DCS460', *Photogrammetric Record*, 17(97), 38-61.
- Charlton, M. E., Fuller, I. C., Large, A. R. G., Passmore, D. G., Newson, M. D. and Heritage, G. L. 2001, 'Airborne LIDAR and ground survey for exploring channel dynamics'. Paper presented to a joint meeting of the Photogrammetric Society and the British Geomorphological Research Group, University of Leeds, 17 January 2001.
- Cheetham, G. H. 1979, 'Flow competence in relation to stream channel form and braiding', *Geological Society of America Bulletin*, 90, 877-886.
- Church, M. 2001, 'Rivers as self-adjusting systems'. Paper presented to the 50th annual meeting of the Canadian Association of Geographers, Montreal, Canada, 29 May - 3 June 2001.
- Church, M., McLean, D. and Wolcott, J. F. 1987, 'River bed gravels: sampling and analysis'. In: *Sediment transport in gravel-bed rivers* (eds. Thorne, C. R., Bathurst, J. C. and Hey, R. D.), Wiley, Chichester, 43-88.
- Clifford, N. J., Robert, A. and Richards, K. S. 1992, 'Estimation of flow roughness in gravel-bedded rivers: a physical explanation for the multiplier of roughness length', *Earth Surface Processes and Landforms*, 17, 111-126.
- Cody, W. D. 1993, 'ALGORITHM 715: SPECFUN - A portable FORTRAN package of special function routines and test drivers', *ACM Transactions on Mathematical Software*, 19, 22-32.
- Coldwell, A. E. 1957, 'Importance of channel erosion as a source of sediment', *Transactions of the American Geophysical Union*, 38, 908-912.
- Collins, S. H. and Moon, G. C. 1979, 'Stereometric measurement of streambank erosion', *Photogrammetric Engineering and Remote Sensing*, 45(2), 183-190.

- Connell, R. J. 2001, 'North Ashburton River - Blands Reach - Aggradation'. In: Gravel bed rivers 2000 CD ROM (eds. Nolan, T. and Thorne, C.), Special Publication of the New Zealand Hydrological Society, Christchurch.
- Cooper, M. A. R. 1998, 'Datums, coordinates and differences'. In: Landform monitoring, modelling and analysis (eds. Lane, S. N., Richards, K. S. and Chandler, J. H.), Wiley, Chichester, 23-36.
- Cooper, M. A. R. and Cross, P. A. 1988, 'Statistical concepts and their application in photogrammetry and surveying', Photogrammetric Record, 12(71), 637-663.
- Cracknell, A. P. 1987, 'Use of satellite and aircraft data for bathymetry studies'. In: 13th Annual Conference of the Remote Sensing Society, University of Nottingham, September 7-11, 1987.
- Cracknell, A. P., MacFarlane, N., McMillan, K., Charlton, J. A., McManus, J. and Ulbricht, K. A. 1982, 'Remote sensing in Scotland using data received from satellites. A study of the Tay Estuary region using Landsat multispectral scanning imagery', International Journal of Remote Sensing, 3(2), 113-137.
- Crickmay, C. H. 1960, 'Lateral activity in a river in North Western Canada', Journal of Geology, 68, 377-391.
- Davies-Colley, R. J., Vant, W. N. and Smith, D. G. 1993, Colour and clarity of natural waters: science and management of optical water quality, Ellis Horwood, Chichester.
- Davis, J. C. 1986, Statistics and data analysis in geology, 2nd edition, Wiley, New York.
- Davis, T. J. and Keller, C. P. 1997, 'Modelling uncertainty in natural resources analysis using fuzzy sets and Monte Carlo simulation', International Journal of Geographical Information Science, 11, 409-434.
- Davoren, A. and Mosley, M. P. 1986, 'Observations of bedload movement, bar development and sediment supply in the braided Ohau River', Earth Surface Processes and Landforms, 11, 643-652.
- Derose, R. C., Gomez, B., Marden, M. and Trustrum, N. A. 1998, 'Gully erosion in Mangatu Forest, New Zealand, estimated from digital elevation models', Earth Surface Processes and Landforms, 23, 1045-1053.
- Desmet, P. J. J. 1997, 'Effects of interpolation errors on the analysis of DEMs', Earth Surface Processes and Landforms, 22, 563-580.
- Deville, E. 1893, 'Lever topographique des Montagnes Rocheuses exécuté par la photographie', Proceedings and Transactions of the Royal Society of Canada, 11(3), 13-15.
- Dickinson, W. T. and Scott, A. M. 1979, 'Analysis of streambank erosion', Canadian Agricultural Engineering, 21(1), 95-116.

- Dietrich, W. E. and Whiting, P. J. 1989, 'Boundary shear stress and sediment transport in river meanders of sand and gravel'. In: River meandering (eds. Ikeda, S. and Parker, G.), American Geophysical Union, Washington DC, 1-50.
- Dietz, R. S. 1947, 'Aerial photographs in the geological study of shore features and processes', *Photogrammetric Engineering*, 13(4), 537-545.
- Dinehart, R. L. 1992, 'Gravel-bed deposition and erosion by bedform migration observed ultrasonically during storm flow, North Fork, Toutle River, Washington', *Journal of Hydrology*, 136(1-4), 51-71.
- Dixon, L. F. J., Barker, R., Farres, P., Hooke, J., Inkpen, R., Merel, A., Payne, D. and Shelford, A. 1998, 'Analytical photogrammetry for geomorphological research'. In: Landform monitoring, modelling and analysis (eds. Lane, S. N., Richards, K. S. and Chandler, J. H.), Wiley, Chichester, 63-94.
- Duntley, S. Q. 1963, 'Light in the sea', *Journal of the Optical Society of America*, 53(2), 214-233.
- Ehlschlaeger, C. R., Shortridge, A. M. and Goodchild, M. F. 1997, 'Visualising spatial data uncertainty using animation', *Computers and Geosciences*, 23, 387-395.
- Eliel, L. T. 1947, 'Progress of photogrammetry in the U.S.', *Photogrammetric Engineering*, 13(1), 12-22.
- ERDAS 1995, IMAGINE Version 8.2: OrthoMAX user's Guide, Vision International and Manchester Computing.
- Evans, S. Y., Peiris, T. and Fields, B. 2001, 'Application of various survey data for hydraulic modelling and floodplain mapping'. Paper presented to a joint meeting of the Photogrammetric Society and the British Geomorphological Research Group, University of Leeds, 17 January 2001.
- Fahnestock, R. K. and Bradley, W. C. 1973, 'Knik and Matanuska rivers, Alaska: a contrast in braiding'. In: Fluvial geomorphology (ed. Morisawa, M.), Allen and Unwin, London.
- Favey, E., Geiger, A., Gudmundsson, G. H. and Wehr, A. 1999, 'Evaluating the potential of an airborne laser-scanning system for measuring volume changes of glaciers', *Geografiska Annaler*, 81A(4), 555-561.
- Felicísmo, A. M. 1994, 'Parametric statistical method for error detection in digital elevation models', *ISPRS Journal of Photogrammetry*, 49(4), 29-33.
- FEMA (Federal Emergency Management Agency) 2000, Map modernisation plan, National Flood Insurance Program,, Washington D.C.
- Fenn, C. R. and Gurnell, A. M. 1987, 'Proglacial channel processes'. In: Glacio-fluvial sediment transfer (eds. Gurnell, A. M. and Clark, M. J.), Wiley, Chichester, 423-472.

- Ferguson, R. I. 1993, 'Understanding braiding processes in gravel-bed rivers: progress and unsolved problems'. In: Braided rivers, Special Publication No. 75 (eds. Best, J. L. and Bristow, C. S.), Geological Society, London, 73-87.
- Ferguson, R. I., Ashmore, P. E., Ashworth, P. J., Paola, C. and Prestegard, K. L. 1992, 'Measurements in a braided river chute and lobe 1: flow pattern, sediment transport and channel change', *Water Resources Research*, 28, 1877-1886.
- Ferguson, R. I. and Ashworth, P. J. 1992, 'Spatial patterns of bedload transport and channel change in braided and near-braided rivers'. In: Dynamics of gravel-bed rivers (eds. Billi, P., Hey, R. D., Thorne, C. R. and Tacconi, P.), Wiley, New York, 477-496.
- Ferguson, R. I. and Werry, A. 1983, 'Bar development and channel changes in the gravelly River Feshie, Scotland'. In: Modern and ancient fluvial systems (eds. Collinson, J. and Lewin, J.), Blackwell Scientific Publications, Oxford, 181-194.
- Fernando, A. D. N. 1966, 'Changes in the course of the Mahaweliganga and their significance', *Ceylon Survey Newsletter*, 41, 33-35.
- Fezer, F. 1971, 'Photo interpretation applied to geomorphology - a review', *Photogrammetria*, 7-53(27), 1.
- Finnegan, D. C., Gomez, B. and Smith, L. C. 2001, 'Using laser altimetry to quantify geomorphic change effected by large-scale flooding'. Paper presented to the 97th Annual Meeting of the American Association of Geographers, New York, USA, 27 February - 3 March 2001.
- Florinsky, I. V. 1998, 'Combined analysis of digital terrain models and remotely sensed data in landscape investigations', *Progress in Physical Geography*, 22(1), 33-60.
- Forrester, W. D. 1960, 'Plotting of water current patterns by photogrammetry', *Photogrammetric Engineering*, 26(5), 726-736.
- Fraser, C., Jonas, D. and Turton, D. 1999, Report on 1998 airborne laser scanner trials, AAM Surveys, Brisbane, Queensland. Available online at <http://www.aamsurveys.com.au/articles.html>.
- Frederiksen, P., Jacobi, O. and Kubik, K. 1986, 'Optimum sampling spacing in digital terrain models', *International Archives of Photogrammetry and Remote Sensing*, 26(3/1), 252-259.
- French, J. R. 2001, 'Airborne LiDAR data in support of hydraulic modelling: representation of form as the key to simulation of process'. Paper presented to a joint meeting of the Photogrammetric Society and the British Geomorphological Research Group, University of Leeds, 17 January 2001.
- Fryer, J. G. 1983, 'A simple system for photogrammetric mapping in shallow water', *Photogrammetric Record*, 11(62), 203-208.
- Fryer, J. G. 1987, 'Innovations in photogrammetry: some student examples', *The Australian Surveyor*, 33(7), 602-616.

- Fryer, J. G., Chandler, J. H. and Cooper, M. A. R. 1994, 'On the accuracy of heighting from aerial photographs and maps: implications to process modellers', *Earth Surface Processes and Landforms*, 19, 577-583.
- Fryer, J. G. and Kniest, H. T. 1985, 'Errors in depth determination caused by waves in through-water photogrammetry', *Photogrammetric Record*, 11(66), 745-753.
- Geary, E. L. 1968, 'Coastal hydrology', *Photogrammetric Engineering*, 34, 44-50.
- Ghosh, S. K. 1988, *Analytical photogrammetry*, Pergamon Press, New York.
- Giles, P. T. and Franklin, S. 1996, 'Comparison of derivative topographic surfaces of a DEM generated from stereoscopic SPOT images with field measurements', *Photogrammetric Engineering and Remote Sensing*, 62(10), 1165-1171.
- Gilvear, D. J., Davies, J. R. and Winterbottom, S. J. 1994, 'Mechanisms of floodbank failure during large flood events on the regulated River Tay, Scotland', *Quarterly Journal of Engineering Geology*, 4, 1-20.
- Gilvear, D. J., Waters, T. M. and Milner, A. M. 1998, 'Image analysis of aerial photography to quantify the effect of gold placer mining on channel morphology, Interior Alaska'. In: *Landform monitoring, modelling and analysis* (eds. Lane, S. N., Richards, K. S. and Chandler, J. H.), Wiley, Chichester, 195-216.
- Gilvear, D. J. and Winterbottom, S. J. 1992, 'Channel changes and flood events since 1783 on the regulated River Tay, Scotland', *Regulated Rivers: Research and Management*, 7, 247-260.
- Glova, G. J., Jellyman, D. J. and Bonnett, M. L. 1998, 'Factors associated with the distribution and habitat of eels (*Anguilla* spp) in three New Zealand lowland streams', *New Zealand Journal of Marine and Freshwater Research*, 32(2), 255-269.
- Goff, J. R. and Ashmore, P. 1994, 'Gravel transport and morphological change in braided Sunwapta River, Alberta, Canada', *Earth Surface Processes and Landforms*, 19, 195-212.
- Gomes Pereira, L. M. and Wicherson, R. J. 1999, 'Suitability of laser data for deriving geographical information. A case study in the context of management of fluvial zones', *ISPRS Journal of Photogrammetry and Remote Sensing*, 54, 105-114.
- Gomez, B., Hubbell, D. W. and Stevens, H. H. 1990, 'At-a-point bedload sampling in the presence of dunes', *Water Resources Research*, 26, 2717-2731.
- Gong, J., Li, Z., Zhu, Q., Sui, H. and Zhou, Y. 2000, 'Effects of various factors on the accuracy of DEMs: an intensive experimental investigation', *Photogrammetric Engineering and Remote Sensing*, 66(9), 1113-1117.
- Gooch, M. J., Chandler, J. H. and Stojic, M. 1999, 'Accuracy assessment of digital elevation models generated using the ERDAS Imagine OrthoMAX digital photogrammetric system', *Photogrammetric Record*, 16(93), 519-531.

- Grange Moore, J. 1946, 'The determination of the depths and extinction coefficients of shallow water by air photography using colour filters', *Philosophical Transactions of the Royal Society of London*, 240A(816), 163-217.
- Granshaw, S. I. 1980, 'Bundle adjustment methods in engineering photogrammetry', *Photogrammetric Record*, 10, 181-207.
- Green, A. A., Whitehouse, G. and Outhet, D. 1983, 'Causes of flood streamlines observed on Landsat images and their use as indicators of floodways', *International Journal of Remote Sensing*, 4, 5-16.
- Griffiths, G. A. 1979a, 'High sediment yields from major rivers of the western Southern Alps, New Zealand', *Nature*, 282, 61-63.
- Griffiths, G. A. 1979b, 'Recent sedimentation history of the Waimakariri River, New Zealand', *Journal of Hydrology (New Zealand)*, 18(1), 6-28.
- Griffiths, G. A. 1991, (Draft) Waimakariri River Floodplain Management Plan, Canterbury Regional Council, Christchurch. Internal report R91(9).
- Griffiths, G. A. 1993, 'Sediment translation waves in braided gravel-bed rivers', *Journal of Hydraulic Engineering*, 119(8), 924-937.
- Guenther, G. C., Brooks, M. W. and LaRocque, P. E. 2000, 'New capabilities of the "SHOALS" airborne lidar bathymeter', *Remote Sensing of Environment*, 73(2), 247-255.
- Gugan, D. J. and Dowman, I. J. 1988, 'Topographic mapping from SPOT imagery', *Photogrammetric Engineering and Remote Sensing*, 54, 1409-1414.
- Gurnell, A. M., Downward, S. R. and Jones, R. 1994, 'Channel planform change on the River Dee meanders, 1876-1992', *Regulated Rivers: Research and Management*, 9, 187-204.
- Ham, D. G. and Church, M. 2000, 'Bed-material transport estimated from channel morphodynamics: Chilliwack River, British Columbia', *Earth Surface Processes and Landforms*, 25(10), 1123-1142.
- Hamilton, S. K. and Lewis, W. M. 1990, 'Physical characteristics of the fringing floodplain of the Orinoco River, Venezuela', *Interciencia*, 15(6), 491-500.
- Hannah, M. J. 1981, 'Error detection and correction in digital terrain models', *Photogrammetric Engineering and Remote Sensing*, 47(1), 63-69.
- Hansen, J. and Jonas, D. 2000, Airborne laser scanning or aerial photogrammetry for the mine surveyor, AAM Surveys, Brisbane, Queensland. Available online at <http://www.aamsurveys.com.au/articles.html>.
- Hardisty, J., Middleton, R., Whyatt, D. and Rouse, H. 1998, 'Geomorphological and hydrodynamic results from digital terrain models of the Humber Estuary'. In: *Landform monitoring, modelling and analysis* (eds. Lane, S. N., Richards, K. S. and Chandler, J. H.), Wiley, Chichester, 421-433.

- Hardy, T. B., Anderson, P. C., Neale, C. M. U. and Stevens, D. K. 1994, 'Application of multispectral videography for the delineation of riverine depths and mesoscale hydraulic features'. In: Effects of human-induced changes on hydrologic systems (eds. Marson, R. and Hasfurther, V.), American Water Resources Association, Maryland, 445-454.
- Harris, M. M., Mesick, H. C., Byrnes, H. J., Curran, T. P. and Cantarino, V. M. 1987, 'A laser sounder for US hydrographers'. In: Proceedings of the International Geoscience and Remote Sensing Symposium, Ann Arbor, Michigan, USA, 791-796.
- Harris, W. D. and Umbach, M. J. 1972, 'Underwater mapping', Photogrammetric Engineering, 38(8), 765-772.
- Harvey, E. S. and Shortis, M. R. 1996, 'A system for stereo-video of sub-tidal organisms', Journal of the Marine Technology Society, 29(4), 10-22.
- Hassan, M. and Reid, I. 1990, 'The influence of microform bed roughness elements on flow and sediment transport in gravel-bed rivers', Earth Surface Processes and Landforms, 15, 739-750.
- Helgeson, G. A. 1970, 'Water depth and distance penetration', Photogrammetric Engineering, 36(2), 164-172.
- Heritage, G. L., Fuller, I. C., Charlton, M. E., Brewer, P. and Passmore, D. 1998, 'CDW photogrammetry of low relief fluvial features: accuracy and implications for reach-scale sediment budgeting', Earth Surface Processes and Landforms, 23(13), 1219-1233.
- Hickman, G. D. and Hogg, J. E. 1969, 'Application of an airborne pulsed laser for near shore bathymetric measurements', Remote Sensing of Environment, 1, 47-58.
- Hicks, D. M., Duncan, M. J., Walsh, J., Lane, S. N. and Westaway, R. M. 1999b, Braided River Morphodynamics: Research Plan for 1999-2000 and 1998-1999 Fieldwork, National Institute of Water and Atmosphere, Christchurch. Technical Report 51.
- Hicks, D. M., Duncan, M. J., Walsh, J. M., Westaway, R. M., Lane, S. N. and Jonas, D. L. 2001a, 'The braided Waimakariri River: new views of form and process from high-density topographic surveys and time-lapse imagery'. In: Gravel bed rivers 2000 CD ROM (eds. Nolan, T. and Thorne, C.), Special Publication of the New Zealand Hydrological Society, Christchurch.
- Hicks, D. M. and Jonas, D. 2000, 'Research into Freshwater River Systems', Scanning The Horizons - Journal of AAM Surveys, Aug/Sep 2000.
- Hicks, D. M., Walsh, J. and Nikora, V. 1999a, 'Some scaling and fractal properties of braided rivers on the Canterbury Plains', Paper presented to New Zealand Hydrological Society 1999 Symposium, Napier, New Zealand, 23-26 November 1999.

- Hitchcock, D. 1977, 'Channel pattern changes in divided reaches: an example in the coarse bed material of the Forest of Bowland'. In: River channel changes (ed. Gregory, K. J.), Wiley, Chichester, 207-220.
- Hoey, T. 1994, 'Patterns of sediment storage in the Kowai River, Torlesse Range, New Zealand', *Journal of Hydrology (New Zealand)*, 32(1), 1-15.
- Hofton, M. A., Blair, J. B., Minster, J.-B., Ridgway, J. R., Williams, N. P., Bufton, J. L. and Rabine, D. L. 2000, 'An airborne laser altimetry survey of Long Valley, California', *International Journal of Remote Sensing*, 21(12), 2413-2437.
- Höhle, J. 1971, 'Reconstruction of the underwater object', *Photogrammetric Engineering*, 37(9), 948-954.
- Holmes, A. M. 1982, Underwater mapping using photogrammetry, Final Year Project, University of Newcastle, New South Wales, Australia.
- Horritt, M. S. and Bates, P. D. 2001, 'Predicting floodplain inundation: raster-based modelling versus the finite-element approach', *Hydrological Processes*, 15(5), 825-842.
- Howe, R. H. L. 1960, 'The application of aerial photographic interpretation to the investigation of hydrologic problems', *Photogrammetric Engineering*, 26(1), 85-95.
- Huang, Y. D. 2000, 'Evaluation of information loss in digital elevation models with digital photogrammetric systems', *Photogrammetric Record*, 16(95), 781-791.
- Huisng, E. J. and Gomes Pereira, L. M. 1999, 'Errors and accuracy estimates of laser data acquired by various laser scanning systems for topographic applications', *ISPRS Journal of Photogrammetry and Remote Sensing*, 53, 245-261.
- Hunter, G. J. and Goodchild, M. F. 1997, 'Modeling the uncertainty of slope and aspect estimates derived from spatial databases', *Geographical Analysis*, 29(1), 35-49.
- Ibrahim, M. and Cracknell, A. P. 1990, 'Bathymetry using Landsat MSS data of Penang Island in Malaysia', *International Journal of Remote Sensing*, 11(4), 557-559.
- Iriondo, M. H. 1972, 'A rapid method for size analysis of coarse sediments', *Journal of Sedimentary Petrology*, 42, 985-986.
- Irish, J. L. and Lillycrop, W. J. 1999, 'Scanning laser mapping of the coastal zone: the SHOALS system', *ISPRS Journal of Photogrammetry and Remote Sensing*, 54, 123-129.
- Jacobberger, P. A. 1988, 'Mapping abandoned river channels in Mali through directional filtering of Thematic Mapper data', *Remote Sensing of Environment*, 26, 161-170.
- Jensen, J. R. 1996, 'Issues involving the creation of digital elevation models and terrain corrected orthoimagery using soft-copy photogrammetry'. In: Digital photogrammetry: an addendum to the manual of photogrammetry (ed. Greve, C. W.), American Society of Photogrammetry and Remote Sensing, Bethesda, 167-179.
- Jerlov, N. G. 1976, Marine optics, Elsevier Publishing, Amsterdam.

- Jia, Y., Kitamura, T. and Wang, S. 2001, 'Simulation of scour process in plunging pool of loose bed-material', ASCE Journal of Hydraulic Engineering, 127(3), 219-229.
- Jonas, D. 2001a, Dunwich irrigation area - comparing airborne laser scanning with photogrammetry, AAM Surveys, Brisbane, Queensland. Available online at <http://www.aamsurveys.com.au/articles.html>.
- Jonas, D. 2001b, Spatial data suitable for visualisation of built environments, AAM Surveys, Brisbane, Queensland. Available online at <http://www.aamsurveys.com.au/articles.html>.
- Jonas, D. and Byrne, P. 1999, 'Extension of topographical modelling capability with airborne laser scanning'. In: Paper presented at 6th South East Asian Surveyors Congress, Fremantle, Western Australia, 1 - 6 November 1999., 11 pages.
- Keim, R. F., Skaugset, A. E. and Bateman, D. S. 1999, 'Digital terrain modeling of small stream channels with a total-station theodolite', Advanced Water Resources, 23(1), 41-48.
- Kelly, W. A. and McGuire, D. J. 1955, 'Exceptional meander scars and their significance in determining the direction of stream flow', Photogrammetric Engineering, 21(1), 110-112.
- Kersarwani, A., Gomez, B., Jacobsen, R. and Smith, L. 2001, 'Using laser altimetry for rapid assessment of post-flood erosional and depositional changes'. Paper presented to the 97th Annual Meeting of the American Association of Geographers, New York, USA, 27 February - 3 March 2001.
- Klingeman, P. C. 1998, 'Introduction'. In: Gravel-bed rivers in the environment (eds. Klingeman, P. C., Beschta, R. L., Komar, P. D. and Bradley, J. B.), Water Resources Publications, Highlands Ranch, Colorado, USA, 1-4.
- Kneist, H. T. 1990, Photogrammetry through an air-water interface, Department of Civil Engineering and Surveying, University of Newcastle, New South Wales, Australia. Research report no. 055.11.1990.
- Koch, K.-R. 1987, Parameter estimation and hypothesis testing in linear models, Springer-Verlag, Berlin.
- Kondolf, G. M. and Swanson, M. L. 1993, 'Channel adjustments to reservoir construction and gravel extraction along Stony Creek, California', Environmental Geology, 21, 256-269.
- Kraus, K. and Pfeifer, N. 1998, 'Determination of terrain models in wooded areas with airborne laser scanner data', ISPRS Journal of Photogrammetry and Remote Sensing, 53(4), 193-203.
- Kubik, K. and Botman, A. G. 1976, 'Interpolation accuracy for topographic and geological surfaces', ITC Journal, 2, 236-276.
- Kumar, K. V., Palit, A. and Bhan, S. K. 1997, 'Bathymetric mapping in Rupnarayan-Hooghly River confluence using Indian remote sensing satellite data', International Journal of Remote Sensing, 18(11), 2269-2270.

- Kyriakidis, P. C., Shortridge, A. M. and Goodchild, M. F. 1999, 'Geostatistics for conflation and accuracy assessment of digital elevation models', *International Journal of Geographical Information Science*, 13(7), 677-707.
- La Barbera, P. and Rosso, R. 1989, 'On the fractal dimension of stream networks', *Water Resources Research*, 25, 735-741.
- Lane, S. N. 1990, An evaluation of how short term changes in channel morphology relate to the hydraulics of flow in the braided reach of a gravel-bedded proglacial stream, unpublished undergraduate dissertation, University of Cambridge.
- Lane, S. N. 1994, Monitoring and modelling morphology, flow and sediment transport in a gravel-bed stream, unpublished PhD thesis, University of Cambridge.
- Lane, S. N. 1997, 'The reconstruction of bed material yield and supply histories in gravel-bed streams', *Catena*, 30, 183-196.
- Lane, S. N. 1998, 'The use of digital terrain modelling in the understanding of dynamic river channel systems'. In: *Landform monitoring, modelling and analysis* (eds. Lane, S. N., Richards, K. S. and Chandler, J. H.), Wiley, Chichester, 311-342.
- Lane, S. N. 2000, 'The measurement of river channel morphology using digital photogrammetry', *Photogrammetric Record*, 16(96), 937-957.
- Lane, S. N. 2001, 'The measurement of river channel morphology'. In: *Gravel bed rivers V* (ed. Mosely, M. P.), New Zealand Hydrological Society, Wellington, New Zealand.
- Lane, S. N., James, T. D. and Crowell, M. D. 2000, 'Application of digital photogrammetry to complex topography for geomorphological research', *Photogrammetric Record*, 16(95), 793-821.
- Lane, S. N., Reid, S. C., Westaway, R. M. and Hicks, D. M. in prep., 'Remotely-sensed topographic data for river channel research: the identification, explanation and management of error'.
- Lane, S. N. and Richards, K. S. 1997, 'Linking river channel form and process: time, space and causality revisited', *Earth Surface Processes and Landforms*, 22, 349-368.
- Lane, S. N. and Richards, K. S. 1998, 'High resolution, two-dimensional spatial modelling of flow processes in a multi-thread channel', *Hydrological Processes*, 12(8), 1279-1298.
- Lane, S. N., Richards, K. S. and Chandler, J. H. 1993, 'Developments in photogrammetry: the geomorphological potential', *Progress in Physical Geography*, 17(3), 306-328.
- Lane, S. N., Richards, K. S. and Chandler, J. H. 1994, 'Developments in monitoring and terrain modelling of small-scale riverbed topography', *Earth Surface Processes and Landforms*, 19, 349-368.
- Lane, S. N., Richards, K. S. and Chandler, J. H. 1995a, 'Morphological estimation of the time-integrated bed-load transport rate', *Water Resources Research*, 31(3), 761-772.

- Lane, S. N., Richards, K. S. and Chandler, J. H. 1995b, 'Within-reach spatial patterns of process and channel adjustment'. In: *River geomorphology* (ed. Hickin, E. J.), Wiley, Chichester, 105-130.
- Lane, S. N., Richards, K. S. and Chandler, J. H. 1996, 'Discharge and sediment supply controls on erosion and deposition in a dynamic alluvial channel', *Geomorphology*, 15, 1-15.
- Lankes, L. R. 1970, 'Optics and the physical parameters of the sea', *Optical Spectra*, 4, 42-29.
- Lapointe, M. F., Secretan, Y., Driscoll, S., Bergeron, N. and Leclerc, M. 1998, 'Response of the Ha! Ha! river to the flood of July 1996 in the Saguenay region of Quebec: large-scale avulsion in a glaciated valley', *Water Resources Research*, 34(9), 2383-2392.
- Laronne, J. B. and Duncan, M. J. 1992, 'Bedload transport paths and gravel bar formation'. In: *Dynamics of Gravel-bed rivers*, eds. Billi, P., Hey, R. D., Thorne, C. R. and Tacconi, P.), Wiley, Florence, Italy, 673.
- Lawler, D. M. 1993, 'The measurement of river bank erosion and lateral channel change: a review', *Earth Surface Processes and Landforms*, 18, 777-821.
- Lee, J., Snyder, P. K. and Fisher, P. F. 1992, 'Modeling the effect of data errors on feature-extraction from digital elevation models', *Photogrammetric Engineering and Remote Sensing*, 58(10), 1461-1467.
- Lee, W. T. 1922, *The face of the earth as seen from the air: a study in the application of airplane photography to geography*, New York.
- Lee, Z., Carder, K. L., Mobley, C. D., Steward, R. G. and Patch, J. S. 1999, 'Hyperspectral remote sensing for shallow waters: 2. Deriving bottom depths and water properties by optimization', *Applied Optics*, 38(18), 3831-3843.
- Leeks, G. J., Lewin, J. and Newson, M. D. 1988, 'Channel change, fluvial geomorphology and river engineering: the case of the Afon Trannon, mid-Wales', *Earth Surface Processes and Landforms*, 13, 207-223.
- Lepley, L. K. 1968, 'Coastal water clarity from space photographs', *Photogrammetric Engineering*, 34(7), 667-674.
- Lewin, J. 1990, 'River channels'. In: *Geomorphological techniques*, 2nd edition (ed. Goudie, A. S.), Unwin Hyman, London, 280-301.
- Lewin, J. and Hughes, D. 1976, 'Assessing channel change on Welsh rivers', Cambria, 3, 1-10.
- Lewin, J. and Manton, M. M. M. 1975, 'Welsh floodplain studies: the nature of floodplain geometry', *Journal of Hydrology*, 25, 37-50.
- Lewin, J. and Weir, M. J. C. 1977, 'Morphology and recent history of the Lower Spey', *Scottish Geographical Magazine*, 93, 45-51.
- Ley, R. G. 1986, 'Accuracy assessment of digital terrain models'. In: *Proceedings AutoCarto London*, Autocarto London, London, 455-464.

- Li, Z. 1988, 'On the measure of digital terrain model accuracy', *Photogrammetric Record*, 12(72), 873-877.
- Li, Z. 1992, 'Variation of the accuracy of digital terrain models with sampling interval', *Photogrammetric Record*, 14(79), 113-128.
- Li, Z. 1993a, 'Theoretical models of the accuracy of digital terrain models: an evaluation and some observations', *Photogrammetric Record*, 14(82), 651-660.
- Li, Z. 1993b, 'Mathematical models of the accuracy of digital terrain model surfaces linearly constructed from square gridded data', *Photogrammetric Record*, 14(82), 661-674.
- Li, Z. 1994, 'A comparative study of the accuracy of digital terrain models (DTMs) based on various data models', *ISPRS Journal of Photogrammetry and Remote Sensing*, 49(1), 2-11.
- Lindsay, J. B. and Ashmore, P. E. submitted, 'Error in the measurement of gravel-bed topography and topographic change. Part 2: the effects of survey frequency on estimates of scour and fill in a braided river model'.
- Lindsay, J. B., Ashmore, P. E. and Smart, C. C. submitted, 'Error in the measurement of gravel-bed topography and topographic change. Part 1: error in elevation measurements caused by bed roughness'.
- Linton, D. L. 1952, 'Air photographs as tools of geographical research'. In: Rapporté commission utiliser photographie aériennes études géographie, Congress International Géographique, Washington, Paris, 17-28.
- Liu, H. and Jezek, K. C. 1999, 'Investigating DEM error patterns by directional variograms and Fourier analysis', *Geographical Analysis*, 31(3), 249-266.
- Lo, C. P. and Wong, F. Y. 1973, 'Micro-scale geomorphological features', *Photogrammetric Engineering*, 39(39), 12.
- Lohman, S. W. and Robinove, C. J. 1964, 'Photographic description and appraisal of water resources', *Photogrammetria*, 19(3), 87-103.
- Lopez, C. 1997, 'Locating some types of random errors in digital terrain models', *International Journal of Geographical Information Science*, 11(7), 677-698.
- Lueder, D. R. 1959, *Aerial photographic interpretation*, McGraw-Hill, New York.
- Lyon, J. G., Lunetta, R. S. and Williams, D. C. 1992, 'Airborne multispectral scanner data for evaluating bottom sediment types and water depths of the St Marys River, Michigan', *Photogrammetric Engineering and Remote Sensing*, 58(7), 951-956.
- Lyzenga, D. R. 1978, 'Passive remote sensing techniques for mapping water depth and bottom features', *Applied Optics*, 17(3), 379-383.

- Lyzenga, D. R. 1981, 'Remote sensing of bottom reflectance and water attenuation parameters in shallow water using aircraft and Landsat data', *International Journal of Remote Sensing*, 2(1), 71-82.
- Lyzenga, D. R. 1985, 'Shallow-water bathymetry using combined lidar and passive multispectral scanner data', *International Journal of Remote Sensing*, 6(1), 115-125.
- MacPhee, S. B., Dow, A. J., Anderson, N. M., Reid, D. B. and Lapp, P. A. 1981, 'Aerial hydrography laser bathymetry and air photo techniques for obtaining inshore hydrography', *The Hydrographic Journal*, 22, 19-22.
- Makarovici, B. 1972, 'Information transfer in reconstruction of data from sampled points', *Photogrammetria*, 28(4), 111-130.
- Makarovici, B. 1974, 'Conversion of fidelity into accuracy', *ITC Journal*, 4, 506-517.
- Marcus, W. A., Legleiter, C., Rasmussen, J., Ahl, R. and Halligan, K. 2001, 'Evaluation of high spatial resolution hyperspectral imagery for stream mapping'. In: Paper presented to 97th annual meeting of the American Association of Geographers, New York, 27 February - 3 March 2001.
- Marks, K. and Bates, P. 2000, 'Integration of high-resolution topographic data with floodplain flow models', *Hydrological Processes*, 14(11-12), 2109-2212.
- Martin, Y. and Church, M. 1995, 'Bed-material transport estimated from channel surveys: Vedder River, British Columbia', *Earth Surface Processes and Landforms*, 20, 347-361.
- McEwan, I. K., Habersack, H. M. and Heald, J. G. C. 2001, 'Discrete particle modelling and active tracers: new techniques for studying sediment transport as a lagrangian phenomenon'. In: *Gravel bed rivers V* (ed. Mosley, M. P.), New Zealand Hydrological Society, Wellington.
- McLean, D. G. and Church, M. 1999, 'Sediment transport along lower Fraser River. 2. Estimates based on long-term gravel budget', *Water Resources Research*, 35(8), 2549-2559.
- Meijer, W. O. J. G. 1964, 'Formula for conversion of stereoscopically observed apparent depth of water to true depth, numerical examples and discussion', *Photogrammetric Engineering*, 30(6), 1037-1045.
- Mertes, L., Smith, M. O. and Adams, J. B. 1993, 'Estimating suspended sediment concentrations in surface waters of the Amazon wetlands from Landsat images', *Remote Sensing of Environment*, 43, 281-301.
- Miles, M. 1976, 'An investigation of riverbank and coastal erosion, Banks Island, District of Franklin', *Geological Survey of Canada Paper*, 76(1A), 195-200.
- Miller, C. L. and LaFlamme, R. A. 1958, 'The digital terrain model - theory and application', *Photogrammetric Engineering*, 24, 433-442.

- Milton, E. J., Gilvear, D. J. and Hooper, I. D. 1995, 'Investigating change in fluvial systems using remotely sensed data'. In: *Changing river channels* (eds. Gurnell, A. M. and Petts, G. E.), Wiley, Chichester, 277-301.
- Monckton, C. G. 1994, 'An investigation into the spatial structure of error in digital elevation data'. In: *Innovations in GIS 1* (ed. Worboys, M. F.), Taylor and Francis, London, 201-211.
- Montgomery, D. R., Dietrich, W. E. and Sullivan, K. 1998, 'The role of GIS in watershed analysis'. In: *Landform monitoring, modelling and analysis* (eds. Lane, S. N., Richards, K. S. and Chandler, J. H.), Wiley, Chichester, 241-261.
- Moore, I. D., Grayson, R. B. and Ladson, A. R. 1991, 'Digital terrain models: a review of hydrological, geomorphological, and biological applications', *Hydrological Processes*, 5, 3-30.
- Morang, A., Larson, R. and Gorman, L. 1997, 'Monitoring the coastal environment 3: geophysical and research methods', *Journal of Coastal Research*, 13(4), 1064-1085.
- Muller, E. 1992, *Evaluation de la bande TM5 pour la cartographie morpho-hydrogéologique de la moyenne vallée de la Garonne (Project SPOT 4/MIR)*, CNES, Paris.
- Muller, E., Décamps, H. and Dobson, M. K. 1993, 'Contribution of space remote sensing to river studies', *Freshwater Biology*, 29, 301-312.
- Murray, A. B. and Paola, C. 1994, 'A cellular model of braided rivers', *Nature*, 371, 54-57.
- Murray, A. B. and Paola, C. 1997, 'Properties of a cellular braided stream model', *Earth Surface Processes and Landforms*, 22, 1001-1025.
- Nagao, M., Mukai, Y., Ayabe, K., Arai, K. and Nakazawa, T. 1988, 'A study of reducing abnormal elevations in automatic computations of elevations from satellite data', *Archives of Photogrammetry and Remote Sensing*, 27(B4), 280-288.
- Nagarajan, R., Marathe, G. T. and Collins, W. G. 1993, 'Identification of flood prone regions of the Rapti River using temporal remotely-sensed data', *International Journal of Remote Sensing*, 14(7), 1297-1303.
- Neill, C. R. 1969, 'Bed forms in the Lower Red Deer River, Alberta', *Journal of Hydrology*, 7, 58-85.
- Neill, C. R. 1971, 'River bed transport related to meander migration rates', *ASCE Journal of the Waterways and Harbours Division*, 97, 783-786.
- Nellis, M. D., Harington, J. A. J. and Wu, J. 1998, 'Remote sensing of temporal and spatial variations in pool size, suspended sediment, turbidity and Secchi depth in Tuttle Creek Reservoir, Kansas: 1993.', *Geomorphology*, 21(3-4), 281-293.

- Newton, I. 1989, 'Underwater photogrammetry'. In: Non-topographic photogrammetry, 2nd edition (ed. Karara, H. M.), American Society for Photogrammetry and Remote Sensing, Falls Church, Virginia, USA.
- Nicholas, A. P. 2001, 'Computational fluid dynamics modelling of boundary roughness in gravel-bed rivers: An investigation of the effects of random variability in bed elevation', *Earth Surface Processes and Landforms*, 26(4), 345-362.
- Nicholas, A. P. and Sambrook-Smith, G. H. 1998, 'Relationships between flow hydraulics, sediment supply, bedload transport and channel stability in the proglacial Virkisa River, Iceland', *Geografiska Annaler*, 80A(2), 111-122.
- Nicholas, A. P. and Sambrook-Smith, G. H. 1999, 'Numerical simulation of three-dimensional flow hydraulics in a braided channel', *Hydrological Processes*, 13(6), 913-929.
- Nikora, V. I. 1991, 'Fractal structures of river plan forms', *Water Resources Research*, 27(6), 1327-1333.
- Norcliffe, G. B. 1977, Inferential statistics for geographers, Hutchinson & Co, London.
- Nykanen, D. K., Foufoula-Georgiou, E. and Sapozhnikov, V. B. 1998, 'Study of scaling in braided river patterns using synthetic aperture radar imagery', *Water Resources Research*, 34(7), 1795-1807.
- Openshaw, S., Carver, M. and Carver, S. 1991, 'Error propagation: A Monte Carlo simulation'. In: Handling geographical information: methodology and potential applications (eds. Masser, I. and Blackemore, M.), Bath Press, Bath, 78-102.
- Oros, C. N. 1952, 'River current data from aerial photography', *Photogrammetric Engineering*, 18(1), 96-99.
- OS (Ordnance Survey) 1992, 1:50000 scale height data user manual, Ordnance Survey, Southampton.
- Painter, R. B., Blyth, K., Mosedale, J. C. and Kelly, M. 1974, 'The effect of afforestation on erosion processes and sediment yield'. In: Effects of man on the interface of the hydrological cycle with the physical environment, International Association of Hydrological Sciences Publication, Paris, 62-68.
- Paola, C. 2001, 'Modelling stream braiding over a range of scales'. In: Gravel bed rivers V (ed. Mosley, M. P.), New Zealand Hydrological Society, Wellington.
- Paredes, J. M. and Spero, R. E. 1983, 'Water depth mapping from passive remote sensing data under a generalised ratio assumption', *Applied Optics*, 22(8), 1134-1135.
- Parker, D. E., Lee, G. B. and Milfred, C. J. 1970, 'Flood plain delineation with pan and colour', *Photogrammetric Engineering*, 36(10), 1059-1063.
- Parker, G., Dhamotharan, S. and Stefan, H. 1982, 'Model experiments on mobile, paved, gravel-bed streams', *Water Resources Research*, 18, 1395-1408.

- Peckham, S. D. 1995, 'New results for self-similar trees with application to river networks', *Water Resources Research*, 31, 1023-1029.
- Pels, S. 1964, 'The present and ancestral Murray River system', *Australian Geographical Studies*, 2(2-3), 111-120.
- Pelzer, H. 1979, 'Criteria for the reliability of geodetic networks'. In: *Optimisation of the design and computation of control networks* (eds. Halmos, F. and Somogyi, J.), Akademiai Kaido, Budapest, 553-562.
- Penny, M. F., Billard, B. and Abbot, R. H. 1989, 'LADS - the Australian laser airborne depth sounder', *International Journal of Remote Sensing*, 10, 1463-1479.
- Pethick, J. S. 1998, 'Coastal management and sea level rise: a morphological approach'. In: *Landform monitoring, modelling and analysis* (eds. Lane, S. N., Richards, K. S. and Chandler, J. H.), Wiley, Chichester, 405-419.
- Petrie, G. 1997, 'Developments in Digital Photogrammetric Systems for Topographic Mapping and GIS/LIS Applications', *ITC Journal*, 2, 121-135.
- Petzold, B., Reiss, P. and Stössel, W. 1999, 'Laser scanning - surveying and mapping agencies are using a new technique for the derivation of digital terrain models', *ISPRS Journal of Photogrammetry and Remote Sensing*, 54, 95-104.
- Philip, G., Gupta, R. P. and Bhattacharya, A. 1989, 'Channel migration studies in the middle Ganga basin, India, using remote-sensing data', *International Journal of Remote Sensing*, 10(6), 1141-1149.
- Phillips, J. D. 1995, 'Self-organisation and landscape evolution', *Progress in Physical Geography*, 19, 309-321.
- Philpot, W. D. 1989, 'Bathymetric mapping with passive multispectral imagery', *Applied Optics*, 28(8), 1569-1578.
- Pike, R. J. 1995, 'Geomorphometry - progress, practice and prospect', *Zeitschrift für Geomorphologie*, Supplementband, 101, 221-238.
- Pike, R. J. 2000, 'Geomorphometry - diversity in qualitative surface analysis', *Progress in Physical Geography*, 24(1), 1-20.
- Polidori, L., Chorowicz, J. and Guillande, R. 1991, 'Description of terrain as a fractal surface, and application to digital elevation model quality assessment', *Photogrammetric Engineering and Remote Sensing*, 57(10), 1329-1332.
- Popov, I. V. 1962, 'Application of morphological analysis to the evaluation of the general channel deformation of the River Ob', *Soviet Hydrology*, 3, 267-324.
- Price, R. J. 1965, 'The changing proglacial environment of the Casement Glacier, Glacier Bay, Alaska', *Transactions of the Institute of British Geographers*, 36, 107-116.

- Putnam, W. C. 1947, 'Aerial photographs in geology', *Photogrammetric Engineering*, 13(4), 557-565.
- Pyle, C. J., Chandler, J. H. and Richards, K. S. 1997, 'Digital photogrammetric monitoring of river bank erosion', *Photogrammetric Record*, 15, 753-764.
- Quinn, P. F., Beven, K. J., Chevallier, P. and Planchon, O. 1991, 'The prediction of hillslope flow paths for distributed hydrological modelling using digital terrain models', *Hydrological Processes*, 5, 59-79.
- Ramasamy, S. M., Bakiwal, P. C. and Verma, R. P. 1991, 'Remote sensing and river migration in western India', *International Journal of Remote Sensing*, 12, 2597-2609.
- Reeves, D. M. 1927, *Aerial photographs: characteristics and military applications*, Ronald Press, New York.
- Reid, R. E. and Poynter, R. H. 1982, *The Waimakariri Improvement Scheme 1982 Review*, North Canterbury Catchment Board and Regional Water Board, Christchurch.
- Reid, S. C. 2001, Investigation of controls upon error in photogrammetrically-derived digital elevation models of large braided rivers, with specific reference to the River Waimakariri, New Zealand, unpublished MGeog dissertation, University of Leeds.
- Reilly, S. E. 1965, 'Submarine topography and its delineation', *The Australian Surveyor*, 20(5), 325-340.
- Reinfelds, I. 1995, 'Evidence for high magnitude floods along the Waimakariri River, South Island, New Zealand', *Journal of Hydrology (New Zealand)*, 34(2), 95-110.
- Reinfelds, I. 1997, 'Reconstruction of changes in bankfull width. A comparison of surveyed cross-sections and aerial photography', *Applied Geography*, 17(3), 203-213.
- Rhoads, B. L. and Thorn, C. E. 1996, 'Observation in Geomorphology'. In: *The scientific nature of geomorphology* (eds. Rhoads, B. L. and Thorn, C. E.), Wiley, Chichester, 21-56.
- Richards, K. S. 1988, 'Fluvial geomorphology', *Progress in Physical Geography*, 12, 435-456.
- Rinaldo, A., Rodríguez-Iturbe, I. and Rigon, R. 1998, 'Channel networks'. In: *Annual review of earth and planetary sciences*, 26 (eds. Jeanloz, R., Albee, A. L. and Burke, K. C.), Annual Reviews, Palo Alto, California, 289-327.
- Rinner, K. 1969, 'Problems of two-medium photogrammetry', *Photogrammetric Engineering*, 35(3), 275-282.
- Ritchie, J. C. 1996, 'Remote sensing applications to hydrology: airborne laser altimeters', *Hydrological Sciences*, 41(4), 625-636.
- Ritchie, J. C., Grissinger, E. H., Murphrey, J. B. and Garbrecht, J. D. 1994, 'Measuring channel and gully cross-sections with an airborne laser altimeter', *Hydrological Processes*, 8, 237-243.

- Rodríguez-Iturbe, I., Ijjasz-Vasquez, E., Bras, R. and Tarboton, D. 1992, 'Power law distributions of discharge mass and energy in river basins', *Water Resources Research*, 28, 1089-1093.
- Romanowicz, R., Beven, K., Freer, J. and Moore, R. 1993, 'TOPMODEL as an application module within WIS'. In: *Application of geographic information systems in hydrology and water resources*, 211 (eds. Kovar, K. and Nachtnebel, H. P.), International Association of Hydrological Sciences, Wallingford, 211-223.
- Rosenshein, J. S., Goodwin, C. R. and Jurado, A. 1977, 'Bottom configuration and environment of Tampa Bay', *Photogrammetric Engineering*, 43(6), 693-699.
- Rundle, A. 1985, 'Braid morphology and the formation of multiple channels: The Rakaia, New Zealand', *Zeitschrift fur Geomorphologie*, Suppl.-Bd 55, 15-37.
- Sabins, F. F. 1987, *Remote sensing: principles and interpretation*, 2nd edition, W.H. Freeman and Co., New York.
- Saleh, R. A. 1996, 'Photogrammetry and the quest for digitization', *Photogrammetric Engineering and Remote Sensing*, 62(6), 675-678.
- Salgueiro, P. R. 1965, 'Landslide investigation by means of photogrammetry', *Photogrammetria*, 20(3), 107-114.
- Salo, J., Kalliola, R., Häkkinen, I., Mäkinen, Y., Niemelä, P., Puhakka, M. and Coley, P. D. 1986, 'River dynamics and the diversity of the Amazon lowland forest', *Nature*, 322, 254-258.
- Sapozhnikov, V. and Foufoula-Georgiou, E. 1996, 'Self-affinity in braided rivers', *Water Resources Research*, 32(5), 1429-1439.
- Sapozhnikov, V. and Foufoula-Georgiou, E. 1997, 'Experimental evidence of dynamic scaling and indications of self-organized criticality in braided rivers', *Water Resources Research*, 33(8), 1983-1991.
- Sapozhnikov, V. and Foufoula-Georgiou, E. 1999, 'Horizontal and vertical self-organization of braided rivers toward a critical state', *Water Resources Research*, 35(3), 843-851.
- Sapozhnikov, V. B., Murray, A. B., Paola, C. and Foufoula-Georgiou, E. 1998, 'Validation of braided-stream models: Spatial state-space plots, self-affine scaling, and island shapes', *Water Resources Research*, 34(9), 2353-2364.
- Satalich, J. and Ricketson, R. 1998, 'Field test of Trimble 4000 real-time kinematic GPS survey system', *Journal of Surveying Engineering*, 124(1), 40-48.
- Schmidt, L. B., Schill, S. R., Raber, G. T., Jensen, J. R. and Hodgson, M. E. 2001, 'Evaluation of the utility and accuracy of LIDAR and IFSAR derived DEMs for flood plain mapping'. Paper presented to the 97th Annual Meeting of the American Association of Geographers, New York, USA, 27 February - 3 March 2001.

- Schmutter, B. and Bonfiglioli, L. 1967, 'Orientation problems in two-medium photogrammetry', *Photogrammetric Engineering*, 33(12), 1421-1428.
- Schneider, W. J. 1968, 'Color photographs for water resource studies', *Photogrammetric Engineering*, 34(3), 257-262.
- Schumann, R. R. 1989, 'Morphology of Red Creek, Wyoming, an arid-region anastomosing channel system', *Earth Surface Processes and Landforms*, 14, 277-288.
- Schumm, S. A. and Lichty, R. W. 1963, 'Channel widening and floodplain construction along Cimarron River, in south-western Kansas', United States Geological Survey Professional Paper, 352(D).
- Sear, D. A. and Milne, J. A. 2000, 'Surface modelling of upland river channel topography and sedimentology using GIS', *Physics and Chemistry of the Earth Part B - Hydrology, Oceans and Atmosphere*, 25(4), 399-406.
- Shan, J. 1994, 'Relative orientation for 2-media photogrammetry', *Photogrammetric Record*, 14(84), 993-999.
- Shaw, S. H. 1953, 'The value of air photographs in the analysis of drainage patterns', *Photogrammetric Record*, 1(2), 4-15.
- Shearer, J. W. 1990, 'The accuracy of digital terrain models'. In: *Terrain modelling in surveying and civil engineering* (eds. Petrie, G. and Kennie, T. J. M.), Whittles, London, 315-316.
- Sherstone, D. A. 1983, 'Sediment removal during an extreme summer storm: Muskwa River, North-eastern British Columbia', *Canadian Geotechnical Journal*, 20(2), 329-335.
- Shortis, M. R. and Harvey, E. S. 1998, 'Design and calibration of an underwater stereo-video system for the monitoring of marine fauna populations', *International Archives of Photogrammetry and Remote Sensing*, 32(5), 792-799.
- Slama, C. C. 1980, *The manual of photogrammetry*, 4th edition, American Society of Photogrammetrists, Falls Church, Virginia.
- Smart, G., Walsh, J. and Duncan, M. J. 2001, 'Roughness and flow resistance'. In: *Gravel bed rivers 2000 CD ROM* (eds. Nolan, T. and Thorne, C.), Special Publication of the New Zealand Hydrological Society, Christchurch.
- Smart, R. and Brasington, J. 2001, 'Three dimensional morphometric analysis of a small channel evolution'. In: Presented to the Joint Technical Symposium of the Photogrammetric Society and the British Geomorphological Research Group, University of Leeds, 17 January 2001.
- Smith, D. G. 1997, Digital photogrammetry for elevation modelling, unpublished PhD thesis, University of Nottingham.
- Smith, H. T. U. 1941, 'Aerial photographs in geomorphic studies', *Journal of Geomorphology*, 4(3), 170-205.

- Smith, H. T. U. 1943, Aerial photographs and their applications, D. Appleton-Century, New York.
- Smith, L. C., Alsdorf, D. E., Magilligan, F. J., Gomez, B., Mertes, L. A. K., Smith, N. D. and Garvin, J. B. 2000, 'Estimation of erosion, deposition and net volumetric change caused by the 1996 Skeiðarársandur jökulhlaup, Iceland, from synthetic aperture radar interferometry', *Water Resources Research*, 36(6), 1583-1594.
- Smith, M. J., Smith, D. G., Tragheim, D. G. and Holt, M. 1997, 'DEM's and ortho-images from aerial photographs', *Photogrammetric Record*, 15(90), 945-950.
- Specht, M. R., Needler, D. and Fritz, N. L. 1973, 'New color film for water-photography penetration', *Photogrammetric Engineering*, 39(4), 359-369.
- Speight, J. G. 1965a, 'Meander spectra of the Angabunga River', *Journal of Hydrology*, 3(1), 1-15.
- Speight, J. G. 1965b, 'Flow and channel characteristics of the Angabunga River, Papua', *Journal of Hydrology*, 3, 16-36.
- Spitzer, D. and Dirks, R. W. J. 1987, 'Bottom influence on the reflectance of the sea', *International Journal of Remote Sensing*, 8(3), 279-290.
- Squires, G. L. 1968, Practical physics, McGraw-Hill, London.
- Sternberg, I. 1961, 'Drainage studies from aerial surveys', *Photogrammetric Engineering*, 27, 638-644.
- Stojic, M. 2001, River channel modeling using oblique imagery, ERDAS, Atlanta, Georgia, USA. Available online at <http://www.geosystems.de/anwendungen>.
- Stojic, M., Chandler, J. H., Ashmore, P. and Luce, J. 1998, 'The assessment of sediment transport rates by automated digital photogrammetry', *Photogrammetric Engineering and Remote Sensing*, 64(5), 387-395.
- Stølum, H.-H. 1996, 'River meandering as a self-organization process', *Science*, 271, 1710-1713.
- Sundborg, A. 1956, 'The river Klaräven, a study of fluvial processes', *Geografiska Annaler*, 38(A), 125-316.
- Tan, K. H. 1983, The effect of surface waves on photography through water, unpublished Final Year Project, University of Newcastle, New South Wales, Australia.
- Tarboton, D. G., Bras, R. L. and Rodríguez-Iturbe, I. 1988, 'The fractal nature of river networks', *Water Resources Research*, 24, 1317-1322.
- Tateishi, R. and Akutsu, A. 1992, 'Relative DEM production from SPOT data without GCP', *International Journal of Remote Sensing*, 13(14), 2517-2530.
- Taylor, J. R. 1997, An introduction to error analysis: the study of uncertainties in physical measurements, 2nd edition, University Science Books, Sausalito, California, USA.

- Templfi, K. 1980, 'Spectral analysis of terrain relief for the accuracy estimation of digital terrain models', *ITC Journal*, 3, 478-510.
- Tewinkel, G. C. 1963, 'Water depths from aerial photographs', *Photogrammetric Engineering*, 29(6), 1037-1042.
- Thompson, G. W. and Maune, D. F. 2001, Remapping the North Carolina floodplains with LIDAR, part 1, North Carolina Floodplain Mapping Program. Available online at <http://www.ncfloodmaps.com/pubdocs/default.htm>.
- Thorne, C. R., Russell, A. P. G. and Alam, M. K. 1993, 'Planform pattern and channel evolution of the Brahmaputra River, Bangladesh'. In: Braided rivers, Special Publication No. 75 (eds. Best, J. L. and Bristow, C. S.), Geological Society, London, 257-276.
- Thornes, J. B. and Brunsden, D. 1977, Geomorphology and time, Methuen, London.
- Torgersen, C. E., Faux, R. N., McIntosh, B. A., Poage, N. J. and Norton, D. J. 2001, 'Airborne remote sensing for water temperature assessment in rivers and streams', *Remote Sensing of Environment*, 76(3), 386-398.
- Torlegård, K., Östman, A. and Lindgren, R. 1986, 'A comparative test of photogrammetrically sampled digital elevation models', *Photogrammetria*, 41, 1-16.
- Townsend, P. A. and Walsh, S. J. 1998, 'Modeling floodplain inundation using an integrated GIS with radar and optical remote sensing', *Geomorphology*, 21, 295-312.
- Turpin, O. C., Ferguson, R. I. and Clark, C. D. 1998, 'The transient snowline on glaciers: topographic controls and implications for melt predictions'. In: Landform monitoring, modelling and analysis (eds. Lane, S. N., Richards, K. S. and Chandler, J. H.), Wiley, Chichester, 363-383.
- Turton, D. and Jonas, D. 1999, Airborne laser scanning: a new technology for the supply of spatial data, AAM Surveys, Brisbane, Queensland. Available online at <http://www.aamsurveys.com.au/articles.html>.
- USGS (United States Geological Survey) 1987, Digital elevation models data users guide, Technical Instructions, Data Users Guide 5, National Mapping Program, United States Geological Survey, Reston, Virginia.
- Van Sickle, J. 1996, GPS for land surveyors, Ann-Habor Press, Michigan, USA.
- Walker, J. P. and Wilgoose, G. R. 1999, 'On the effect of digital elevation model accuracy on hydrology and geomorphology', *Water Resources Research*, 35(7), 2259-2268.
- Wallbridge, S., Vouilgaris, G., Tomlinson, B. N. and Collins, M. B. 1999, 'Initial motion and pivoting characteristics of sand particles in uniform and heterogeneous beds: experiments and modelling', *Sedimentology*, 46(1), 17-32.
- Warburton, J., Davies, T. R. H. and Mandl, M. G. 1993, 'A meso-scale investigation of channel change and floodplain characteristics in an upland braided gravel-bed river, New

- Zealand'. In: Braide7d rivers (eds. Best, J. L. and Bristow, C. S.), Geological Society, London, 241-255.
- Webb, E. K. 1995, 'Simulation of braided channel topology and topography', *Water Resources Research*, 31(10), 2603-2611.
- Wehr, A. and Lohr, U. 1999, 'Airborne laser scanning - an introduction and overview', *ISPRS Journal of Photogrammetry and Remote Sensing*, 54, 68-82.
- Welch, R. and Jordan, T. R. 1983, 'Analytical non-metric close-range photogrammetry for monitoring stream channel erosion', *Photogrammetric Engineering and Remote Sensing*, 49(3), 367-374.
- Werner, B. T. 1999, 'Complexity in natural landform patterns', *Science*, 284, 102-104.
- Werrity, A. and Ferguson, R. I. 1980, 'Pattern changes in a Scottish braided river over 1, 30 and 200 years'. In: Timescales in geomorphology (eds. Cullingford, R. A., Davidson, D. A. and Lewin, J.), Wiley, Chichester, 53-68.
- Whitehouse, F. W. 1944, 'The natural drainage of some very flat monsoonal lands', *Australian Geographer*, 4, 183-196.
- Williams, D. R., Romeril, P. M. and Mitchell, R. J. 1979, 'Riverbank erosion and recession in the Ottawa area', *Canadian Geotechnical Journal*, 16(4), 641-650.
- Williman, E. B. and Low, H. S. 1988, Waimakariri Floodplain Management Plan: cross section data processing and data analysis, Department of Scientific and Industrial Research, Christchurch, New Zealand. Hydrology Centre Report HC88.02.
- Willis, I. C., Arnold, N. S., Sharp, M. J., Bonvin, J.-M. and Hubbard, B. P. 1998, 'Mass balance and flow variations of Haut Glacier d'Arolla, Switzerland, calculated using digital terrain modelling techniques'. In: Landform monitoring, modelling and analysis (eds. Lane, S. N., Richards, K. S. and Chandler, J. H.), Wiley, Chichester, 343-361.
- Willsman, A. 1995, North Ashburton River survey, NIWA, Christchurch. Unpublished report.
- Willsman, A. 1999, North Ashburton River survey: Part 2, NIWA, Christchurch. Unpublished report.
- Winterbottom, S. J. 2000, 'Medium and short-term channel planform changes on the Rivers Tay and Tummel, Scotland', *Geomorphology*, 34(3-4), 195-208.
- Winterbottom, S. J. and Gilvear, D. J. 1997, 'Quantification of channel bed morphology in gravel-bed rivers using airborne multispectral imagery and aerial photography', *Regulated Rivers: Research and Management*, 13, 489-499.
- Wise, S. 1998, 'The effect of GIS interpolation errors on the use of DEMs in geomorphology'. In: Landform monitoring, modelling and analysis (eds. Lane, S. N., Richards, K. S. and Chandler, J. H.), Wiley, Chichester, 139-164.

- Witte, C., Norman, P., Denham, R., Turton, D., Jonas, D. and Tickle, P. 2000, Airborne laser scanning - a tool for monitoring and assessing the forests and woodlands of Australia, Department of Natural Resources, Queensland Government, Brisbane, Queensland. Available online at <http://www.aamsurveys.com.au/articles.html>.
- Wolf, P. R. 1983, Elements of photogrammetry, 2nd edition, McGraw Hill, New York.
- Wolf, P. R. and Dewitt, B. A. 2000, Elements of photogrammetry with applications in GIS, 3rd edition, McGraw-Hill, London.
- Wolman, M. G. 1967, 'A cycle of sedimentation and erosion in urban river channels', *Geografiska Annaler*, 49, 385-395.
- Wood, J. 1994, 'Visualizing contour interpolation accuracy in digital elevation models'. In: Visualization in geographical information systems (eds. Hearnshaw, H. M. and Unwin, D. J.), Wiley, Chichester, 168-180.
- Wright, A., Marcus, W. A. and Aspinall, R. 2000, 'Evaluation of multispectral, fine scale digital imagery as a tool for mapping stream morphology', *Geomorphology*, 33(1-2), 107-120.
- Yong, S. J. 1984, The effect of surface waves on low altitude photogrammetry through artificially calmed water, unpublished Final Year Project, University of Newcastle, New South Wales, Australia.
- Yost, E. and Wenderoth, S. 1968, 'Coastal water penetration using multispectral methods'. In: Proceedings of the Fifth Symposium on Remote Sensing of Environment, Ann Arbor, Michigan, April 1968.